Winter 12-15-2018

# Neural Mechanisms of Drosophila Circadian Rhythms

Xitong Liang
*Washington University in St. Louis*

WASHINGTON UNIVERSITY IN ST. LOUIS

Division of Biology and Biomedical Sciences
Neurosciences

Dissertation Examination Committee:
Paul Taghert, Chair
Timothy Holy, Co-Chair
Martha Bagnall
Erik Herzog
Daniel Kerschensteiner

# Neural Mechanisms of *Drosophila* Circadian Rhythms

by

Xitong Liang

A dissertation presented to
The Graduate School
of Washington University in
partial fulfillment of the
requirements for the degree
of Doctor of Philosophy

December 2018
St. Louis, Missouri

# Table of Contents

# List of Figures

Chapter 5



Chapter 6

# List of Tables

# Acknowledgments

I thank my advisor Dr. Paul Taghert for guidance, support, and training in the past six years. I thank him for accommodating me as an undergraduate intern in the lab, initiating the collaboration with Dr. Tim Holy for my thesis project, and being fully involved in every step of this project. I also thank him for his efforts on improving my writing and presentation skills and for giving me opportunities to conferences and peer reviews. I would also like to thank my co-advisor Dr. Tim Holy. I benefit not only from his expertise in imaging techniques and quantitative/system neurosciences, but also from his enthusiasm and imagination in science.

I am grateful to my thesis committee. I thank Dr. Erik Herzog for his help during the quantifying exam, for his great classes, for helpful discussions in all different meetings, and for always being the first reader of my manuscripts. I thank Dr. Martha Bagnall and Dr. Daniel Kerschensteiner for their insightful and constructive suggestions in committee meetings and joint lab meetings. I also want to thank Dr. Yehuda Ben-Shahar and Dr. Bruce Carlson for enjoyable rotations in their labs. I also thank mentors in my undergraduate lab, Dr. Yi Zhong and Qian Li, for training in fly behavioral genetics and bringing me into the fly field.

I thank all members in Taghert lab and Holy lab for their support and valuable suggestions. Weihua Li taught me the behavioral assay and immunostaining and he always takes care of my flies when I'm absent. Laura Duvall taught me the cAMP imaging. Jennifer Trigg helped with molecular cloning. Cody Greer built the new generation of OCPI microscope and helped whenever I met any technical problems. Dae Woo Kim upgraded the software for OCPI microscope with new features designed for my experiments. Terra Barnes supervised me when I rotated in the lab and always gives me generous advice since then. I also thank Dennis Oakley for training on microscopes. I am grateful to the DBBS Neuroscience program and the

Department of Neuroscience. I also appreciate the Clocks community at Washington University, especially Matt Tso, Jiajia Li, Cristina Mazuski, Jeff Jones, and Krishna Melnattur for their generous help and valuable advice.

Thanks to my collaborators, Dr. Mark Wu, Margaret Ho, and Ting Xie, for providing their insights in dopamine biology, sharing reagents, and helping revise the manuscript reprinted in Chapter 4. I would like to thank Dr. Orie Shafer for his careful read and constructive comments on the manuscripts reprinted in Chapter 2 & 3. I thank Orie Shafer, Francois Rouyer, Gerry Rubin, Heather Dionne, Aljoscha Nern, Markus Affolter, S. Lawrence Zipursky, Gaiti Hasan, Mark Schnitzer, Yulong Li, Charles Nichols, Michael Rosbash, Erik Johnson, Peter Evans, Vienna Drosophila Resource center, Bloomington Stock Center, and Janelia Research Center for sharing fly lines and reagents. Thanks to the research grants from National Institute of Health and Washington University McDonnell Center for Cellular and Molecular Neurobiology.

I would like to thank all my friends in St. Louis and in other places, especially my roommates Cheng Cheng and Qihao Ren, Wan Shi, Matt Tso, and Zhen Peng. I also thank my animal friends, the cat Cat, Latte, Toothless and Sophie, the chameleon Neuvo, and two parakeets.

I would like to thank my parents and my partner Xueying Li for their love and support.

Xitong Liang

*Washington University in St. Louis*

*December 2018*

Dedicated to *life*.

# ABSTRACT OF THE DISSERTATION

Neural Mechanisms of *Drosophila* Circadian Rhythms

by

Xitong Liang

Doctor of Philosophy in Biology and Biomedical Sciences

Neuroscience

Washington University in St. Louis, 2018

Professor Paul Taghert, Chair

Professor Timothy Holy, Co-Chair

Animals show circadian rhythms in a variety of physiological functions and behaviors. In *Drosophila melanogaster*, behavioral rhythms are driven by circadian clock genes that are oscillating in ~150 circadian pacemaker neurons. To explain how circadian neurons encode time and regulate different behavioral rhythms, I performed 24-hour *in vivo* whole-brain calcium imaging using light-sheet microscopy. First, I found that different groups of circadian neurons show circadian rhythms in spontaneous neural activity with diverse phases. The neural activity phases of the M and E pacemaker groups, which are associated with the morning and evening locomotor activities respectively, occur ~4 hours before their respective behaviors. I also showed that neural activity rhythms are generated by circadian clock gene oscillations, which regulate the expression of *IP3R* and T-type calcium channels. Next, I asked how the diverse phases of neural activity are generated from the in-phase clock gene oscillations. Groups of circadian neurons inhibit each other via long-duration neuromodulation, mediated by neuropeptides PDF and sNPF, such that their activity phases are properly staggered across the day and night. Certain

activity phases are also regulated by environmental light inputs. I then identified an output pathway by which circadian neurons regulate the locomotor activity rhythm. M and E pacemaker groups independently activate a common pre-motor center (termed ellipsoid body ring neurons) through the agency of specific dopaminergic interneurons. Finally, using methods including whole-brain pan-neuronal imaging, I further identified several output circuits downstream of circadian neurons. Circadian neural activity rhythms propagate through these circuits to regulate different behavioral outputs including sleep, olfaction, mating, and feeding rhythms. Together, my findings show how circadian clocks regulate diverse behavioral outputs by two steps; first, circadian clock genes generate diverse circadian neural activity rhythms within a network of interacting pacemaker neurons; then, sequentially-active pacemaker neurons independently and together regulate diverse behavioral outputs by generating diverse circadian neural activity rhythms in different downstream output circuits.

# Chapter 1

# Introduction

### Circadian clocks

## 1.1 Circadian rhythms

Most organisms coordinate their metabolism, physiology, and behavior with daily cyclic environmental changes (Herzog 2007). These environmental changes, including changes in light/dark, temperature, food availability, predatory threats, and other survival-relevant factors that are imposed by the self-rotation of the Earth, repeat every day in a highly predictable manner. Organisms that can anticipate the daily environmental changes can fit themselves into unique and optimal temporal niches.

The fruit fly *Drosophila melanogaster* has two daily activity bouts occurring around dawn and dusk. In the laboratory condition, with 12-hour light: 12-hour dark (LD) cycles, flies align the two bouts at the transients from dark-to-light and from light-to-dark, respectively (Figure 1). Although the light/dark transients in the laboratory condition are instantaneous, the locomotor activity of the fly increases gradually before light-on or light-off, suggesting that, with just a few cycles of experience with this environmental alternation, the fly anticipates the timing of light/dark switches. These predictable extrinsic events are anticipated by an internal biological clock. Therefore, even under constant environmental conditions: constant darkness and constant temperature, the fly still shows daily two peaks of locomotor activity around the dawn and the dusk (Figure 1). This daily rhythm in behavior persists under constant conditions at a period close to 24 hours (~23.5 hours). This period is the intrinsic period of the organism's circadian

clock which free runs under constant conditions, but which can be adjusted to a range of periods (~20 to ~28 hours) under different environmental light/dark cycles (Pittendrigh *et al.* 1958).

In addition to locomotor activity rhythms, circadian clocks also drive rhythms in different biological processes, such as eclosion (the emergence of adult flies following the completion of metamorphosis), sleep/wake cycle, light responses, temperature preference, feeding and metabolism, courtship and mating, chemosensation, cognition like learning and memory, immune response, *et cetera* (Allada and Chung 2010). As such, and because many different biological processes are involved, the disruption of circadian clocks might affect the timing or severity of stroke, cardiac arrest, mood disorders, sleep disorders, and metabolic syndrome. The disruption of circadian clocks can occur under pathological conditions like neurodegenerative diseases and also in daily life such as by jet-lag, shift-work and sleep disturbances. Therefore, the goal of my thesis is to promote a fundamental understanding of the biological basis of circadian clocks. I hope especially to better understand how the outputs of circadian clocks regulate different biological processes.

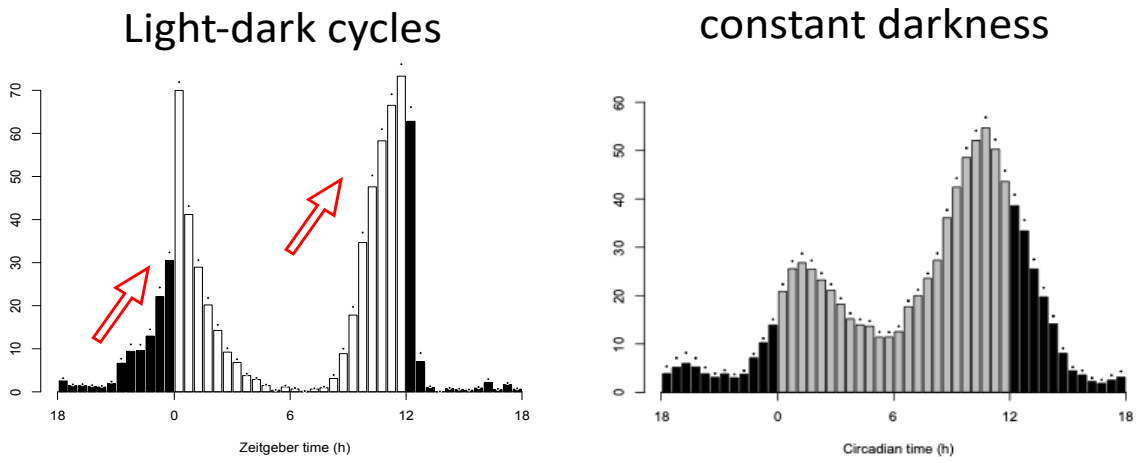


**Figure 1. Daily locomotor activity pattern of Drosophila under light/dark cycles and constant darkness.** Red arrows indicate that the increase of daily locomotor activity precedes the environmental light/dark switches.

## 1.2 Molecular circadian clocks

The circadian clock has been well studied in terms of molecular mechanism. In eukaryotes, the core molecular machinery of circadian clock timing is based on a transcription-translation negative-feedback loop (TTFL), by which the proteins of core clock genes suppress their own transcription with a ~24-hour delay. In animals, the TTFL operates by a set of evolutionarily-conserved circadian clock genes (Herzog 2007). In *Drosophila melanogaster*, two transcription factors with bHLH-PAS domains CYCLE and CLOCK (BMAL1 and CLOCK in mammals) form a CYC-CLK heterodimer. The heterodimer then binds to certain promotor sequences, which represent a subset of ones containing binding motif termed the E-box, to activate transcription of clock-regulated genes. Among the products of these regulated genes, two negative circadian elements PERIOD (PER) and TIMLESS (TIM) (PER1/2 and CRY1/2 in mammals) also form a heterodimer, called PER-TIM. That heterodimer feeds back to repress *per* and *tim* transcription by inhibiting the activity of CYC-CLK, and consequently it represses the transcription of all other clock-regulated genes in that day's cycle. As a result, this feedback loop drives oscillations in the expression of PER/TIM, in the transcriptional activity of CYC-CLK, and in the expression of other clock-regulated genes according to a ~24-hour period, thus forming a stable molecular clock (Hall 2003).

The oscillations of molecular clocks are self-sustained yet can be regulated by different factors. Every day, the levels of PER and TIM proteins in *Drosophila* peak in the morning and exert maximal inhibition on CYC-CLK activity. Then PER/TIM proteins are degraded over the course of the day. The degradation of PER/TIM is facilitated by light. The external light activates an internal photoreceptor CRYPTOCHROME (CRY) (Emery *et al.* 1998; Stanewsky *et al.* 1998). CRY then activates the degradation of TIM, mediated by a E3 ligase JETLAG (Koh *et*

*al.* 2006). During the nighttime, PER and TIM accumulate in the cytoplasm and eventually enter nucleus to repress CYC-CLK during the late night (Shafer *et al.* 2002). Nuclear entry of PER and TIM is gated by their levels and their phosphorylation states. The phosphorylation of PER/TIM is regulated by several kinases including glycogen synthase kinase 3 shaggy (SGG), casein kinase I doubletime (DBT), and casein kinase 2 (Price *et al.* 1998; Kloss *et al.* 1998; Martinek *et al.* 2001; Lin *et al.* 2002; Akten *et al.* 2003). Together, the regulation of PER/TIM determines the 24-hour delay of the oscillation and aligns the phase of the oscillation to the environmental day/night cycles.

In the brain of *Drosophila melanogaster*, circadian molecular clockworks prominently cycle in about 150 neurons (termed circadian pacemakers) and are essential for circadian behavior (Kaneko and Hall 2000). However, it is poorly understood how the molecular oscillations control the cellular and especially the neuronal properties of the pacemaker neurons. Likewise, there is little information with which we can explain how pacemakers ultimately control daily behavioral rhythms. These two issues motivated much of the work in my thesis studies.

### 1.3 Circadian pacemaker neurons

The clock genes are evolutionarily-conserved in animals, from flies to mammals (Herzog 2007). In mammals, the suprachiasmatic nucleus (SCN) coordinates many circadian rhythmic outputs (Stephan and Zucher 1972, Ralph *et al.* 1990). Organotypic SCN slice cultures have been a useful model in which to study the molecular, cellular and circuit properties of circadian pacemaker neurons. Studies in SCN strongly suggest that mechanism at the circuit level is essential to understand how molecular clocks control circadian behavior.

First, physiological properties of SCN neurons display circadian rhythms (Schwartz and Gainer 1977, Welsh *et al.* 1995). These rhythms are modulated via clock-dependent changes in the expression and activity levels of several ion channels (Pennartz *et al.* 2002, Lundkvist *et al.* 2005, Itri *et al.* 2005, Meredith *et al.* 2006). As the outputs of molecular clocks, circadian rhythms in neuronal properties are necessary for circadian behavior. Second, SCN neurons are heterogeneous in their oscillatory activities. Their oscillatory phases display a dorsomedial to ventrolateral progression across the nucleus (Enoki *et al.* 2012, Hong *et al.* 2012, Brancaccio *et al.* 2013). Third, SCN neurons are heterogeneous in in their responses to environment inputs. The ventral SCN neurons respond to extrinsic influences, like photoperiod changes, more quickly than do dorsal neurons (Aton and Herzog 2005, Meijer *et al.* 2010, Evans *et al.* 2013). Fourth, interactions between heterogeneous pacemakers are essential for the balance of plasticity and robustness of internal clocks (Hogenesch and Herzog 2011, An *et al.* 2013). In sum, the SCN is a hierarchical multi-oscillator system, in which mechanisms on the circuit level play crucial roles.

However, without on-going reference to sensory inputs, SCN slices are not anatomically complete. There remains a pressing need to provide complimentary information from an intact multi-pacemaker circadian neural system *in vivo* and to describe its normal phasic activity patterns over the course of a 24hr day. To do so, I have studied Drosophila in which cellular resolution is high and pacemaker identities can be directly related to distinct phases of behavior. Although the neuronal and network properties in Drosophila pacemakers remain elusive, evidence suggest similarity with mammals in these four fundamental aspects I described above.

### 1.3.1 Rhythmic neural activity

The electrical activity in subsets of pacemakers (l-LNv, s-LNv, and DN1) fluctuates according to time of day, as measured in acutely-dissected brains (Cao and Nitabach 2008, Sheeba *et al.* 2008, Cao *et al.* 2013, Kunst *et al.* 2014, Flourakis *et al.* 2015). These observations suggest circadian rhythmicity in pacemaker neural activity. In DN1 pacemakers, the neural activity rhythm involves the sodium leak channel *narrow abdomen* (NA) whose rhythmic expression depends on molecular clocks (Flourakis *et al.* 2015). In the NA mutant, or following acute electrical silencing behavioral rhythmicity is greatly reduced while molecular clocks are not disrupted: this further suggests that neural activity is a fundamental output (Depetris-Chauvin *et al.* 2011, Lear *et al.* 2005). However, without defining the spatiotemporal pattern of neural activity throughout the 150 circadian pacemakers in vivo, how pacemakers' neural activity precisely controls circadian behavior cannot be properly evaluated.

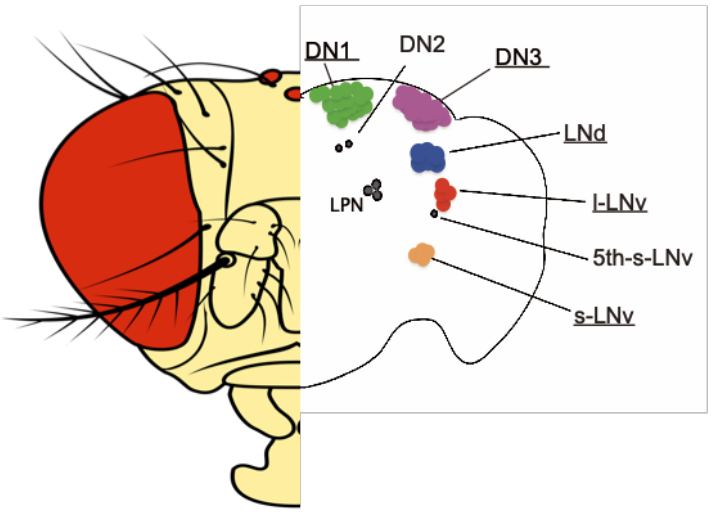


**Figure 2. A map of circadian pacemaker neurons** (following Helfrich-Forster 2003). The different pacemaker groups are marked in different colors.

### 1.3.2 Heterogeneity

In Drosophila, the pacemaker network is anatomically clustered into eight groups: three groups of dorsal neurons (DN1, DN2, and DN3), lateral posterior neurons (LPN), dorsolateral neurons (LNd), large and small ventrolateral neurons (l-LNv and s-LNv), and the 5th small ventrolateral neuron (5th s-LNv) (Figure 2) (Nitabach and Taghert 2008). Each group is

anatomically identifiable and genetically targetable across fly individuals. Genetic mosaic experiments have revealed functional heterogeneity among different pacemaker groups, as exemplified by the categorization of M (morning) and E (evening) cells, primarily responsible for driving the morning and evening peaks of locomotor activity (Stoleru *et al.* 2004, Grima *et al.* 2004, Yoshii *et al.* 2004, Zhang *et al.* 2010). M and E cell categorization supports a classic model of seasonal adaptation (Pittendrigh and Daan 1976) wherein a two-oscillator system responds differentially to light, and so can track dawn and dusk independently. For example, under long day conditions (summer), light accelerates a "morning" clock and decelerates an "evening" clock, leading to advanced morning activity peak and delayed evening activity peak.

In addition to M and E cells, other pacemaker groups also have different functions. The l-LNv group serves an arousal function and promotes the waking state (Parisky *et al.* 2008; Shang *et al.* 2008, 2013). The DN1 group regulates both the morning and evening peaks of locomotor activity under certain circumstances (Zhang L. *et al.* 2010, Zhang Y. *et al.* 2010, Chatterjee *et al.* 2018). Meanwhile, different subsets of DN1 also regulate sleep at different times of day in different manners (Kunst *et al.* 2014, Guo *et al.* 2016, Lamaze *et al.* 2018, Guo *et al.* 2018). The functional diversity of pacemaker neurons expands the functionality of the molecular clock. However, there is strong consensus that molecular clocks in the majority of *Drosophila* circadian pacemaker neurons are highly synchronized (Yoshii et a 2009, Menegazzi *et al.* 2013). By comparing temporal patterns of their neural activity as described in Chapters 2 & 3, I have asked how different pacemaker groups with synchronous molecular clocks control distinct behavior at different times of day?

### 1.3.3 Interactions between pacemakers

A crucial interaction between *Drosophila* circadian pacemakers is mediated by the neuropeptide pigment-dispersing factor (PDF). Two groups of pacemakers (PDF neurons, including s-LNv and l-LNv) release PDF to synchronize molecular clocks of other clock neurons with them (Renn *et al.* 1999). In the absence of PDF release, molecular clocks throughout circadian circuit become increasingly desynchronized under constant conditions, and files exhibit abnormal activity patterns, including arrhythmicity, phase shifts, and multi-rhythmicity (Peng *et al.* 2003, Lin *et al.* 2004, Wülbeck *et al.* 2008, Yoshii *et al.* 2009). Besides PDF, other known interactions between pacemakers are mediated by: glutamate (Hamasaka *et al.* 2007, Collins *et al.* 2012, 2014), diuretic hormone 31 (DH31) (Shafer *et al.* 2007, Kunst *et al.* 2014), short neuropeptide F (sNPF) (Johard *et al.* 2009, Shang *et al.* 2013), neuropeptide F (NPF), and ion transport peptide (ITP) (Johard *et al.* 2009) (also see Table 1). However, when and how these interactions occur and to what extent they influence the spatiotemporal neural activity pattern in the pacemaker network is largely unexplored.

## 1.4 Inputs to the circadian circuit

Light is the most important environmental cue for circadian clocks to entrain to local time. Differentially timed light inputs phase-shift circadian clocks in different manners, as described by the phase response curve (PRC) (Winfree 1970, Saunders *et al.* 1994). A light pulse in the early night, indicating a delayed dusk, causes a phase delay, while a light pulse in the late night, indicating an advanced dawn, causes a phase advance. The mechanism of circadian photoreception in *Drosophila* was largely considered cell-autonomous, via the intracellular photoreceptor CRY (Emery *et al.* 1998, Stanewsky *et al.* 1998) and a recently

identified rhodopsin Rh7 (Ni *et al.* 2017), both of which express in subsets of circadian neurons. However, recent evidence suggests that circadian photoreception requires neural signaling and network mechanisms. First, molecular clocks in different pacemaker groups responded to light by degrading TIMELESS in different manners (Tang *et al.* 2010) and regardless of whether or not they express CRY (Yoshii *et al.* 2009). In whole-brain explants, a single light pulse induced transient desynchrony in the pacemaker network over the course of 1-2 cycles (Roberts *et al.* 2015). Second, as with studies that restrict the molecular clockworks, mosaic analysis showed that restricting photoreception to subsets of pacemaker groups resets behavior phases in different manners (Emery *et al.* 2000, Stoleru *et al.* 2007, Shang *et al.* 2008, Lamba *et al.* 2014, Yoshii *et al.* 2015). Third, besides the cell autonomous CRY expression, the visual systems convey light inputs to PDF-positive pacemakers (LNvs) (Ashmore and Sehgal 2003). Furthermore, LNvs have been suggested to convey light information to other pacemaker groups through PDF signaling (Cusumano *et al.* 2009, Guo *et al.* 2014). Finally, eye-inputs are broadly conveyed to numerous pacemaker cells via direct synaptic contacts made in the Accessory Medulla (Li *et al.* 2018). Therefore, by studying light induced neural response in vivo in living flies, I asked how environmental inputs are processed in the circadian system, to shift neural activity patterns and thus help adapt behavioral outputs.

## 1.5 Outputs of the circadian circuit

Circadian pacemaker neurons show daily rhythmic neural outputs and control different behavioral rhythms. Many circadian neurons release one or more neuropeptides. Compared to small molecule neurotransmitters, neuropeptides can modulate neuronal activity over larger temporal and spatial ranges (Nässel 2018). Many of these neuropeptides have been shown to regulate different behavioral rhythms, such as locomotor activity, sleep/wake cycles, and eclosion, which is summarized in Table 1. Among these neuropeptides, the pigment-dispensing factor (PDF) is the best-characterized one. In addition to mediating the interaction between pacemakers, PDF receptors also express in non-clock neurons (Im and Taghert 2010) and potentially signal the circadian regulation to neurons downstream of clock neurons (Pírez *et al.* 2013, Chen *et al.* 2016, Potdar and Sheeba 2018). Besides PDF, other neuropeptides such as ITP, sNPF, NPF, and DH31 also might be involved as outputs of the clocks to regulate different downstream circuits. Downstream output circuits then convey the circadian information to drive rhythms in different biological processes.

Recently, a series of studies have identified several output circuits downstream of the circadian neurons, by screening for neurons and neuropeptides outside of circadian neurons that cause deficits behavioral rhythms. These findings are summarized in Table 2. Three criteria are used to define a downstream output circuit; first, the circuit regulates certain behavioral or physiological rhythms; second, the neural activity of the circuit is regulated directly or indirectly by circadian pacemaker neurons; third, disruption of its neural activity disrupts the behavioral rhythms without affecting the molecular clocks in pacemaker neurons.

However, output circuits identified so far suggest that the output pathways are possibly redundant, because disrupting any of them weakened but didn't eliminate the behavioral

rhythms. Therefore, screening for strong behavioral deficits is likely to miss those redundant and parallel pathways. To characterize the complete neural pathways of circadian outputs, I use a complemental strategy in Chapters 4 & 5 by searching for non-clock neurons that show clock-dependent circadian rhythms in their spontaneous neural activity. Then I study how circadian neurons regulate these candidate output neurons by selectively manipulating a subset of circadian neurons and also link the neural activity rhythms of these output neurons to different behavioral rhythms.

**Table 1. Summary of neuropeptides released from circadian pacemaker neurons.**

| **Output signals** | **Behavior(s)** | **Released by** | **References** |
|---|---|---|---|
| DH31 | Promote wake | DN1p | Kunst *et al.* 2014 |
| ITP | Locomotor rhythms | 5$^{th}$ sLNv & 1 LNd | Hermann-Luibl *et al.* 2014 |
| NPF | Locomotor rhythms<br>Fat body rhythms | 4 LNd & l-LNv | Hermann *et al.* 2012<br>Erion *et al.* 2016 |
| sNPF | Promote sleep | 2 LNd & 4 s-LNv | Shang *et al.* 2013 |
| IPNa/CCHa1 | Locomotor rhythms | DN1a | Shafer *et al.* 2006<br>Fujiwara *et al.* 2018 |
| Ast-C | Locomotor rhythms | DN3 & LPN | Díaz *et al.* 2018 |
| PDF | Locomotor rhythms | s-LNv & l-LNv | Renn *et al.* 1999 |

**Table 2. Summary of candidate output neurons downstream of circadian pacemaker circuit described in previous studies.**

| Neurons | Behavior(s) | Downstream of clock | Connections | References |
|---|---|---|---|---|
| DH44 ->Hugin | Locomotor rhythms | Yes | Indirectly by PDF via DN1 | Cavanaugh *et al.* 2014<br>King *et al.* 2017 |
| SIFa | Locomotor rhythms<br>Promote sleep | Yes | via DN1 | Cavanaugh *et al.* 2014<br>Park *et al.* 2014<br>Bai *et al.* 2018 |
| ILPs | Feeding<br>Promote wake | Yes | PDF<br>via DN1 | Barber *et al.* 2017<br>Crocker *et al.* 2010 |
| LK | Locomotor rhythms<br>Feeding | Yes | Indirectly by PDF | Cavey *et al.* 2016<br>Yurgel *et al.* 2018<br>Zawandala *et al.* 2018 |
| Ast-A | Feeding<br>Promote sleep | unknown | By PDF | Chen *et al.* 2016 |
| PTTH | Eclosion | Yes | By sNPF from sLNv | Selcho *et al.* 2017 |
| Ellipsoid body | Locomotion<br>Sleep homeostasis | unknown | By PDF;<br>via DN1 | Pírez *et al.* 2013<br>Liu *et al.* 2016 |
| Mushroom body | Sleep/wake<br>Locomotor rhythms | unknown | unknown | Joiner *et al.* 2006<br>Pitman *et al.* 2006<br>Mabuchi *et al.* 2016 |

**Calcium imaging with light-sheet microscopy**

The major technical challenge in this study was how to record the neural activity in living flies for an entire 24-hour day *in vivo*. I pursued *in vivo* recordings because: (i) Compared to mammalian SCN slice culture or *Drosophila* whole-brain explants, *in vivo* preparations maintain brain-wide connectivity and also receive normal sensory inputs. An *in vivo* model would be optimally placed to study how the system processes environmental inputs. (ii) The *in vivo* microenvironment (if properly maintained) helps to sustain neural tissue health and will avoid tissue deformation during long-term recordings.

To overcome the technical barriers of long-term neural activity recordings in living flies, I use genetically encoded calcium indicator, mostly the GCaMP6s (Chen *et al.* 2013) to do calcium imaging. Calcium imaging has several advantages, including: (a) Compared to electrophysiological recordings, optical recording is non-invasive and thus readily permits long term recording. (b) The genetically-encoded calcium indicators restrict the signal to cells of interest. (c) Imaging can simultaneously monitor a large population of neurons, from the entire circadian pacemaker circuit (all 150 neurons) which are distributed throughout the brain, and conceivably could monitor all neurons in the brain. (d) However, since the circadian clock is highly sensitive to light (Vinayak *et al.* 2013, Fogle *et al.* 2011), imaging methods run the risk of artificially stimulating clock-resetting signals. Further complications could follow due to generation of photobleaching processes by illumination during imaging: these degrade the fidelity of the circadian signals. Illumination could also inadvertently cause phototoxicity and so damage the normal function of the cells. To help overcome these concerns, I use objective-coupled planar illumination (OCPI) microscopy (Holekamp *et al.* 2008), which employs a light sheet to illuminate an entire focal plane simultaneously. The illumination by a light sheet can

avoid the emission and detection of light from out-of-focus tissue planes by optical sectioning. Optical sectioning can be achieved by other ways, such as laser scanning microscopy (like two-photon microscopy), which illuminates a single point in space at a time. However, the speed of laser scanning microscopy is limited because it requires serially scanning each excitation point (pixel) in the three-dimensional space. Each pixel requires a minimal dwell time ($10^{-6}$ s). In contrast, the light-sheet microscopy parallels the acquisition of the entire plane (2048 pixels X 2048 pixels), which can theoretically increase the speed by as much as six orders of magnitude. In addition, by the same factor, light-sheet microscopy can substantially reduce the amount of excitation light needed to achieve the same imaging speed and quality as the laser scanning microscope. Therefore, this method greatly accelerates volumetric imaging and reduces the amount of illumination and possible photobleaching.

Recent advances in imaging methods and data analysis permit acquisition of increasingly more detailed information regarding network phenomena. The circadian pacemaker system studied here is advantageous in that it produces activity spontaneously and rhythmically. Especially in *Drosophila*, the circadian system is smaller than that in mammals (~150 vs. ~20,000 neurons) but it still represents a highly interactive network. Importantly, within this network, pacemaker identities can be reliable recognized, genetically manipulated, and directly related to distinct phases of behavior, as I show in later Chapters.

**Focus of dissertation work**

The goal of the thesis is to understand two major questions: (i) how do circadian molecular clocks control the outputs of circadian pacemaker neurons, and (ii) how do the outputs of circadian pacemaker neurons control rhythms in different biological processes. I took the advantages of modern imaging techniques and developed an *in vivo* calcium imaging method to monitor brain-wide neural activity in living flies for 24 hours using light-sheet microscopy.

The first question, how molecular circadian clocks control the outputs of circadian pacemaker neurons is addressed in Chapter 2, Chapter 3, and Chapter 6. In Chapter 2, I used this imaging technique to measure the 24-hour neural activity patterns of *Drosophila* circadian pacemaker circuit. I found that different groups of circadian neurons show circadian rhythms in spontaneous neural activity with diverse phases. The neural activity phases are associated with their distinct behavioral outputs. In Chapter 3, combining the imaging platform with genetic and pharmacological manipulations, I asked how the diverse phases of neural activity are generated from the in-phase clock gene oscillations. I found that groups of circadian neurons inhibit each other via long-term neuromodulations, mediated by neuropeptides PDF and sNPF, such that their activity phases are staggered. Certain groups' activity phases are also regulated by external light inputs. Finally, in Chapter 6, I show that circadian neurons display circadian rhythms in both basal calcium levels and in fast calcium fluctuations. These two cellular rhythms may be generated by clock regulation of *IP3R* and T-type calcium channels, respectively.

The second question, how the outputs of circadian pacemaker neurons control rhythms in different biological processes is addressed in Chapter 4 and Chapter 5, by imaging the 24-hour neural activity patterns outside of the circadian pacemaker circuit. In Chapter 4, I identified an output pathway by which circadian neurons regulate the locomotor activity rhythm. Distinct

groups of circadian neurons independently regulate a common pre-motor center, the ellipsoid body ring neurons, through the agency of identified dopaminergic interneurons called PPM3-EB. In Chapter 5, I identified several output circuits downstream of circadian neurons, including different groups of dopaminergic neurons, and different groups of peptidergic neuroendocrine cells. Using methods including whole-brain pan-neuronal imaging, I showed that circadian neural activity rhythms propagate through these circuits to regulate different behavioral outputs including sleep, olfaction, mating, and feeding rhythms.

Therefore, by studying these two questions, my findings began to show how circadian clocks regulate diverse behavioral outputs. First circadian molecular clocks indirectly generate multi-phasic circadian rhythms of pacemakers' outputs; Second, the multi-phasic outputs from pacemakers independently regulate distinct biological processes by generating diverse circadian neural activity rhythms in different downstream output circuits.

# Chapter 2

# 24-hour neural activity patterns of *Drosophila* circadian neural circuit

This chapter is adapted from the following publication:

Liang, X., Holy, T. E., & Taghert, P. H. (2016). Synchronous *Drosophila* circadian pacemakers display nonsynchronous $Ca^{2+}$ rhythms in vivo. ***Science***, *351*(6276), 976-981.

**Abstract**:

In Drosophila, molecular clocks control circadian rhythmic behavior through a network of ~150 pacemaker neurons. To explain how the network's neuronal properties encode time, we performed brainwide calcium imaging of groups of pacemaker neurons in vivo for 24 hours. Pacemakers exhibited daily rhythmic changes in intracellular $Ca^{2+}$ that were entrained by environmental cues and timed by molecular clocks. However, these rhythms were not synchronous, as each group exhibited its own phase of activation. $Ca^{2+}$ rhythms displayed by pacemaker groups that were associated with the morning or evening locomotor activities occurred ~4 hours before their respective behaviors. Loss of the receptor for the neuropeptide PDF promoted synchrony of $Ca^{2+}$ waves. Thus, neuropeptide modulation is required to sequentially time outputs from a network of synchronous molecular pacemakers.

**Main Text:**

Circadian clocks help animals adapt their physiology and behavior to local time. The clocks require a highly-conserved set of genes and proteins (Lim and Allada 2013) operating through molecular feedback loops to generate robust rhythms that produce a 24-hour timing signal (Partch *et al.* 2014). These clocks are expressed by pacemaker neurons which themselves are assembled into an interactive network (Welsh *et al.* 2010). Through network encoding and cellular interactions, pacemaker neurons in the suprachiasmatic nucleus (SCN) of the mammalian brain coordinate many circadian rhythmic outputs (Freeman *et al.* 2013, Inagaki *et al.* 2007, Evans *et al.* 2013, Brancaccio *et al.* 2013). To study how molecular clocks couple to network encoding, and how network encoding relates to specific behavioral outputs, we conducted an *in vivo* brain-wide analysis of the circadian pacemaker network in *Drosophila* across an entire 24-hour day.

This network contains ~150 synchronized pacemaker neurons (Yoshii *et al.* 2009, Roberts *et al.* 2015) (Fig S1) yet it produces biphasic behavioral outputs - the morning and evening peaks of locomotor activity (Fig. 1A). The molecular clocks are entrained by environmental cues and by network interactions, for example by release of the neuropeptide pigment-dispersing factor (PDF) (Lin *et al.* 2004). Genetic mosaic studies indicate that morning and evening peaks of locomotor activity are controlled by distinct pacemaker groups (Stoleru *et al.* 2004, Grima *et al.* 2004, Yoshii *et al.* 2004, Zhang *et al.* 2010) (Fig. 1B). We reasoned that: (i) synchronous signals from the pacemaker network might diverge in downstream circuits or (ii) the pacemaker network might itself generate different timing signals to downstream circuits. To explore this, we developed an *in vivo* imaging assay to monitor the intracellular $Ca^{2+}$ concentration ($[Ca^{2+}]_i$), in pacemaker cell bodies over a ~24-hour period (Fig. 1C and methods). Intracellular $Ca^{2+}$

dynamics directly reflect amounts of neuronal activity and $Ca^{2+}$ imaging allows monitoring activity across neuronal ensembles (Chen *et al.* 2013).

We used objective-coupled planar illumination (OCPI) microscopy (Holekamp *et al.* 2008), which illuminates an entire focal plane simultaneously; this method accelerates volumetric imaging and reduces phototoxicity caused by repeated illumination. To permit imaging, we made cranial holes in the heads of living *tim > GCaMP6s* flies, which express the $Ca^{2+}$ sensor GCaMP6s in all pacemaker neurons (Chen *et al.* 2013)(Fig. 1C), and monitored $[Ca^{2+}]_i$ in five of the eight major pacemaker groups: small Lateral Neuron ventral (s-LNv), large Lateral Neuron ventral (l-LNv), Lateral Neuron dorsal (LNd), Dorsal Neuron 1 (DN1) and Dorsal Neuron 3 (DN3) (Fig. 1D). Each of the five groups displayed a prominent peak of $[Ca^{2+}]_i$ during the 24-hour recording sessions and each peak had distinct timing (Fig. 1E). To test whether these $Ca^{2+}$ dynamics reflected intrinsic circadian patterning, we began 24 hour recording sessions at different Zeitgeber times (ZT). In all such recordings, the peaks of $Ca^{2+}$ activity reflected the pacemaker group identity, not the time at which recordings began (Fig. S2). Thus, $Ca^{2+}$ varies in pacemaker neurons systematically as a function of the time of day based on biologically-defined rules of entrainment (Fig. 1F).Three *Drosophila* pacemaker groups (l-LNv, s-LNv and DN1p) show morning peaks of electrical activity when measured in acutely-dissected brains (Cao *et al.* 2008, 2013, Flourakis *et al.* 2015). Thus, the phases of $Ca^{2+}$ rhythms we observed are roughly coincident with, or slightly anticipate their peak electrical activity. $Ca^{2+}$ rhythms produced by different pacemaker groups were similar in amplitude (Fig. 1F), yet different in waveform (Fig. S3) and phase (Fig.1G). We confirmed our results using the FRET-based cameleon2.1 imaging method (Miyawaki *et al.* 1999), for which the ratio of fluorescence from the Yellow Fluorescence Protein to that of the Cyan Fluorescent protein reflects $[Ca^{2+}]_i$, independent of the

abundance of the sensor. $[Ca^{2+}]_i$ estimated by this assay exhibited ~2-fold circadian variation with temporal patterns consistent with those obtained with GCaMP6s (Fig. S4). These observations demonstrate that the *Drosophila* pacemaker network exhibits stereotyped and diverse spatiotemporal patterns of $Ca^{2+}$ activity during the course of the 24-hour day.

We compared this diversity of $Ca^{2+}$ activity patterns with the diversity of pacemaker functions. Pacemaker functions have been revealed by genetic mosaic experiments, as exemplified by the categorization of M (morning) and E (evening) cells (Stoleru *et al.* 2004, Grima *et al.* 2004, Yoshii *et al.* 2004, Zhang *et al.* 2010). These autonomous oscillators primarily drive the morning and evening peaks of locomotor activity, respectively. The phase relationships ($\Psi_{M/E}$) between the peaks of $Ca^{2+}$ rhythms in canonical M (s-LNv) and E (LNd) cells and the two daily peaks of locomotor activity were highly correlated (Fig 1H-J). In M cells, the $Ca^{2+}$ rhythm peaked towards the end of the subjective night, whereas in E cells it peaked towards the end of the subjective day (Fig. 1F). The ~10-hour phase difference between $Ca^{2+}$ rhythms in M and E pacemakers is similar to the ~10 hour phase difference between the morning and evening behavioral peaks (Fig. 1J). Thus, M and E pacemaker $Ca^{2+}$ activations precede by ~4 hours the behavioral outputs they control. The distinct phases of $Ca^{2+}$ rhythms in the other three pacemaker groups (l-LNv, DN1 and DN3) may also involve the morning and evening behavioral peaks, or may regulate other, distinct circadian-gated outputs.

The E category of pacemakers includes the LNd as well as the $5^{th}$ s-LNv (Stoleru *et al.* 2004, Grima *et al.* 2004, Yoshii *et al.* 2004, Zhang *et al.* 2010). However, the LNd is a heterogeneous group of neurons that exhibits diverse entrainment properties (Yao and Shafer 2014); likewise, the critical $5^{th}$ s-LNv could not be unambiguously identified with *tim*-GAL4. To better understand the function of these subsets of E pacemakers, we used a PDF receptor (*pdfr)*(B)

GAL4 driver (Im and Taghert 2010); this driver restricts GCaMP6s expression to s-LNv, to three of six LNd and to the single 5$^{th}$ s-LNv (Fig. 2A). The three PDFR-expressing LNd and the 5$^{th}$ s-LNv displayed the same basic E cell pattern of $Ca^{2+}$ activity – a peak in late subjective day, suggesting they both function as circadian pacemakers (Fig. 2B). Thus, the phase difference between $Ca^{2+}$ rhythms in these PDFR-expressing M and E cell groups again matched that between the morning and evening behavioral activity peaks (Fig. 2, C through F).

M and E cell categorization supports a classic model of seasonal adaptation (Pittendrigh and Daan 1976) wherein a two-oscillator system responds differentially to light, and so can track dawn and dusk independently. For example, under long-day conditions, light accelerates a "morning" clock and decelerates an "evening" clock. If these $Ca^{2+}$ rhythms are critical output features of M and E cells, their properties may also reflect differences in photoperiodic entrainment. We entrained flies under either long-day (16 hour light: 8 hour dark) or short-day (8 hour light: 16 hour dark) conditions. In these flies, the phase difference between the morning and evening behavioral activity peaks tracked dawn and dusk (Fig S6). Likewise, the phases of pacemaker $Ca^{2+}$ rhythms were also tracked dawn and dusk (Fig. 3, A and B, E and F, and Fig. S7). Regardless of the photoperiodic schedule, the s-LNv (M cells) always peaked around dawn, while the LNd (E cells) always peaked before dusk (Fig. 3, B through D and F through H). Thus, $Ca^{2+}$ activity patterns within the pacemaker network correspond to the circadian temporal landmarks of dawn and dusk.

We tested whether changes in the molecular oscillator would alter the patterns of $[Ca^{2+}]_i$. We used different alleles of the gene *period*, which encodes a state variable of the *Drosophila* circadian clock. In $per^{01}$ (null) mutant flies, which lack inherent rhythmicity in their molecular oscillators and in free-running behavior (Konopka and Benzer 1971, Hardin *et al.* 1990) (Fig.

S8), all clock neurons showed reduced rhythmicity in $[Ca^{2+}]_i$. The amplitudes of $Ca^{2+}$ fluctuations were reduced by half (Fig. 3, I and K) and coherence was lost within groups (Rayleigh test, p>0.5; Fig. 3J and Table S1). In fast-running $per^S$ mutant flies, which have ~19 h free-running period (Konopka and Benzer 1971, Hardin *et al.* 1990) (Fig. S9), the $Ca^{2+}$ rhythms were phase-shifted (Fig. 3, L and M, and Fig. S10) consonant with the direction of behavioral phase shifts (Fig. 3N and Fig. S9). The phase difference between $Ca^{2+}$ rhythm peaks in $per^S$ M and E pacemakers still matched the phase difference between M and E behavioral peaks (Fig 3, N and O). Thus, molecular clocks determine the pace of $Ca^{2+}$ rhythms in the pacemaker network.

To explore how synchronous molecular clocks can have staggered phases of $Ca^{2+}$ activation by many hours, we tested whether PDF, which mediates interactions between pacemakers, was required. Flies bearing the severely hypomorphic $han^{5304}$ mutation of the PDF receptor show unimodal or arrhythmic behavior patterns under DD (Hyun *et al.* 2005) (Fig. S11 and Table S2). In these flies, we found that the $Ca^{2+}$ rhythms in M cells (s-LNv and DN1) were unaffected, but they were phase-shifted in LNd and DN3, such that these two groups now produced $Ca^{2+}$ rhythms around dawn, roughly in synchrony with M cells (Fig. 4, A and B). The phase of l-LNv did not change, consistent with the absence of PDF sensitivity by this pacemaker group (Shafer *et al.* 2008). The phase shifts in LNd and DN3 were fully restored by the expression of complete *pdfr* from a BAC transgene (Fig. 4, C through E "rescue 1", and Fig. S11). Thus PDF, which promotes synchronization of molecular clocks under constant conditions (Lin *et al.* 2004, Yoshii *et al.* 2009), is also needed to properly stagger their $Ca^{2+}$ activity phases across the day. Whether the phases of the l-LNv and DN3 are set by other intercellular signals remains to be determined.

We further examined the *pdfr* mutant phenotype at higher cellular resolution (*pdfr(B)>GCaMP6s*; Fig. 2A). The PDFR-expressing E cell groups (the 3 PDFR-expressing LNd and the

5th s-LNv) displayed phase shifts similar to those of the entire LNd group (Fig. 4, F and G). When *pdfr* expression was restored just in these subsets of pacemaker neurons (with GAL4-UAS), both behavior and $Ca^{2+}$ rhythms were partially restored (Fig. 4, H through J, "rescue 2", Fig. S11, and Table S2). The phase of the 5th s-LNv was fully restored, suggesting PDFR signaling is required for cell-autonomously setting of $Ca^{2+}$ phase in this pacemaker group. However, in "rescue 2", a single LNd remained typically active around dawn whereas two LNd were active around dusk (Fig. S12), which indicates either a partial restoration or a non-autonomous phase-setting mechanism for LNd.

Our results suggest that molecular clocks drive circadian rhythms in the neural activity of pacemakers.. Temporally patterned neural activity encodes different temporal landmarks of the day in a manner that reflects the different functions of the pacemaker groups. The homogeneous molecular clock produces staggered activity peaks by a mechanism dependent upon PDFR signaling. By generating diverse phases of neural activity in different pacemaker groups, the circadian clock greatly expands its functional output.

**Materials and Methods:**

Fly rearing, fly stocks and molecular biology

All flies were reared at 23°C on standard food medium. Male adult flies were then entrained at 25°C for 3 to 5 days under 12 hour light:12 hour dark standard conditions, 16 hour light:8 hour dark long-day conditions, or 8 hour light:16 hour dark short-day conditions). The *tim>GCaMPS6s*, *mCherry*; $cry^{01}$ flies were entrained for more than 6 days as were flies entrained under different photoperiods. In order to begin 24 hour recording sessions systematically at different Zeitgeber times (ZT) and to avoid the influence of any unknown temporal factor in the ambient recording environment, two groups of flies were entrained separately in two separate incubators with an 8 hour phase difference in their LD cycles.

All *gal4* and UAS lines used in this study have been described previously: *tim(UAS)-gal4*(Blau and Young 1999), *pdfr(B)-gal4*(Im and Taghert 2010), *UAS-GCaMP6s*(Chen *et al.* 2013), *UAS-mCherry.NLS*(Caussinus *et al.* 2008), *UAS-cameleon2.1*(Miyawaki *et al.* 1999, Fiala and Spall 2003), and *UAS-pdfr-16* (Mertens *et al.* 2005), and also the BAC-recombineered *pdfr-myc* transgene line (Im and Taghert 2010). All mutant lines have also been described previously: $cry^{01}$ (Dolezelova *et al.* 2007), $per^{01}$ and $per^{S}$ (Konopka and Benzer 1971), and $pdfr^{han5403}$ (Hyun *et al.* 2005).

We confirmed the genotype of the *tim>GCaMP6s,mCherry;* $cry^{01}$ flies by single-fly PCR using the following primers: (1) 5' flanking region: 5'- TAAACCGCTTGGAGCTTCGT-3' and 5'-GAAAGGCAAACGAAGCCAGG-3'; (2) 3' flanking region: 5'-GAAAGGCAAACGAAGCCAGG-3' and 5'-GAAAGGCAACGAAGCCAGG-3'; (3) *cry* coding region as a negative control to prove it was homozygous: 5'-

AAGCCGAACGAAAATCTCCT-3' and 5'-TGGTTGCTTGAGATTGTTGAA-3' The sequence of 5' flanking region PCR product is available upon request.

*In vivo* preparations

Each fly was anesthetized by $CO_2$. The neck of the fly was inserted into a narrow cut on an aluminum foil. Thus, the foil separated the head from the thorax. Only the head was immersed in ice-cold calcium-free fly saline (46 mM NaCl, 5 mM KCl, and 10 mM Tris (pH 7.2)), leaving the other part of the body dry. One hemisphere of the fly brain was then exposed by partial removal of the head capsule and sometime part of the compound eye, if necessary. After this surgery, fly saline was replaced by room temperature haemolymph-like saline (HL3), containing 70 mM NaCl, 5 mM KCl, 1.5 mM CaCl2, 20 mM MgCl2, 10 mM $NaHCO_3$, 5 mM trehalose, 115 mM sucrose, and 5 mM HEPES (pH 7.1)(Stewart *et al.* 1994). During imaging, fresh HL3 saline was perfused continuously (0.1-0.2 mL/min).

GCaMP-based calcium imaging

Imaging was performed on a custom Objective Coupled Planar Illumination microscope (Holekamp *et al.* 2008). This microscope had the following features. The illumination was performed by a ~5µm thick light sheet. The light sheet was generated from a 488nm laser that went through an optical fiber, a light collimator and light sheet–forming cylindrical lens. The light sheet was set to the focal plane of the microscope objective. The objective was a water-immersion 0.5NA 20× (Olympus). Images were captured on an iXon DV885-KCS-VP cooled EM-CCD (Andor). Images were acquired by scanning the light sheet across the fly brain through

the cranial window. For 24-hour recordings, stacks were acquired every 10min and the total scanning time for each image stack was less than 3s.

Cameleon-based calcium imaging

At certain zeitgeber times, living brains expressing Gal4-driven cameleon2.1 were dissected in ice-cold calcium-free fly saline and placed at the bottom of a poly-l-lysine-coated 35*10 mm plastic FALCON Petri dish (Becton Dickenson Labware), incubated in HL3. Epifluorescent FRET imaging was performed through a LUMPL 606/1.10 water objective with immersion cone and correction collar (Olympus) on an Olympus BX61 microscope. Excitation and emission filter wheels were driven by a Lambda 10-3 optical filter changer and shutter control system (Sutter Instrument Company) and controlled with SLIDEBOOK 4.1 software (Intelligent Imaging Innovations). Images were captured on a Hamamatsu Orca ER cooled CCD camera (Hamamatsu Photonics). FRET imaging was performed on individual cell bodies. YFP-FRET and CFP donor images were captured sequentially at each time point. Exposure times were 20 ms for YFP- FRET and 500 ms for CFP donor, as these were the shortest exposure times that allowed for clear images and yielded approximately equal ranges of values for YFP-FRET and CFP-donor emissions (Fiala and Spall 2003). For each cell, 12 images were captured with 10s interval. For different cells, images were captured sequentially by moving stage in X, Y, and Z dimensions using a Prior H101Plan Power Stage.

Imaging data analysis

For GCaMP-based calcium imaging, images were acquired by custom software Image 2.0 and were processed in MATLAB R2014b (MathWorks, Natick, MA, USA) using custom

software described previously (Turaga and Holy 2012), and ImageJ-based Fiji (Schindelin *et al.* 2012). After registration of images (StackReg plugin in Fiji) (Thévenaz *et al.* 1998), regions of interest (ROIs) were manually selected over individual cells or groups of cells. An ROI was defined as a subtype of clock neurons based on anatomical location. Average intensities of ROIs were measured through the time course. For each time point, the average intensity of ROI was divided by average of the whole image to subtract background noise. For each time trace, intensity (F) throughout the time course were subtracted by the minimal intensity ($dF=F-F_{min}$) and then divided by the mean intensity (dF/F). These time traces were then compared based on different features. To show $Ca^{2+}$ level in certain pacemaker groups as a function of circadian time, intensity traces of certain cell type ROIs were firstly aligned based on Zeitgeber Time and averaged across different animals.

For waveform comparison, intensity traces of certain cell type ROIs were firstly linearly normalized into 0-100 ranges, shifted for maximal correlation, and averaged across different animals. For phase comparison, all normalized traces were pooled, paired, and analyzed through a cross-correlation analysis. The lag for maximum across-correlation was regarded as the phase difference between two traces. By registering the average peak time for traces from each cell type, phases of all traces were plotted on a 24-hour-clock circular plot reflecting both peak time and phase relationship of traces. This phase relationship was then tested statistically by Rayleigh test of uniformity and Watson-Williams test for homogeneity of means (Levine *et al.* 2002). Intensity trace analysis and statistics were performed using R 3.1.2 and Prism 6 (GraphPad, San Diego CA).

For cameleon-based calcium imaging, the intensity of ROIs was measured in SLIDEBOOK 4.1 software (Intelligent Imaging Innovations). The ratio of YFP/CFP for each cell was the

average of 12 images. The ratio values of certain cell types at two Zeitgeber Times (ZT6 and ZT18) were compared by Mann-Whitney test. For each Zeitgeber Time point, the ratio values of certain cell types were collected from at least 30 cells that were found in at least 10 brains. To estimate intracellular $Ca^{2+}$ concentration, the ratio was reduced to minimal level (0.91 ± 0.013) by chelation of $Ca^{2+}$ with EGTA (20 mM) and BAPTA-AM (30 μM). The ratio was elevated to maximal level (1.41 ±0.016) by the high $Ca^{2+}$ HL3 (20 mM) with $Ca^{2+}$ ionophore (10 μM ionomycin). The calcium concentration was estimated based on the Hill coefficient and the $K_d$ of cameleon2.1 (1.0 and 100 nM, respectively)(Enoki *et al.* 2012). Data were analyzed in Excel 2013 (Microsoft, Redmond, WA) and Prism 6 (GraphPad, San Diego CA).

Locomotor activity

After eclosion, male flies were entrained at 25°C for 4-6 days under different conditions (standard, long-day, or short-day conditions). The locomotor activity of individual flies was monitored using Trikinetics Activity Monitors for 6 days under light-dark condition and then for another 9 days under constant darkness (DD) condition, or constant light (LL) condition for $cry^{01}$ mutants. The DD1 actograms were plotted on Zeitgeber Time scale (instead of circadian time scale) for better comparison with 24-h $Ca^{2+}$ imaging. To find the phases of morning and evening peaks, DD1 activity profiles of individual animals were smoothed through moving averages of five 30-min bins. The time of the midday ‘‘siesta’’ was manually selected. The morning and evening peaks were then determined by the maximum activities before and after the midday ‘‘siesta’’. Data were analyzed in R 3.1.2. For Table S2, flies were entrained to 12:12 hr LD cycles for 6 days and then released into DD or LL for 9 days. To estimate rhythmicity and period, locomotor activity from DD Days 1–9 was then normalized for a $\chi^2$ periodogram with a

95% confidence cutoff and SNR analysis (Levine *et al.* 2002). Arrhythmic flies were defined by having a power value less than 10 and width lower than 1, or if having a period less than 18 or more than 30 hr.

Immunocytochemistry

The flies were entrained for 6 days under 12-hour light:12-hour dark standard conditions, then underwent *in vivo* GCaMP-based calcium imaging for 6 hour: from (i) ZT12 to ZT18, or from (ii) ZT18 to ZT24. Immediately after imaging, fly brains were dissected in $Ca^{2+}$-free fly saline and fixed for 15 min at room temperature in 4% paraformaldehyde and 7% picric acid in phosphate buffered saline (PBS). After washes with PBS and PBS-Tx (0.3% Triton X-100), the brains were blocked in 3% normal goat serum in PBS-TX for 1 hr at room temperature. The brains were then incubated in 1:5000 diluted Rabbit anti-PER primary antibodies (Stanewsky *et al.* 1997) for 24 hour at 4°C and 1:1000 diluted secondary antibodies for 2 hour at room temperature. Secondary antibodies were conjugated to Alexa 633. After washes with PBS-Tx and PBS, the brains were dehydrated in 70% glycerol and mounted on slides with Vectashield HardSet Mounting Medium (Vector Laboratories, Burlingame, CA, USA). All images were acquired on the Nikon A1Rsi+ Confocal microscope with the same imaging settings. PER immunostaining intensity was quantified in ImageJ-based Fiji (Schindelin *et al.* 2012).

**Supplementary Text**

**Spontaneous $Ca^{2+}$ activity patterns are CRY-independent**

In *Drosophila*, the photoreceptor CRYPTOCHROME (CRY) is critical for circadian photoreception (Emery *et al.* 1998, Stanewsky *et al.* 1998): it is expressed in most pacemaker groups (Yoshii *et al.* 2008) and can provoke rapid membrane depolarization in response to light (Fogle *et al.* 2011). Because CRY and the GCaMP6s calcium indicator are activated by similar wavelengths, we tested whether CRY-mediated light responses contributed to the $Ca^{2+}$ rhythms we measured. $Ca^{2+}$ rhythms in $cry^{01}$ (null) flies displayed patterns similar to those of control flies (Fig. S5, A through C, and G), showing a strong correlation with daily behavior patterns (Fig. S5, D through F). We conclude that light stimulation of CRY does not measurably affect the patterns of $Ca^{2+}$ activity in pacemaker neurons.

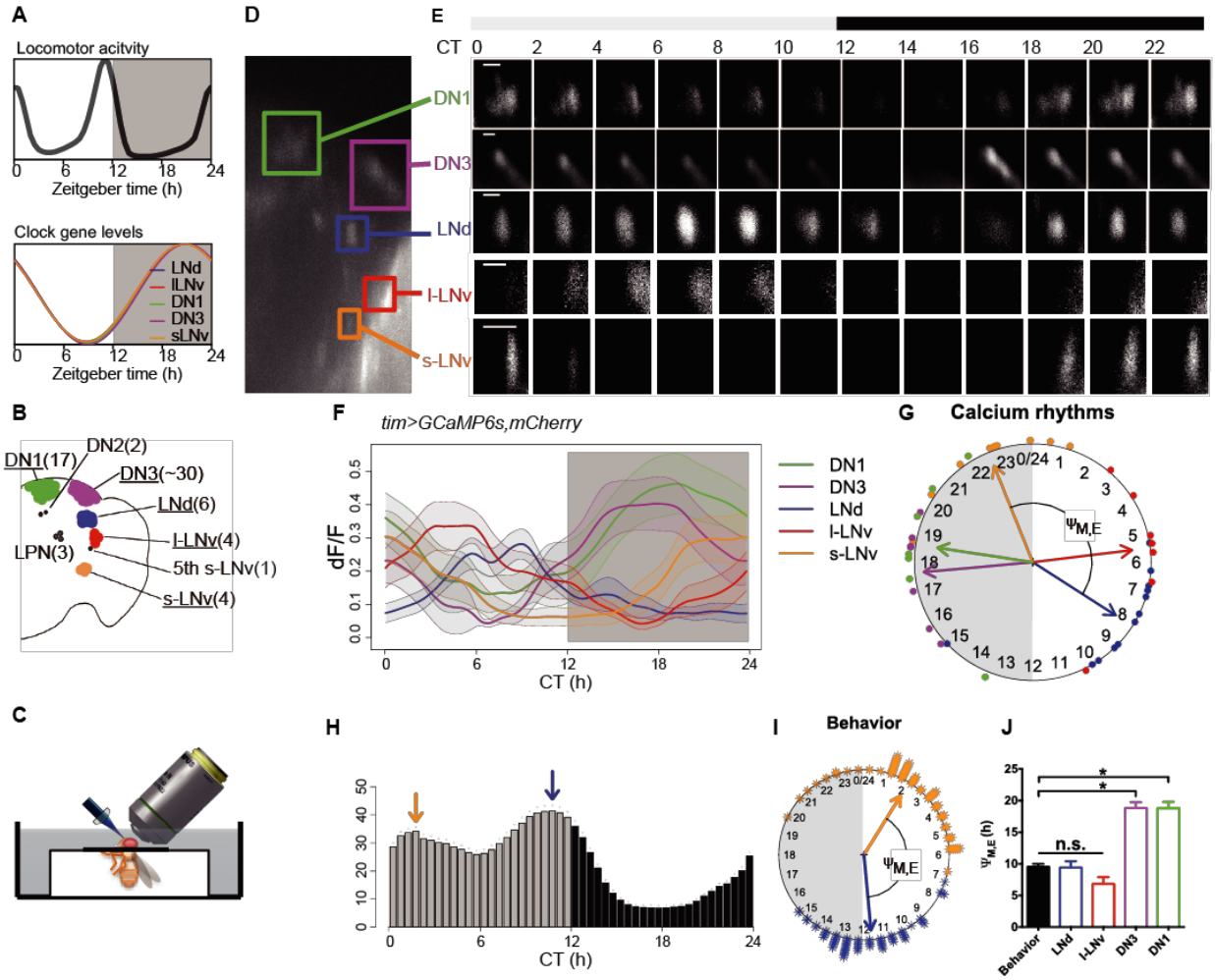


**Fig.1. $Ca^{2+}$ activity patterns in circadian pacemaker neurons *in vivo*. (A)** Schematic representation of synchronous, unimodal molecular clocks that drive bimodal behavioral rhythms. **(B)** Map of the eight major clock pacemaker groups in the fly brain. **(C)** Schematic to illustrate method for long-term *in vivo* imaging; the head is immersed in saline while the body remains in an air-filled enclosure (see Methods for details). **(D)** A representative image of *tim>GCaMP6s* signals showing the locations of five identifiable pacemaker groups. **(E)** Representative images showing 24-h $Ca^{2+}$ activity patterns of five identifiable groups. **(F)** Average $Ca^{2+}$ transients in the five pacemaker groups as a function of Circadian Time (n=13 flies). Gray aspect indicates the period of lights-off during the preceding six days of 12hour:12hour photoentrainment. **(G)** Phase distributions of 24-hour $Ca^{2+}$ transients in different pacemaker groups (data from F). Each colored dot outside of the clockface represents the calculated peak phase of one group in one fly as described in Methods. Colored arrows are mean vectors for the different clock neuron groups. The arrow magnitude describes the phase coherence of $Ca^{2+}$ transients in a specific pacemaker group among different flies (n=13, not all 5 groups were visible in each fly due to the size of the cranial windows – see Table S1). $\Psi_{M,E}$ is the phase difference between M cells (s-LNv) and E cells (LNd). **(H)** The average activity

histogram of *tim>GCaMP6s,mCherry.NLS* flies in the first day under constant darkness (DD1). Arrows indicate behavioral peak phases (orange: morning, blue: evening). Dots indicate SEM (n=47 flies). **(I)** Phase distributions of behavioral peaks indicated by arrows in (H) (asterisks: peak phases of individual flies; orange: morning, blue: evening). $\Psi_{M, E}$ is the phase difference between morning and evening behavioral peaks. **(J)** Phase difference from M cells (s-LNv) to other pacemaker groups compared to behavioral $\Psi_{M, E}$. n.s. = not significant; "*" denotes significantly different groups ($P < 0.05$) by ANOVA followed by post hoc Tukey tests. $\Psi_{M,LNd}$ matched behavioral $\Psi_{M, E}$ (t-test, p=0.91; f-test, p=0.65). Error bars denote SEM.

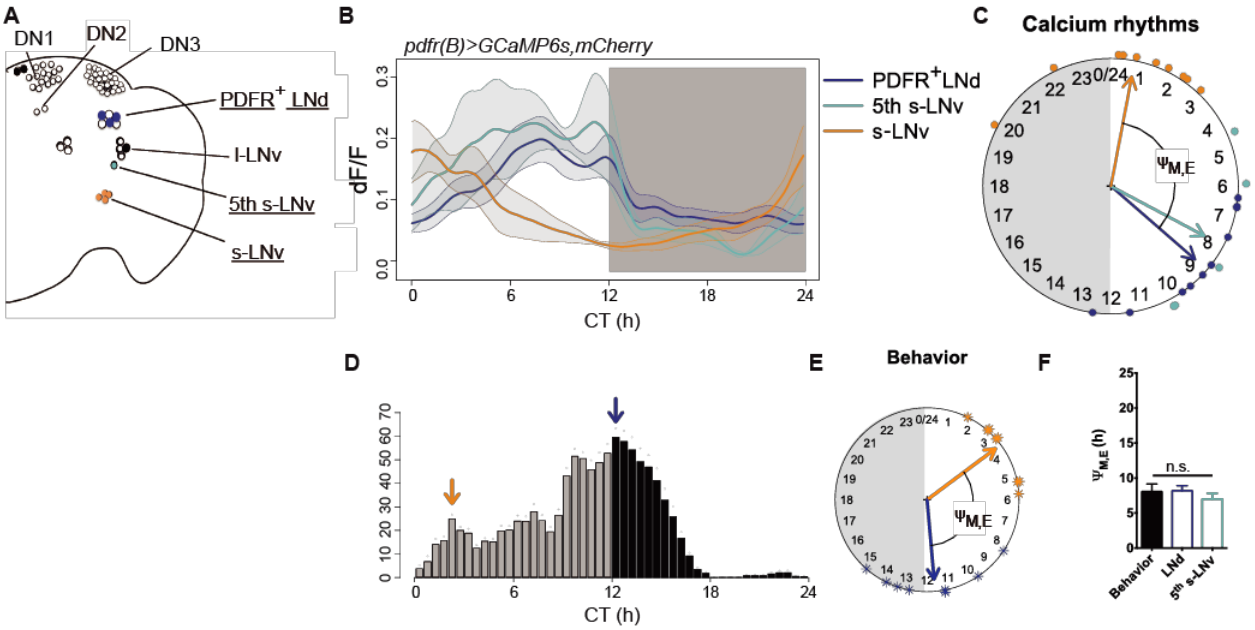


**Fig.2. $Ca^{2+}$ rhythms can be resolved within individual components of the E pacemaker groups.**(**A**) Schematic of PDFR-expressing clock neurons. Neuronal groups and subgroups driven by *pdfr(B)-gal4* are filled and color-coded; those imaged for GCaMP6s signals are underlined. (**B** to **F**) As in Fig. 1, F to J: (B) $Ca^{2+}$ transients in three PDFR+ clock neuron groups and subgroups (n = 10 flies). Activities in the three PDFR+ LNds and in the single fifth s-LNv are similar (Pearson's r = 0.89). (C) $Ca^{2+}$ rhythm phases from (B). (D) The DD1 locomotor activity of *pdfr(B)>GCaMP6s, mCherry.NLS* flies (n = 8). (E) The phases of behavioral peaks from (D). (F) Phase differences from M cells (s-LNv) to both LNd and the fifth s-LNv matched behavioral $\Psi_{M,E}$ (ANOVA, P = 0.7239).

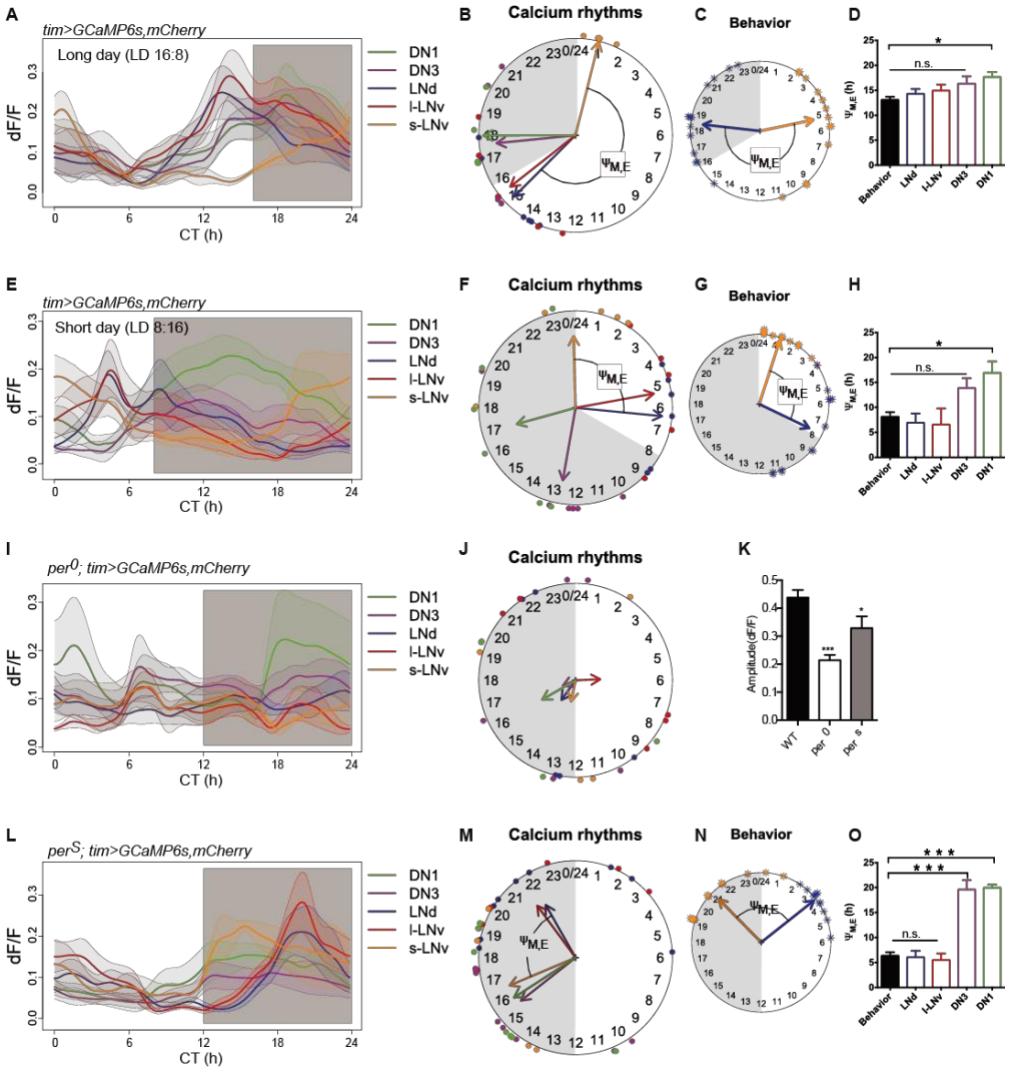


**Fig.3. Effects of environmental information and molecular clocks on the spatiotemporal patterns of $Ca^{2+}$ activity in the pacemaker network. (A** and **E)** $Ca^{2+}$ transients: (A) under long (16:8 LD) photoperiod (n=6 flies) and (E) under short (8:16 LD) photoperiod (n=6 flies). **(B** and **F)** $Ca^{2+}$ rhythm phases (B) under long photoperiod and (F) under short photoperiod. The shaded circular sectors indicate the 8 hours (B) and 16 hours (F) lights-out periods. Note that M cells (s-LNv, orange) peaked around lights-on and E cells (LNd, blue) peaked before lights-off regardless of photoperiod. **(C** and **G)** The phases of behavioral peaks in DD1 after 6 days of photoperiodic entrainment: (C) long photoperiod (n=13 flies) and (G) short photoperiod (n=12 flies). (See Fig S5 for more details). **(D** and **H)** $\Psi_{M,LNd}$ matches behavioral $\Psi_{M,E}$ under long photoperiod (t-test, p=0.32; f-test, p=0.88) and under short photoperiod (t-test, p=0.30; f-test, p=0.16). **(I)** Arrhythmic $Ca^{2+}$ transients in *per*$^{01}$ mutants (n=5 flies). **(J)** Phase coherence of $Ca^{2+}$ transients was poor among *per*$^{01}$ flies. **(K)** Amplitude of $Ca^{2+}$ transients (maximum dF/F) was significantly smaller in *per*$^{01}$ and in *per*$^{S}$ mutants (vs. control flies, Mann-Whitney test, *p<0.1, ***p<0.001). **(L)** $Ca^{2+}$ transients in *per*$^{S}$ mutants (n=6 flies). **(M)** $Ca^{2+}$ rhythm phases of *per*$^{S}$ mutants. **(N)** Phases of behavioral peaks corresponding to $Ca^{2+}$ rhythm phases in panel (M) (n=16 flies). **(O)** $\Psi_{M,LNd}$ matched behavioral $\Psi_{M,E}$ (t-test, p=0.83; f-test, p=0.13).

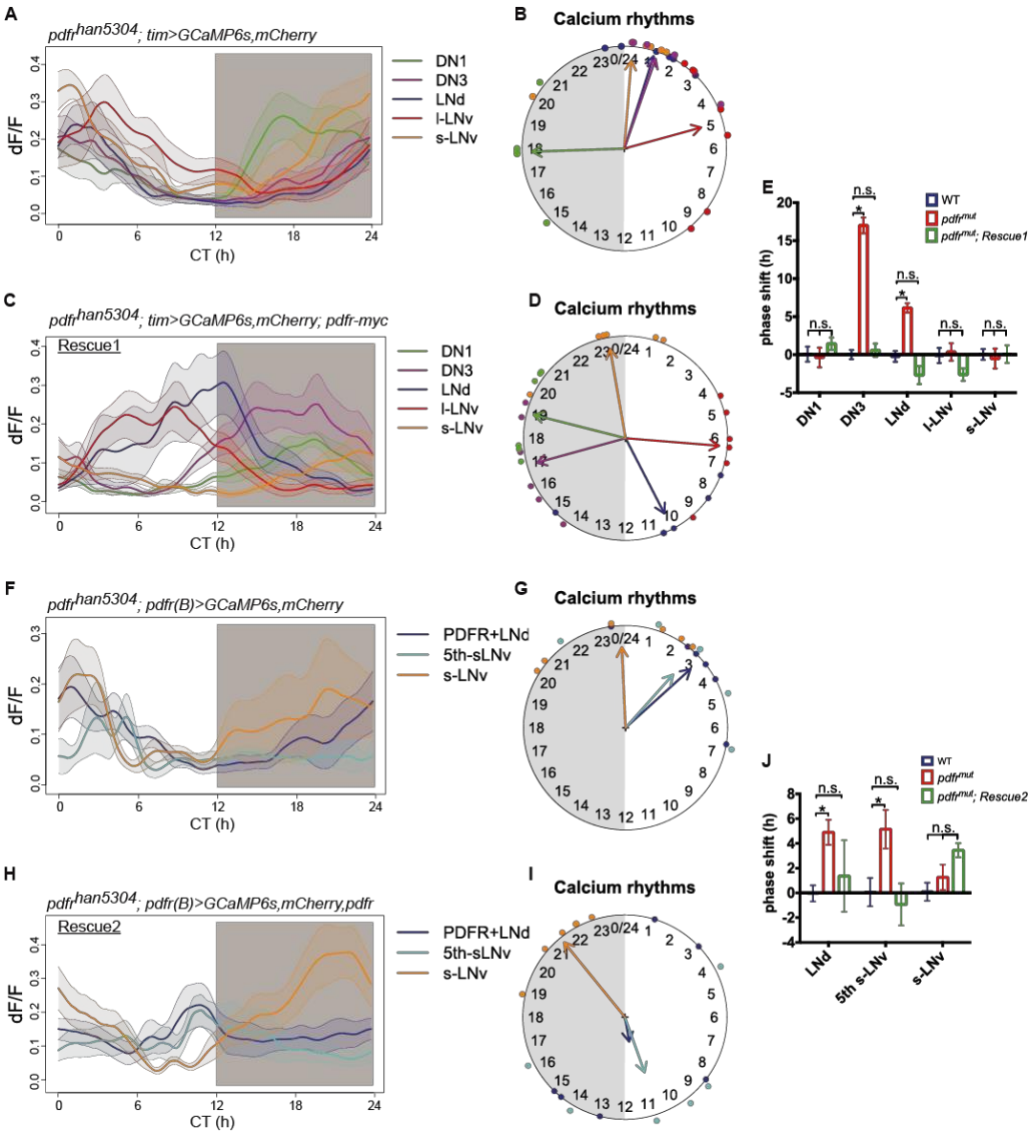


**Fig.4. Requirement of PDFR signaling for staggered waves of $Ca^{2+}$ transients among the pacemaker groups. (A)** $Ca^{2+}$ transients in five pacemaker groups in *pdfr*$^{han5304}$ mutants (n=7 flies). **(B)** $Ca^{2+}$ rhythm phases from panel (A): LNd and DN3 were phase-shifted towards s-LNv**. (C)** $Ca^{2+}$ transients in *pdfr* mutant flies that are restored by a large BAC-recombineered *pdfr-myc* transgene (Rescue 1, n=6 flies). **(D)** $Ca^{2+}$ rhythm phases from panel (C). **(E)** The phase shifts in mutants were fully rescued by restoring PDFR (two-way ANOVA followed by a Bonferroni post-hoc test, *p<0.001). Colors in this panel indicate genotype. **(F)** $Ca^{2+}$ transients in three pacemaker groups targeted by *pdfr(B)-gal4* in *pdfr*$^{han5304}$ mutants (n=6 flies). **(G)** $Ca^{2+}$ rhythm phases from (F). **(H)** $Ca^{2+}$ transients in *pdfr* mutant flies that are restored by *pdfr(B)-gal4>pdfr* (Rescue 2, n=6 flies). **(I)** $Ca^{2+}$ rhythm phases from (H): the PDFR+ LNd and the single 5$^{th}$ s-LNv display restored phases, but lack strong phase coherence (Rayleigh test, p>0.1) (also see Fig. S12). **(J)** Phase shifts in mutant flies were partially restored by restoring *pdfr* in subsets of $PDFR^{+}$ cells (two-way ANOVA followed by a Bonferroni post-hoc test, *p<0.001). Colors in this panel indicate genotype.

Fig S1

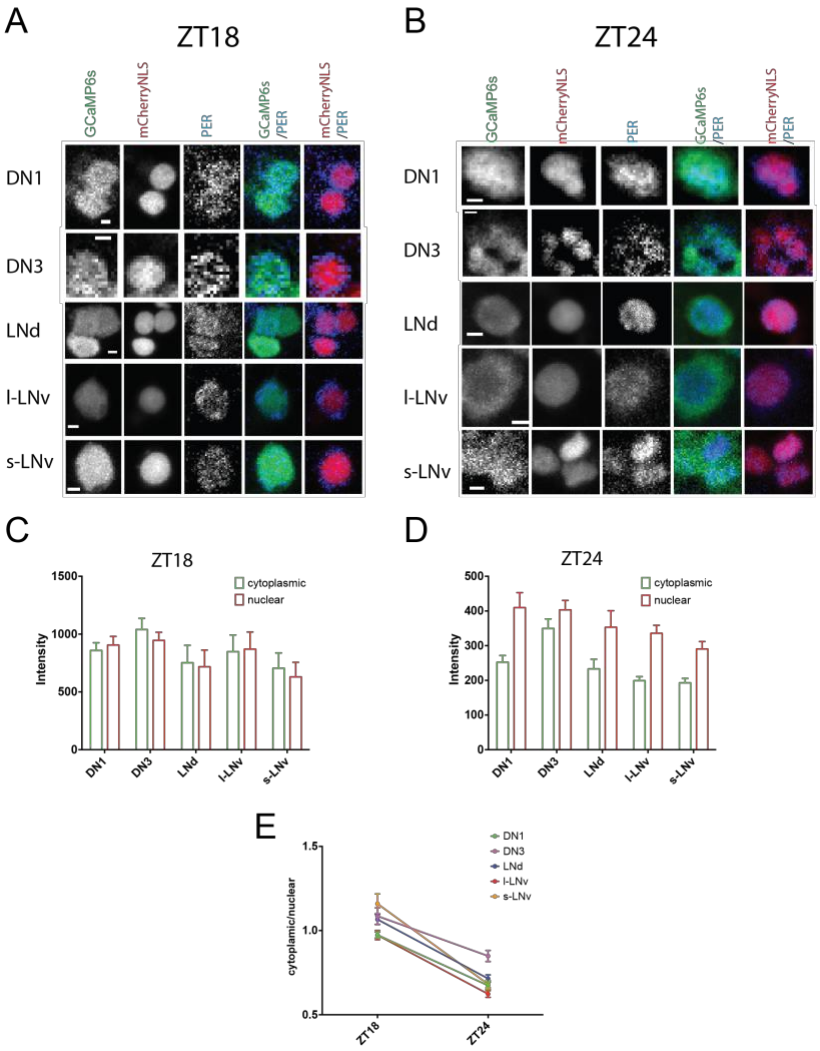


Fig. S1.

**The molecular clocks are synchronous among the different pacemaker groups in vivo during lightsheet-based $Ca^{2+}$ imaging.** Imaging was performed during the dark phase of a 12:12 LD cycle. **(A** and **B)** Immunostaining of PER protein in *tim>GCaMP6s, mCherryNLS* flies, following 6 hr of $Ca^{2+}$imaging: (**A**) starting at ZT12 and ending at ZT18, or (**B**) starting at ZT18 and ending at ZT24. In all five main pacemaker groups, at ZT18 (A), PER accumulated in the cytoplasm, while at ZT24 (**B**) PER was primarily located within nuclei. **(C** and **D)** Quantification of cytoplasmic and nuclear PER staining in (A and B). The cytoplasmic region of each neuron was identified by GCaMP6s signal. The nuclear region of each neuron was identified by mCherryNLS signal. **(E)** The ratio of cytoplasmic over nuclear PER intensity decreased from ZT18 to ZT24 in all five pacemaker groups. Scale bars, 2 µm

Fig S2

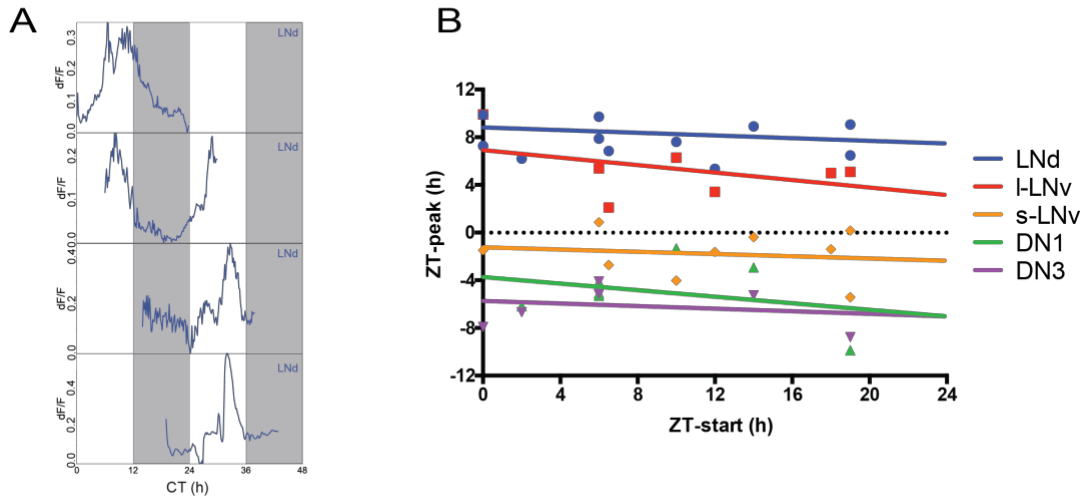


Fig. S2

**The phases of $Ca^{2+}$ signal peaks are independent of recording start times. (A)** Four representative examples of 24-h $Ca^{2+}$ activity traces of the identifiable LNd pacemaker group: recordings were started at different times of day but all examples produced the highest $Ca^{2+}$ signals around the same time of day. **(B)** Plot of the Zeitgeber Time when each trial started vs. the Zeitgeber Time when $Ca^{2+}$ signals peaked in each pacemaker group. Linear regressions suggest no correlation. (LNd: slope= -0.05631 ± 0.1209, $p_{slope\neq0}$= 0.6515, $R^2$= 0.02122, n=12; l-LNv: slope=-0.1567 ± 0.1455, $p_{slope\neq0}$= 0.3307, $R^2$= 0.1883, n=7; s-LNv: slope=-0.04688 ± 0.1132; $p_{slope\neq0}$= 0.6911, $R^2$= 0.02393, n=9; DN1: slope=-0.1374 ± 0.1989, $p_{slope\neq0}$= 0.5204, $R^2$= 0.08713, n=7; DN3: slope -0.05417 ± 0.1119, $p_{slope\neq0}$= 0.6487, $R^2$= 0.0448, n=7). The genotype of these flies was *yw; tim> GCaMP6s, mCherry-NLS*.

Fig S3

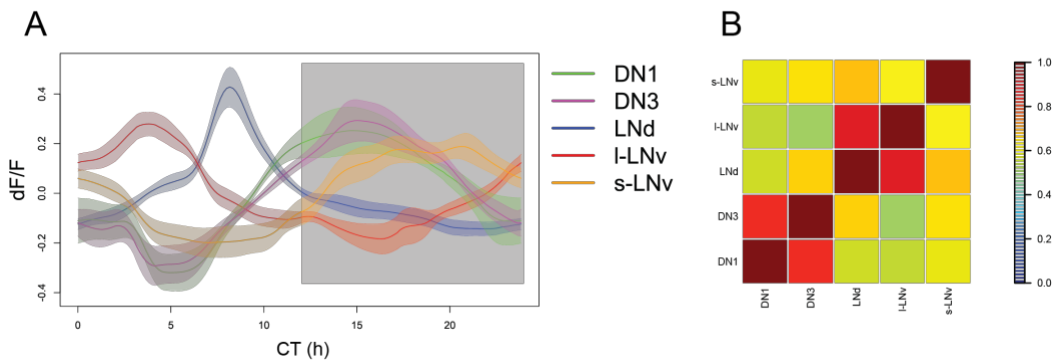


Fig. S3

**Different pacemaker groups have distinct $Ca^{2+}$ rhythm waveforms. (A)** Average $Ca^{2+}$ transients of normalized traces aligned by maximum correlation (the same data as Figure 2A, see methods). **(B)** Average of maximum lagged cross-correlation coefficient between different pacemaker groups. The shapes of the different waveforms are most similar between l-LNv and LNd, and between DN1 and DN3. The genotype of the flies was *tim> GCaMP6s, mCherry-NLS*.

Fig S4

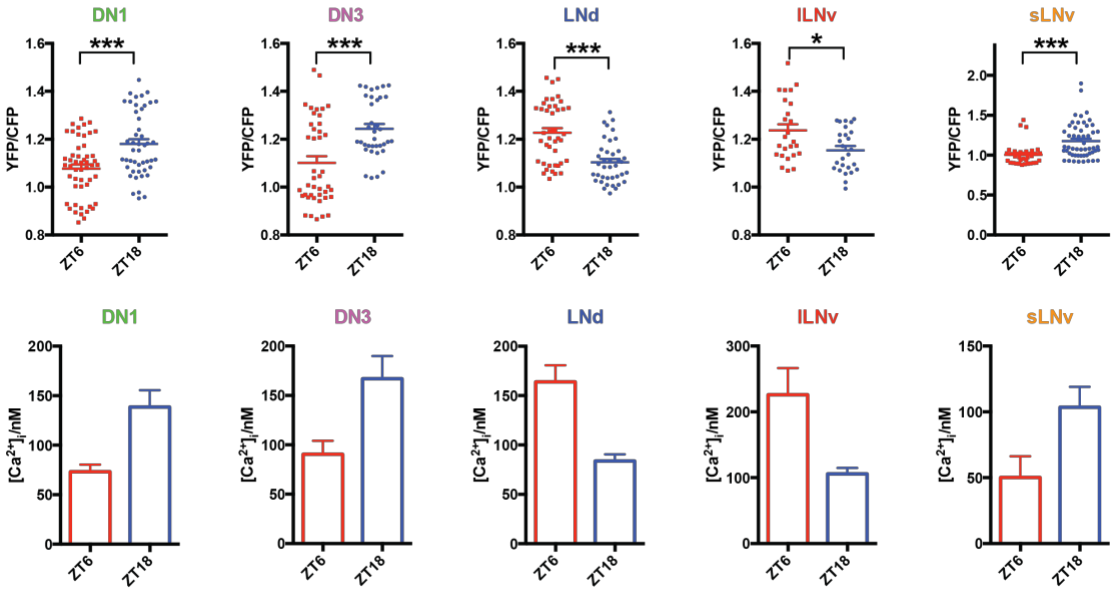


Fig. S4

**Spatiotemporal patterns of $[Ca^{2+}]_i$ in different pacemaker groups revealed by FRET-based Cameleon2.1 imaging.** (Upper panels) The ratio of YFP and CFP signals were significantly different between clock neurons acutely exposed at ZT6 and ZT18 (Mann-Whitney test, *p<0.1, ***p<0.001; n=47 vs. 51, 36 vs. 42, 39 vs. 42, 26 vs. 25, and 54 vs. 36). (Lower panels) $[Ca^{2+}]_i$ estimated by FRET signals from upper panels (see Methods).

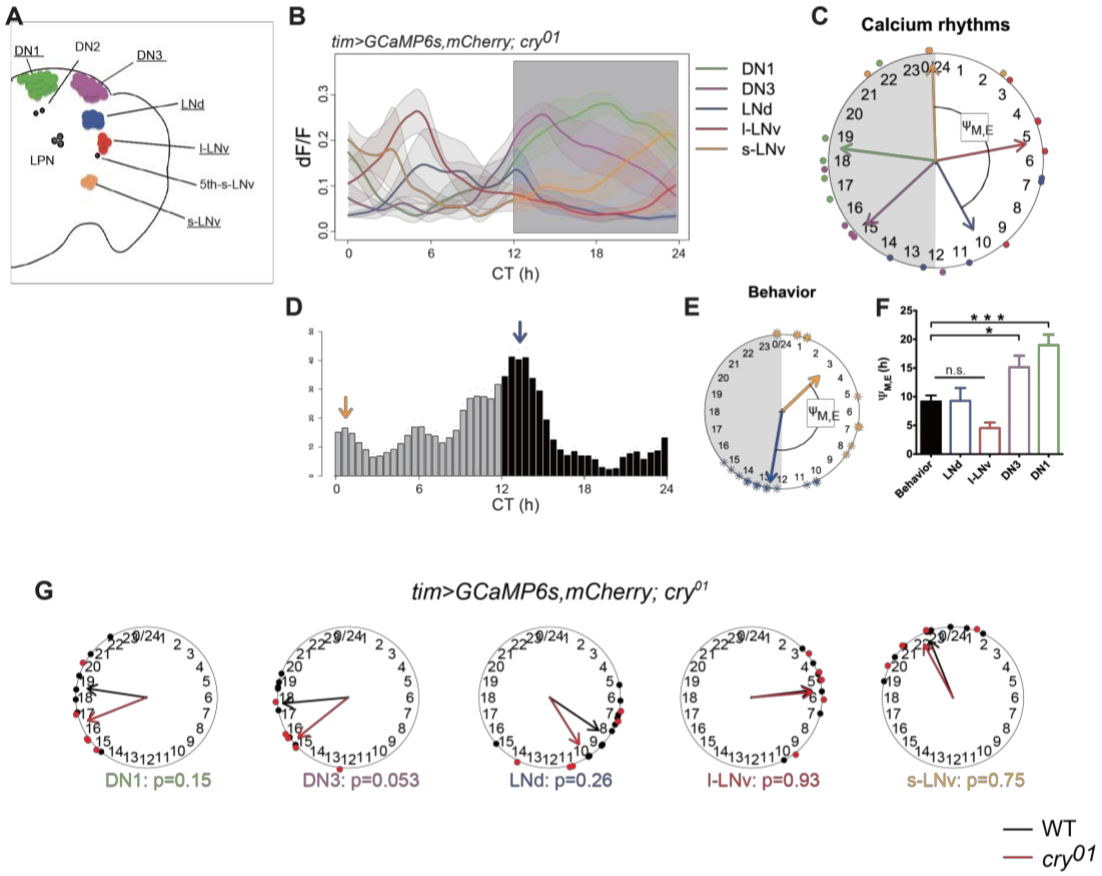


Fig. S5

**Spontaneous $Ca^{2+}$ activity patterns are CRY-independent (A)** Schematic of fly clock neuron network: neuronal groups driven by *tim-gal4* are color-coded; those imaged for GCaMP6s signals are underlined. **(B-F)** As Fig. 1G-K: **(B)** $Ca^{2+}$ transients in five pacemaker groups in homozygous *cry*$^{01}$ mutants (n=5 flies). **(C)** $Ca^{2+}$ rhythm phases from panel (B) **(D)** The DD1 locomotor activity of *tim>GCaMP6s,mCherryNLS; cry*$^{01}$ flies (n=11). **(E)** The phases of behavioral peaks from panel (D). **(F)** $\Psi_{M,LNd}$ matches behavioral $\Psi_{M,E}$ in DD1 (t-test, p=0.96; f-test, p=0.46). **(G)** The peak phases of $Ca^{2+}$ rhythms in different pacemaker groups in *cry*$^{01}$ mutants (red arrow) were not significantly different from those in control flies (black arrows). (p values computed by Watson-Williams test ).

Fig S6

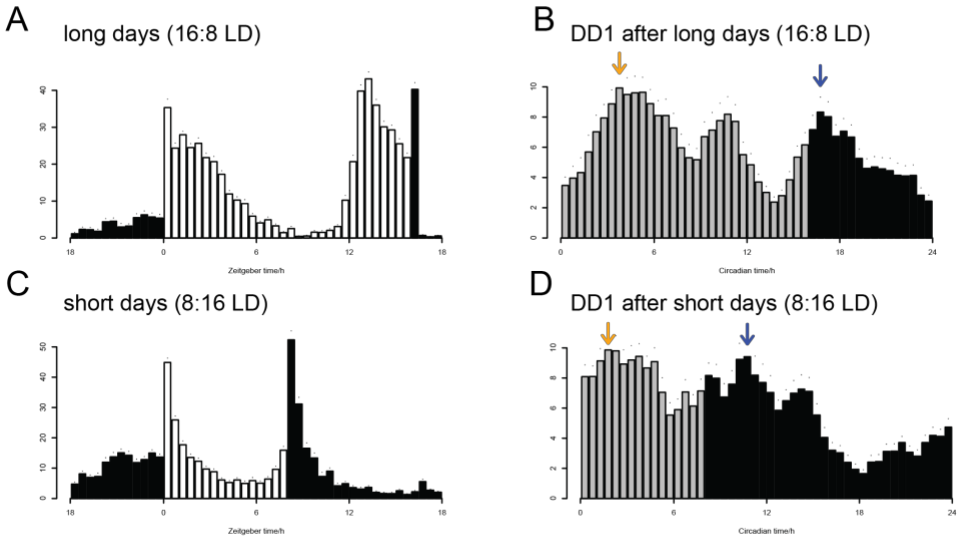


Fig. S6

**Locomotor behavioral phases reflect environmental photoperiods.** (A and C) The average activity histogram shows the locomotor activity under different photoperiod entrainment in constant temperature: (A) long-day condition (16:8 LD; n=13 flies) and (C) short-day condition (8:16 LD; n=12 flies). (B and D) The average activity histogram shows the locomotor activity in the first day under constant darkness (DD1) and in constant temperature, after 6 days of photoentrainment: (B) DD1 behavior following long-day condition (16:8 LD; n=13 flies) and (D) DD1 behavior following short-day condition (8:16 LD; n=12 flies). The genotype of the flies was *yw; tim> GCaMP6s*, mCherry-NLS. Orange and blue arrows indicate peak time for subjective morning and evening peaks of activity

Fig S7


Fig. S7

**Changes in the peak phases of $Ca^{2+}$ rhythms in different pacemaker groups under different environmental photoperiodic conditions compared with 12:12 LD conditions.** (p values computed by Watson-Williams test ). In all cases, the black arrows indicate data from flies entrained under a 12:12 condition; the red arrows indicate data from: (upper panels) 18:6 (long) and (lower panels) 6:18 (short) conditions respectively.

Fig S8

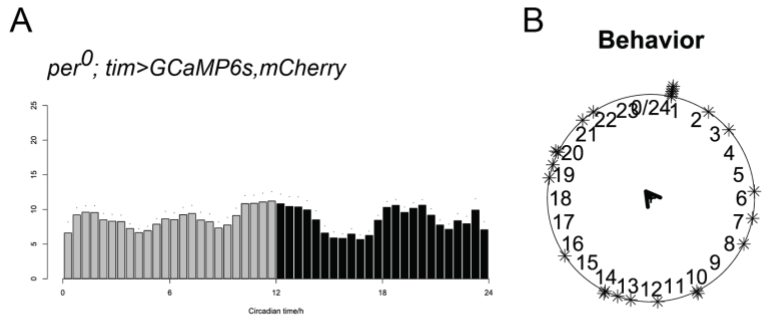


Fig. S8

***per*$^{01}$ mutants lose circadian behavioral rhythmicity under constant darkness conditions.** **(A)** Locomotor activity in DD1 was arrhythmic in *per*$^{01}$ mutants (n=16 flies). **(B)** Behavioral peaks lost phase coherence among *per*$^{01}$ flies. Behavioral peak phases were determined by the time of maximal bin in DD1 locomotor activity profile.

Fig S9

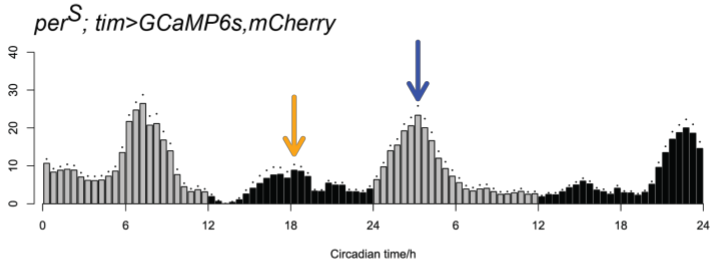


Fig. S9

**In *per*$^S$ mutant flies, which exhibit a ~19 h free-running period, behavioral peaks are dramatically phase-shifted in DD 1-2 under constant darkness.** The average activity histogram shows the locomotor activity of *per*$^S$ mutants in the first two days under constant darkness (DD1-2). Arrows indicate behavioral peak phases corresponding to $Ca^{2+}$ rhythm phases in Fig. 3M (orange: morning, blue: evening). Dots indicate SEM (n=16 flies).

Fig S10

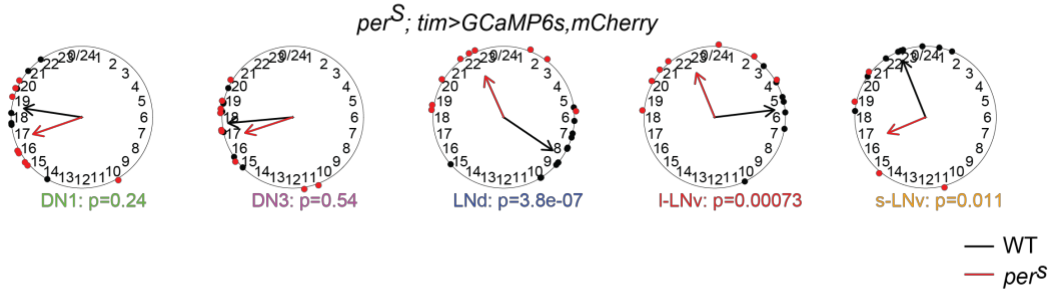


Fig. S10

Changes in the peak phases of $Ca^{2+}$ rhythms in different pacemaker groups in *per*$^{s}$ mutants (red arrow) compared with those in control flies (black arrows). (p values computed by Watson-Williams test )

Fig S11

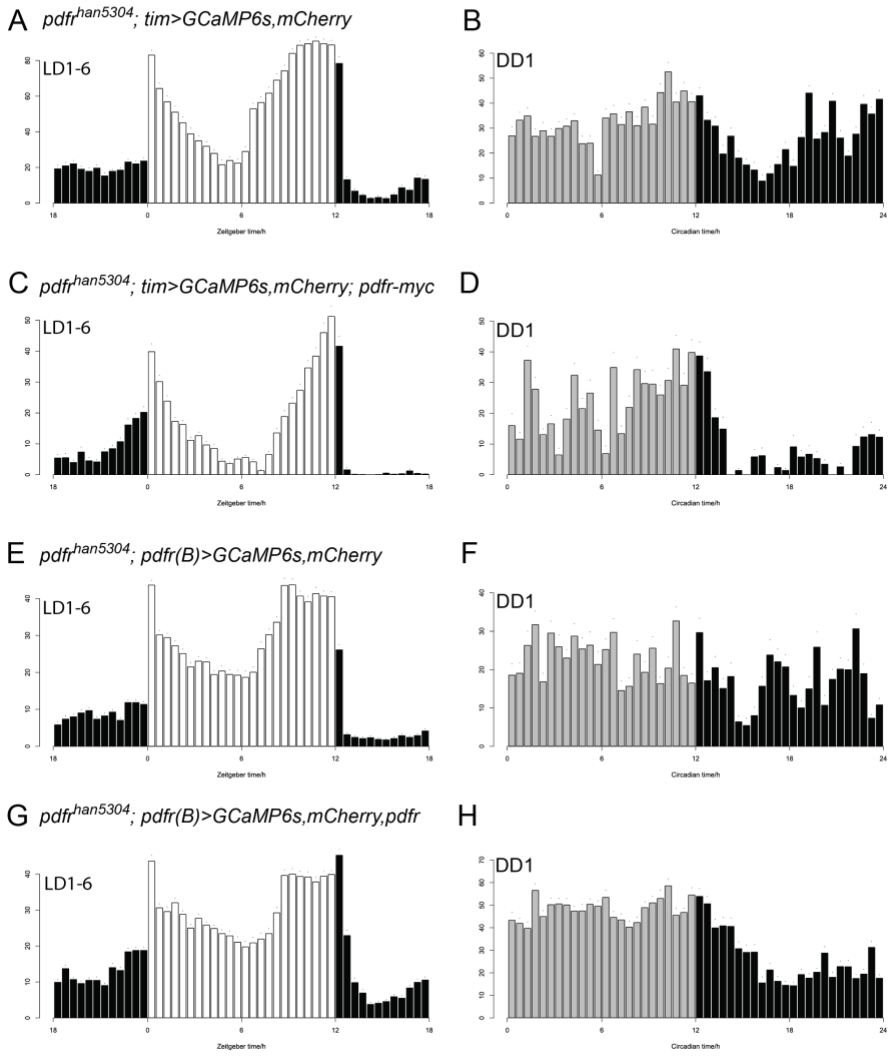


Fig. S11

**Circadian behavior is rescued in *pdfr*$^{han5403}$ mutants by restoring PDFR in pacemaker neurons. (A** and **E)** Under light-dark cycles (LD), the average activity histogram shows that the locomotor activity of *pdfr*$^{han5403}$ mutants lack morning anticipation and display broad, advanced evening phases. **(B** and **F)** In DD1, *pdfr*$^{han5403}$ mutants did not exhibit bimodal behavioral rhythms. Half of them became arrhythmic in constant darkness (see Table S2). **(C** and **D)** The recombineered *pdfr-myc* transgene rescued *pdfr* mutant behavioral defects. **(G** and **H)** The restoration of *Pdfr* in subsets of PDFR$^{+}$ cells using *pdfr(B)-Gal4* partially rescued *pdfr* mutant behavioral defects: (G) in LD, morning anticipation appeared but was weaker; (H) in DD1 flies showed bimodal behavioral rhythms and became more rhythmic in following days under constant darkness (see Table 2S).

Fig S12

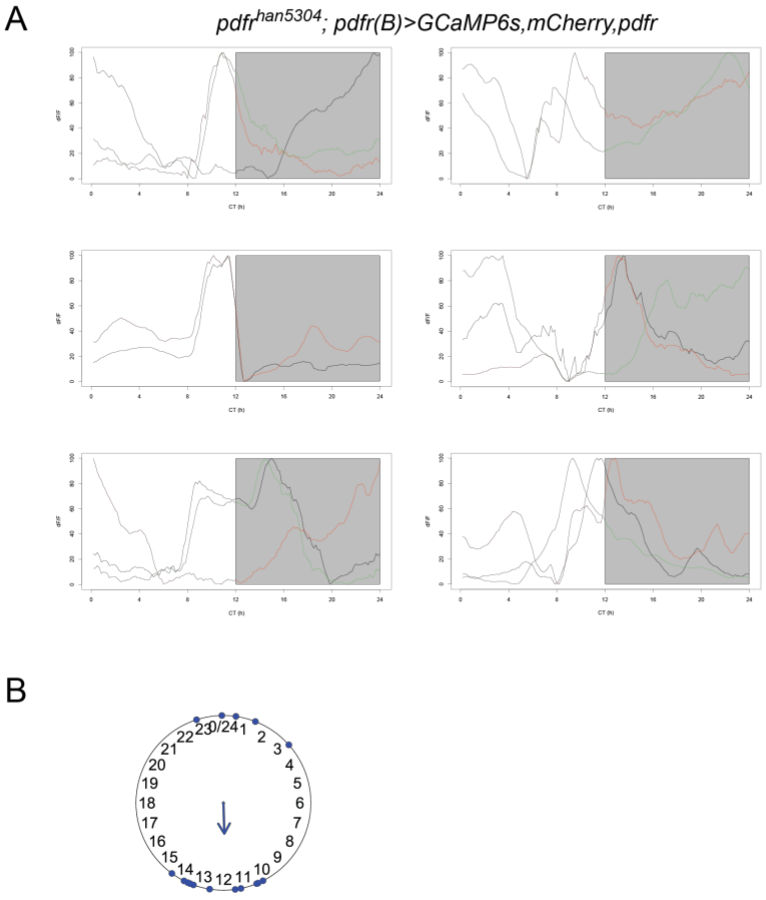


Fig. S12

When PDFR is restored in three PDFR+ LNd by Rescue 2, $Ca^{2+}$ rhythm phases in two, and sometimes all three, are rescued. (A) Normalized $Ca^{2+}$ transients traces of individual LNd neurons. Each panel shows up to three LNd traces from the same fly. Except for the example in the bottom right, for all observations with 3 LNd traces, one LNd was active around dawn, while two were active around dusk. (B) Phase distributions of $Ca^{2+}$ transients in rescued PDFR+ LNd neurons (data from A)

Table S1
Summary of quantification of $Ca^{2+}$ transients in different pacemaker groups.

| Genotype | Pacemaker groups | Peak phase (ZT) | Circular variance (h) | Rayleigh test p-value | Amplitude (dF/F) | sem | Width (h) | sem | N |
|---|---|---|---|---|---|---|---|---|---|
| tim>GCaMP6s, mCherry.NLS | LNd | 8.2 | 0.17 | 2.70E-05 | 0.44 | 0.038 | 5.6 | 0.78 | 12 |
| | lLNv | 5.5 | 0.16 | 0.0029 | 0.4 | 0.061 | 12 | 2.4 | 7 |
| | sLNv | 22.5 | 0.12 | 0.00013 | 0.36 | 0.073 | 16 | 2.2 | 7 |
| | DN3 | 17.7 | 0.076 | 0.00036 | 0.46 | 0.088 | 11 | 0.53 | 7 |
| | DN1 | 18.6 | 0.19 | 0.0051 | 0.49 | 0.091 | 12 | 1.2 | 9 |
| pdfr(B)>GCaMP6s, mCherry.NLS | LNd | 8.7 | 0.13 | 3.90E-05 | 0.28 | 0.036 | 9.2 | 1.5 | 10 |
| | sLNv | 0.72 | 0.13 | 4.10E-05 | 0.23 | 0.044 | 8.5 | 2.1 | 10 |
| | fifth_sLNv | 7.9 | 0.17 | 0.023 | 0.39 | 0.054 | 8.8 | 2.6 | 5 |
| tim>GCaMP6s, mCherry.NLS;$cry^{01}$ | LNd | 10 | 0.27 | 0.063 | 0.26 | 0.062 | 7.9 | 1.3 | 5 |
| | lLNv | 5.3 | 0.15 | 0.018 | 0.33 | 0.018 | 5 | 0.58 | 5 |
| | sLNv | 23.86 | 0.11 | 0.029 | 0.3 | 0.062 | 18 | 2.7 | 4 |
| | DN3 | 15.1 | 0.12 | 0.012 | 0.29 | 0.031 | 9.4 | 1.1 | 5 |
| | DN1 | 18.5 | 0.11 | 0.01 | 0.33 | 0.018 | 14 | 3 | 5 |
| tim>GCaMP6s, mCherry.NLS (Long day: 16:8LD) | LNd | 15 | 0.1 | 0.0029 | 0.29 | 0.057 | 9.2 | 2.7 | 6 |
| | lLNv | 15.5 | 0.14 | 0.0061 | 0.33 | 0.054 | 10 | 2.7 | 6 |
| | sLNv | 0.93 | 0.006 | 0.0013 | 0.22 | 0.045 | 9.3 | 3.7 | 5 |
| | DN3 | 17.6 | 0.18 | 0.025 | 0.31 | 0.046 | 9.8 | 2.5 | 5 |
| | DN1 | 18 | 0.048 | 0.014 | 0.25 | 0.068 | 11 | 1.6 | 4 |
| tim>GCaMP6s, mCherry.NLS (Short day: 8:16LD) | LNd | 6.4 | 0.1 | 0.0029 | 0.27 | 0.052 | 10 | 2.9 | 6 |
| | lLNv | 5.3 | 0.18 | 0.025 | 0.24 | 0.062 | 9.5 | 3.8 | 5 |
| | sLNv | 23.89 | 0.26 | 0.058 | 0.24 | 0.055 | 14 | 3.3 | 5 |
| | DN3 | 13 | 0.24 | 0.024 | 0.15 | 0.023 | 12 | 2 | 6 |
| | DN1 | 17 | 0.37 | 0.09 | 0.25 | 0.043 | 14 | 1.2 | 6 |

Table S1

| Genotype | Pacemaker groups | Peak phase (ZT) | Circular variance (h) | Rayleigh test p-value | Amplitude (dF/F) | sem | Width (h) | sem | N |
|---|---|---|---|---|---|---|---|---|---|
| $per^{01}$;tim>GCaMP6s, mCherry.NLS | LNd | 14.4 | 0.75 | 0.75 | 0.2 | 0.016 | 14 | 2.9 | 5 |
| | lLNv | 5.8 | 0.75 | 0.74 | 0.17 | 0.031 | 8 | 2.4 | 5 |
| | sLNv | 13 | 0.78 | 0.84 | 0.13 | 0.036 | 14 | 3.4 | 4 |
| | DN3 | 16.4 | 0.86 | 0.91 | 0.25 | 0.041 | 12 | 2.7 | 5 |
| | DN1 | 16 | 0.6 | 0.56 | 0.3 | 0.08 | 10 | 2.4 | 4 |
| $per^{S}$;tim>GCaMP6s, mCherry.NLS | LNd | 22 | 0.38 | 0.025 | 0.33 | 0.058 | 8.8 | 2.5 | 9 |
| | lLNv | 21.6 | 0.33 | 0.039 | 0.38 | 0.065 | 12 | 3.7 | 7 |
| | sLNv | 16.5 | 0.22 | 0.04 | 0.3 | 0.033 | 10 | 3.8 | 4 |
| | DN3 | 15.5 | 0.28 | 0.0063 | 0.18 | 0.033 | 8.9 | 2.1 | 9 |
| | DN1 | 15.8 | 0.24 | 0.0061 | 0.23 | 0.037 | 12 | 2.6 | 8 |

| Genotype | Pacemaker groups | Peak phase (ZT) | Circular variance (h) | Rayleigh test p-value | Amplitude (dF/F) | sem | Width (h) | sem | N |
|---|---|---|---|---|---|---|---|---|---|
| $pdfr^{han5304}$; tim>GCaMP6s,mCherry.NLS | LNd | 1.2 | 0.052 | 0.00082 | 0.3 | 0.056 | 15 | 3.9 | 6 |
| | l-LNv | 5 | 0.22 | 0.0087 | 0.39 | 0.049 | 13 | 3.5 | 7 |
| | s-LNv | 0.31 | 0.14 | 0.015 | 0.39 | 0.039 | 13 | 4 | 5 |
| | DN3 | 1.3 | 0.071 | 0.0014 | 0.25 | 0.045 | 13 | 3.4 | 6 |
| | DN1 | 17.9 | 0.098 | 0.0085 | 0.3 | 0.053 | 16 | 3.2 | 5 |
| $pdfr^{han5304}$; tim>GCaMP6s,mCherry.NLS;pdfr-myc | LNd | 10 | 0.17 | 0.0096 | 0.39 | 0.097 | 8.8 | 1.4 | 6 |
| | l-LNv | 6.3 | 0.081 | 0.0018 | 0.32 | 0.057 | 7.5 | 1.7 | 6 |
| | s-LNv | 23.34 | 0.11 | 0.0036 | 0.17 | 0.046 | 16 | 3.5 | 6 |
| | DN3 | 17 | 0.099 | 0.0027 | 0.31 | 0.074 | 12 | 2 | 6 |
| | DN1 | 18.9 | 0.072 | 0.0014 | 0.19 | 0.019 | 10 | 2.9 | 6 |
| $pdfr^{han5304}$; pdfr(B)>GCaMP6s,mCherry.NLS | PDFR+LNd | 3.2 | 0.14 | 0.0062 | 0.26 | 0.046 | 11 | 2.8 | 6 |
| | s-LNv | 23.82 | 0.21 | 0.017 | 0.34 | 0.081 | 7.7 | 2.6 | 6 |
| | 5th-sLNv | 2.8 | 0.3 | 0.084 | 0.24 | 0.046 | 3.3 | 0.6 | 5 |
| $pdfr^{han5304}$; pdfr(B)>GCaMP6s,mCherry.NLS,pdfr | PDFR+LNd | 14.5 | 0.72 | 0.65 | 0.34 | 0.041 | 9.7 | 1.9 | 6 |
| | s-LNv | 21.4 | 0.056 | 0.00094 | 0.44 | 0.076 | 13 | 3.5 | 6 |
| | 5th-sLNv | 11 | 0.43 | 0.14 | 0.35 | 0.027 | 9 | 2.8 | 6 |

Table S2.
Summary of Circadian Behavior Rhythms Under Constant Conditions (DD or LL1-9)

| Genotype | N | %AR | Period | pwr | wid | SNR | ACT-day | ACT-night | ACT-cycle |
|---|---|---|---|---|---|---|---|---|---|
| **DD** | | | | | | | | | |
| w1118 | 16 | 12.5% | 23.9 | 46.8 | 6.8 | 1.4 | 34.8 | 15.5 | 25.1 |
| tim-gal4;uas-GCaMP6s,mCherryNLS | 28 | 53.6% | 24.3 | 28.1 | 4.2 | 0.7 | 11.8 | 6.5 | 9.1 |
| tim-gal4/+;uas-GCaMP6s,mCherryNLS/+ | 14 | 14.3% | 24.0 | 79.2 | 4.8 | 0.8 | 14.0 | 5.9 | 10.0 |
| pdfr(B)gal4/uas-GCaMP6s,mCherryNLS/+ | 20 | 10.0% | 24.0 | 114.8 | 5.4 | 1.3 | 12.6 | 10.5 | 11.5 |
| timgal4/uas-GCaMP6s,mCherryNLS;cry01 | 15 | 13.3% | 23.0 | 44.7 | 3.3 | 0.9 | 14.4 | 9.5 | 11.9 |
| $per^{s}$;tim-gal4/+;uas-GCaMP6s,mCheryNLS/+ | 16 | 25.0% | 19.5 | 51.3 | 3.3 | 0.9 | 10.1 | 10.4 | 10.3 |
| $per^{01}$;tim-gal4/+;uas-GCaMP6s,mCheryNLS/+ | 30 | 96.7% | 24.0 | 12.7 | 1.5 | 0.4 | 8.1 | 10.8 | 9.5 |
| $pdfr^{han5304}$;tim-gal4/+;uas-GCaMP6s,mCheryNLS/+ | 16 | 56.3% | 22.8 | 25.5 | 3.3 | 0.9 | 21.7 | 19.8 | 20.7 |
| $pdfr^{han5304}$;tim-gal4/+;uas-GCaMP6s,mCheryNLS/pdfr-myc | 17 | 11.8% | 24.5 | 25.2 | 3.7 | 0.6 | 18.2 | 8.1 | 13.1 |
| $pdfr^{han5304}$;pdfr(B)-gal4/+;uas-GCaMP6s,mCheryNLS/+ | 14 | 64.3% | 22.7 | 23.1 | 2.4 | 0.5 | 11.7 | 11.1 | 11.4 |
| $pdfr^{han5304}$;pdfr(B)-gal4/+;uas-GCaMP6s,mCheryNLS/uas-pdfr | 11 | 36.4% | 24.9 | 46.3 | 5.6 | 1.1 | 14.3 | 9.7 | 12 |
| **LL** | | | | | | | | | |
| tim-gal4/+;uas-GCaMP6s,mCherryNLS/+ | 8 | 100.0% | - | - | - | 1.1 | 10.4 | 7.9 | 9.2 |
| timgal4/uas-GCaMP6s,mCherryNLS;$cry^{01}$ | 20 | 50.0% | 26.1 | 39.7 | 4.1 | 0.6 | 7.1 | 8.2 | 7.7 |

# Chapter 3

# Neuromodulations and environmental inputs to circadian neural circuit

This chapter is adapted from the following publication:

Liang, X., Holy, T. E., & Taghert, P. H. (2017). A series of suppressive signals within the *Drosophila* circadian neural circuit generates sequential daily outputs. ***Neuron***, 94, 1173–1189.

**Abstract**:

We studied the *Drosophila* circadian neural circuit using whole brain imaging *in vivo*. Five major groups of pacemaker neurons display synchronized molecular clocks, yet each exhibits a distinct phase of daily $Ca^{2+}$ activation. Light and neuropeptide PDF from morning cells (s-LNv) together delay the phase of the evening (LNd) group by ~12 h; PDF alone delays the phase of the DN3 group, by ~17 h. Neuropeptide sNPF, released from s-LNv and LNd pacemakers, produces latenight $Ca^{2+}$ activation in the DN1 group. The circuit also features negative feedback by PDF to truncate the s-LNv $Ca^{2+}$ wave and terminate PDF release. Both PDF and sNPF suppress basal $Ca^{2+}$ levels in target pacemakers with long durations by cell autonomous actions. Thus, light and neuropeptides act dynamically at distinct hubs of the circuit to produce multiple suppressive events that create the proper tempo and sequence of circadian pacemaker neuronal activities.

## INTRODUCTION

Circadian rhythms in behavior, helping animals to adapt to environmental day-night cycles, are generated by small groups of pacemaker neurons in the brain (Herzog, 2007), many of which display self-sustained oscillations in both gene expression and neural activity (Welsh *et al.* 1995). These pacemakers are coupled together into a highly interactive network, from which unique network properties emerge, including the synchronization of molecular oscillations, the coordination of responses to external inputs, and the generation of multiple temporal outputs, such as circadian rhythms in locomotor activity, feeding, and sleep (Welsh *et al.* 2010; Hastings *et al.* 2014). The network mechanisms promoting the synchronization of molecular oscillations have been well characterized (Lin *et al.* 2004; Aton and Herzog, 2005; Li *et al.* 2014). Recently, several studies have focused on the coordination of pacemakers' molecular rhythms with their neuronal properties and the coordination with the network properties of inputs and outputs (e.g., Coomans *et al.* 2015; Flourakis *et al.* 2015), yet these critical aspects of circadian neuronal oscillators remain incompletely understood. Using the *Drosophila* circadian network as a model system, here we study how the neural network processes external light inputs and how it generates sequential outputs during the course of the 24-h day.

The *Drosophila* circadian network contains ~150 pacemaker neurons organized into seven groups (Nitabach and Taghert, 2008). Previously we reported (Liang *et al.* 2016)that five major groups from this network became sequentially active at specific times of day (Figure 1A): for several groups, these times can be associated with their unique functions in behavioral outputs. The small lateral neuron ventral (s-LNv) group, previously associated with the morning peak of locomotor activity (Renn *et al.* 1999), is active around dawn (Liang *et al.* 2016) and is operationally termed a Morning (M) cell. Likewise, the large lateral neuron ventral (l-LNv)

group, that serves an arousal function and promotes the waking state (Parisky *et al.* 2008; Shang *et al.* 2008, 2013) is active just following the s-LNv in the morning. Activity by the Evening (E)-cell group (including the lateral neuron dorsal (LNd) and the 5$^{th}$ s-LNv) was previously associated with the evening peak of locomotor activity (Grima *et al.* 2004; Stoleru *et al.* 2004): its neural activity anticipates dusk (Liang *et al.* 2016). Two additional groups, the dorsal neuron 3 (DN3) and the dorsal neuron 1 (DN1) display distinct activity bouts during the nighttime. Thus the network generates sequential neural outputs to control different behavioral rhythms throughout the day and night.

We previously reported that without neuropeptide pigment dispersing factor (PDF) receptor signaling, the daily neural activity patterns of the E-cell and DN3 groups became co-phasic with the M group around dawn (Liang *et al.* 2016). This observation suggested that such neuropeptide-mediated pacemaker interactions stagger neural activity patterns across the different groups in the circadian network. However several fundamental questions remain. By what mechanism does PDF signaling alter neural activity phases by several hours, and how does it promote different, group-specific phases? Also, the activity patterns of certain pacemaker groups (l-LNv and DN1) are strikingly indifferent to PDF signaling: do other neuropeptides released within the network contribute to setting their specific phasic activities? Interactions between pacemakers are not only crucial for generating multiple temporal outputs, but also for responding to external inputs. Light information can cell-autonomously adjust *Drosophila* molecular clocks through the internal photoreceptor Cryptochrome (CRY) (Ceriani *et al.* 1999; Emery *et al.* 2000) and non-cell-autonomously via pacemaker interactions (Cusumano *et al.* 2009; Guo *et al.* 2014). Yet, how such light information from different inputs eventually translates to multiple neural network outputs remains largely undefined.

To begin addressing these fundamental problems, here we investigate how the 24-h neural activity pattern of the entire *Drosophila* circadian network *in vivo* is regulated by light inputs and neuropeptides. We report three principal findings. First, PDF provides forward and feedback information within the network and that light cycles act in concert with PDF to provide the proper phase for E cell $Ca^{2+}$ activity. Second, short light pulses rapidly phase-shift the 24-h neural activity patterns in all pacemaker groups, via both CRY and visual system pathways. Third, short Neuropeptide F (sNPF) is required for the nighttime phasing of the DN1 group. PDF and sNPF share phase-setting mechanisms by both suppressing $Ca^{2+}$ activity in different pacemaker groups. Together, these results indicate that the *Drosophila* circadian pacemakers interact primarily by delay-based mechanisms, through light and neuropeptide-mediated inhibition. We propose this is a generalized process by which a neural network can variably produce sequentially-timed outputs.

## RESULTS

### Light inputs and PDF modulation converge to set Evening Cell $Ca^{2+}$ phase.

Previously we reported on pacemaker $Ca^{2+}$ activities under constant conditions (DD: lacking external timing cues) (Liang *et al.* 2016). To consider the possible influence of light, we performed *in vivo* 24h $Ca^{2+}$ imaging in a 12h light: 12h dark (LD) cycle. Wild type (WT) patterns of $Ca^{2+}$ activity in the majority of pacemaker groups in LD were not altered, except in the E-cell group, LNd: its $Ca^{2+}$ activity peak in LD was delayed by 3.8±0.6h (Figure 1AB), to the end the 12h photophase (ZT12). We next asked whether PDF is required for the delaying effect of light on LNd by comparing the pacemaker $Ca^{2+}$ rhythms of $pdf^{01}$ mutants under DD with those under LD cycles (Figure 1CD). Under DD and compared to WT controls, $Ca^{2+}$ rhythms were phase-shifted in both LNd and DN3 of $pdf^{01}$ mutants (Figure 1D). Both pacemaker groups became less consistent among animals and roughly co-active with the s-LNv around presumptive dawn, phenocopying $Ca^{2+}$ patterns in *pdfr* mutants (Liang *et al.* 2016). However, under LD, $pdf^{01}$ mutant LNd were selectively delayed compared to DD by 7.8±0.5h (Figure 1C-E). The results indicate that PDF/PDFR signaling is not required for the delaying effect of light on LNd $Ca^{2+}$ activity.

The LNd group is operationally termed an Evening (E) cell group: in WT animals and as measured in DD, its $Ca^{2+}$ activity peak is phase-locked to the evening behavioral peak (Liang *et al.* 2016). With the PDF-independent delay effect of light, under an LD cycle, the $pdf^{01}$ mutant LNd peaked 2.7±0.5h earlier than WT, consistent with the 1-2h advanced evening behavioral phase of *pdf/pdfr* mutants (Renn *et al.* 1999; Hyun *et al.* 2005)(Figure 1FG). It is also worth noting that, for both WT and *pdf* mutants, LNd rhythms became more consistent across flies under cycling LD conditions than under DD (F-test for variances within genotypes, $p<0.05$). In

contrast to the LNd group, the DN3 pacemaker group's $Ca^{2+}$ rhythms were not different between LD vs DD in either genotype (Figure 1A-D). Therefore, PDF>PDFR signaling alone sets the proper phase of DN3 $Ca^{2+}$ rhythms, whereas PDF>PDFR signaling and light inputs together set the proper phase of LNd $Ca^{2+}$ rhythms.

**PDF receptor signaling alters $Ca^{2+}$ rhythms in E cells and in M cells.**

To define the mechanism by which neuropeptide PDF signaling sets $Ca^{2+}$ phases, we first asked whether PDFR signaling acts cell autonomously in different pacemaker groups. We used the Gal4:UAS system to selectively express PDFR in alternate pacemaker subsets in the hypomorphic *pdfr* mutant $han^{5304}$ (Hyun *et al.* 2005). In conjunction, we used *cry*-lexA>lexAop-*GCaMP6s* to independently express the calcium sensor throughout the pacemaker network. Using this lexA reporter system in both WT and the $han^{5304}$ (*Pdfr*) mutant background, we recapitulated results we obtained previously with *tim>GCaMP6s* for WT and $pdf^{01}$, respectively (Figure 2A and B). We first restricted PDFR rescue to a subset of E cells (the 5$^{th}$ sLNv and the three LNd, all four of which are normally $CRY^+/PDFR^+$) (Im and Taghert, 2010; Yao and Shafer, 2014)(Figure 2C and S1A). In this case, the LNd $Ca^{2+}$ peaked 14.1±1.0h later than in the *pdfr* mutant (Figure 2B), and 5.2±1.0h later than in a control genotype (Figure 2B). These mosaic flies also displayed a later evening behavioral phase than in the *pdfr* mutant (Figure S1; cf. Lear *et al.* 2009). In this mosaic design, DN3 still lacked PDFR and did not display any rescue of the $Ca^{2+}$ rhythm phase. In contrast, when we restricted PDF receptors to M cells only (s-LNv), the distribution of $Ca^{2+}$ phases among the different pacemaker groups was the same as in the *pdfr* mutant (Figure 2D and S1B). However, the width of the $Ca^{2+}$ wave in the s-LNv was longer in the $pdfr^{mut}$, and also longer in the 'Rescue: E cell', than in the WT (Figure 2F). When

PDFR expression was restored to the s-LNv ('Rescue: M-cell'), the width of the s-LNv wave was shortened and no longer different from the WT value (Figure 2F). This result suggested that PDFR functions in s-LNv to help terminate the period of $Ca^{2+}$ activation in s-LNv in cell-autonomous fashion. Collectively, these PDFR different rescues displayed distinct actions on $Ca^{2+}$ activities in E versus in M cells: in the forward direction (i.e., to E cells), it delays the $Ca^{2+}$ phase; in the feedback direction, (i.e., to M cells), it helps terminate the $Ca^{2+}$ peak.

**Pharmacological tests of PDF-mediated suppression of $Ca^{2+}$ in vivo.**

PDFR signaling in M vs. in E pacemakers may reflect a common mechanism - suppression of $Ca^{2+}$ levels. To test this hypothesis, we applied synthetic PDF while imaging *in vivo*. We compared pacemaker responses between WT and *pdfr* (*han*$^{5304}$) mutant genotypes by imaging them concurrently, as yoked pairs, to reduce measurement variance derived from non-genetic factors (Figure 3A). We restricted the GCaMP6s sensor expression to s-LNv and three out of six LNd with *pdfr*(*B*)-GAL4 (Im and Taghert, 2010). WT s-LNv and LNd both responded to PDF by 8.7±1.5% and 10.4±1.0% peak reductions in $Ca^{2+}$ signals respectively (Figure 3B): these reductions developed over many hours. The net reduction of $Ca^{2+}$ levels in WT LNd was ~25.5% compared to the vehicle control, as we performed the experiments during the normal $Ca^{2+}$ peak of LNd (CT6-12) (Figure 3CD). In *pdfr* mutants, s-LNv and LNd showed no significant responses to the same applications of PDF. Together these results demonstrate PDF>PDFR signaling potently suppresses basal $Ca^{2+}$ levels in both E cells (LNd) and M cells (s-LNv).

We next asked whether suppression of $Ca^{2+}$ levels by PDF>PDFR signaling is sufficient to delay the daily $Ca^{2+}$ phases in LNd and DN3 by applying synthetic PDF, while imaging *pdf*

mutants *in vivo*. PDF applied at the $Ca^{2+}$ peak time (CT0) of the s-LNv delayed $Ca^{2+}$ phases in both LNd by 3.4±0.5h and DN3 by 3.3±0.8h (Figure 3EF). Two serial applications of synthetic PDF at CT0 and at CT5 (at the $Ca^{2+}$ peak time of the l-LNv PDF-releasing group) further delayed $Ca^{2+}$ phases by a total of 6.2±0.3h (LNd) and by 4.9±1.3h (DN3) (Figure 3E-I). In contrast, a single application of PDF at CT5, after the peaks in LNd and DN3, did not induce delays in $Ca^{2+}$ activity peaks in either group (Figure 3G). These results demonstrate that PDF can in principle affect $Ca^{2+}$ phases in LNd and DN3 *in vivo* by delaying the onset of their incipient, clock-driven $Ca^{2+}$activations.

**Ectopic PDFR confers sensitivity to the phase-delaying effects of PDF.**

We also tested the cell autonomous effects of PDFR signaling on pacemaker $Ca^{2+}$ activity with gain of function experiments. The l-LNv pacemaker group is not responsive to PDF, but becomes responsive with ectopic receptor expression (Shafer *et al.* 2008). Consistent with its lack of pharmacological sensitivity, the normal l-LNv $Ca^{2+}$ phase is not altered in either the *pdfr* (Liang *et al.* 2016) or the *pdf* mutants (Figure 1B). When we overexpressed PDFR in all pacemaker neurons in the *pdfr* mutant background (thereby including the l-LNv), the phases of $Ca^{2+}$ activity patterns that were aberrant in the mutant backgrounds (those of the LNd and DN3) were fully restored to their normal values. In addition, this experiment produced a 4.2±1.3h delay in the phase of l-LNv (Figure 4A). To test whether this PDFR-dependent delay in l-LNv $Ca^{2+}$ was cell autonomous, we restricted ectopic PDFR expression within the pacemaker network to only the l-LNv in an otherwise WT background (*pdf>pdfr,* Figure 4B) and separately in a *pdfr* mutant background (*han; c929>pdfr,* Figure 4C). In both cases, ectopic PDFR expression in l-LNv delayed its $Ca^{2+}$ phase: by 4.9±0.4h (compared to WT) and by 8.7±1.0h (compared to the

*pdfr* mutant) (Figure 4F). The increased delay of the $Ca^{2+}$ phase in the l-LNv in the *han; c929>pdfr* compared to that in the *pdf>pdfr* genotype is likely due to the lack of PDFR in the s-LNv. As described above, PDFR in the s-LNv mediates negative feedback to help terminate activity in that cell, hence a longer period of s-LNv activity produces greater delay in the l-LNv phase. In sum, gain-of-function genetic experiments support the hypothesis that PDFR signaling normally delays $Ca^{2+}$ phases in diverse pacemakers by a cell-autonomous mechanism.

**PDFR signaling in M cells provides negative feedback.**

Based on the sensitivity of the $Ca^{2+}$ wave duration in the s-LNv to cell autonomous *pdfr* signaling (Figure 2 D&F), we speculated that a shorter period of $Ca^{2+}$ activation would diminish neuropeptide PDF release and hence, diminish PDF signaling. To further examine this possibility, we used *pdf*-Gal80 to restrict *tim>pdfr* overexpression to only non-M pacemakers. Consistent with the predictions of the hypothesis (lack of M cell PDFR extends the duration of PDF cell signaling), we observed significantly delayed $Ca^{2+}$ phases in DN1, DN3, and LNd, by an average of 4.5±0.6h (Figure 4D), as well as delayed evening behavioral phases (Figure S2). Independently, we observed similar E cell $Ca^{2+}$ phase delays (3.8±1.1h) when PDFR expression was restricted to only a subset of E cells (PDFR-positive LNd and the $5^{th}$ s-LNv) (Figure 4E&G). Collectively, these results support the hypothesis that PDFR signaling delays $Ca^{2+}$ activations in non-M cells and, by negative feedback, terminates $Ca^{2+}$ activation in M cells.

**Light pulses rapidly phase-shift the $Ca^{2+}$ rhythms.**

We further probed pacemaker interactions with the environment, we delivered light pulse stimuli at the phase-delaying zone (ZT17) or the phase-advancing zone (ZT21), and also in DD1

at the dead zone (CT9) (Figure S3). Before, or at different times after the light pulses, we performed 24h $Ca^{2+}$ imaging sessions and tiled them together to unify the records across a three-day post-stimulus period (Figure 5AB & Figure S3B). A dead zone light pulse (CT9) did not phase-shift pacemaker $Ca^{2+}$ rhythms (Figure 5B-E). In contrast, phase-delaying light pulses delayed $Ca^{2+}$ rhythms in all pacemakers within the first circadian cycle (Figure 5C). During the second day, LNd and s-LNv further delayed their $Ca^{2+}$ phases, while DN1 and DN3 became less coherent (Figure 5B&D). By the third day, the pacemaker network re-established a normal phase pattern with an overall 5.5±0.6h delay, compared to the pattern in flies that received no light pulse (Figure 5E). With phase-advancing light pulses, only the s-LNv responded during the first day post-stimulus, with a 8.5±1.0h phase advance (Figure 5C). During the second day, the s-LNv $Ca^{2+}$ phase advance became smaller (4.6±0.8h) and all other pacemaker groups now displayed in $Ca^{2+}$ phases advances that were roughly similar (5.3±0.4h) (Figure 5D); this pattern was maintained into the third day (Figure 5E). Together, these results show that the circadian pacemaker network responds rapidly to short light pulses, especially for phase delays.

**Light inputs via CRY and PDF.**

We further investigated the mechanism for light inputs to regulate $Ca^{2+}$ activity patterns of circadian pacemakers. The light-input pathways include the intracellular photoreceptor CRY and the visual systems (perhaps relayed by PDF signals). To examine these two pathways, we repeated the tests in *cry null* mutants and in *pdf* mutants independently, during the first post-stimulus cycle.

We previously found that in DD, the $Ca^{2+}$ activity patterns of circadian pacemakers in *cry* nulls were not different from those of WT flies (Liang *et al.* 2016). However, phase-delaying

light pulses in *cry* mutants failed to induce any $Ca^{2+}$ phase shifts during the first circadian cycle (Figure S4A). In contrast phase-advancing light stimuli shifted *cry* mutant s-LNv, albeit by only half as much as WT controls (Figure S4B). In contrast, pacemaker groups in *pdf null* mutant flies responded rapidly to both phase-delaying and phase-advancing light pulses in the first circadian cycle. Of note, the phase-delaying light pulse caused a much larger $Ca^{2+}$ phase shift in *pdf* mutant s-LNv (12.4±1.0h) than controls (4.4±0.6h) (Figure S4CD). Consistent with the poor rhythmicity in behavior under DD (Table S1), *pdf* null mutant flies had generally poorer coherence in $Ca^{2+}$ phases among mutant flies than did control flies. These results indicate that the normal pattern of light induced $Ca^{2+}$ phase shifts is partially modulated by PDF signaling.

**sNPF modulation sets DN1 $Ca^{2+}$ phase by suppressing daytime DN1 $Ca^{2+}$ levels.**

PDF signaling is not required for the proper $Ca^{2+}$ phases of the l-LNv or the DN1 (Liang *et al.* 2016 and see Figure 1). We therefore screened for the potential involvement of other neuropeptides (and cognate their receptors) that are known to be expressed by subsets of pacemaker neurons, including short neuropeptide F (sNPF - Johard *et al.* 2009), diuretic hormone 31 (DH31 - Kunst *et al.* 2014), ion transport peptide (ITP - Johard *et al.* 2009), and neuropeptide F (NPF - Hermann *et al.* 2012). Manipulation of DH31 signaling suggested possible changes: a strongly hypomorphic mutation of *DH31* and the knockdown of one of the DH31 receptors (CG17415 – Johnson *et al.* 2005) displayed a trend toward lower coherence of l-LNv $Ca^{2+}$ activity among different flies ($p=0.16$ (DH31) and $p=0.38$ (CG17415): Rayleigh test; Figure S5). However, neither the amplitudes of daily $Ca^{2+}$ fluctuations ($p>0.5$: t-test) nor the mean $Ca^{2+}$ phases ($p>0.5$: Watson-Williams test) were significantly altered compared to WT controls. Likewise, the expression of RNAi constructs of *itp*, *npf*, *npfr* did not cause major

alterations in the daily $Ca^{2+}$ activity patterns in the network or of locomotor activity rhythms (Figure S5; Table S1).

In contrast, we observed complete arrhythmicity in $Ca^{2+}$ activity of the DN1 group following RNAi-knock down of the neuropeptide sNPF within the pacemaker network (*tim>sNPF* RNAi - Figure 6A). The amplitudes of $Ca^{2+}$ fluctuations in DN1 were reduced (t-test, $p<0.05$) and coherence among different flies was lost (Rayleigh test, $p=0.81$). However, this manipulation did not alter the pacing of molecular clocks in DN1 cells (Figure S6A). RNAi knockdown of the *sNPF receptor*, using *tim*-Gal4, produced a very similar outcome (Figure S6D). These congruent effects suggested DN1 $Ca^{2+}$ rhythms normally require neuropeptide sNPF signaling. Since sNPF was knocked down by an RNAi that targeted its 3'UTR sequence, we tested genetic specificity with a rescue experiment that overexpressed the sNPF coding sequence in the *sNPF* knockdown background (Figure S6E). In these flies, the phase and coherence of the $Ca^{2+}$ activity in DN1 were fully rescued.

Within the *tim*-GAL4 pattern of pacemakers, sNPF is normally expressed in both M (four s-LNv) and E (two of six LNd) cells (Johard *et al.* 2009). We therefore asked whether sNPF released by M versus E groups had different functions. We selectively knocked down sNPF in M cells and found surprisingly, that $Ca^{2+}$ activity in DN1 was rhythmic and coherent, but now with a peak at dawn, co-phasic with M cells (Figure 6B). We observed this same effect under cyclic LD conditions (Figure 6CD). Together these results suggest that E-cell derived sNPF is sufficient for rhythmic $Ca^{2+}$ in DN1, but is not sufficient for its proper $Ca^{2+}$ phase.

When sNPF or sNPFR was 'knocked-down' in all pacemakers, we observed a slight increase of nighttime locomotor activity under LD (Figure 6EG, compared to WT in Figure 1F; Figure S6B; Table S1). However, when sNPF knockdown was restricted to M-cells (*Pdf*-cells),

behavioral activity patterns were substantially altered (Figure 6FH, compared to WT in Figure 1F; Figure S6C). These flies lost morning anticipation under LD and displayed a phase-delayed morning peak within the first DD cycle. Therefore, M-cell specific knockdown of sNPF produces a strong behavioral phenotype correlated with the phase shift it produced in the DN1 $Ca^{2+}$ activity.

When the sNPF knockdown was restricted to E cells, the DN1 $Ca^{2+}$ rhythm was not different from control, and locomotor behavior likewise displayed no alterations (Figure S6F), suggesting that M-cell sNPF is sufficient to support rhythmic DN1 activity when E-cell sNPF is missing. Impairing sNPF or PDF signals from s-LNv caused the $Ca^{2+}$ activity of DN1 in the case of lost sNPF, or LNd and DN3 in the case of lost PDF, to become co-phasic with s-LNv around dawn. When PDF neurons (s-LNv and l-LNv) were ablated by expressing the cell death genes (*hid* and *rpr*) (Renn *et al.* 1999), LNd and DN3 were phase-shifted to a morning peak, while DN1 still displayed a normal activity pattern, peaking at nighttime and remaining anti-phasic with LNd (Figure S7). We speculate that when LNd became active around dawn in this genotype, they could replace the role of s-LNv to set DN1 activity at the nighttime. Together these four sets of results suggest that sNPF from both M cells and E cells produces the normal $Ca^{2+}$ activity pattern and behavioral output of DN1.

**Pharmacological Tests of sNPF-Mediated Suppression in vivo.**

We hypothesized that the normal circadian function of sNPF, by analogy to that of PDF (Figure 3), is to suppress DN1 $Ca^{2+}$ activity during the daytime, sequentially by M cells and then by E cells. To test this hypothesis, we pharmacologically applied sNPF onto WT brains during 12 hr episodes of $Ca^{2+}$ imaging (Figure 7A). We again employed a design of 'yoked' fly pairs,

now simultaneously testing flies that previously entrained to LD schedules with an 8h phase difference. Therefore, one fly of each pair began the recording session at CT4 and the other at CT12. CT4 pacemakers did not exhibit $Ca^{2+}$ signal changes in response to single applications of synthetic sNPF (we propose this is because the intrinsic $Ca^{2+}$ activity in DN1 was low due to intrinsic sNPF signaling at this time). Conversely, pacemakers staged to begin testing at CT12 exhibited a 12.8±2.3% reduction in $Ca^{2+}$ signals in response to synthetic sNPF exposure, and they subsequently recovered to a higher level (Figure 7B-D). The net reduction of $Ca^{2+}$ signal in DN1 pacemakers from CT12 was ~27.0%, compared to the vehicle control. These results demonstrated that sNPF can suppress the $Ca^{2+}$ activity of DN1 *in vivo*.

## DISCUSSION

Each day, neuronal activity patterns in the *Drosophila* pacemaker network proceed sequentially in a wave from lateral to dorsal aspects of the brain: the relative phases are such that each pacemaker group occupies a distinct temporal niche (Liang *et al.* 2016). To understand how this 24-h neural activity pattern is organized and regulated, we tested many of the known interactions between pacemakers. We found that light and the neuropeptides PDF and sNPF are involved. PDF released from M cells affects the sequence in two ways: it terminates $Ca^{2+}$ activity in M cells, and it delays $Ca^{2+}$ activations in E cells and DN3 cells away from a morning phase. The proper phase of the E cells is in fact the product of delay from both PDF and light signals. sNPF, released from M and E cells, is required for $Ca^{2+}$ rhythms in another pacemaker group, the DN1. We also found that light inputs arriving through both the internal photoreceptor CRYPTOCHROME and via the visual systems rapidly phase-shift $Ca^{2+}$ waves. Therefore, neuropeptides and light coordinately produce sequentially-timed outputs from a network of otherwise synchronous molecular pacemakers.

### Circadian pacemakers are coupled by neuropeptide-meditated inhibitions.

How can synchronous molecular clocks generate a pattern of sequential activities? We identified two neuropeptides, PDF and sNPF, that mediate much of the critical interactions between pacemaker groups to set the diverse $Ca^{2+}$ activity phases (Figure 8AB). First, we suggest that neuropeptide PDF delays the $Ca^{2+}$ activity peaks of the E cells (LNd/$5^{th}$ s-LNv) and DN3 groups, away from a morning phase they would otherwise share with the s-LNv. This model is based on four lines of evidence: (i) in both *pdf*$^-$ and *pdfr*$^-$ mutants, $Ca^{2+}$ activation in E cells and in DN3 were co-active at prospective dawn (Figure 1D & 2B); (ii) restoring *pdfr*

expression selectively to the LNd E cell-group autonomously delayed (rescued) their $Ca^{2+}$ activation to an evening phase, but produced no rescue on the DN3 phase (Figure 2C); (iii) ectopic PDFR by l-LNv delayed its $Ca^{2+}$ activation (Figure 4A-C); (iv) acute administration of synthetic PDF delayed $Ca^{2+}$ activation in E cells (LNd) and DN3; this delay increased with serial PDF administration (Figure 3E-I). Therefore, PDF staggers $Ca^{2+}$ activity phases between PDF-releasing neurons and PDF-receiving neurons by a cell autonomous, delay mechanism. However, our model cannot explain by what mechanism the same PDF signal causes different phase-delaying effects in $Ca^{2+}$ activity in the E cells (7.4±1.4h) versus in the DN3 (16.4±1.5h).

We also found that neuropeptide sNPF determines the rhythmicity and phase of DN1 $Ca^{2+}$ activity. Selectively impairing sNPF signals from M-cells (s-LNv) altered DN1 $Ca^{2+}$ phase (Figure 6B), while impairing sNPF signals from both groups severely diminished the amplitude of the DN1 $Ca^{2+}$ rhythms (Figure 6A). Together with the evidence that synthetic sNPF administration reduced DN1 $Ca^{2+}$ level (Figure 7), we suggest the following model. Without sNPF inhibition, DN1 $Ca^{2+}$ levels are constitutively high throughout the day with no evidence of a rhythmic change. A daily rhythm is imposed by sequential sNPF signals mediating daytime inhibition: strong inhibition from M cells in the morning is followed by more temperate inhibition from E cells in the afternoon. Thus, DN1 display an 'activity peak' during the nighttime, representing a period of dis-inhibition from sNPF released by the lateral pacemaker groups. These proposed sNPF effects on DN1 are further interesting in that both sNPF and the DN1 pacemakers have been implicated in the regulation of sleep (Shang *et al.* 2013; Guo *et al.* 2016). Consistent with previous observations (Hermann-Luibl, 2014), we found that all-pacemaker downregulation of sNPF increased night time locomotor activity (Figure 6G and S6B), which we interpret as the loss of night time sleep promotion by the mid-night activity peak

of the DN1s. In addition, we found M-pacemaker specific downregulation of sNPF impaired morning anticipatory activity (Figure 6H and S6C). We interpret this to indicate a suppression/delay of the morning locomotor activity peak by DN1 activity coincident with s-LNv activity. DN1s inhibit s-LNv neurons via glutamatergic transmission (Collins *et al.* 2012). Previous findings also suggest that DN1s integrate multiple circadian outputs and they regulate both morning and evening behavior (Zhang *et al.* 2010a, Zhang *et al.* 2010b, Cavanaugh *et al.* 2014). Our results suggest that both M cells and E cells modulate DN1s, which represents a convergence of sNPF signals, and thus provides a mechanistic basis to help explain the integrating function of DN1.

The $Ca^{2+}$ activity of the LNd appears highly correlated with the evening behavior. Yet, anomolously, in DD1 the LNd $Ca^{2+}$ phase of the $pdf^{01}$ mutant is advanced by ~ 8hr (Liang *et al.* 2016), while the phase of the evening behavior is only advanced by ~1.5 hr (Renn *et al.* 1999). How can this difference be reconciled with LNd control of the phase of the evening behavior? We propose the explanation involves a parallel delaying effect of light on the LNd pacemaker group, as revealed by measurements in $pdf^{01}$ mutants in an LD cycle (Figure 1): the net advance in the LNd $Ca^{2+}$ wave in that condition is only ~ 2 hr. Thus the phase of $Ca^{2+}$ activity in the LNd remains highly correlated in both WT and *pdf* mutant conditions with the phase of the evening behavior. Likewise, the phase of the $Ca^{2+}$ activity in the DN1 remains highly correlated in both WT and *sNPF* knockdowns with the presence, or the delay/absence of the morning peak of behavior. Together these data independently support the hypothesis that $Ca^{2+}$ dynamics in pacemaker neurons are inextricably linked to specific behavioral outputs.

Furthermore, we found that PDF and sNPF may modulate daily activity patterns broadly among different pacemaker groups by suppressing $Ca^{2+}$ activity (Figure 3A-D & Figure 7). In

the literature, the effects of PDF on neuronal activity in insects vary (Seluzicki *et al.* 2014; Vecsey *et al.* 2014). With functional expression of PDFR in *hEK-293* cells, PDF caused rapid elevations of both cAMP and $Ca^{2+}$ (Mertens *et al.* 2005). In contrast, our present studies mainly focused on the *in vivo* effects of PDF that develop over many hours. Previous studies also suggested long term cell inhibition by PDF signaling (Choi *et al.* 2012). The documented effects of sNPF are likewise varied (Root *et al.* 2011; Shang *et al.* 2013). Future studies that detail the actual signaling pathways leading from PDF and sNPF receptors to suppress $Ca^{2+}$ activities will be helpful.

We also found a suppressing effect of PDF on the M cell s-LNvs, mediated by the PDF receptor. We propose that negative feedback by PDF shortens the period during which s-LNv release PDF, and in so doing shortens the time window for PDF action across the pacemaker network. This model is based on two lines of evidence: selectively impairing the PDFR autoreceptor in s-LNv (i) prolonged s-LNv $Ca^{2+}$ activity further into the morning (Figure 2F) and (ii) delayed the $Ca^{2+}$ activation of LNd, DN3, and DN1, consistent with a longer duration of PDF-mediated delay (Figure 4G). Negative feedback by autoreceptors is a phenomenon common to many fast neurotransmitters. Choi *et al.* (2012)reported that chronic activation of PDFR autoreceptors (by a tethered-PDF design) increased morning behavioral activity. Thus, they argued that the PDFR autoreceptor normally regulates PDF secretion in a positive feedback mode. In that study, chronic PDFR autoreceptor activation also advanced the evening behavioral phase and shortened the free-running period under constant darkness. This phenotype is similar to those of both *pdf* and *pdfr* mutants (Renn *et al.* 1999; Hyun *et al.* 2005), two situations in which PDF signaling is diminished. By that analogy, we reason that PDFR autoreceptors may depress PDF secretion.

Our working model of phase control in the *Drosophila* circadian network suggests that morning (dawn) is the cardinal phase for periodic 24-h elevations of $Ca^{2+}$. Yet all pacemaker groups except the s-LNv normally display a non-morning phase: we have shown that they are forced to do so by a series of delaying signals, mediated by light and neuropeptides. This model builds on a strong foundation of work highlighting the importance of cell interactions to generate circadian rhythmicity as an emergent property from the *Drosophila* neuronal network (e.g., Renn *et al.* 1999; Peng *et al.* 2003; Grima *et al.* 2004; Lin *et al.* 2004; Stoleru *et al.* 2004; Dissel *et al.* 2014; Yao and Shafer, 2014). We have so far identified signals that delay all pacemaker groups except the l-LNv to display group-specific, non-morning phases of activity (Figure 8A). The l-LNv $Ca^{2+}$ phase was moderately altered by loss-of-function genetic manipulations for neuropeptide DH31 and the DH31-R1. However, the strength of the effects we observed were modest, suggesting other factor(s) regulating l-LNv $Ca^{2+}$ activity remain to be identified.

Based on our observations, we generated a quantitative model of coupled oscillators. By optimizing parameters for PDF and sNPF inhibition strength to each pacemaker group, this model fits the sequential pattern of the WT pacemakers' $Ca^{2+}$ activities. Importantly, it predicts pacemakers' $Ca^{2+}$ activity patterns for nearly all genetic manipulations performed in this study (Figure S8). With only a single exception, the model supports the contention that PDF and sNPF neuropeptide-mediated inhibitions are sufficient to explain much of the details of the $Ca^{2+}$ activity patterns in this pacemaker network. The exception is the failure to accurately predict the phenotype of PDFR overexpression in a *pdfr* mutant background that is shown in Figure 4D. Here DN3 and DN1 were both phase-shifted to a prospective dawn phase. Thus, DN1 $Ca^{2+}$ phases were unaltered by *pdf/pdfr* loss-of-function mutants, but, anomalously, they were altered by gain-of-function PDFR signaling. In fact, seven of the 15 DN1s normally express

endogenous PDFR (Im *et al.* 2011). Therefore, a possible explanation is that the altered $Ca^{2+}$ activity pattern we observed in this gain-of-function state represents the anomalous responses of the eight DN1 that are normally PDFR-negative. This single inconsistency between the theoretical model and the experimental observation also suggested that the interactions between DN1 and s-LNv might be reciprocal, as indicated by previous work (Collins *et al.* 2012; Guo *et al.* 2016). We also noted that M-cell-specific sNPF knockdown in the *pdfr* mutant background restored their morning anticipation behavior (Figure S6G), which was impaired in either *pdfr* mutant background or the M-cell-specific sNPF knockdown in a $pdfr^{+}$ background (Figure S1C & Figure 6H). This result reveals an unexpected interaction between sNPF and PDF signals and more complex interactions between pacemakers than have been so far described.

In the mammalian suprachiasmatic nucleus (SCN), circadian pacemaker neurons also show spatiotemporal patterns in $Ca^{2+}$ activity (e.g. Ikeda *et al.* 2003; Enoki *et al.* 2012). The activity patterns in SCN were disrupted by manipulating neuropeptidergic G-coupled signaling (Aton *et al.* 2006), suggesting that such patterns might also be regulated by neuropeptide-mediated interactions. SCN pacemaker $Ca^{2+}$ rhythms require ryanodine-sensitive $Ca^{2+}$ stores (Ikeda *et al.* 2003), but a complete understanding of how neuropeptidergic G protein-coupled signaling regulates these internal $Ca^{2+}$ stores is not yet at hand.

**PDF and light signaling pathways converge to set pacemakers' activity phases.**

We found that a 12:12 LD cycle delayed $Ca^{2+}$ activation in the E-cell LNd (Figure 1 and Figure 8A). The functional significance of the LNd $Ca^{2+}$ phase under the regulation of light is that LNd encodes the length of daytime (Liang *et al.* 2016). These results suggest that the PDF and light signaling pathways converge to set the phase of E-cell LNd $Ca^{2+}$ activity. Previous

studies have indicated a close interaction between PDF and light in the *Drosophila* circadian system. First, PDF receptor and the circadian photoreceptor CRY display coordinate expression by a subset of pacemakers (Im *et al.* 2011; Yao and Shafer, 2014). Second, *cry* interacts genetically with both *pdf* and *pdfr*, causing severe disruptions of molecular PER oscillations in E cells and behavioral rhythms (Cusumano *et al.* 2009; Zhang *et al.* 2009; Im *et al.* 2011). Third, PDF neurons use PDF to relay light inputs from visual systems to the rest of pacemaker network (Guo *et al.* 2014), suggesting that PDF signals may constitute critical parts of the network's light signaling pathways.

The balance between PDF and CRY signals may be crucial for light input processing. Indeed, when one signal is reduced, the other may become stronger (Guo *et al.* 2014). Responses to light pulses in molecular clocks (Li *et al.* 2014) and $Ca^{2+}$ rhythms (Figure S4CD) were larger in $pdf^{01}$ than in WT. Therefore, the coordinate actions of PDF and light signals affect all levels of the pacemaker network, from molecules to neurons to behavior. VIP signaling in the mammalian SCN appears orthologous to *Drosophila* PDF signaling in many respects (Vosko *et al.* 2007). Pharmacologically, VIP induced phase delays and 'phase tumbling' of molecular clocks among the SCN cells (An *et al.* 2013). Furthermore, VIP signaling is needed to encode seasonal information, as *VIP* knock out mice show greatly diminished adaptation to either long or short days (Lucassen *et al.* 2012). Finally, Hughes *et al.* (2015) recently showed that constant light improves rhythmicity in mice deficient for the VIP receptor. These observations suggest further parallelism between PDF and VIP signaling in coordination with light inputs.

**Light inputs change pacemaker interactions.**

Short light pulses regulate the molecular clock (Roberts *et al.* 2015) ; here we found they also regulate the 24-h neural activity patterns of circadian pacemakers within the first day post-stimulus. Both these changes preceded phase changes in rhythmic behavior, since the light-induced behavioral phase shift does not occur until in the second and third circadian cycle (Pittendrigh *et al.* 1958) (Figure S3A. Furthermore, in the first day post-stimulus, phase-delaying pulses rapidly delayed $Ca^{2+}$ phases in all pacemaker groups, while a phase-advancing light pulse only advanced that of the s-LNv. In the following two days, other pacemaker groups were gradually advanced, possibly driven by s-LNv. Recently, Eck *et al.* (2016) reported that directly activating all pacemakers could induce both behavioral phase advances and delays, while activating s-LNv alone could only induce phase advances, but not phase delays. Those outcomes appear consistent with our observations: phase-delaying effects may need all pacemaker groups responding in coordination, while phase-advancing effects only involve s-LNv responses; the latter then recruits other groups to subsequently advance.

These data lead us to re-consider the relationship between $Ca^{2+}$ dynamics and the molecular clock. We previously found that all $Ca^{2+}$ dynamics are lost in the chronic absence of the PER-based clock (Liang *et al.* 2016). Therefore, the mechanism underlying differential light responsiveness in $Ca^{2+}$ activities and behavioral effects (Figure 5) could be differential responsiveness in the molecular clocks (Lin *et al.* 2004; Yoshii *et al.* 2008). A phase-advancing light pulse instantaneously de-synchronizes molecular clocks among pacemaker groups *ex vivo*; they re-synchronize over the subsequent 2-3 cycles (Roberts *et al.* 2015). While more experiments are needed, the data at present lead us to suggest that phase shifts in molecular clocks cannot fully explain the phase shifts we observe in $Ca^{2+}$ activity patterns. The generation

of $Ca^{2+}$ rhythms within a specific group may likewise be independent of that cell's PER clock: the knockdown of sNPF (Figure 6) diminished the DN1 calcium activation without affecting the rhythm of the PER cycle in that pacemaker group. Thus $Ca^{2+}$ rhythms could be imposed by other pacemaker groups in a manner that is independent of the target pacemaker's PER-clock.

In summary, our study provides a new framework to help understand how 24-h neural activity patterns are generated in the *Drosophila* circadian pacemaker network. Among different groups of pacemakers, sequential oscillations in their neural activities are established by neuropeptide-mediated inhibition and delay (including by PDF and sNPF), and as well by light-mediated delay. These coupling mechanisms help ensure that dawn and dusk light pulses produce the appropriate advancing and delaying phase shifts for pacemaker entrainment (Meijer and Schwartz, 2003) and the proper sequencing of multiple, sequentially-timed neuronal outputs.

## EXPERIMENTAL MODEL AND SUBJECT DETAILS

## KEY RESOURCES TABLE

| REAGENT or RESOURCE | SOURCE | IDENTIFIER |
|---|---|---|
| Chemicals, Peptides, and Recombinant Proteins | | |
| Drosophila pigment dispersing factor (PDF) | Neo-MPS | NA |
| Drosophila small neuropeptide F-2 | Gift from P. Evans, (Feng *et al.* 2003) | NA |
| Experimental Models: Organisms/Strains | | |
| Drosophila: *tim(UAS)-gal4* | *(Blau and Young, 1999)* | NA |
| Drosophila:*pdfr(B)-gal4* | Taghert Lab, *(Im and Taghert, 2010)* | NA |
| Drosophila:*pdf-gal4* | Taghert Lab, *(Renn et al. 1999)* | NA |
| Drosophila:*c929-gal4* | Taghert Lab, *(Hewes et al. 2003)* | NA |
| Drosophila:*pdf-gal80* | *(Stoleru et al. 2004)* | NA |
| Drosophila:*20XUAS-IVS-GCaMP6s(attP40)* | Bloomington *(Chen et al. 2013)* | BL#42746 |
| Drosophila:*13XLexAop2-IVS-GCaMP6s-p10(su(Hw)attP1)* | Bloomington *(Chen et al. 2013)* | BL#44274 |
| Drosophila: *UAS-mCherry.NLS* | *(Caussinus et al. 2008)* | NA |
| Drosophila: *UAS-pdfr-16* | Taghert Lab, (Mertens *et al.* 2005) | NA |
| Drosophila: UAS-*sNPF* | *(Lee et al. 2004)* | NA |
| Drosophila: *cry-LexA::GAD* | F. Rouyer (CNRS Gyf, Paris) | NA |
| Drosophila: *GMR_SS00681-Gal4* | H. Dionne, A. Nern and G. Rubin (Janelia Research Center, VA) | NA |
| Drosophila: *GMR_MB122B-Gal4* | H. Dionne, A. Nern and G. Rubin (Janelia Research Center, VA) | NA |
| Drosophila: $cry^{01}$ | (Dolezelova *et al.* 2007) | NA |

| | | |
|---|---|---|
| Drosophila: *per*$^{01}$ | (Konopka and Benzer, 1971) | NA |
| Drosophila: *pdfr*$^{han5403}$ | (Hyun *et al.* 2005) | NA |
| Drosophila: *pdf*$^{01}$ | Taghert Lab, (Renn *et al.* 1999) | NA |
| Drosophila: *Dh31*$^{01}$ | E. Johnson (Wake Forest, NC) | NA |
| Drosophila: *CG4395*-RNAi | VDRC | GD724 |
| Drosophila: *CG17415*-RNAi | TRiP, Bloomington | TRiP.JF01945 |
| Drosophila: *sNPF-R*-RNAi | VDRC | GD661 |
| Drosophila: *sNPF*-RNAi | TRiP, Bloomington | TRiP.JF01906 |
| Drosophila: *ITP*-RNAi | TRiP, Bloomington | TRiP.JF01817 |
| Drosophila: *NPF*-RNAi | TRiP, Bloomington | TRiP.JF02444 |
| Drosophila: *NPFR*-RNAi | VDRC | KK112704 |
| Drosophila: *UAS-dcr2* | Bloomington | BL#24648 |
| Software and Algorithms | | |
| MATLAB | MathWorks | Version: R2015b |
| R | http://www.R-project.org | Version: 3.3.3 |
| Prism 7 | GraphPad | https://www.graphpad.com/ |
| Fiji | (Schindelin *et al.* 2012) | https://fiji.sc/ |
| Imagine | (Holekamp *et al.* 2008) | http://holylab.wustl.edu/ |

Fly Rearing and Stocks

Flies were reared at room temperature on standard yeast-supplemented cornmeal/agar food. Males were entrained under 12 h light: 12 h dark (LD) cycles at 25°C for at least 3 days. The *tim>GCaMPS6s, mCherry; cry*$^{01}$ flies were entrained for more than 6 days.

The *cry-LexA::GAD* line was a gift from Dr. F Rouyer (CNRS Gyf, Paris): it is strongly expressed in CRY-expressing neurons and shows weaker expression in other clock neurons in addition to some non-clock cells, similarly to the *cry*-Gal439 pattern described by Klarsfeld *et al.* (2004). *cry-LexA* was recombined with *LexAop-GCaMP6s* into the same third chromosome. RNAi was tested along with *UAS-dcr2* to increase the efficiency of RNAi-

mediated knockdown. A stable line: *UAS-dcr2; tim(UAS)-gal4; UAS-GCaMP6s, UAS-mCherry.NLS* was created for RNAi screening of neuropeptides and their receptors. This line was then crossed with individual RNAi lines. In male progeny from these crosses, we measured locomotor behavior and calcium rhythms. Table S1 provides the complete genotype for flies used in this study. The age/developmental stage of experimental models was 3-10 days after eclosion.

**METHOD DETAILS**

Light stimulation

Light stimulation before or during *in vivo* calcium imaging was delivered by a white Rebel LED (Luxeon) that was powered by a LED driver (350 mA, externally dimmable, BuckPuck DC driver). The output of the driver was controlled by an Arduino UNO board (Smart Projects, Italy). The Arduino was timed by a real-time clock module (DS3231). The light intensity was measured by light meter (W/RS-232, VWR Scientific) and adjusted to ~3000 lux.

For the light stimulation before calcium imaging, the LED was programmed to deliver the first regular 12 h light: 12 h dark (LD) cycles followed with constant darkness (DD). During the dark period, 15 min light pulse was delivered 5 h (CT17), 9 h (CT21), or 21 h (CT9) after light off. The flies that received light stimulation remained in darkness for different periods of time (varying from 3 to 62 hr) and then underwent surgery. We previously described the surgical procedure (Liang *et al.* 2016): briefly, the pacemaker neurons on one side of the brain were exposed by removing a portion of the dorso-anterior head capsule on one side of the head. The entire surgery was typically 20 min in duration, and was performed under dim red light to avoid additional light stimulation. Immediately after surgery, *in vivo* 24-h calcium imaging was

performed. Different 24h calcium imaging sessions were systematically tiled to create synthetic, uninterrupted ~72 h observation periods. For the light stimulation during calcium imaging, we performed surgery on flies that previously entrained to a 12:12 LD cycle and began imaging at the beginning of the dark period. During the imaging, the LED delivered a 15 min light pulse at CT17 (5 h after light-off). For the LD cycle stimulation during calcium imaging, the 24-h calcium imaging sessions began systematically at different Zeitgeber times (ZT). The LED delivered the 12 h light: 12 h dark cycles according to the original schedule by which the flies were entrained. During the light period, the LED was shut off for 10 seconds every 10 min, allowing the microscope to acquire complete volume brain scans.

*In vivo* calcium imaging

Imaging was performed on a custom Objective Coupled Planar Illumination (OCPI) microscope (Holekamp *et al.* 2008), as described in (Liang *et al.* 2016). Briefly, OCPI illuminated samples with a ~5µm thick light sheet set to the focal plane of the objective. The light sheet was generated from a 488nm laser that went through an optical fiber, a light collimator and light sheet–forming cylindrical lens. The objective was a water-immersion 0.5NA 20× (Olympus). Images were captured on an iXon DV885-KCS-VP cooled EM-CCD (Andor). The microscope was operated by a custom software (Imagine). To characterize the circadian properties of neural activity, GCaMP6s signals from circadian neurons were imaged every 10 min for 24 hr. Each stack of images was acquired by scanning the light sheet across the fly brain through the cranial window. Stacks contained 20 to 30 separate images with step size of 10 microns. The total scanning time for each brain stack was less than 3s. During the 24-h imaging, fresh haemolymph-like saline (HL3), containing 70 mM NaCl, 5 mM KCl, 1.5 mM CaCl2, 20 mM

MgCl2, 10 mM NaHCO3, 5 mM trehalose, 115 mM sucrose, and 5 mM HEPES (pH 7.1), was perfused continuously (0.1-0.2 mL/min). For experiments that included light stimulation and pharmacological treatments, two brains were imaged simultaneously.

Pharmacology

For pharmacological tests of PDF during 24 h $Ca^{2+}$ imaging *in vivo* (Fig 7A-B), imaging was started at CT0. ~10 minutes prior to the start of recording, PDF was pre-mixed in the bath at $10^{-5}$ M (the first dose at CT0). In the double PDF application experiments (Fig 7B), a second dose of PDF was added dropwise to the bath at CT5 (1mL of $10^{-4}$ M PDF solution added into the 10 ml bath over a ~10 s period). For pharmacological tests of PDF during 6 h $Ca^{2+}$ imaging *in vivo* (Fig 7D-E), $Ca^{2+}$ imaging started at CT6. PDF (1mL of $10^{-4}$ M PDF) was then added dropwise over a ~10 s period to the 10 ml bath at CT7.

For pharmacological tests of sNPF during 12 h $Ca^{2+}$ imaging *in vivo*, flies were separately entrained to LD schedules with an 8h phase difference for at least 3 days before experiments. Therefore, for one fly of the pair, the $Ca^{2+}$ imaging was started at CT4, while for the other it started at CT12. sNPF-2 (1mL of $10^{-4}$ M) was then added dropwise to the bath over a ~10 s period one hour after $Ca^{2+}$ imaging was started (CT5 for one fly and CT13 for the other).

In all drug experiments, fresh HL3 saline was perfused continuously at a rate comparable to that of other experiments. Using bromophenol blue measurements, we estimate the perfusion system reduced the concentration of free PDF in the solution bathing the brain by 10-fold over 7 hr. PDF was purchased from Neo-MPS (San Diego, CA, USA) at a purity of 86%. sNPF-2 was kindly provided by Dr. P. Evans (Cambridge, U.K.).

Locomotor activity

The locomotor activity of 4-6 day old male flies was recorded using Trikinetics Activity Monitors. Flies were entrained to 12:12 h LD cycles for 6 days and then released into constant darkness (DD) for 9 days.

Mathematical Modeling

The quantitative model of oscillators coupled with PDF- and sNPF-mediated suppressions was generated in R 3.3.2. The $Ca^{2+}$ rhythms of five circadian pacemaker groups were simplified as five identical simple harmonic oscillators. The $Ca^{2+}$ level (x) for each group was set to oscillate with a 24 h period:

$$\frac{d^2x}{dt^2} = -\left(\frac{12}{\pi}\right)^2 x$$

For pacemaker groups those release the designated neuropeptides (PDF and/or sNPF), the peptides were released when the $Ca^{2+}$ level reached a threshold ($\theta_{release}$). Levels of secreted neuropeptide (P) decayed at a constant rate ($k_{decay}$) and followed the equation:

$$\frac{dP}{dt} = N(x - \theta) - k_{decay}P$$

N was a binary parameter representing whether the pacemaker group expresses a specific neuropeptide. The suppressing effect of neuropeptides on the $Ca^{2+}$ level of a pacemaker group followed this equation once the neuropeptide level achieved a threshold ($\theta_{effect}$):

$$\frac{dx}{dt} = x + \sum Rk_{effect}P$$

R was a binary parameter representing whether a pacemaker group expresses the specific PDF and/or the sNPF neuropeptide receptor. $k_{effect}$ was a constant for the strength of neuropeptide effects.

The model was fit to experimental data of $Ca^{2+}$ phases in five pacemaker groups in WT controls shown in Figure 2B with parameter values: $\theta_{release.PDF}$=0.17, $k_{decay.PDF}$=0.55, $\theta_{effect.PDF.s\text{-}LNv}$= 0.37, $\theta_{effect.PDF.l\text{-}LNv}$= 0.50, $\theta_{effect.PDF.LNd}$= 0.36, $\theta_{effect.PDF.DN3}$= 0.46, $\theta_{effect.PDF.DN1}$= 1.69, $k_{effect.PDF.s\text{-}LNv}$=-0.79, $k_{effect.PDF.LNd}$=-0.73, $k_{effect.PDF.l\text{-}LNv}$=-2.00, $k_{effect.PDF.DN3}$=-1.41, $k_{effect.PDF.DN1}$=-1.18, $\theta_{release.sNPF.s\text{-}LNv}$=0.37, $\theta_{release.sNPF.LNd}$=0.91, , $k_{decay.PDF}$=0.10, $\theta_{effect.sNPF.DN1}$=0.09, and $k_{effect.sNPF.DN1}$=-1.03.

Based on these parameters and initial values of x for each groups ($x_{s\text{-}LNv}$=1; $x_{l\text{-}LNv}$=0.09, $x_{LNd}$=1, $x_{DN3}$=1, and $x_{DN1}$=0), we added or removed neuropeptide interactions by manipulating the N and R values for each group to predict the $Ca^{2+}$ phases in genetic manipulations done in this study. The differential equations were solved using lsoda solver.

Replication

For all *in vivo* calcium imaging experiments, at least 5 biological replications have done for each genotype and/or condition. For all behavioral experiments, at least 8 biological replications have done for each genotype and/or condition.

Strategy for randomization and/or stratification

In order to avoid the influence of the imaging preparation and any unknown temporal factor in the ambient recording environment, 24 hour recording sessions were randomly began at different Zeitgeber times (ZT) except for pharmacological experiments, which were began at the same ZT.

In light pulse stimulation experiment (Figure 5 and Figure S3), 24 hour recording sub-sessions were began after the flies receiving light stimulation and remaining in darkness for random periods of time (varying from 3 to 62 hr).

Blinding at any stage of the study

The information about genotypes, light or pharmacological treatments, and the circadian time for each recording was blinded at the stage of image processes, ROIs selection, and time traces measurements.

Sample-size estimation and statistical method of computation

The sample size information was listed along with any statistical method used in figure legend.

Inclusion and exclusion criteria of any data or subjects

The behavioral data of flies died during the analysis window (Day 1-6 in LD and Day 1-9 in DD) was excluded. In calcium imaging data, any group of pacemakers that didn't display detectable signal throughout entire recording period (usually 24 hours) was not included.

## QUANTIFICATION AND STATISTICAL ANALYSIS

Imaging data analysis

Calcium imaging data was analyzed as described in (Liang *et al.* 2016). Images were processed in MATLAB R2015b (MathWorks, Natick, MA, USA) using custom software described previously (Holekamp *et al.* 2008) and ImageJ-based Fiji. Regions of interest (ROIs) were manually selected over individual cells or groups of cells. Average intensities of ROIs were

measured through the time course and divided by average of the whole image to subtract background noise. For each time trace, the calcium transient was then calculated as $dF/F=(F-F_{min})/F_{mean}$. The phase relationship between traces was estimated by cross-correlation analysis. Phases of traces were plotted on a 24-hr-clock circular plot reflecting both peak time and phase relationship of traces. This phase relationship was then tested statistically by the Rayleigh test of uniformity and the Watson-Williams test for homogeneity of means (Levine *et al.* 2002). For the light pulse stimulation experiments, as the $Ca^{2+}$ dynamics were expected to vary among three circadian cycles, additional analysis was applied as described immediately following.

In light pulse stimulation experiments, traces were aligned by the time after the light pulse. 24-h traces from different animals, which were distributed and overlaid within three day period after light pulses, were then merged to simulate a continuous three day record. In other experiments, traces were aligned by Zeitgeber Time. Traces of the same cell type were then averaged across different animals.

Peak phases in three cycles after light pulses were estimated separately by cross-over analysis, because the circadian cycles might be phase-shifted and mismatched between cell types. For each cell type, averaged traces were first filtered by 8 hr, and then by 24 hr. The crossover points of two different filtered traces were identified as rising and falling phase markers for each cycle. In each cycle, the local maximum between the rising and falling phase markers was then identified as the peak phase. After identifying the peak phase of the averaged trace, traces from different animals falling in that cycle were then pooled together to estimate the phase coherence among these animals. In other experiments (no light pulses), all traces were considered within the same cycle. The phase relationship between traces from the same cycle was estimated by cross-correlation analysis. Phases of traces were plotted on a 24-hr-clock circular plot reflecting

both peak time and phase relationship of traces. This phase relationship was then tested statistically by the Rayleigh test of uniformity and the Watson-Williams test for homogeneity of means (Levine *et al.* 2002). Trace analyses and statistics were performed using R 3.3.3 and Prism 7 (GraphPad, San Diego CA).

Behavioral experiment analysis

Locomotor activity from DD Days 1–9 was then normalized for a $\chi^2$ periodogram with a 95% confidence cutoff and SNR analysis, to estimate circadian rhythmicity (Levine *et al.* 2002). Arrhythmic flies were defined by a power value less than 10 and width lower than 1, or a period less than 18, or more than 30 h. Data were analyzed in R 3.3.3 and MATLAB R2015 (MathWorks, Natick, MA, USA).

Fig 1

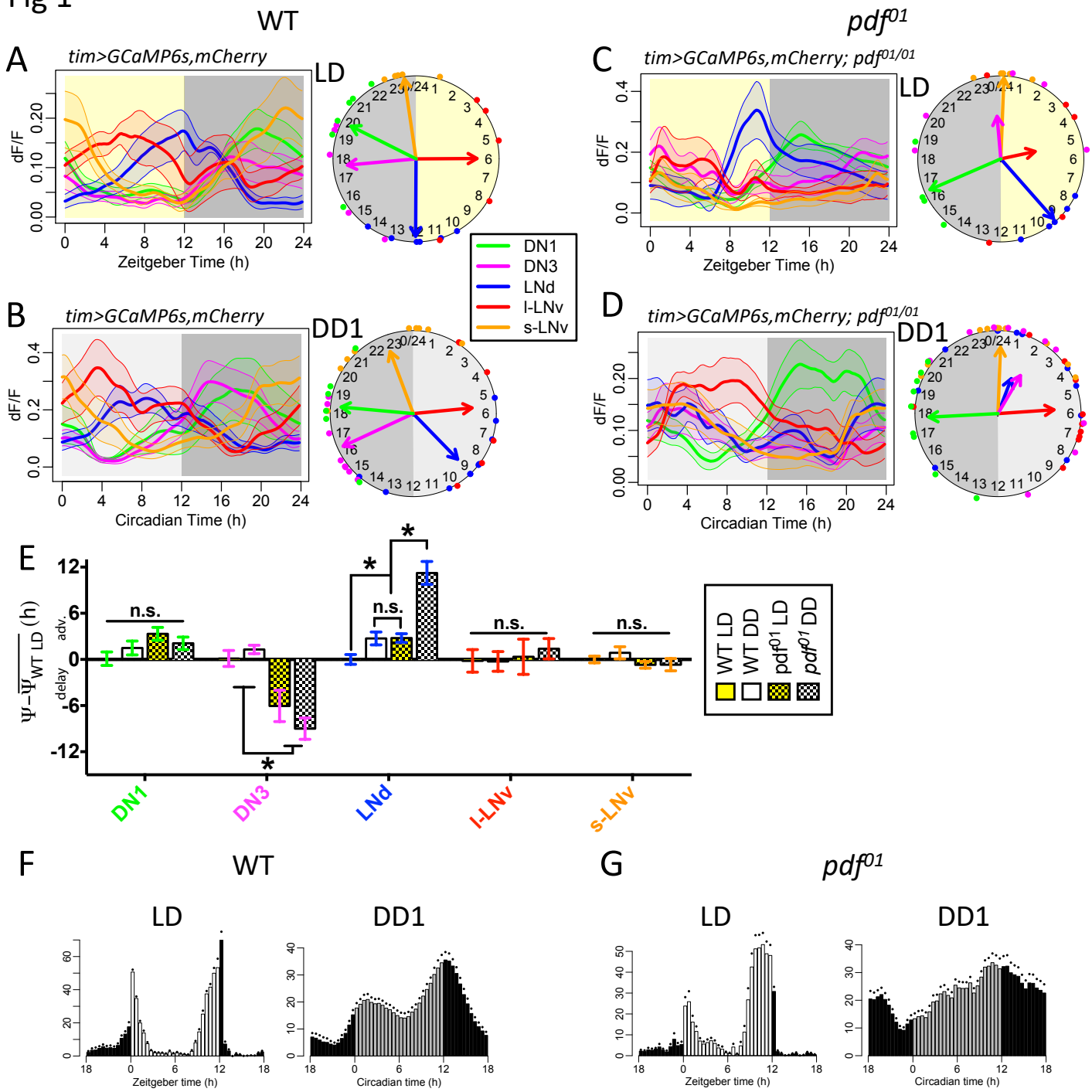


**Figure 1. PDF and cyclic light-dark conditions phase-delay the $Ca^{2+}$ rhythm of E-pacemaker LNd.**
(A) Daily $Ca^{2+}$ activity patterns of five major *Drosophila* circadian pacemaker groups in wild type (WT) flies under 12h light: 12h dark (LD) cycle (n = 6 flies). Left, average $Ca^{2+}$ transients. Right, $Ca^{2+}$ phase distribution: each colored dot represents calculated peak phase of one group in one fly; colored arrows are mean vectors for different groups; the arrow magnitude describes the $Ca^{2+}$ phase coherence among different flies in a specific pacemaker group. Yellow aspect indicates 12 h period of light stimulation. (B) Daily $Ca^{2+}$ activity patterns in WT flies under constant darkness (DD) conditions (n = 12 flies). Darker gray aspect indicates subjective night. (C) Daily $Ca^{2+}$ activity patterns in *pdf*$^{01}$ mutants under LD cycle (n = 5 flies). (D) Daily $Ca^{2+}$ activity patterns in *pdf*$^{01}$ mutants under DD (n = 11 flies). (E) Quantification of $Ca^{2+}$ phase shifts described in panels (A-D). The mean phase of each group in WT controls under LD is set to zero (*p<0.01: Watson-Williams test). Error bars denote SEM. (F) Average locomotor activity of WT flies (n = 16 flies) in LD cycles (averaged across 6 days) and in the first day under DD (DD1). Dots indicate SEM. (G) Average locomotor activity of *pdf*$^{01}$ mutants (n = 15 flies) in LD and DD1.

Fig 2

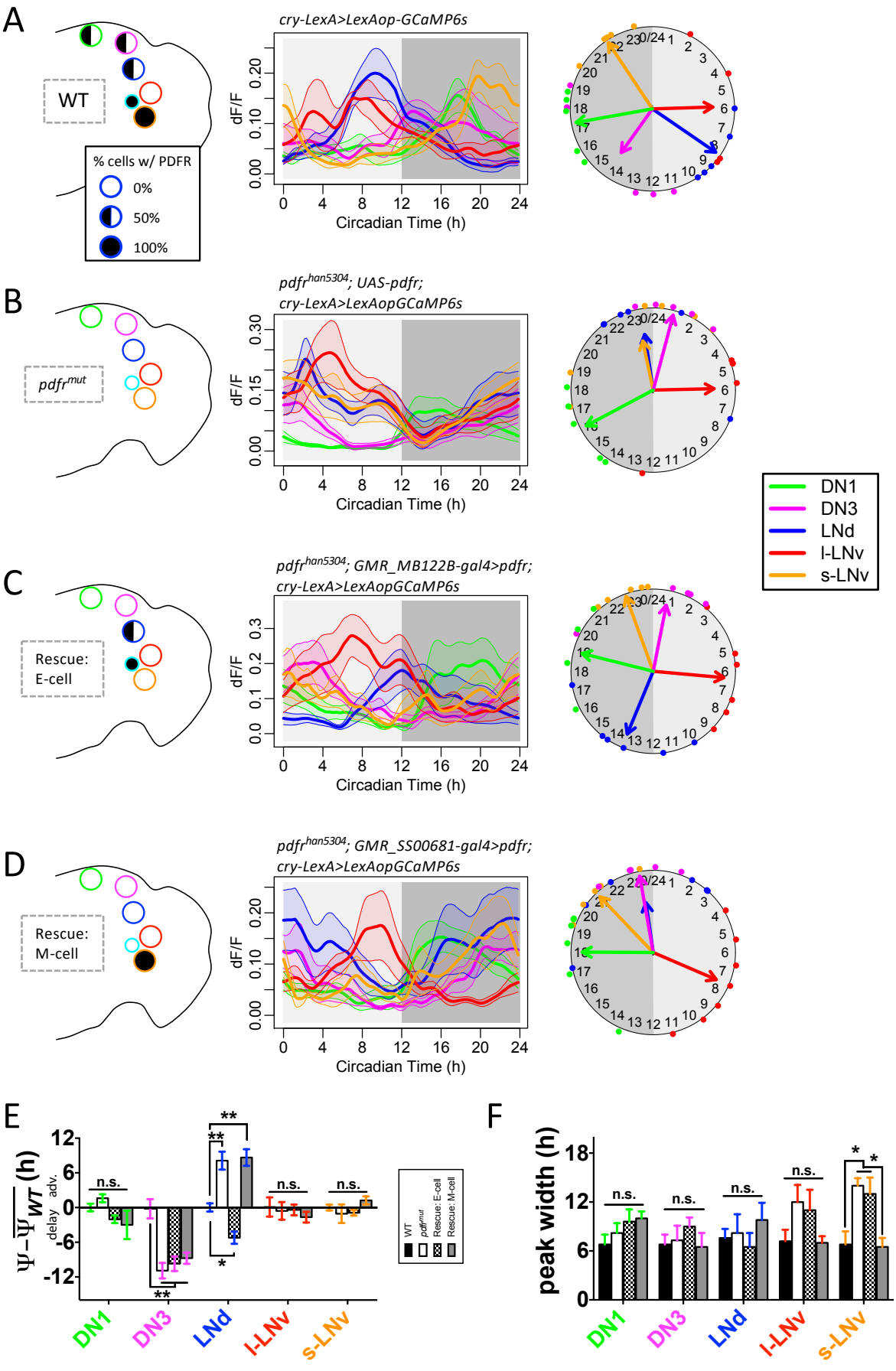
A
WT
% cells w/ PDFR
0%
50%
100%
cry-LexA>LexAop-GCaMP6s
dF/F
Circadian Time (h)
B
pdfr^mut
pdfr^han5304; UAS-pdfr;
cry-LexA>LexAopGCaMP6s
C
Rescue: E-cell
pdfr^han5304; GMR_MB122B-gal4>pdfr;
cry-LexA>LexAopGCaMP6s
D
Rescue: M-cell
pdfr^han5304; GMR_SS00681-gal4>pdfr;
cry-LexA>LexAopGCaMP6s
DN1
DN3
LNd
l-LNv
s-LNv
E
Ψ−Ψ_WT (h)
delay adv.
n.s.
WT
pdfr^mut
Rescue: E-cell
Rescue: M-cell
F
peak width (h)

**Figure 2. PDFR signaling regulates $Ca^{2+}$ rhythms in M and E pacemakers by cell autonomous mechanisms.**

(A-D) Daily $Ca^{2+}$ activity patterns of five major pacemaker groups under DD (A) in WT flies (n = 5 flies), (B) in *pdfr* mutants (n = 6 flies), (C) in an E cell rescue design - wherein E pacemakers (three out of six LNd and the $5^{th}$ s-LNv) express PDFR in the *pdfr* mutant background (n = 6 flies), and (D) in an M cell rescue – wherein flies with M pacemakers (four PDF-positive sLNv) express PDFR in the *pdfr* mutant background (n = 8 flies). Left, schematics of PDFR expression patterns in major pacemaker groups. Filled circles indicate all cells in the group express PDFR. Half circles indicate approximately half of cells in the group express PDFR. Middle, average $Ca^{2+}$ transients. Right, $Ca^{2+}$ phase distributions.

(E) Quantification of $Ca^{2+}$ phase shifts described in panels (A-D). The mean phase of each group in WT controls under DD is set to zero (*$p<0.05$, **$p<0.01$, and n.s. - not significant: Watson-Williams test). Error bars denote SEM.

(F) Quantification of peak widths (the full width at half maximum) for $Ca^{2+}$ transients in all groups and conditions (*$p<0.05$: Two-way ANOVA, followed by Bonferroni *post hoc* test).

Fig 3

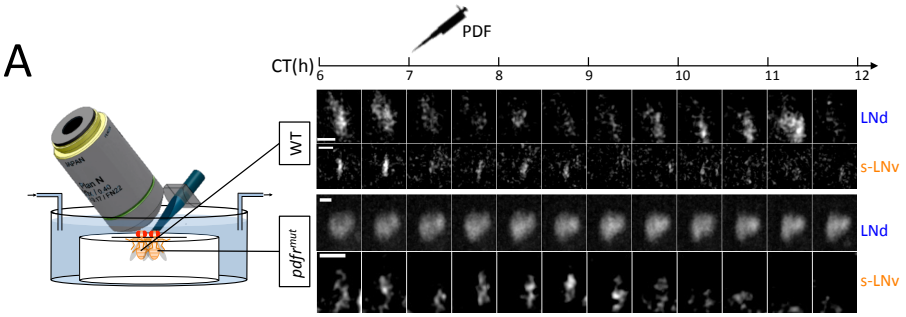


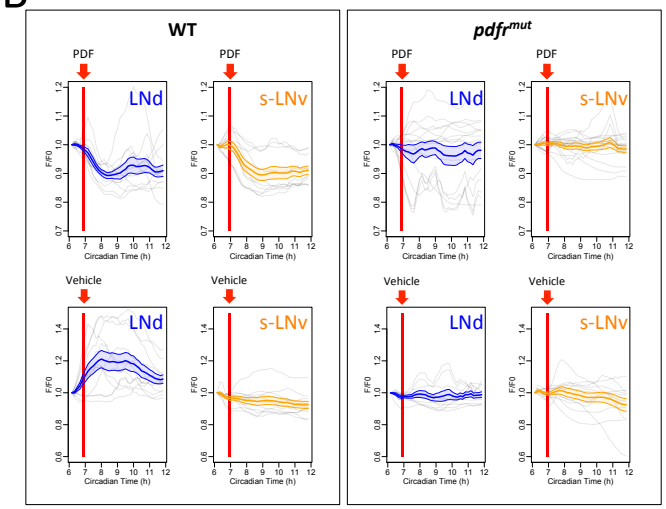


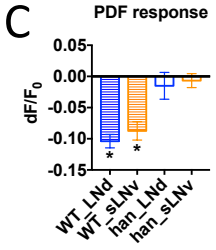


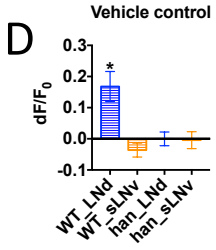


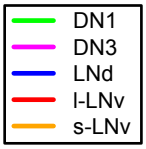


*tim>GCaMP6s,mCherry; pdf^01/01*

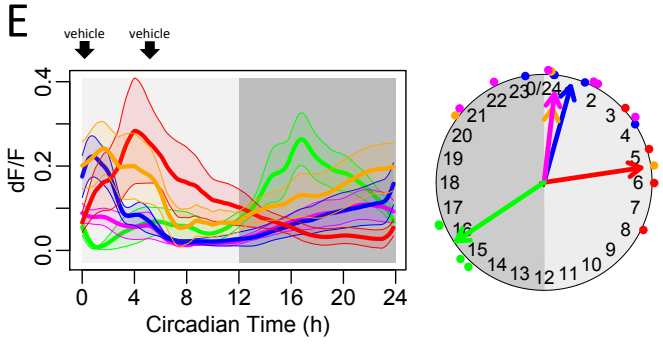


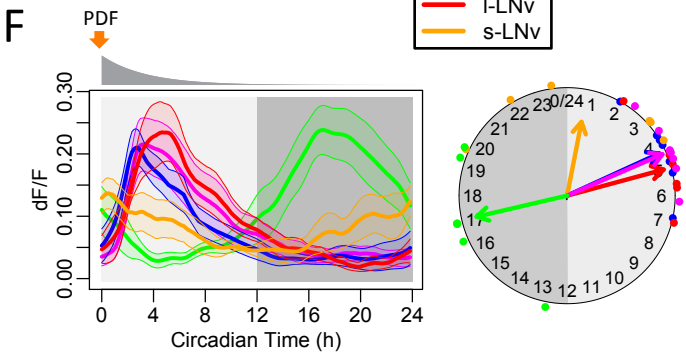


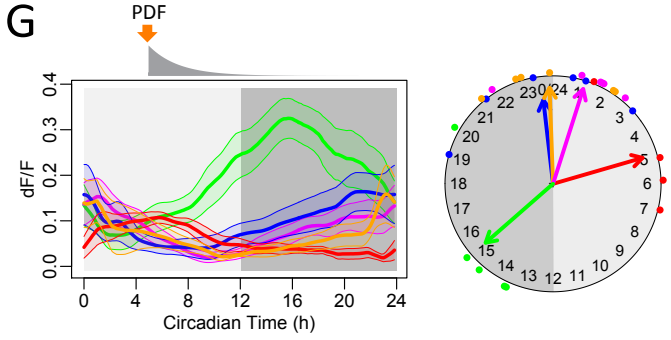


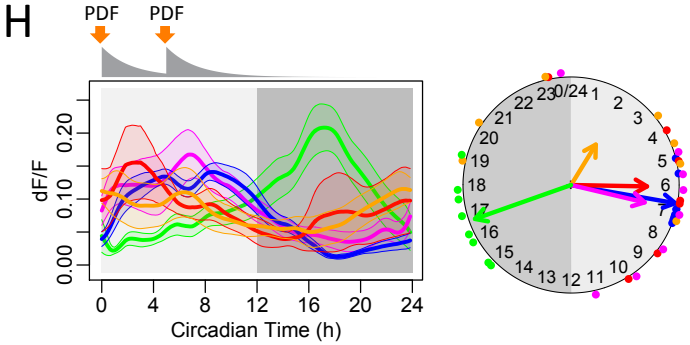


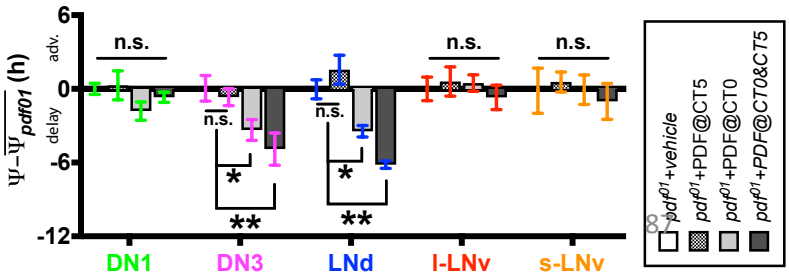

**Figure 3. Synthetic PDF application suppresses and/or delays $Ca^{2+}$ activity *in vivo*.**
(A) Left, schematic illustrating yoked pairs of WT and *pdfr* mutant flies for pharmacological tests. Right, representative images of LNd and s-LNv pacemakers in such *Drosophila* pairs responding differentially to $10^{-05}$M synthetic PDF. Axis above denotes the circadian time of recordings and the CT7 time point of synthetic PDF application.
(B) Averaged $Ca^{2+}$ transients of M pacemakers (s-LNv, orange) and E pacemakers (LNd, blue) responding to (top) PDF or (bottom) vehicle from (left) WT or (right) *pdfr* mutant flies. Gray traces represent individual cells in trials (PDF: n = 5 pairs; vehicle: n= 4 pairs).
(C-D) $Ca^{2+}$ signal changes by (C) PDF treatment or (D) vehicle treatment measured at the point that WT pacemakers displayed a maximal reduction in response to PDF (*$p<0.01$: single-sample t-test). The average increase in $Ca^{2+}$ signals in WT LNd with vehicle treatment represents their normal daily $Ca^{2+}$ peak that occurs during these recording periods (cf. Figure 1C).
(E) $Ca^{2+}$ activity responses in $pdf^{01}$ mutants to application of vehicle saline at the time indicated by vertical arrows under DD (n = 6 flies).
(F) $Ca^{2+}$ activity responses in $pdf^{01}$ mutants to single synthetic PDF application under DD (n = 5 flies). PDF was present in the initial saline bath as indicated by the vertical orange arrow at a peak concentration of $10^{-5}$ M. This initial time point represents the peak time of $Ca^{2+}$ in s-LNv (CT0 – orange arrow). PDF was slowly washed out by perfusion (gray curve below the orange arrow denotes PDF concentration).
(G) $Ca^{2+}$ activity responses in $pdf^{01}$ mutants to single synthetic PDF application at CT5 under DD (n = 6 flies).
(H) $Ca^{2+}$ activity responses to two serial applications of synthetic PDF in $pdf^{01}$ mutants under DD (n = 6 flies). The first dose was at CT0 (as in panel F), and the second at CT5 (~ at the l-LNv $Ca^{2+}$ peak time) both denoted by vertical orange arrows; constant perfusion followed each application.
(I) Quantification of $Ca^{2+}$ phase shifts produced by synthetic PDF; the mean phase of each group in $pdf^{01}$ mutants under DD is set to zero (*$p<0.05$: Watson-Williams test).

Fig 4

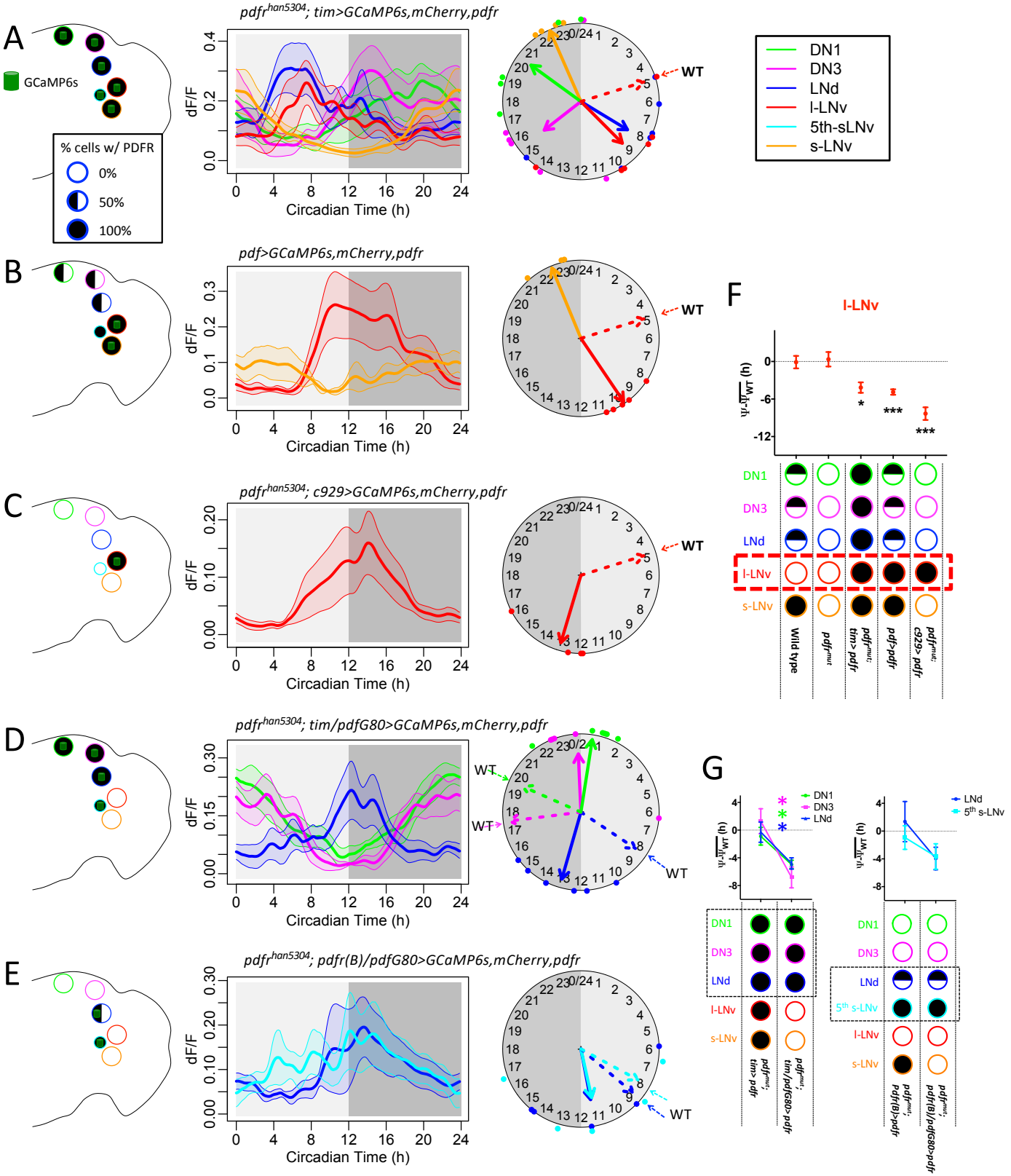
A
GCaMP6s
% cells w/ PDFR
0%
50%
100%
pdfr^han5304; tim>GCaMP6s,mCherry,pdfr
dF/F
Circadian Time (h)
WT
DN1
DN3
LNd
l-LNv
5th-sLNv
s-LNv
B
pdf>GCaMP6s,mCherry,pdfr
C
pdfr^han5304; c929>GCaMP6s,mCherry,pdfr
D
pdfr^han5304; tim/pdfG80>GCaMP6s,mCherry,pdfr
E
pdfr^han5304; pdfr(B)/pdfG80>GCaMP6s,mCherry,pdfr
F
l-LNv
Ψ-Ψ_WT (h)
Wild type
pdfr^mut
pdfr^mut; tim> pdfr
pdf>pdfr
pdfr^mut; c929> pdfr
G
LNd
5th s-LNv
pdfr^mut; tim/pdfG80> pdfr
pdfr^mut; PdfR(B)>pdfr
pdfr^mut; pdfr(B)/pdfG80>pdfr

**Figure 4. PDFR signaling delays $Ca^{2+}$ activation in diverse pacemakers.**
(A-E) Daily $Ca^{2+}$ activity patterns of five major pacemaker groups under DD (A) in flies with all pacemakers over-expressing PDFR in *pdfr* mutants (n = 6 flies); (B) in flies with PDF-positive neurons (s-LNv and l-LNv) over-expressing PDFR in an otherwise WT background (n = 5 flies); (C) in flies with l-LNv over-expressing PDFR in *pdfr* mutants (n = 6 flies); (D) in flies with l-LNv alone over-expressing PDFR (by *c929*-gal4) in *pdfr* mutants (n = 4 flies); (D) in flies with all pacemakers except PDF-positive neurons over-expressing PDFR in *pdfr* mutants (n = 6 flies); and (E) in flies with E pacemakers (three out of six LNd and the 5$^{th}$ s-LNv) expressing PDFR in *pdfr* mutants (n = 5 flies). Dashed arrows on the clock face indicate the mean phases of those groups in WT flies (cf. Figure 1A).
(F) Quantification of l-LNv $Ca^{2+}$ phase shifts described in panels (A-C). The mean phase of each group in WT controls under DD is set to zero (cf. Figure 1C; *$p<0.05$, ***$p<0.001$: Watson-Williams test).
(G) Quantification of $Ca^{2+}$ phase shifts in PDF-negative, PDFR-positive pacemakers described in panels (D-E). The mean phase of each group in WT controls under DD is set to zero (cf. Figure 1C; the colors of the asterisks correspond to the cognate pacemaker groups; *$p<0.001$: Watson-Williams test).

Fig 5

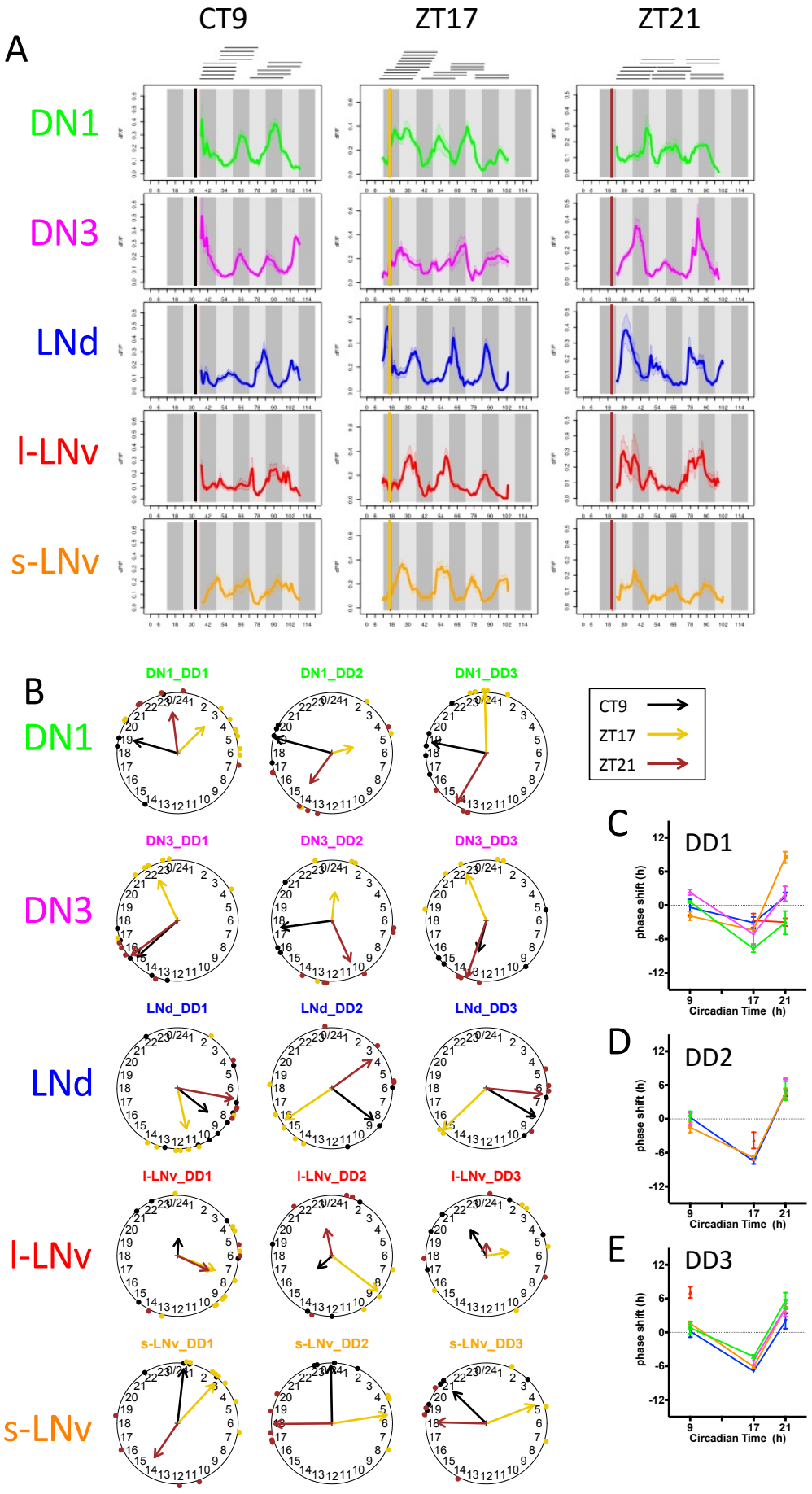
A
CT9
ZT17
ZT21
DN1
DN3
LNd
l-LNv
s-LNv
B
DN1_DD1
DN1_DD2
DN1_DD3
DN3_DD1
DN3_DD2
DN3_DD3
LNd_DD1
LNd_DD2
LNd_DD3
l-LNv_DD1
l-LNv_DD2
l-LNv_DD3
s-LNv_DD1
s-LNv_DD2
s-LNv_DD3
CT9
ZT17
ZT21
C
DD1
D
DD2
E
DD3
phase shift (h)
Circadian Time (h)

**Figure 5. Light pulses phase-shift circadian pacemaker $Ca^{2+}$ rhythms *in vivo*.**
(A) Averaged $Ca^{2+}$ transients in the five circadian pacemaker groups in the three days following 15 min light pulses delivered either in the dead zone (CT9), or in the phase-delay zone (ZT17), or in the phase-advance zone (ZT21). Bars indicate the time of light pulses. Horizontal lines on top indicate separate 24 h imaging sessions for individual flies that were tiled to synthesize three-day patterns (CT9: n = 14 flies; ZT17: n = 18 flies; ZT21: n = 14 flies).
(B) $Ca^{2+}$ phase distributions of five circadian pacemaker groups in three circadian cycles immediately following the three different light pulse stimuli: CT9, ZT17, and ZT21.
(C-E) $Ca^{2+}$ phase response curves (PRC) plotted over the course of the three circadian cycles: (C) day one, (D) day two, and (E) day three. The $Ca^{2+}$ phase shifts compared to $Ca^{2+}$ phases in unstimulated flies (from Figure 1A) after three different light pulse stimuli. Phase-shifts that lacked coherence ($p>0.05$: Rayleigh test) were excluded.

Fig 6

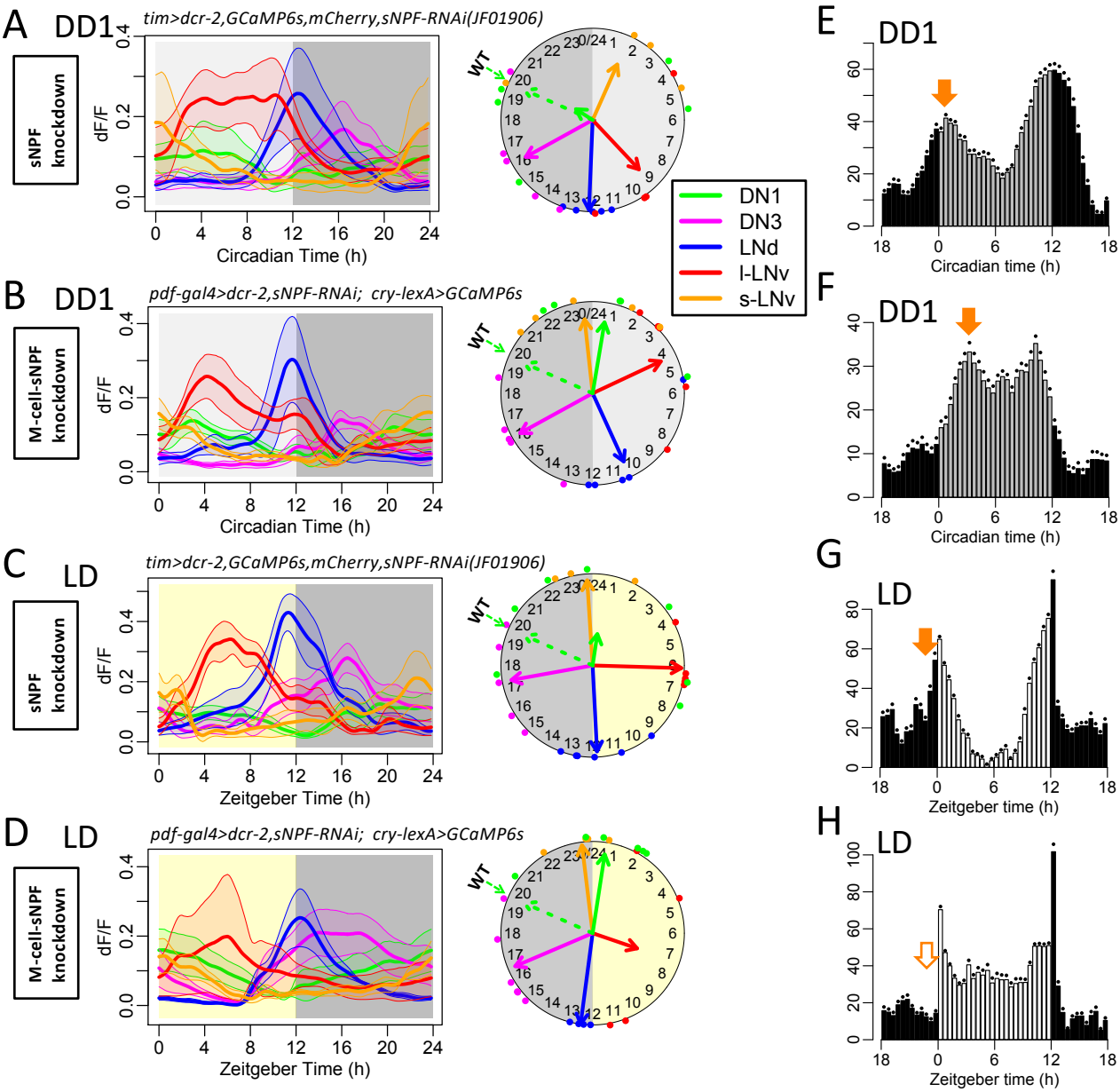


**Figure 6. sNPF is required for DN1 $Ca^{2+}$ rhythms *in vivo*.**

(A) Daily $Ca^{2+}$ activity patterns in *tim > sNPF RNAi* flies (sNPF knockdown) under DD conditions (n = 5 flies). Dashed arrows on the clock face indicate the mean phases of DN1 in WT flies (cf. Figure 1C). DN1 $Ca^{2+}$ activity displayed poor phase coherence among flies (p>0.1: Rayleigh test).

(B) Daily $Ca^{2+}$ activity patterns in flies with sNPF knockdown in M pacemakers, *pdf > sNPF RNAi* under DD conditions (n = 5 flies). DN1 $Ca^{2+}$ activity was rhythmic but phase-shifted compared to WT controls (p<0.01: Watson-Williams test).

(C-D) Daily $Ca^{2+}$ activity patterns under LD cycles in (C) *tim > sNPF RNAi* flies (n = 7 flies) and (C) *pdf > sNPF RNAi* flies (n = 6 flies).

(E-F) Average locomotor activity in the first day under DD of (E) *tim > sNPF RNAi* flies (n = 15 flies) and (F) *pdf > sNPF RNAi* flies (n = 32 flies). Dots indicate SEM. See Figure 1F for a comparison to locomotor profiles in a control (WT) genotype.

(G-H) Average locomotor activity in LD cycles (averaged across 6 days) of (G) *tim > sNPF RNAi* flies and (H) *pdf > sNPF RNAi* flies. See Figure 1F for a comparison to locomotor profiles in a control (WT) genotype.

Fig 7

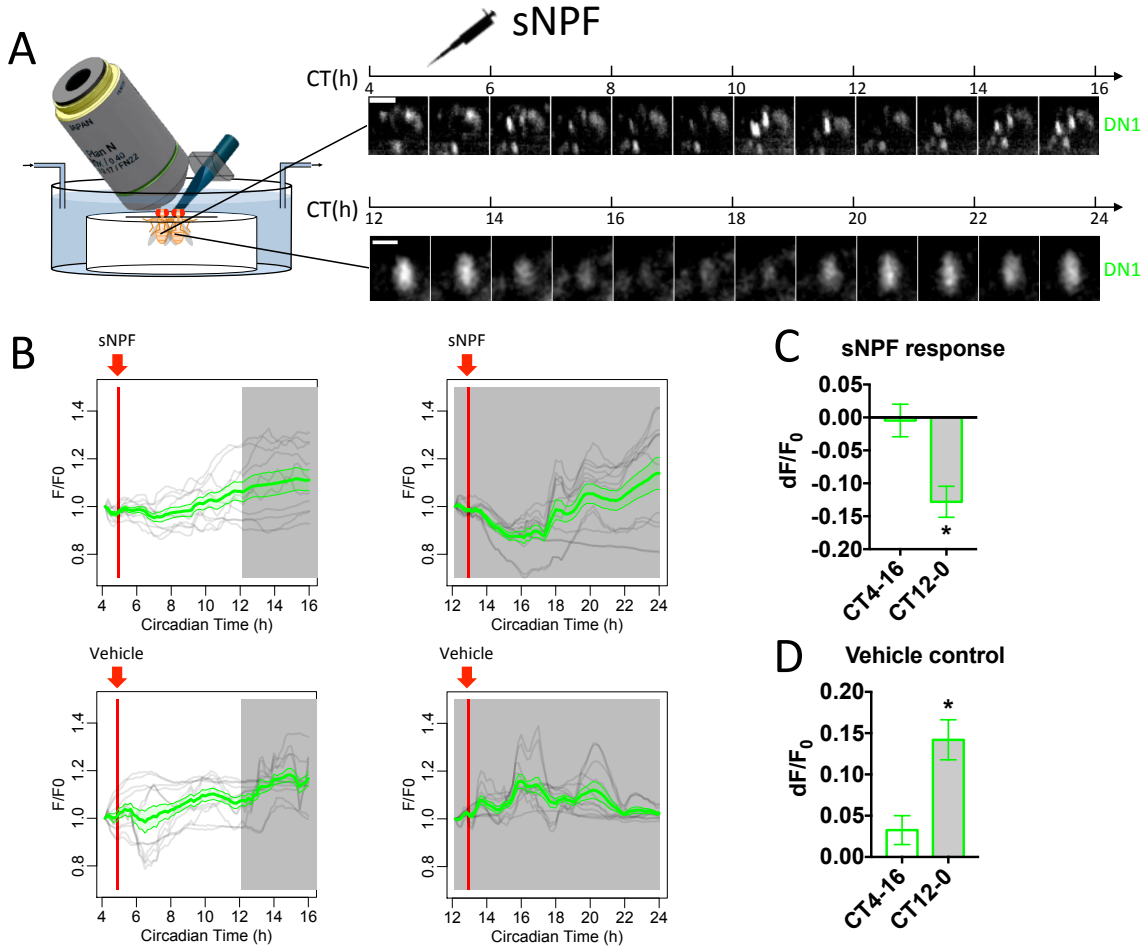


**Figure 7. sNPF suppresses DN1 $Ca^{2+}$ activity.**
(A-D) As in Figure 3A-D, yoked pairs of WT flies entrained to different circadian time (PDF: n = 3 pairs; vehicle: n= 3 pairs). DN1 $Ca^{2+}$ signals from flies in subjective night were reduced by $10^{-05}$M synthetic sNPF application. The nighttime DN1 $Ca^{2+}$ signals increased with vehicle treatment, reflecting their normal peak phase (cf. Figure 1C).

Fig 8

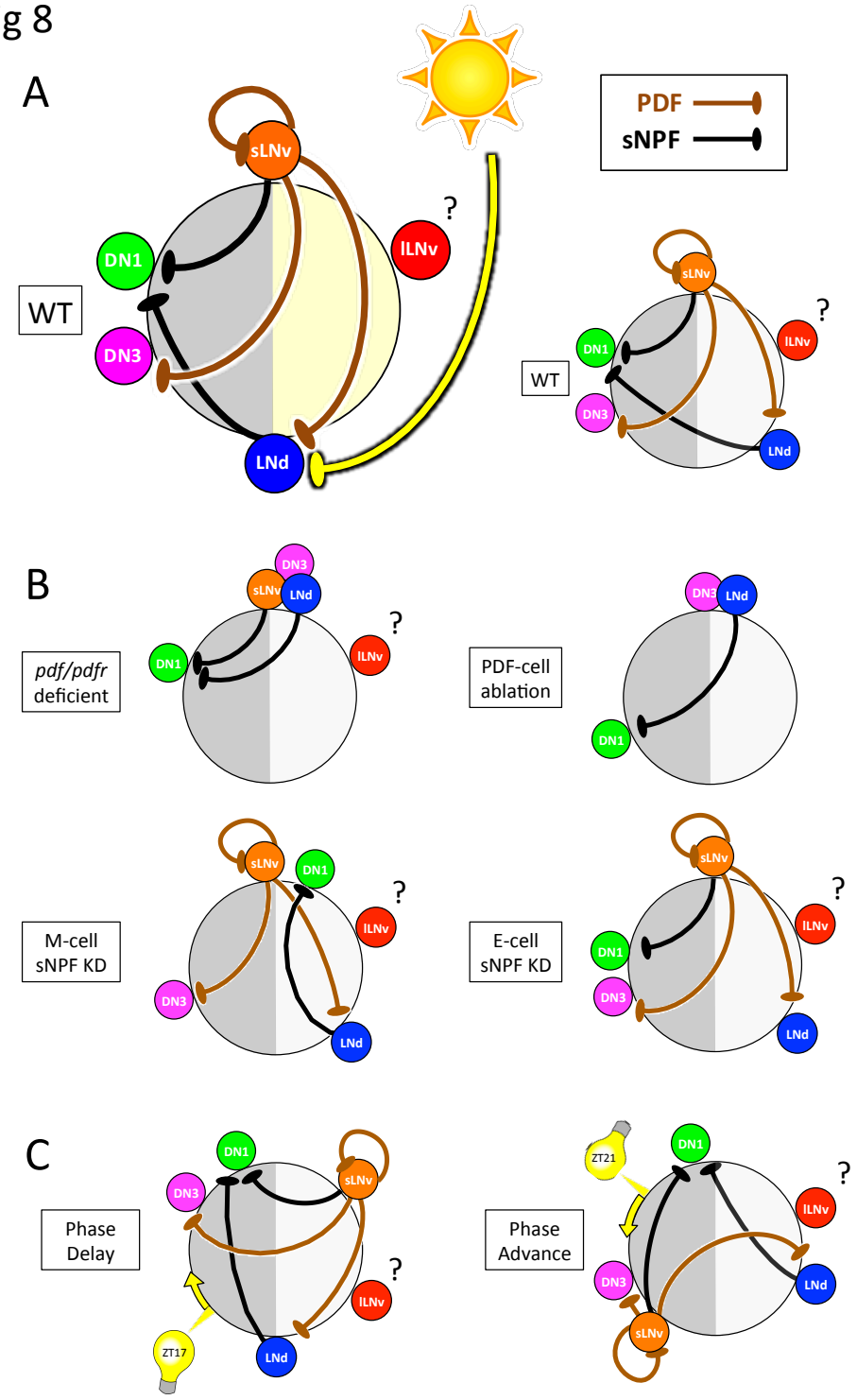


**Figure 8. Model of PDF-, sNPF- and light-mediated interactions that in concert set sequential Ca2+ activity phases of the different pacemaker groups.** (A) The position of each pacemaker group on the circle indicates its $Ca^{2+}$ peak phase. Both PDF and sNPF signals suppress the receivers (LNd and DN3 for PDF; DN1 for sNPF) from being active when senders (s-LNv for PDF; s-LNv and LNd for sNPF) are active. Light cycles act together with PDF to delay LNd $Ca^{2+}$ phases (Figure 1A&C). (B) Loss of neuropeptide-mediated interactions caused alterations in network $Ca^{2+}$ activity patterns: *pdf/pdfr* deficient (Figure 1D and Figure 2B), M-cell *sNPF* knockdown (Figure 7B), E-cell *sNPF* knockdown (Figure S6F), and PDF cell ablation (Figure S7). (C) $Ca^{2+}$ phase shifts occurring within 24 h following 15 min light pulses suggest that light also regulates PDF and sNPF signals (Figure 5).

# Fig S1 Related to Figure 2

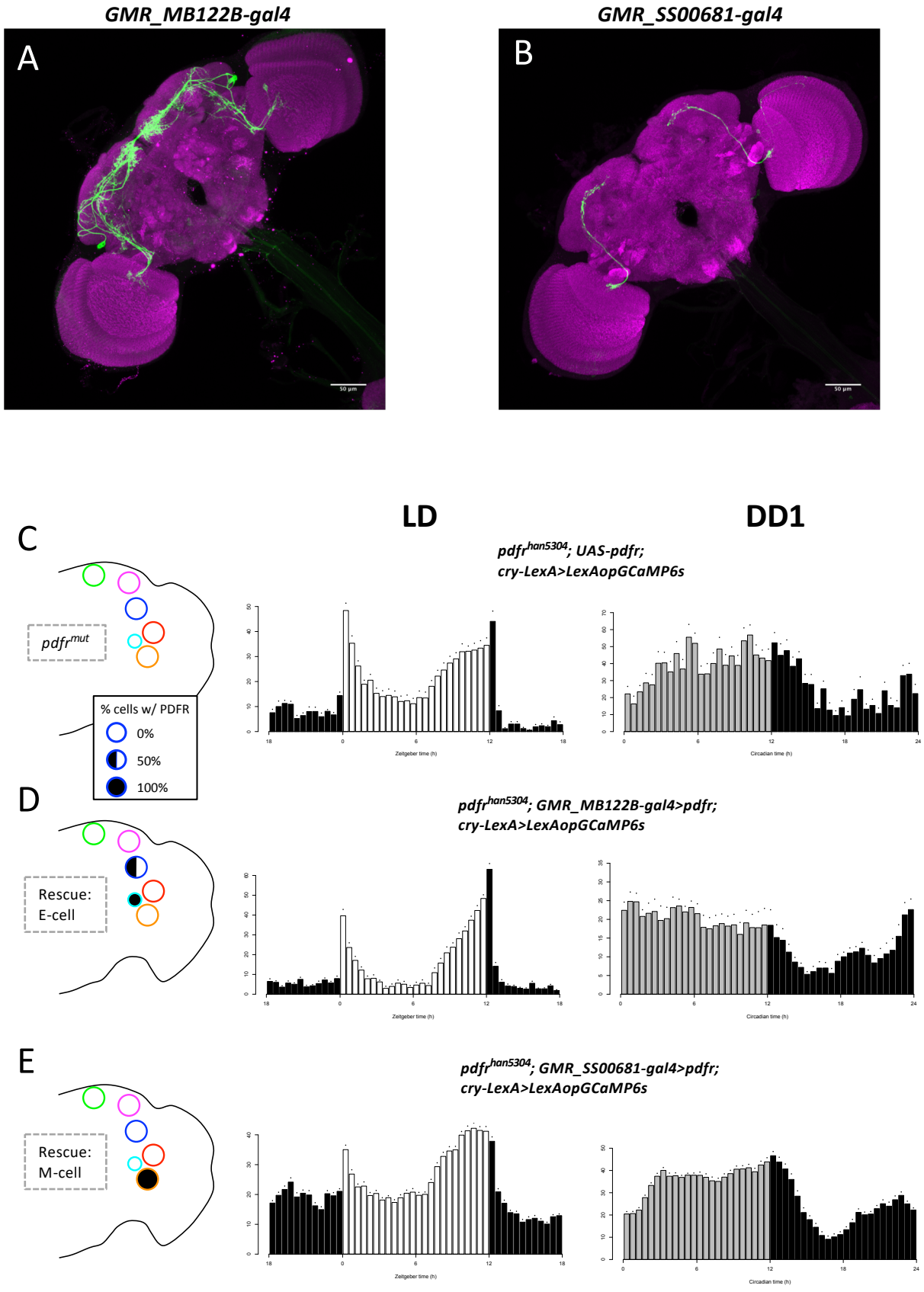

**Figure S1. Restoring PDFR in E pacemakers partially rescued the evening behavioral phase in *pdfr* mutants.** Related to Figure 2.

(A-B) The expression patterns of (A) MB122B-GAL4 and (B) SS00681-GAL4. The maximum intensity projections of 20x confocal stacks; the reference pattern is anti-Brp and the split-GAL4 patterns were visualized using a membrane targeted marker
( pJFRC225-5XUAS-IVS-myr::smGFP-FLAG). More detailed characterization of these lines will be presented in: H. Dionne, G. Rubin and A. Nern (in preparation).

(C-E) Average locomotor activity in the same genotypes which are used for imaging in Figure 2 B-D under LD cycles (left) and in first day under DD (right); also see Table S1. Restoring PDFR in M pacemakers did not provide such rescue. These results confirm previously published work by Lear et al. (2009) and by Im and Taghert (2010).

Fig S2. Related to Figure 4

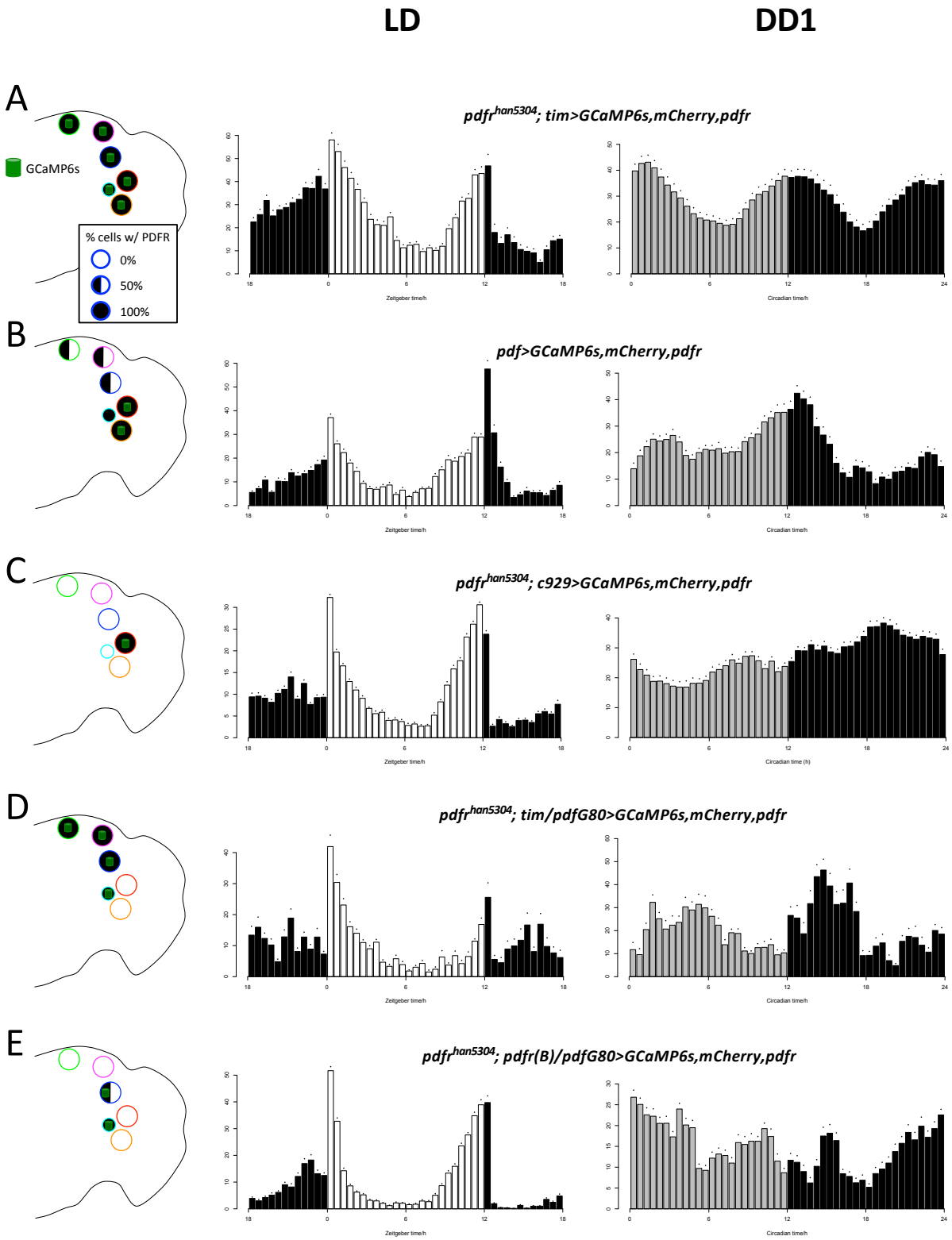


**Figure S2. Behavioral patterns resulting from PDFR gain-of-function experiments.** Related to Figure 4.
(A-E) Average locomotor activity under LD cycles (left) and in first day under DD (right) in in the same genotypes which were used for imaging in Figure 4 A-E (also see Table S1).

Fig S3 Related to Figure 5

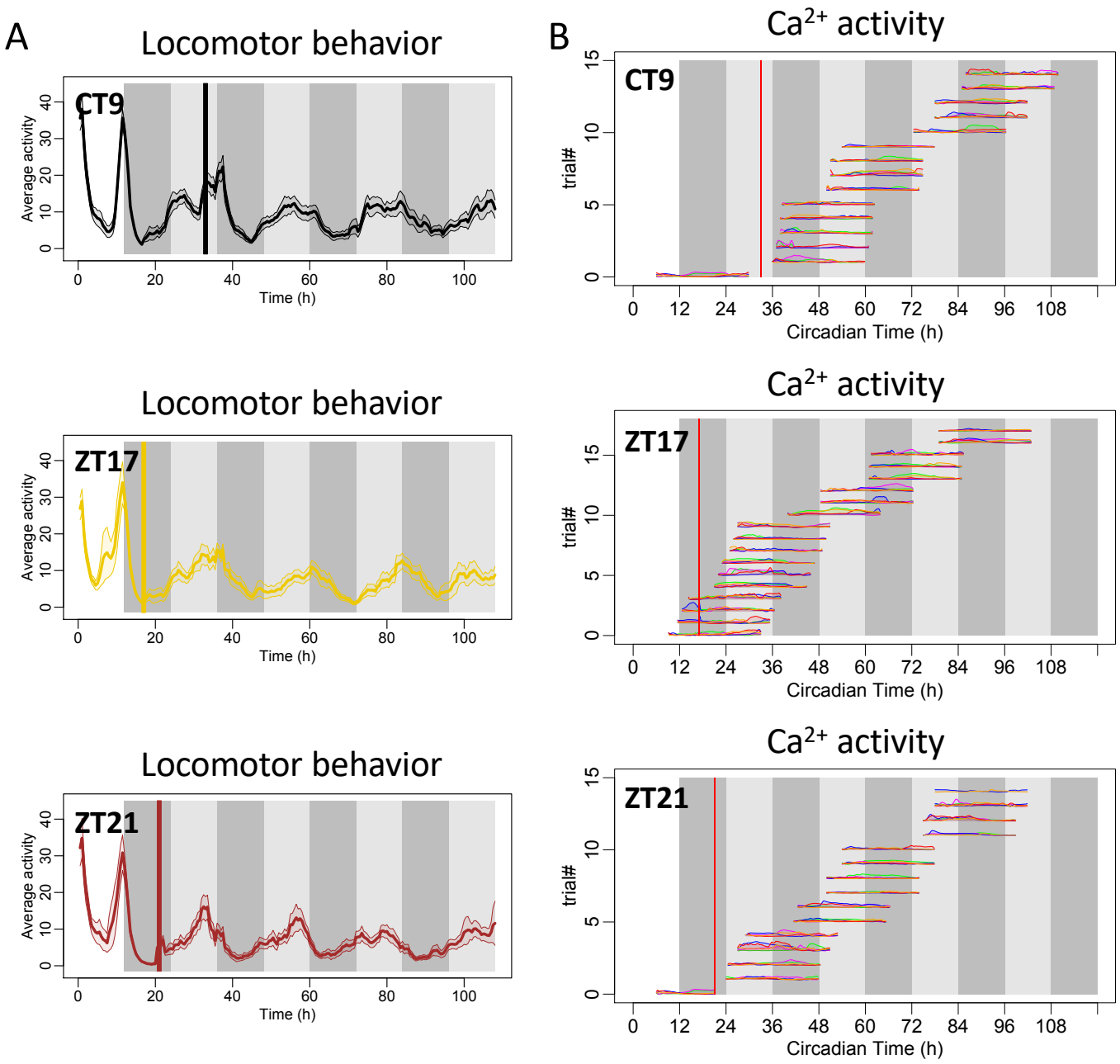


**Figure S3. Behavior and $Ca^{2+}$ activity phase-shifts by light pulses.** Related to Figure 5.
(A) Average locomotor activity in the three days following 15 min light pulses delivered either in the dead zone (CT9), or in the phase-delay zone (ZT17), or in the phase-advance zone (ZT21). Bars indicate the time of light pulses. (n= 16 flies).
(B) $Ca^{2+}$ activity traces of light pulse experiments. Each line represents a single imaging episode measuring 24 h $Ca^{2+}$ transients in the different pacemaker groups in one fly. Group-specific traces were then tiled and averaged to synthesize the three-day patterns in Figure 5A. Red bars indicate the time of light pulses.

# Fig S4. Related to Figure 5

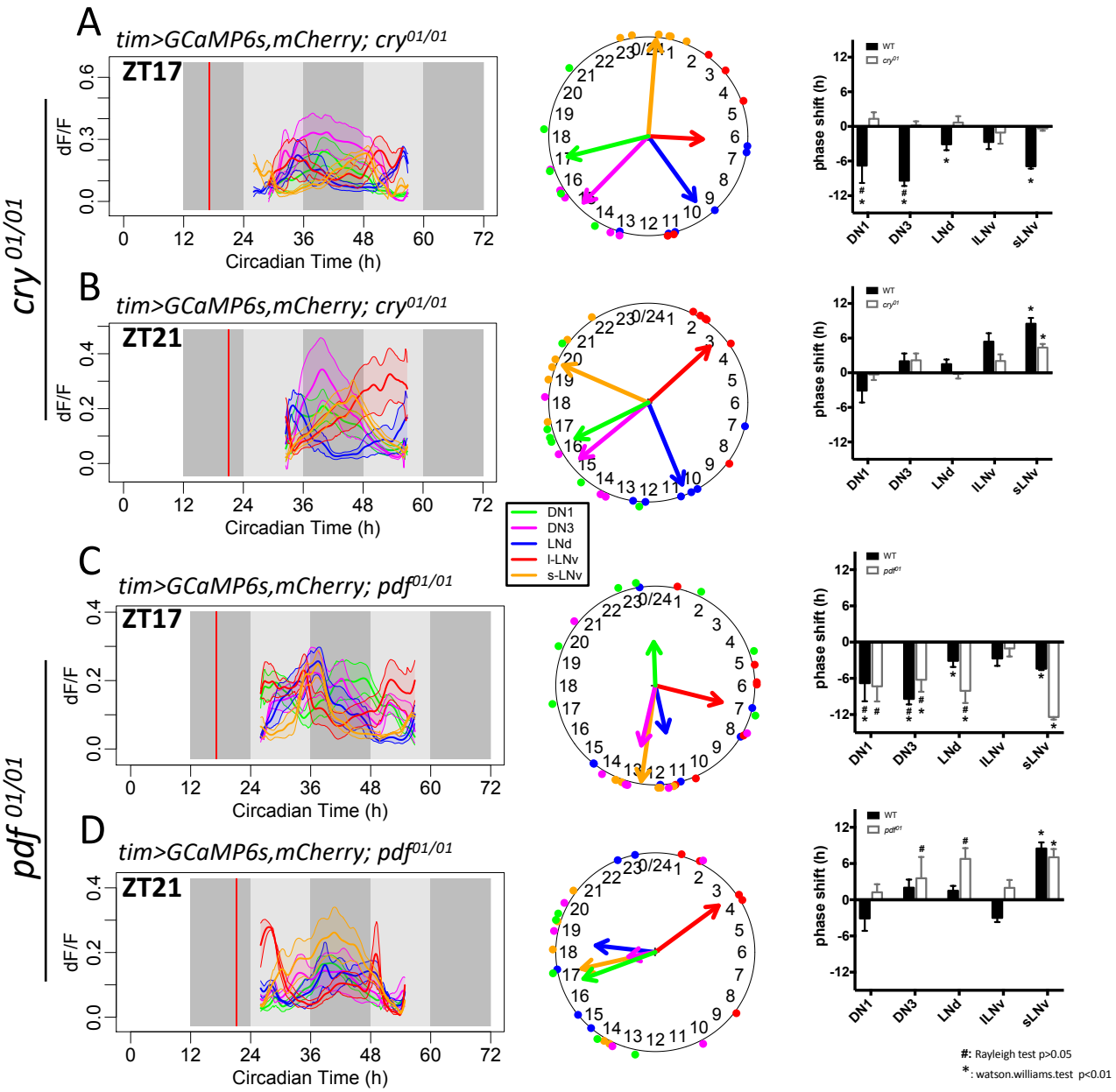


**Figure S4. Light-induced $Ca^{2+}$ phase-shifts require CRY and PDF.** Related to Figure 5.
(A-B) Measurements of $Ca^{2+}$ phase-shifts in the five major pacemaker groups in *cry*$^{01}$ mutants *in vivo*, during the first day after light pulses: (A) in the phase-delay zone (ZT17; n = 6 flies) and (B) in the phase-advance zone (ZT21; n = 6 flies). Left, $Ca^{2+}$ transients. Middle, $Ca^{2+}$ phase distributions. Right, $Ca^{2+}$ phase shifts by light pulses in WT controls (filled bars) and *cry*$^{01}$ mutants (empty bars) compared to unstimulated WT controls and *cry*$^{01}$ mutants respectively. Hashes (#) denote those groups losing coherence of $Ca^{2+}$ activity (p>0.05: Rayleigh test). Asterisks denote those groups with significant phase-shifts (p<0.01: Watson-Williams test).
(C-D) Measurements of $Ca^{2+}$ phase-shifts in the five major pacemaker groups *in vivo* in *pdf*$^{01}$ mutants in the first day after light pulses (C) in the phase-delay zone (ZT17; n = 7 flies) and (D) in the phase-advance zone (ZT21; n = 5 flies).

Fig S5. Related to Figure 6

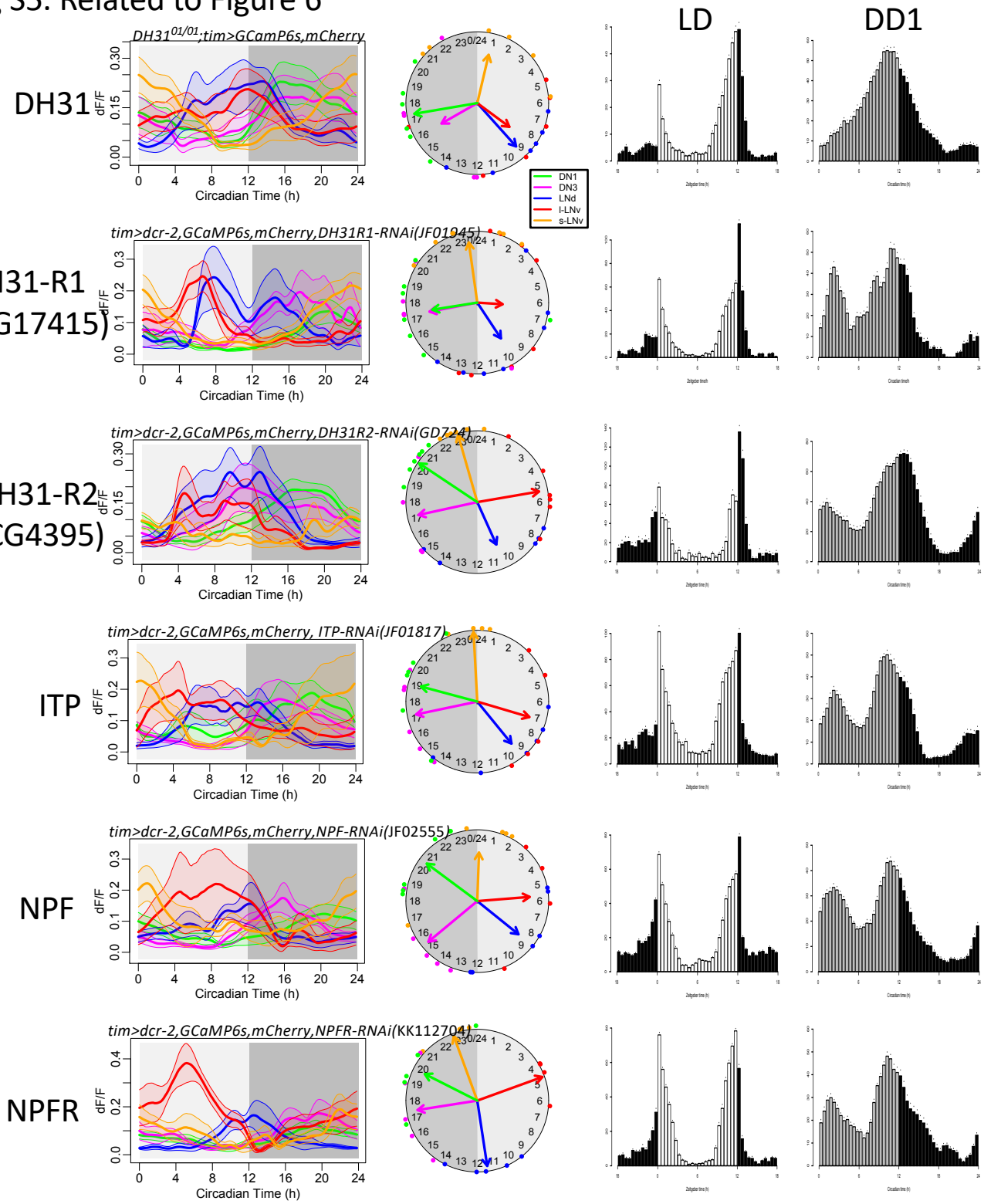


**Figure S5. A screen for neuropeptides and cognate receptors that contribute to wild type patterns of $Ca^{2+}$ rhythms.** Related to Figure 6. (**Left**) Daily $Ca^{2+}$ activity patterns of the five major pacemaker groups under DD in flies with neuropeptide mutants or pan-pacemaker RNAi knockdown of neuropeptides or receptors. Left, average $Ca^{2+}$ transients. Right, $Ca^{2+}$ phase distributions. (DH31: n = 6 flies; DH31R1: n = 8 flies; DH31R2: n = 7 flies; ITP: n = 6 flies; NPF: n = 6 flies; NPFR: n = 5 flies) (**Right**) Average locomotor activity under LD cycles and in first day under DD (DD1) in genotypes that were screened in the left panel (also see Table S1). The absence of a morning activity in *dh31*$^{01}$ homozygotes has previously been ascribed to an unrelated genetic background effect (Kunst et al., 2014).

# Fig S6. Related to Figure 6

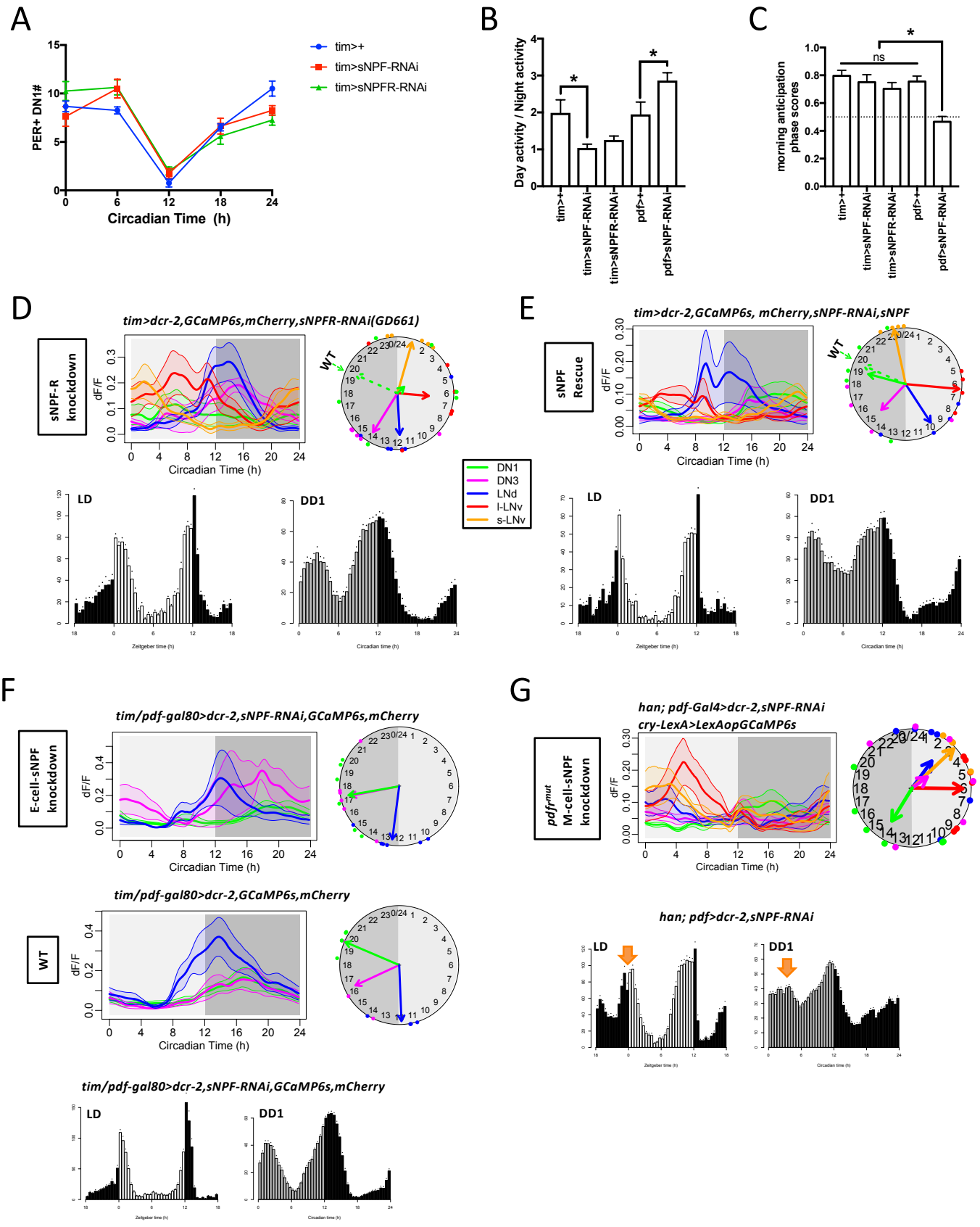

**Figure S6. Additional characterization for the role of sNPF on regulating $Ca^{2+}$ activity in DN1 pacemakers.** Related to Figure 6.

(A) PER oscillations in DN1 groups were unaffected by sNPF/sNPFR knockdown. Quantifications of PER immunostaining brains from WT controls, pan-pacemaker RNAi knockdown of *sNPF*, and pan-pacemaker RNAi knockdown of *sNPFR* flies in first day under DD. PER(+) DN1 neurons were counted in each hemisphere. Error bars denote SEM (n = 6-10 hemispheres per time point). No significant differences were noted between genotypes.

(B) All-pacemaker sNPF knockdown decreases daytime locomotor activity and increases nighttime locomotor activity. M pacemaker sNPF knockdown increases daytime activity and decreases night activity. The amount of locomotor activity during the daytime or nighttime represents averages during a 6-day period under LD (*p<0.05; Mann-Whitney test). These results confirm previous work by Hermann-Luibl et al. (2014).

(C) M pacemaker sNPF knockdown impairs morning anticipatory behavior. Morning anticipation phase scores in different genotypes of control and sNPF knockdown flies (*p<0.01; ns, not significant: ANOVA followed by t-test). Scores below the dashed line indicate no anticipation.

(D) Above - Daily $Ca^{2+}$ activity patterns in flies with sNPF receptor knockdown in all circadian pacemakers under DD (n = 6 flies), and their daily behavioral patterns under LD (below-left) and DD (below-right) conditions. WT refers to the peak value of the DN1 $Ca^{2+}$ pattern in control flies.

(E) Above - Daily patterns in *tim* > *sNPF RNAi*, *sNPF* demonstrating full genetic rescue of the coherence and phase of DN1 $Ca^{2+}$ activity under DD (n = 5 flies), and their daily behavioral patterns under LD (below-left) and DD (below-right) conditions.

(F) Daily $Ca^{2+}$ activity and behavioral patterns of E-cell-specific sNPF knockdown flies. Average 24 hr $Ca^{2+}$ transients (left) and $Ca^{2+}$ phase distributions (right) under DD of three circadian pacemaker groups: the E-cell LNd group, the DN3, and DN1. Driven by *tim*-gal4/*pdf*-gal80, these three groups expressed both the $Ca^{2+}$ sensor and *sNPF*-RNAi (above - n = 6 flies) and only the $Ca^{2+}$ sensor as WT controls (middle - n = 5 flies). DN1 $Ca^{2+}$ activity was rhythmic (p<0.01: Rayleigh test) and displayed a non-significant trend of phase-advance in E-cell-specific sNPF knockdown (p=0.058: Watson-Williams test). (Below) Average locomotor activity under LD cycles (below-left) and in first day under DD (below-right) in flies with *sNPF* knockdown in E pacemakers, *tim*-gal4, *pdf-gal80* > *sNPF RNAi.*

(G) Morning anticipatory behavior of *pdfr* mutants is restored by M-cell-specific sNPF knockdown. (Above) Average $Ca^{2+}$ transients (left) and $Ca^{2+}$ phase distributions (right) five major pacemaker groups in $pdfr^{han5304}$*;pdf > sNPF-RNAi* flies in the first day under DD (n = 6 flies). (Below) Average locomotor activity of $pdfr^{han5304}$*;pdf > sNPF-RNAi* flies under LD cycles (below-left) and in first day under DD (below-right); also see Table S1). In LD, these flies displayed strong morning anticipatory behavior (orange arrow), which is normally absent in *pdfr* mutants (Figure S2A) and in M-cell-specific sNPF knockdown flies (cf. Figure 6H). Note that the phase-advance of evening activity period in LD is not rescued.

# Fig S7. Related to Figure 6

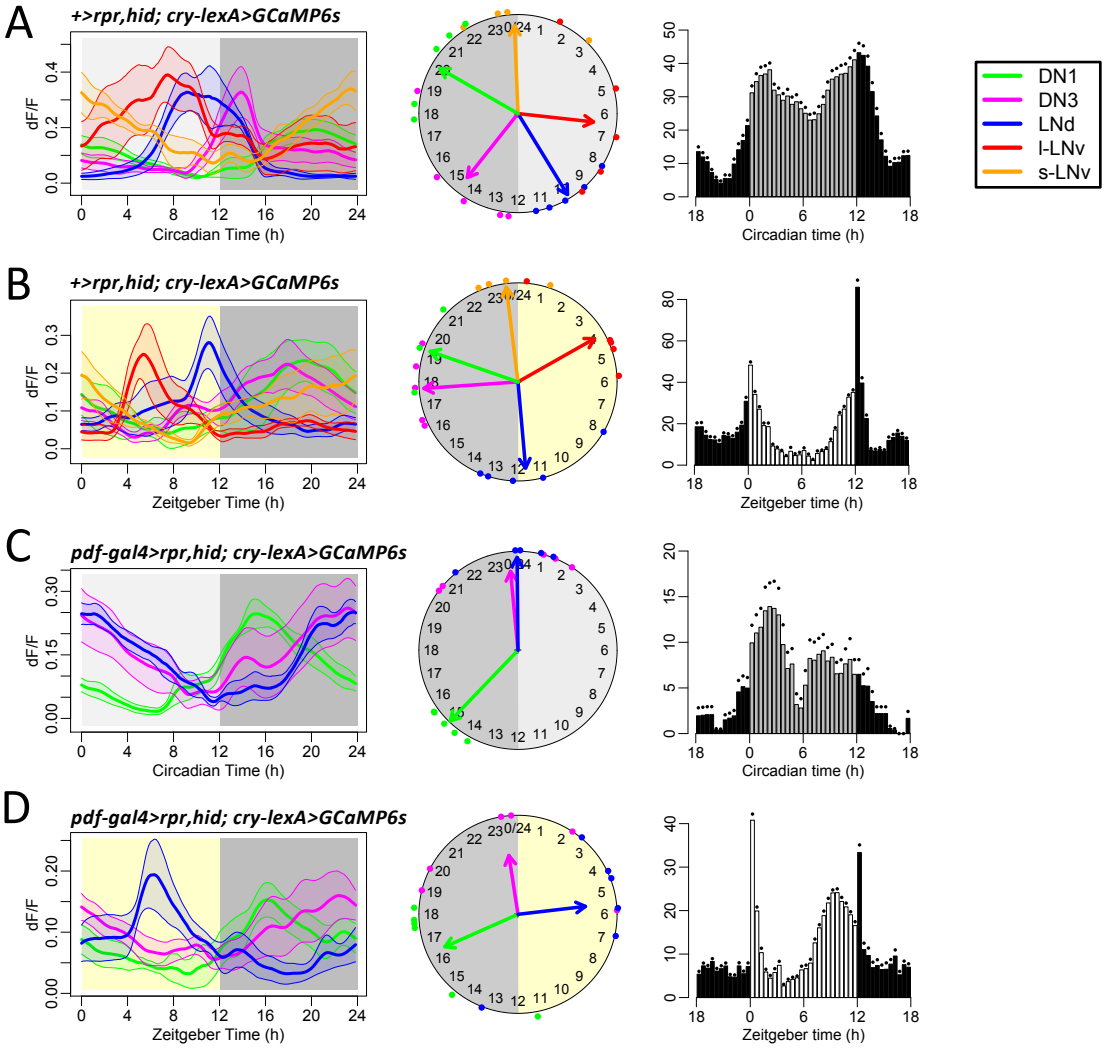


**Figure S7. Daily $Ca^{2+}$ activities and behavioral patterns of PDF-cell-ablated flies.** Related to Figure 6.
(A-B) Average $Ca^{2+}$ transients (left), $Ca^{2+}$ phase distributions (middle) and average locomotor activity (right) in WT (no Gal4) controls (A) in the first day under DD (n = 5 flies) and (B) under LD cycles (n = 5 flies).
(C-D) The $Ca^{2+}$ activity patterns of three PDF-negative pacemaker groups in flies without PDF-positive neurons (s-LNv and l-LNv), and behavioral patterns of *pdf>rpr,hid*; *cry*>GCaMP6s flies. (C) In DD, compared to controls, LNd and DN3 were phase-shifted to dawn, while DN1 displayed a phase-advance ($p<0.01$: Watson-Williams test; n = 5 flies). (D) In LD, LNd phases were delayed, compared to values in DD, panel C) ($p<0.01$: Watson-Williams test; n = 6 flies); cf. Fig 1B.

# Fig S8. Related to Figure 8

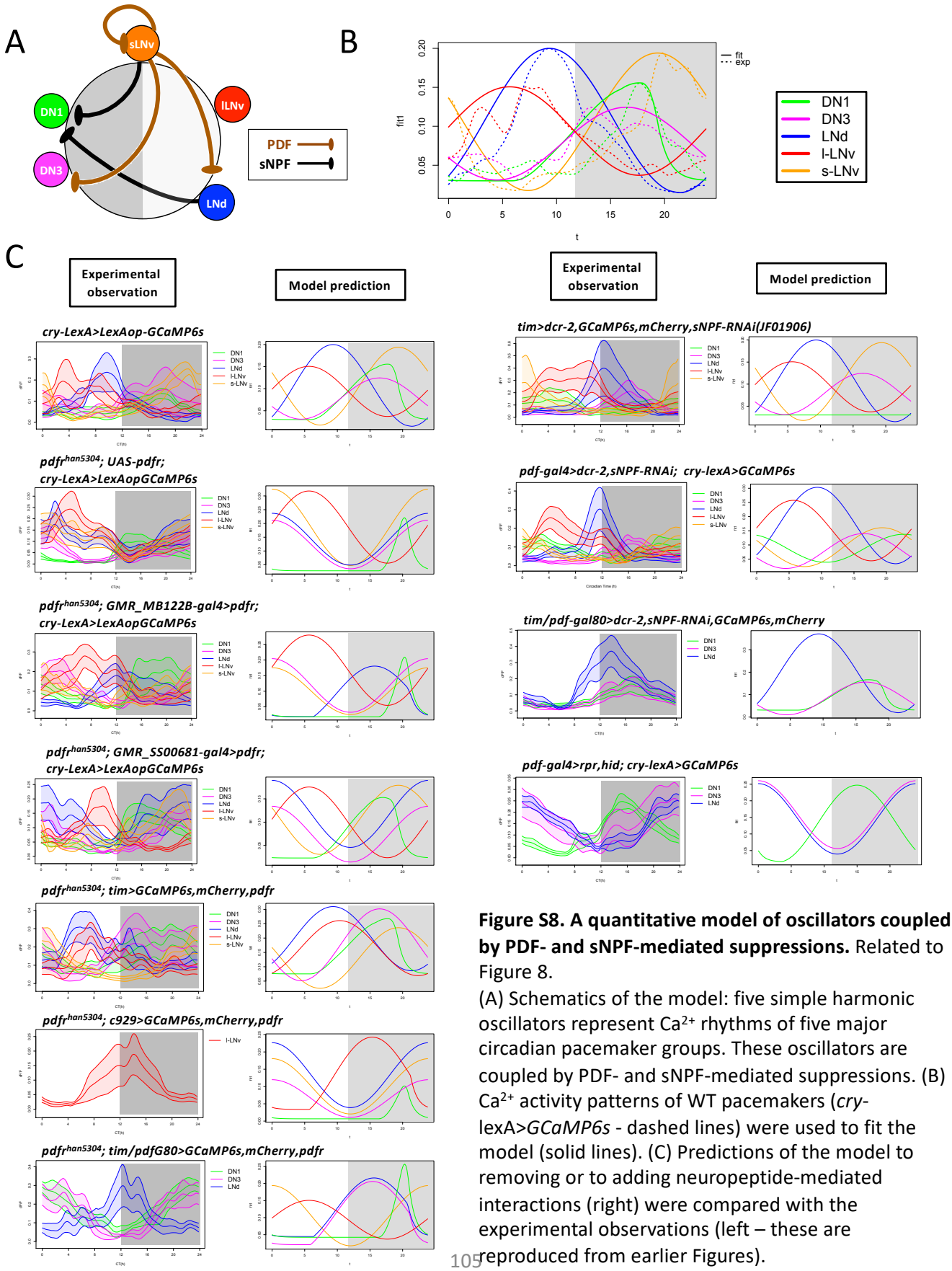


**Figure S8. A quantitative model of oscillators coupled by PDF- and sNPF-mediated suppressions.** Related to Figure 8.

(A) Schematics of the model: five simple harmonic oscillators represent $Ca^{2+}$ rhythms of five major circadian pacemaker groups. These oscillators are coupled by PDF- and sNPF-mediated suppressions. (B) $Ca^{2+}$ activity patterns of WT pacemakers (*cry*-lexA>*GCaMP6s* - dashed lines) were used to fit the model (solid lines). (C) Predictions of the model to removing or to adding neuropeptide-mediated interactions (right) were compared with the experimental observations (left – these are reproduced from earlier Figures).

**Table S1. Summary of Circadian Behavior Rhythms.** Related to Figure 1, 2, 4, and 6 and Figure S1, S2, S5, S6, and S7.

| Genotype | N | %AR | Period | pwr | wid | SNR | ACT-day | ACT-night | ACT-cycle | E-phase* (ZT) | SEM |
|---|---|---|---|---|---|---|---|---|---|---|---|
| **tim-gal4;uas-GCaMP6s,mCherry** | 16 | 44% | 24.3 | 29.0 | 3.1 | 0.4 | 12.3 | 8.2 | 10.2 | 12.2 | 0.1 |
| **tim-gal4,uas-GCaMP6s;pdf01** | 14 | 79% | 22.3 | 38.2 | 4.3 | 0.5 | 14.4 | 13.2 | 13.8 | 11.4 | 0.1 |
| **han/y;uas-pdfr/+; cryLexA,LexAop-GCaMP6s/+** | 16 | 56% | 24.1 | 34.6 | 4.9 | 1.0 | 19.9 | 12.2 | 16.1 | 11.2 | 0.1 |
| **han/y;GMRSS00681/uas-pdfr;cryLexA,LexAop-GCaMP6s/+** | 15 | 53% | 23.5 | 20.6 | 3.0 | 0.4 | 30.6 | 22.6 | 26.6 | 11.2 | 0.1 |
| **han/y;GMRMB122B/uas-pdfr; cryLexA,LexAop-GCaMP6s/+** | 8 | 63% | 23.5 | 25.6 | 5.7 | 0.9 | 13.8 | 10.2 | 12.0 | 11.8 | 0.2 |
| **han/y;tim-gal4/ uas-pdfr;uas-GCaMP6s,mCherry/+** | 11 | 36% | 23.6 | 44.8 | 4.0 | 1.6 | 19.2 | 26.2 | 22.7 | 12.6 | 0.4 |
| **han/y;pdfgal80/uas-pdfr;tim-gal4/uas-GCaMP6s,mCherry** | 12 | 50% | 23.7 | 22.6 | 2.7 | 0.7 | 3.9 | 4.5 | 4.2 | 11.6 | 0.7 |
| **han/y;pdf-gal80/uas-pdfr;pdfr(B)-gal4/uas-GCaMP6s,mCherry** | 15 | 40% | 23.8 | 19.1 | 2.5 | 0.4 | 7.7 | 8.7 | 8.2 | 11.2 | 0.2 |
| **han/y;c929-gal4/uas-pdfr; uas-GCaMP6s,mCherry/+** | 10 | 70% | 23.7 | 6.3 | 1.3 | 0.6 | 12.7 | 10.1 | 11.4 | 11.8 | 0.1 |
| **pdf-gal4/uas-pdfr; GCaMP6s,mCherry/+** | 14 | 43% | 24.5 | 37.2 | 4.4 | 0.5 | 15.4 | 12.2 | 13.8 | 12.0 | 0.3 |
| **DH31[01];timgal4/uas-GCaMP6s** | 15 | 7% | 24.7 | 37.9 | 4.4 | 0.7 | 7.4 | 5.5 | 6.5 | 12.1 | 0.1 |
| **dcr2/y;timgal4/+;GCaMP6s,mCherry/CG17415(JF01945)-RNAi** | 15 | 20% | 24.3 | 39.2 | 5.3 | 0.6 | 20.1 | 10.1 | 15.1 | 11.5 | 0.2 |
| **dcr2/y;timgal4/+;GCaMP6s,mCherry/ GC4395(GD724)-RNAi** | 15 | 0% | 23.5 | 70.8 | 7.9 | 2.4 | 34.3 | 22.1 | 28.2 | 12.8 | 0.2 |
| **dcr2/y;timgal4/ITP(JF01817)-RNAi; GCaMP6s,mCherry/+** | 7 | 0% | 23.6 | 39.2 | 4.3 | 1.4 | 30.5 | 15.7 | 23.1 | 12.2 | 0.1 |
| **dcr2/y;timgal4/+;GCaMP6s,mCherry/ NPF(JF02555)-RNAi** | 16 | 6% | 24.1 | 46.6 | 5.8 | 1.3 | 23.0 | 9.6 | 16.3 | 11.6 | 0.1 |
| **dcr2/y;tim-gal4/+;GCaMP6s,mCherry/ NPFR(KK112704)-RNAi** | 14 | 36% | 25.2 | 22.6 | 4.1 | 0.6 | 15.9 | 12.6 | 14.2 | 11.9 | 0.1 |

| Genotype | N | %AR | Period | pwr | wid | SNR | ACT-day | ACT-night | ACT-cycle | E-phase( ZT) | SEM |
|---|---|---|---|---|---|---|---|---|---|---|---|
| **dcr2/y;tim-gal4/+; GCaMP6s,mCherry/ sNPF(JF01906)-RNAi** | 15 | 0% | 23.9 | 37.0 | 4.4 | 1.1 | 31.6 | 23.4 | 27.5 | 12.0 | 0.1 |
| **pdf-gal4/y;;cry-LexA,LexAop-GCaMP6s** | 15 | 27% | 23.7 | 59.4 | 4.0 | 0.5 | 18.4 | 11.5 | 14.9 | 12.1 | 0.2 |
| **pdf-gal4/y;uas-dcr2/+;cry-LexA,LexAop-GCaMP6s/uas-sNPF(JF01906)-RNAi** | 32 | 19% | 23.6 | 24.4 | 3.0 | 0.5 | 18.1 | 8.9 | 13.4 | 10.0 | 0.2 |
| **dcr2/y;tim-gal4/+;GCaMP6s,mCherry/ sNPFR(GD661)-RNAi** | 22 | 9% | 23.9 | 55.3 | 6.8 | 1.7 | 36.6 | 19.8 | 28.2 | 11.9 | 0.2 |
| **dcr2/y;tim-gal4/ sNPF;GCaMP6s,mCherry /+** | 7 | 29% | 24.5 | 51.4 | 4.6 | 0.7 | 28.8 | 16.6 | 22.7 | 11.7 | 0.2 |
| **dcr2/y;tim-gal4/ sNPF;GCaMP6s,mCherry / sNPF(JF01906)-RNAi** | 8 | 25% | 24.3 | 55.9 | 4.6 | 0.6 | 23.9 | 13.9 | 18.9 | 11.6 | 0.1 |
| **han,pdf-gal4/y;uas-dcr2/+;uas-sNPF(JF01906)-RNAi/+** | 28 | 57% | 23.4 | 16.9 | 2.7 | 0.4 | 43.1 | 30.8 | 36.9 | 11.4 | 0.1 |
| **uas-dcr2/pdf-gal80;tim-gal4,uas-GCaMP6s/uas-sNPF(JF01906)-RNAi** | 16 | 19% | 23.6 | 66.0 | 3.8 | 0.9 | 17.4 | 8.9 | 13.1 | 12.1 | 0.1 |
| **uas-rpr/y;;cry-LexA,LexAop-GCaMP6s** | 14 | 7% | 23.8 | 64.3 | 4.2 | 0.8 | 23.1 | 11.1 | 17.1 | 12.4 | 0.2 |
| **uas-rpr,hid;pdf-gal4;cry-LexA,LexAop-GCaMP6s** | 12 | 100% | NA | 4.8 | 1.0 | 0.5 | 7.0 | 7.5 | 7.2 | 10.1 | 0.2 |

* E-phases and SEM are calculated from behavior in LD cycles. The E-phases are given in Zeitgeber time (ZT), in which the average evening peak fell; SEM represents fly-to-fly variability within a given genotype. The rest of values are calculated from nine-day records of behaviour in DD.

# Chapter 4

## Morning and Evening Circadian Pacemakers Independently Drive Premotor Centers via a Specific Dopamine Relay

This chapter is adapted from the following publication:

Liang, X., Ho, M. C., Wu, M. N., Holy, T. E., & Taghert, P. H. (2018). Morning and evening circadian pacemakers independently drive premotor centers via a specific dopamine relay. ***bioRxiv***, 424499.


**Abstract**

Many animals exhibit morning and evening peaks of locomotor behavior. In *Drosophila*, two corresponding circadian neural oscillators - M (morning) cells and E (evening) cells - each exhibits a corresponding morning or evening neural activity peak. Yet we know little of the neural circuitry by which distinct circadian oscillators produce specific outputs to precisely control behavioral episodes. Here we show that Ring Neurons of the Ellipsoid Body (EB-RNs), display spontaneous morning and evening neural activity peaks *in vivo*: these peaks coincide with the bouts of locomotor activity and result from independent activation by M and E pacemakers. Further, M and E cells regulate EB-RNs via identified PPM3 dopaminergic neurons, which project to the EB and are normally co-active with EB-RNs. These *in vivo* findings establish the fundamental elements of a circadian neuronal output pathway: distinct circadian oscillators independently drive a common pre-motor center, through the agency of specific dopaminergic interneurons.

## INTRODUCTION

Circadian rhythms provide adaptive value by promoting expression of diverse physiological processes and behaviors at specific times of the day. In mammals, rhythms in hormone release, rest/activity cycles, body temperature, and metabolism are all controlled by the multi-oscillator system of pacemakers in the suprachiasmatic nucleus (SCN) of the anterior hypothalamus. Numerous studies have documented that the SCN uses hormonal and neuronal signaling to provide adaptive phasic information across all times of day (Lehman *et al.* 1987; Moore and Klein, 1974; Ralph *et al.* 1990, De la Iglesia *et al.* 2003; Kalsbeek *et al.* 2006; VanderLeest *et al.* 2007). However, the information connecting SCN signaling to neural circuits that translate its outputs is fragmentary. Lacking direct *in vivo* experimental observations, the definition of circadian output networks remains a significant challenge.

In *Drosophila*, a prominent circadian output is the daily locomotor activity rhythm, which peaks once around dawn and again around dusk (Figure 1C). The rhythm is controlled by molecular clocks that cycle synchronously within ~ 150 circadian pacemaker neurons (Nitabach & Taghert, 2008). Among these circadian neurons, two separate groups (termed M cells and E cells) control the morning and evening activity peaks respectively (Stoleru *et al.* 2004; Grima *et al.* 2004; Yoshii *et al.* 2004). Previously we reported that different groups of circadian neurons display rhythmic but asynchronous circadian neural activity *in vivo*: they peak at different yet stereotyped times of day (Liang *et al.* 2016). These neural activity rhythms depend on their synchronous molecular clocks, but their activity peak times are staggered, by neuropeptide-mediated interactions between circadian neuron groups. This allows the network to create multiple phasic time points (Liang *et al.* 2017). Consequently, M cells peak in the morning and E cells peak in the evening. The distinct peak times of M cells and E cells could potentially guide

output motor circuits to generate independent morning and evening locomotor behavioral peaks. To support this emerging network view of pacemaker regulated behavior, we wished to ask which pre-motor centers transduce circadian timing signals to generate morning or evening phase-specific locomotor activity. As a strategy, we reasoned that spontaneous activity patterns corresponding to the daily bimodal activity pattern could help identify the critical pre-motor elements.

Robie *et al.* (2017) performed an unbiased screening of sparsely-labeled neuronal groups to determine which could initiate locomotor activity. By this analysis, the strongest candidates were the Ring Neurons of the Ellipsoid Body (EB-RNs) (Figure 1A). In parallel, silencing these same EB-RNs reduced spontaneous locomotor activity (Martín-Peña *et al.* 2014). EB-RNs are a subset of neurons that constitute the Central Complex - the primary locomotor control center in insects (Strauss and Heisenberg, 1993; Pfeiffer and Homberg, 2014). EB-RNs encode visual landmarks for visuospatial-memory-based orientation and navigation (Neuser *et al.* 2008; Ofstad *et al.* 2011; Seelig and Jayaraman, 2013). In the monarch butterfly, EB-RNs are involved in sun-compass navigation (Heinze and Reppert, 2010), which requires timing information from circadian clocks (Froy *et al.* 2003). In *Drosophila,* EB-RNs might also be regulated by the neuropeptides LK (Cavey *et al.* 2016) and the pigment-dispersing factor (PDF) (Pírez *et al.* 2013). Therefore, we first measured spontaneous activity in EB-RNs *in vivo*, to see if they represent a point of convergent circadian regulation that could lead to daily bouts of locomotor activity.

## RESULTS

### Spontaneous daily bimodal activity in EB-RNs *in vivo*

To test whether EB-RNs regulate circadian locomotor activity, we expressed tetanus toxin light chain (TeTn, Sweeney *et al.* 1995) to block neurotransmission in the majority of ~60 EB-RNs. As expected, the circadian rhythm of locomotor activity in these flies was impaired under DD, as was the general level of activity (Figure 1B and Table S1). Therefore, to learn about the possible involvement of the EB-RNs in normal rhythmic locomotion (Figure 1C), we then measured *in vivo* spontaneous activity exhibited by these neurons in otherwise wild-type flies. Using the genetically encoded calcium sensor GCaMP6s (Chen *et al.* 2013), we performed *in vivo* $Ca^{2+}$ imaging in living flies for 24 hrs using methods previously described (Liang *et al.* 2016, 2017). EB-RNs contains several genetically and morphologically distinct subgroups (Renn *et al.* 1999a). We dissected four EB-RN subgroups using different genetic drivers that use regulatory sequences associated with different circadian clock-related genes: one with sequences from *timeless,* one from *cryptochrome,* and two from *pdfr (pigment-dispersing factor receptor)* (Figure 1D-G and Figure S1A). In both 12-hr light: 12-hr dark (LD) cycles and in constant darkness (DD) conditions, the four different EB-RN subgroups we tested displayed spontaneous, daily $Ca^{2+}$ rhythms (Figure 1D-G). The average $Ca^{2+}$ activity profile of each subgroup was bimodal (Hartigans' dip test, LD: $p<0.0001$, DD: $p<0.05$), with a peak around dawn and another around dusk. These peaks corresponded to the times of day when flies showed daily locomotor activity peaks (Figure 1C). The outer subgroup of EB-RNs caused the strongest effects on locomotor activity according to Robie *et al.* (2017). We tested the same split-GAL4 drivers as reported by Robie *et al.* (2017) and found that these locomotion-promoting EB-RNs likewise displayed a similar spontaneous daily bimodal activity pattern (Figure S1B; Hartigans' dip test,

$p<0.0001$). We also confirmed the daily bimodal activity pattern exhibited by different EB-RN subgroups using a separate, circadian-clock-irrelevant driver line to label the majority of EB-RNs (Figure 1H; Hartigans' dip test, LD: $p<0.001$, DD: $p<0.01$).

To directly test the correlation between EB-RN neural activity and locomotor activity in single flies in our experimental paradigm, we performed *in vivo* 24-hr $Ca^{2+}$ imaging while simultaneously measuring spontaneous leg movements as a proxy for locomotor activity levels (Figure 2A). EB-RN activity was strongly correlated with such behavioral activity in individual flies, both at a daily time scale (Figure 2F-H) as well as at a shorter (hourly) time scale (Figure 2C-E). Analysis of the shorter timescale indicated that increases in EB-RN activity were coincident with increases in behavioral activity; decreases typically preceded decreases in behavioral activity by a few minutes (Figure 2E). Thus, EB-RNs, consistent with their documented roles as pre-motor activity centers, exhibit spontaneous daily neural activity rhythms that precisely correspond to the pattern of circadian locomotor rhythms.

**Circadian pacemaker neurons drive EB-RN activity rhythms**

The daily neural activity rhythms in EB-RNs could reflect rhythmic sensory inputs, either proprioceptive or visual. For example, recent studies suggest that EB-RNs encode self-motion information (Shiozaki & Kazama, 2017). Therefore, to block ascending proprioceptive sensory inputs, we transected connectives between the brain and ventral nerve cord (between subesophageal and first thoracic neuromeres) immediately before $Ca^{2+}$ imaging. EB-RNs still displayed normal bimodal activity rhythms (Figure 3A). These EB-RN rhythms persisted even when the entire body of the fly was removed immediately before imaging (Figure 3B). Therefore, spontaneous bimodal EB-RN activity rhythms are not a consequence of locomotor

behavioral activity. Previous studies also showed that EB-RNs receive large-scale visual inputs (Seeling & Jayaraman, 2013; Omoto *et al.* 2017; Sun *et al.* 2017). We therefore removed visual inputs by testing flies in DD (Figure 1) or by testing genetically blind *norpA*$^{P24}$ mutant flies (Figure 3C): in both cases, normal EB-RN activity rhythms persisted. Together, these results demonstrate that EB-RN activity rhythms are not driven by daily rhythmic sensory inputs.

To determine if EB-RN activity rhythms are driven by molecular clocks, we measured $Ca^{2+}$ activity in circadian-defective *per*$^{01}$ (null) mutant flies (Konopka & Benzer, 1971), which fail to display circadian clock-dependent anticipatory behavior. Although *per*$^{01}$ flies still had two peaks of startle responses (to the lights-on and lights-off stimuli under LD cycles), daily $Ca^{2+}$ activity patterns in EB-RNs were arrhythmic (Figure 3D). Therefore, EB-RN activity rhythms specifically correlate with - and entirely depend on - circadian clock signals that regulate daily behavioral peaks. Notably, EB-RNs exhibit no measurable expression of the core clock gene *period*, which is highly expressed and cycling in circadian pacemaker neurons (Figure S1C) (Kaneko and Hall, 2000). Furthermore, manipulations to alter the pace of circadian clocks in a subset of circadian neurons shifted the locomotor activity phases as previously reported (Stoleru *et al.* 2005; Yao and Shafer, 2014), while the same manipulation within EB-RNs did not affect locomotor behavior (Figure S1D-F). Thus, we conclude that daily EB-RN activity rhythms are downstream of circadian timing information provided by circadian pacemaker neurons. To test whether circadian neurons regulate EB-RNs, we impaired a crucial signal within the pacemaker network, the neuropeptide PDF (Renn *et al.* 1999b). In PDF receptor mutant (*pdfr*$^{han5304}$) flies (Han *et al.* 2005), the EB-RNs activity pattern under LD transformed to a daily unimodal one (Hartigans' dip test, p=0.23): the morning activity peak was lost, and the evening peak was advanced (Figure 3E; Watson-Williams test, p=0.00012). This neural activity pattern mirrors the

changes in locomotor activity pattern typically displayed by *pdfr*$^{han5304}$ flies. Meanwhile, EB-RNs responded to thermogenetic and pharmacogenetic activation of PDF-releasing neurons (Figure S2AB). Thus, EB-RN activity rhythms could be driven (directly or indirectly) by PDF-expressing circadian pacemaker neurons.

**Distinct circadian neurons dictate the separate phases of EB-RN activity**

In contrast to EB-RNs, all circadian pacemaker neurons showed single daily peaks of activity. This difference suggested that the daily two-peak activity pattern of EB-RNs could be generated by a combination of different circadian neuronal outputs. We considered the simplest model, that M cells could drive a morning activity peak in EB-RNs while E cells could independently drive EB-RN evening activity. To begin to test this possibility, we first determined that EB-RNs responded to the selective activation of M cells (four s-LNv) by ATP application to brains expressing ATP-gated cation channel P2X2 (Lima and Miesenböck, 2005) in M cells (Figure 4A). A similar design to selectively activate E cells, the 5$^{th}$ s-LNv and three PDFR-positive LNd (Im and Taghert, 2011), produced correspondent EB-RN responses of comparable amplitude (Figure 4BC and Figure S2D-F). These results support the proposition that both M cells and E cells have functional connections with EB-RNs.

As a more stringent test, we then asked whether selectively accelerating M or E oscillators would selectively influence the phase of either the morning and/or evening peak of EB-RN $Ca^{2+}$ activity. Overexpressing Shaggy (SSG) using *pdf-GAL4* (PDF>SGG) to accelerate the molecular clocks selectively in Morning oscillators advanced the morning peak of locomotor activity (cf. Stoleru *et al.* 2005) and the M-cell activity peak (Figure 4DE). In these flies, we found that only the morning peak of EB-RN $Ca^{2+}$ activity was phase-advanced, while their

evening $Ca^{2+}$ peak phase was unaffected (Figure 4F-H). This result suggests that the morning peak of EB-RNs activity is dictated predominantly by the phase of M cell activity. In parallel, we then asked whether the evening peak of EB-RNs is dictated by the phase of E cell activity. Overexpressing SGG in E cells by using a split-GAL4 line GMR_MB122B (Liang *et al.* 2017) selectively advanced the evening behavioral peak (Figure 4IJ) and the E-cell activity peak (Figure 4K-L). In these flies, we found that only the evening peak of EB-RN $Ca^{2+}$ activity was phase-advanced, and by comparable amplitude to what we previously observed with M cell acceleration and M peak advance (Figure 4K-L). Taken together, these results reveal essential circuit links to demonstrate that M cells and E cells can independently dictate the two distinct phases of EB-RN pre-motor activity.

**Dopaminergic neurons regulate EB-RNs**

None of the ~150 circadian pacemaker neurons in *Drosophila* project directly to the EB (Helfrich-Förster, 2005). We therefore asked through which interneurons M cells and E cells might regulate daily neural activity in EB-RNs. A set of two dopaminergic (DA) neurons (named PPM3-EB) appeared as prominent candidates: they innervate the EB; further, they can initiate locomotor activity and promote ethanol-induced locomotor activity (Kong *et al.* 2010). First we established that PPM3-EB neurons spontaneously displayed a daily bimodal neural activity pattern *in vivo* (Hartigans' dip test, $p<0.0001$), similar to that of the EB-RNs and consistent with their putative involvement in the daily profile of locomotor activity (Figure 5A). To study the precise relationship between activity in EB-RNs and that in PPM3-EBs, we employed dual-color $Ca^{2+}$ imaging in single fly brains (Figure 5B).. This method separated $Ca^{2+}$ activity signals from these two anatomically-overlapping neuron groups, by simultaneously recording a green signal

in PPM3-EB (GCaMP6s), and a red signal in EB-RNs (jGECO1a, Dana *et al.* 2016). We found that the spontaneous $Ca^{2+}$ activity patterns of EB-RNs were highly correlated with those of PPM3-EB, but poorly correlated with those of the l-LNv circadian neurons, which were also labelled by jGECO1a (Figure 5C-F). This result suggests that PPM3-EB and EB-RNs are closely connected: they receive common inputs, and/or one receive synapses from the other. We next turned to anatomical analysis using the GRASP method (GFP reconstitution across synaptic partners - Feinberg *et al.* 2008). We expressed two complementary GFP fragments in PPM3-EB and EB-RNs respectively to demonstrate the connections (potentially synaptic connections) normally exist these two groups of neurons (Figure S3). Furthermore, we asked whether the morning and evening activity peaks in PPM3-EB are independently dictated by M cells and E cells respectively, as we showed for the bimodal activity patterns in the EB-RNs. Again, we overexpressed SSG using *pdf-GAL4* (PDF>SGG) to selectively advance the M-cell activity peak (as in Figure 4DE). In these flies, we found that only the morning peak of PPM3-EB was phase-advanced, while the evening peak phase was unaffected (Figure 5G-I). This result suggested that the daily activity rhythm of PPM3-EB are driven by the same set of circadian neuron outputs as EB-RNs. Both PPM3-EB and EB-RNs responded to the bath-application of PDF and to the pharmacogenetic activation of PDF neurons (Figure S4AB). In response to the activation of PDF neurons, PPM3-EB responded more quickly than did EB-RNs, which is consistent with PPM3-EBs having a physiological 'upstream' of EB-RNs. Together, these results support a model in which circadian pacemaker neurons indirectly activate as many as ~60 pairs of EB-RNs by first activating two pairs of dopaminergic neurons, the PPM3-EB.

We tested this model by blocking neurotransmission in PPM3-EB neurons, thereby asking if their specific output is necessary for proper locomotor rhythmicity. Using intersectional

genetics (*GMR92G05-GAL4* and *TH-Flp*), we restricted the expression of tetanus toxin (TeTn, Sweeney *et al.* 1995) to the two pairs of PPM3-EB. The locomotor activity of these flies was largely arrhythmic under DD (Figure 6AB). This behavioral deficit was comparable with, and even more severe than that caused by blocking neurotransmission in the majority of EB-RNs (Figure 1B and Table S1). Importantly, while the molecular clocks and $Ca^{2+}$ rhythms of circadian pacemaker neurons in these flies were intact (Figure S5), the daily bimodal neural activity pattern of EB-RNs was severely impaired (Figure 6C-E). Likewise, knocking down DA receptors DopR2 or D2R in the majority of EB-RNs also impaired rhythmicity in locomotor activity under DD (Figure 6K and Table S1) Significantly, these same DA receptor knockdowns also suppressed the daily bimodal neural activity pattern of EB-RNs (Figure 6G-K). Hence we propose that dopaminergic input from PPM3-EB neurons forms a critical relay to instruct EB-generated locomotor activity, according to a multi-phasic circadian schedule.

The daily bimodal pattern of PPM3-EB suggested these dopaminergic neurons may release DA twice a day, once in the morning and again in the evening, to modulate the neural activity of EB-RNs. To test this hypothesis, we first measured the responses of EB-RNs to bath-application of dopamine (Figure 7A) and to pharmacogenetic activation of PPM3-EB (Figure 7B). Using a genetically encoded GPCR-activation-based-DA ($GRAB_{DA}$) sensors (Sun *et al.* 2018), we then asked when and how often during the 24 hr day EB-RNs might receive direct DA modulation. $GRAB_{DA}$ sensor in the EB-R3 subgroup increased its fluorescence report with bath application of DA (Figure 7C). When then recorded this signal *in vivo* for 24 hours, we observed a daily bimodal pattern (Figure 7D), similar in pattern and phasing to the $Ca^{2+}$ activity pattern of upstream PPM3-EB neurons and the $Ca^{2+}$ activity pattern of EB-RNs themselves. Collectively, these results suggested that the daily bimodal dopaminergic modulation from PPM-EB to EB-

RNs relays the circadian phase timing from pacemaker neurons. This dopaminergic modulation helps to generate the daily bimodal patterns in the neural activity of EB-RNs and thus the daily bimodal patterns in locomotor activity (Figure 7E).

## DISCUSSION

Locomotor activity in *Drosophila* follows a daily bimodal rhythm that peaks around dawn and again around dusk. By measuring spontaneous neural activity *in vivo* across the 24 hr day, we found that morning and evening circadian oscillators independently activate the pre-motor Ring Neurons of the Ellipsoid Body through the agency of PPM3-EB dopaminergic neurons. These findings provide the most detailed insights available in any model system by which pre-motor pathways are organized in response to phasic circadian pacemaker information. In addition, they indicate an unexpectedly obligate role for dopamine in the neural control of daily rhythmic locomotor activity. We based our conclusions on four lines of evidence: (1) Both PPM3-EB and EB-RNs display daily spontaneous bimodal neural activity patterns that precisely correlate with locomotor activity patterns peaking around dawn and dusk (Figure 1 & 5A). (2) Locomotor activity closely followed changes in EB-RN activity (Figure 2) while EB-RN activity was itself highly correlated with PPM3-EB activity (Figure 5B-F). (3) Different phases of EB-RN circadian-rhythmic neural activity relied on independent inputs from circadian pacemakers, M cells and E cells, but did not rely at all on visual inputs or on the execution of locomotor behavior (Figure 3 and 4). (4) Both EB-RN activity rhythms and normal locomotor activity rhythms required PPM3-EB inputs (Figure 6A-E); normal locomotor activity rhythms also required DA receptors on EB-RNs to receive inputs from PPM3-EB DA neurons (Figure 6F-K). These data together support a model that features outputs from M cells and E cells sequentially

and independently generating the two daily peaks of activity PPM3-EB DA neurons. These non-circadian PPM3-EB DA neurons in turn relay the phasic information to activate as many as ~60 pairs of EB-RNs, thereby generating the bimodal daily locomotor activity rhythm (Figure 7E).

**Output circuits downstream of circadian pacemaker neurons**

Our findings constitute important steps in relating the activities of distinct circadian pacemaker neurons to downstream neural circuits. Selcho *et al.* (2017) recently described circadian pacemaker control of a peripheral clock in *Drosophila* to control steroid hormone secretion and, whose titres gate subsequent adult emergence (eclosion). In that output pathway, s-LNv activate the peptidergic PTTH neurons, which in turn activate the peripheral Prothoracic Gland. With respect to locomotor behavior, we found that M (s-LNv) cells and E (LNd) oscillators independently control the morning and evening neural activity phases in EB-RNs (Figure 4) and in PPM3-EB (Figure 5G-I). Two recent studies linked a different subset of circadian pacemakers (DN1s) to subgroups of EB-RNs, via subsets of neurons in the Anterior Optic Tubercle (Lamaze *et al.* 2018; Guo *et al.* 2018). By manipulating activity in this pathway, both groups found effects on the balance between sleep and wake states. Thus, increasing lines of research indicate circadian- and sleep-regulating circuits impart timing information to govern behavior through the classic pre-motor centers of the Central Complex.

Based on previous limited screens, two other groups of identified peptidergic neurons were implicated as components of output circuits for locomotor activity rhythms in *Drosophila*. The two groups included ones that express the diuretic hormone 44 (DH44), an orthologue of mammalian CRF (Cavanaugh *et al.* 2014), and ones that express leucokinin (LK) (Cavey *et al.* 2016), whose receptor is related to the neurokinin receptors. DH44 neurons receive synaptic

inputs from DN1 pacemaker neurons, and both DH44- and LK- neurons are required for proper locomotor activity rhythms under constant darkness (DD) conditions. However, the connectivity by which these two groups of neuroendocrine neurons promote locomotor activity, and phase-restrict it to morning or evening times, is uncertain. The daily two-peak pattern of locomotor activity is different from the daily activity pattern of either LK neurons (which are more active in the evening - Cavey *et al.* 2016), or that of DH44 neurons (which are more active in mid-day - Bai *et al.* 2018). Additionally, recent studies showed that LK neurons also mediate hunger signals to promote locomotor activity (Yurgel *et al.* 2018; Zandawala *et al.* 2018). These observations suggest that during daily locomotor activity peaks, flies might move to seek food, seek a mate, and/or respond to other internal drives, which might be coupled with circadian timing. Therefore, several parallel pathways may converge within the EB-RN pre-motor circuit to generate and shape daily behavioral patterns.

**Dopaminergic neurons under circadian regulation**

Previous studies in flies and mice have shown that DA modulates circadian pacemaker circuits (Chang *et al.* 2006; Grippo *et al.* 2017; Hirsh *et al.* 2010; Klose *et al.* 2016; Langraf *et al.* 2016; Shang *et al.* 2011, 2013). Our findings here show that circadian pacemaker neurons also regulate DA neuron activity. DA neurons responded to circadian neuron outputs (Figure 4AB) and showed spontaneous circadian neural activity rhythms that were correlated with behavior (Figure 5). These findings correspond to earlier studies in mammals showing that circadian rhythms in DA neuron activity, and in striatal DA content, are dependent on master circadian pacemaker neurons in the suprachiasmatic nuclei (SCN) (Smith *et al.* 1992; Sleipness *et al.* 2006; Luo *et al.* 2008; Fifel *et al.* 2018). Deficits of DA neurons in patients and in animal

models of Parkinson's disease caused dysregulation of circadian locomotor activity patterns and of sleep (Videnovic and Golombek, 2017). Consistent with our model, a DA-deficient mouse model displays dampened and fragmented locomotor activity rhythms, yet possesses normal SCN molecular clocks (Taylor *et al.* 2009; Kudo *et al.* 2011). It remains to be determined whether DA in mammals, as in *Drosophila*, represents the critical agent by which circadian outputs activate pre-motor centers to adaptively schedule locomotor activity.

The effects of DA to organize proper circadian control of locomotor behavior may be related to its well documented effects in *Drosophila* to promote arousal, especially forms of arousal associated with changes in sleep and circadian rhythm states (Andretic *et al.* 2005; Birman, 2005; Kume *et al.* 2005; Lima and Miesenbock, 2005; Lebestky *et al.* 2009; Liu *et al.* 2012). A recent study suggests that PDF signals from circadian neurons promotes wakefulness by suppressing daytime activity in the PPM3 DA neurons (Potdar and Sheeba 2018). However, we favor an alternative model which is based on the results described above, including both manipulations of PPM3 physiology as well as measurements of normal PPM3 24-hr activity patterns *in vivo*. We propose PPM3-DA neurons promote wakefulness and locomotor activity in the morning by excitation from the M oscillators, and perhaps directly by PDF.

**How can circadian timing signals modulate activity in central complex to promote rhythmic locomotor activity?**

Our results suggest that a major focus of circadian timing signals to regulate locomotor activity resides in the Central Complex (CX), the decision-making circuit that dictates the balance between locomotion and rest. Within the CX, EB neurons transform sensory inputs into goal-directed motor outputs (Sun *et al.* 2017; Shiozaki and Kazama, 2017). The final motor

output is subject to many signals reflecting the internal state: for example, hunger signals transmitted through the leucokinin-expressing neurons promote locomotor activity (Yurgel *et al.* 2018; Zandawala *et al.* 2018). Here, we propose that the circadian system promotes locomotor activity in the dawn and dusk episodes by increasing the probability of the EB-RNs to favor activity over rest. A similar action on EB-RNs appears to underlie sleep promotion by dorsal fan-shaped body (dFSB) neurons (Donlea *et al.* 2017). dFSB neurons effectively suppress sensory-triggered movements by inhibiting EB-RNs via helicon cells and thereby instigate less activity and more rest. Thus, sleep and circadian signaling antagonistically converge on the EB-RN system to influence the level of motor output.

In addition to motor outputs, parts of EB circuit also signal the sleep drive: Liu *et al.* (2016) showed that a subgroup of EB-RNs, R2 (called R5 by Omoto *et al.* 2017) registers sleep debt and thereby constitutes an integral part of the sleep homeostat mechanism. How can this be reconciled with our finding that the EB-RNs (including R2s) exhibit neural activity in concert with locomotor behavior? We propose that, because the level of locomotor activity is directly encoded by EB-RN activity, a subgroup of them (R2s) incorporates the amount of locomotor activity along with duration of wakefulness to help generate sleep drive. Therefore, although they receive common circadian pacemaker and DA inputs, and although they exhibit common activation periods at dawn and at dusk, different subgroups of EB-RNs likely have specialized downstream functions in behavioral control.

## METHODS

## KEY RESOURCES TABLE

| REAGENT or RESOURCE | SOURCE | IDENTIFIER |
|---|---|---|
| Chemicals, Peptides, and Recombinant Proteins | | |
| Adenosine 5′-triphosphate | Sigma | A5394 |
| Dopamine hydrochloride | Sigma | H8502 |
| Drosophila pigment dispersing factor (PDF) | Neo-MPS | NA |
| Experimental Models: Organisms/Strains | | |
| *Drosophila: tim(UAS)-GAL4* | (Blau and Young, 1999) | NA |
| *Drosophila:pdfr(B)-GAL4* | Taghert Lab, (Im and Taghert, 2010) | NA |
| *Drosophila:pdfr(F)-GAL4* | Taghert Lab, (Im and Taghert, 2010) | NA |
| *Drosophila:pdf-LexA* | (Shang *et al.* 2008) | NA |
| *Drosophila: LexAop-nSyb-spGFP1-10, UAS-CD4-spGFP11* | Bloomington (Frank *et al.* 2015) | BL#64315 |
| *Drosophila:20XUAS-IVS-GCaMP6s(attP40)* | Bloomington (Chen *et al.* 2013) | BL#42746 |
| *Drosophila:13XLexAop2-IVS-GCaMP6s-p10(su(Hw)attP1)* | Bloomington (Chen *et al.* 2013) | BL#44274 |
| *Drosophila: LexAop-jGECO1a* | Bloomington (Dana *et al.* 2016) | BL#63794 |
| *Drosophila: UAS-(FRT.stop)-TeTn* | Bloomington | BL#67690 |
| *Drosophila: UAS-SGG* | Bloomington (Martinek *et al.* 2001) | BL#5435 |
| *Drosophila: UAS-GRAB$_{DA4.4}$* | Yulong Li (Sun *et al.* 2018) | NA |
| *Drosophila: UAS-P2X2* | Orie Shafer ( Yao *et al.* 2002) | NA |
| *Drosophila: LexAop-P2X2* | Orie Shafer ( Yao *et al.* 2002) | NA |
| *Drosophila: cry-LexA::GAD* | F. Rouyer (CNRS Gyf, Paris) (Liang *et al.* 2017) | NA |
| *Drosophila: TH-LexA* | (Berry *et al.* 2015) | NA |
| *Drosophila: GMR_SS00681* | Gifts from Drs. Dionne, Nern and Rubin (Janelia Research Center, VA) (Liang *et al.* 2017) | NA |

| | | |
|---|---|---|
| *Drosophila: GMR_MB122B* | Gifts from Drs. Dionne, Nern and Rubin (Janelia Research Center, VA) (Liang *et al.* 2017) | NA |
| *Drosophila: GMR_SS002769* | Janelia Research Center (Robie *et al.* 2017) | NA |
| *Drosophila: GMR56H10-GAL4* | Bloomington (Sun *et al.* 2017) | BL#61644 |
| *Drosophila: GMR96F08-GAL4* | Bloomington (Liu *et al.* 2016) | BL#39499 |
| *Drosophila: GMR92G05-GAL4* | Bloomington (Xie *et al.* 2018) | BL#48416 |
| *Drosophila: GMR19C08-LexA* | Bloomington | BL#53543 |
| *Drosophila: norpA$^{P24}$* | Bloomington (Ostroy & Pak 1974) | BL#9048 |
| *Drosophila: per$^{01}$* | (Konopka and Benzer, 1971) | NA |
| *Drosophila: pdfr$^{han5403}$* | (Hyun *et al.* 2005) | NA |
| *Drosophila: UAS-DopR1-miRNA* | Wu Lab (Liu *et al.* 2017) | NA |
| *Drosophila: UAS-DopR2-miRNA* | Wu Lab (Liu *et al.* 2017) | NA |
| *Drosophila: UAS-D2R-miRNA* | Wu Lab (Xie *et al.* 2018) | NA |
| *Drosophila: UAS-DopEcR-miRNA* | Wu Lab (Xie *et al.* 2018) | NA |
| *Drosophila: TH-Flp* | Wu Lab (Xie *et al.* 2018) | NA |
| Software and Algorithms | | |
| R | http://www.R-project.org/ | Version: 3.3.3 |
| Julia | https://julialang.org/ | Version: 0.6 |
| Prism 7 | GraphPad | https://www.graphpad.com/ |
| Fiji | (Schindelin *et al.* 2012) | https://fiji.sc/ |
| Imagine | (Holekamp *et al.* 2008) | http://holylab.wustl.edu/ |

## EXPERIMENTAL MODEL AND SUBJECT DETAILS

**Fly stocks.** Flies were reared on standard cornmeal/agar food at room temperature. Before imaging experiments, flies were entrained under 12 h light: 12 h dark (LD) cycles at 25°C for at least 3 days or under 10 h light: 14 h dark (short day, SD) cycles at 25°C for at least 5 days. The following fly lines were previously described: *tim(UAS)-GAL4* (Blau & Young 1999), *pdfr(F)-GAL4* and *pdfr(B)-GAL4* (Im & Taghert 2011), *GMR56H10-GAL4* (Sun *et al.* 2017), *GMR69F08-GAL4* (Liu *et al.* 2016); split-GAL4 lines: GMR_MB122B and GMR_SS00681 (Liang *et al.* 2017), GMR_SS002769 (Robie *et al.* 2017); *cry-LexA* (Liang *et al.* 2017), *pdf-LexA* (Shang *et al.* 2008), *TH-LexA* (Berry *et al.* 2015); *TH-Flp* (Xie *et al.* 2018); *UAS-SGG* (Martinek *et al.* 2001), *UAS-P2X2* and *LexAop-P2X2* (Yao *et al.* 2002), *LexAop-jGECO1a* (Dana *et al.* 2016), *UAS-GCaMP6s* and *LexAop-GCaMP6s* (Chen *et al.* 2013), *UAS-GRAB$_{DA4.4}$* (Sun *et al.* 2018), *UAS-DopR1-miRNA* and *UAS-DopR2-miRNA* (Liu *et al.* 2017), *UAS-D2R-miRNA* and *UAS-DopEcR-miRNA* (Xie *et al.* 2018); *per$^{01}$* (Konopka & Benzer 1971), *norpA$^{P24}$* (Ostroy & Pak 1974) and *pdfr$^{han5403}$* (Hyun *et al.* 2005).

*UAS-(FRT.stop)-TeTn* (BL67690), *GMR19C08-LexA* (BL52543), *GMR56H10-GAL4* (BL61644), and *GMR92G05-GAL4* (BL48416) were obtained from Bloomington Stock Center. The *cry-LexA* line was a gift from Dr. F Rouyer (CNRS Gyf, Paris).

## METHOD DETAILS

**Nomenclature.** The nomenclature of ellipsoid body (EB) subgroups in this study follows Renn *et al.* (1999a), which was revised by Omoto *et al.* (2017) reflecting the introduction of more specific driver lines. The EB subgroup labelled by *cry-lexA* and *GMR69F08-GAL4* (also see Liu *et al.* 2016) was called R2, they were re-named R5 by Omoto *et al.* (2017). The EB subgroup

labelled by *GMR19C08(pdfr)-lexA* was called R4, they were re-named R2 by Omoto *et al.* (2017).

***In vivo* fly preparations.** The surgical procedure for *Drosophila in vivo* calcium imaging followed methods described in Liang *et al.* (2016, 2017). Following $CO_2$ anesthetization, flies were mounted by inserting the neck into a narrow cut in an aluminum foil base. Thus, the foil permitted immersion of the head by saline during preparatory surgery and *in vivo* imaging, while the body remained in an air-filled enclosure. To access circadian pacemaker neurons on one side of the head, a single antenna, a portion of the dorso-anterior head capsule, and a small part of one compound eye were removed from the side ipsilateral to imaging. To access EB-RNs, both antennae and a portion of the dorso-anterior head capsule were removed, while the compound eyes remained intact. The entire surgery was typically ~15 min in duration. For experiments that entailed transection of connectives, or removal of the entire body, the surgery was conducted with fine forceps prior to brain-exposing surgery. The wounds were then closed by application of a bio-compatible silicone adhesive (Kwik-Sil, WPI, USA).

***In vivo* calcium imaging.** Imaging was conducted with custom Objective Coupled Planar Illumination (OCPI) microscopes (Holekamp *et al.* 2008), as described in Liang *et al.* (2016, 2017). Briefly, OCPI uses a cylindrical lens to generate a ~5µm thick light sheet, which was coupled to the focal plane of the objective. For 24-hr imaging, the objective coupled light sheet was scanned across the fly brain through the cranial window every 10 min to capture stacks of images. Each stack contained 20 to 40 separate images with a step size of 5 to 10 microns. For each image, exposure time was not more than 0.1 s. During 24-hr imaging, fresh hemolymph-

like saline (HL3; 5 mM KCl, 1.5 mM CaCl2, 70 mM NaCl, 20 mM MgCl2, 10 mM NaHCO3, 5 mM trehalose, 115 mM sucrose, and 5 mM HEPES; pH 7.1) was perfused continuously (0.1-0.2 mL/min). Light-dark cycle stimulation during *in vivo* calcium imaging was delivered using a white Rebel LED (Luxeon) controlled by an Arduino UNO board (Smart Projects, Italy) as described in Liang *et al.* (2017). For short term high-frequency imaging, image stacks were captured every 10 s (Figure S2A and S4B), every 2 s (Figure 4A and 7A-C, Figure S2B-F), or every 1 s (Figure 5C-F and Figure S4A). For each image, exposure time was not more than 0.04 s. For pharmacological tests, each fly was treated once. After 1 or 5-min baseline recordings, 1mL of 0.1 mM PDF solution, 1 mM dopamine solution, or 10 mM ATP solution (pH adjusted to 7) was manually added to a 9 mL static HL3 bath over a ~2 s period. PDF was purchased from Neo-MPS (San Diego, CA, USA) at a purity of 86%.

**Locomotor monitoring during imaging.** During 24-hr *in vivo* calcium imaging, *Drosophila* locomotor activity was measured by an infrared detector (LTE-301)/emitter (940nm, LTE-302) circuit. The infrared emitter was aimed toward the body of the fly and the detector received the infrared light transmitted through the fly (shown in Figure 2A). Both the body and leg movements can cause changes in transmitted light intensity. The analog signal from the infrared detector was transmitted through an Arduino UNO board with 100Hz sampling rate. The infrared emitter was shut off for 10 seconds every 10 min, allowing the microscope to acquire complete volume brain scans. The daily fly locomotor activity pattern was then calculated by counting the activity events within each 10-min bin. The activity events were identified by time-points when the infrared detector signal was out of the range for standard deviation by 3-fold. Then the normalized event count trace was aligned with the EB-R2 neuron calcium signal of the same fly

(Figure 2c). The Pearson's correlation coefficient between these two signals was calculated. To test their correlation at an hourly time scale, these two signals then were averaged by a method similar to spike-triggered averaging. 4-hr windows (1 hr before and 3 hr after the trigger point) of calcium signals were aligned by the local maximum (increasing phase) or local minimum (decreasing phase) of calcium signal derivatives. The locomotor signals occurring in these 4-hr windows were then averaged. Analysis was performed using R 3.3.3.

**Locomotor activity.** To examine the circadian rhythms of locomotor activity, individual flies was monitored using Trikinetics *Drosophila* Activity Monitor (DAM) system for 6 days under light-dark (LD) cycles and then for 9 days under constant darkness (DD) condition. $\chi^2$ periodogram with a 95% confidence cutoff and SNR analysis were used to measure circadian rhythmicity and periodicity (Levine *et al.* 2002). Arrhythmicity were defined by a power value ($\chi^2$ power at best period) less than 10, width lower than 1, a period less than 18 hrs or more than 30 hrs. To find the phases of morning and evening peaks, each 24-hr day was split into two halves. For LD, it was split at ZT6. For DD1, it was split at the time of the manually selected midday ''siesta''. Then the morning peak and evening peak were then determined by the maximum activity in each half.

**Immunocytochemistry.** Immunostaining for PER and beta-Gal followed previous descriptions (Liang *et al.* 2016). Briefly, fly brains were dissected in ice-cold, calcium-free saline and fixed for 15m in 4% paraformaldehyde containing 7% picric acid (v/v) in PBS. Primary antibodies included rabbit anti-PER (1:5000; kindly provided by Dr. M. Rosbash, Brandeis Univ.; Stanewsky *et al.* 1997) and mouse anti-beta-galactosidase (1:1000; Promega, Madison, WI, Cat.

#Z3781, Lot #149211). Secondary antisera were Cy3-conjugated (1:1000; Jackson Immunoresearch, West Grove, PA). Images were acquired on the Olympus FV1200 confocal microscope. PER protein immunostaining intensity was measured in ImageJ-based Fiji (Schindelin *et al.* 2012).

**Data reporting.** No statistical methods were used to predetermine sample sizes. The selection of flies from vials for imaging and behavioral tests were randomized. The investigators were not blinded to fly genotypes.

## QUANTIFICATION AND STATISTICAL ANALYSIS

**Imaging data analysis.** Calcium imaging data analysis was as described previously (Liang *et al.* 2016, 2017). Images were acquired by a custom software, Imagine (Holekamp *et al.* 2008) and processed in Julia 0.6 including non-rigid registration, alignment and maximal projection along z-axis. Then ImageJ-based Fiji was used for rigid registration and to manually select regions of interest (ROIs) over individual cells or groups of cells. Average intensities of ROIs were measured through the time course and divided by average of the whole image to subtract background noise. For spontaneous calcium transients, each time trace was then calculated as $dF/F=(F-F_{min})/F_{mean}$. For 24-hr time traces, traces of certain cell type ROIs were first aligned, based on Zeitgeber Time and averaged across different flies. Hartigans' dip test and Silverman's test were used to testify whether the averaged 24-h time traces are unimodal or bimodal (Hartigan & Hartigan, 1985; Silverman, 1981). The phase relationship between traces was estimated by cross-correlation analysis. The 24-hr-clock circular plot of phases reflected both mean peak time and phase relationships of the same cell-group traces from different flies. For

neurons with daily bimodal patterns (EB-RNs and PPM3-EB DA neurons), each trace was split into two parts: ZT18-ZT6 (morning) and ZT6-ZT18 (evening) to estimate the morning and evening peak phases respectively. For dual-color imaging traces, all signals were filtered (high-pass, 1/30 Hz). To 'spike'-triggered average simultaneous traces of three cell types (Figure 5DE), the peaks of selected cell-type signal were identified by the local maximum of that signal after a low-pass filter (0.2Hz). Unfiltered signals of three cell types were then aligned by these peaks to calculate the averaged traces for individual cell types. For pharmacological calcium responses, each time trace was normalized by the initial intensity ($F/F_0$). The maximum change was calculated by the maximum difference of normalized intensities between baseline and after drug application. The latency (onset time constant) was calculated by the duration from drug application to the time when the trace reached 63.2% of maximum change. All statistics tests are two-sided. Trace analysis and statistics were performed using R 3.3.3 and Prism 7 (GraphPad, San Diego CA).

# Figure 1

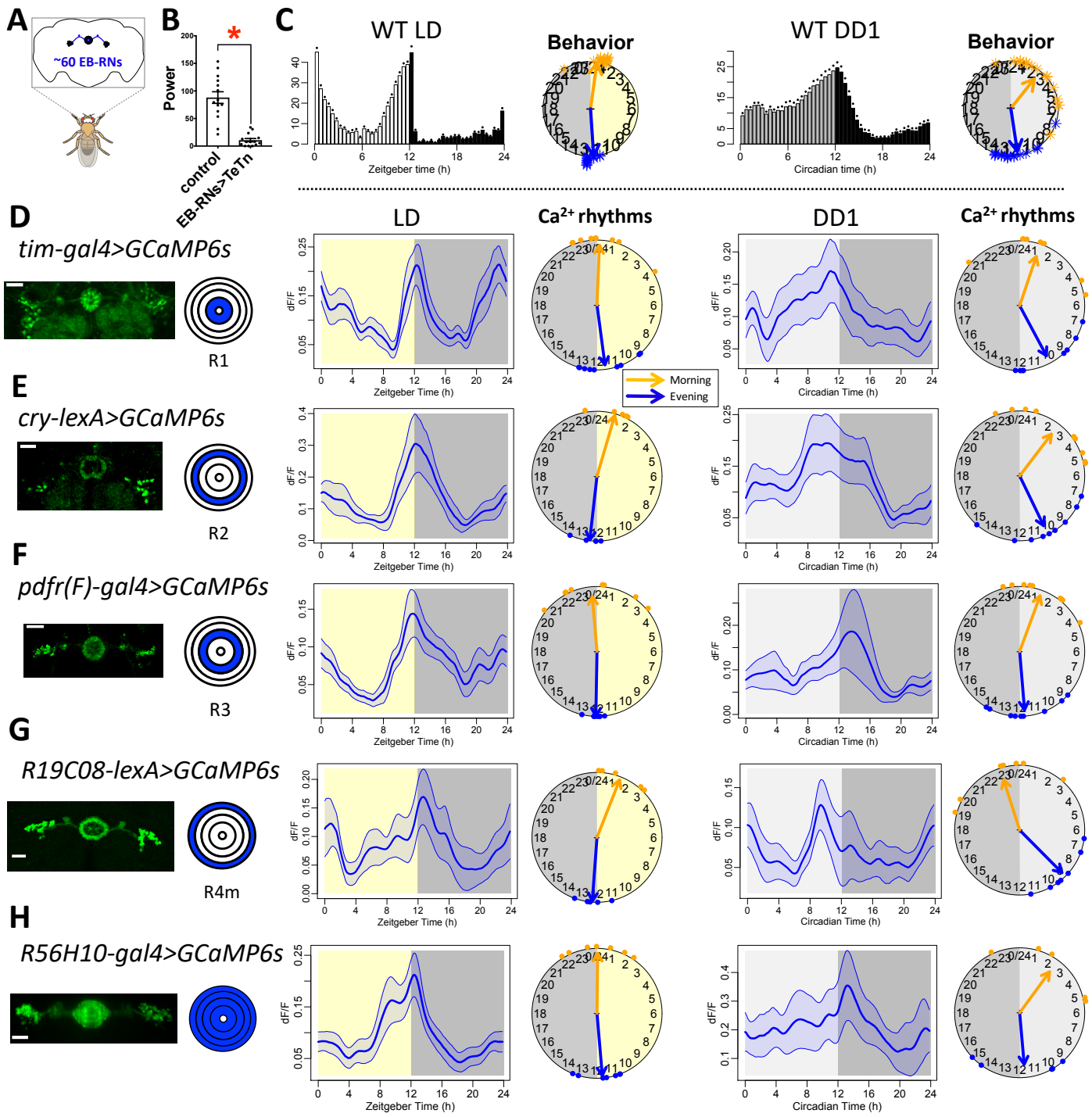


**Figure 1. Daily bimodal neural activity patterns of EB ring neurons.**
(**A**) The ellipsoid body ring neurons (EB-RNs) in the fly brain. (**B**) Average rhythm strength (power) of locomotor activity for 9 days under constant darkness (DD) of control and flies with TeTn expressed in EB-RNs; asterisk denotes significant differences compared to control ($P < 0.0001$, Mann-Whitney test). (**C**) The average locomotor activity histogram and phase distributions of behavioral peaks of wild type *R56H10-GAL4/GCaMP6s* flies (left) under 12-hr light: 12-hr dark (LD) cycle and (right) in the first day under DD (n = 16 flies). Dots indicate SEM. (**D**-**H**) Daily $Ca^{2+}$ activity patterns of the EB ring neuron subgroups: (D) R1 labelled by *tim-GAL4*, (E) R2 labelled by *cry-lexA*, (F) R3 labelled by *pdfr(F)-GAL4*, (G) R4 labelled by *R19H08(pdfr)-lexA*, and (H) R1-4 labelled by *R56H10-GAL4*. Left, confocal images of EB ring neurons and diagrams of their concentric arborization radii; scale bars, 25 µm. Middle and Right, average $Ca^{2+}$ transients and $Ca^{2+}$ phase distribution for both morning peaks (orange dots and arrow) and evening peaks (blue dots and arrow). Middle - under LD; Right - under DD.

# Figure 2

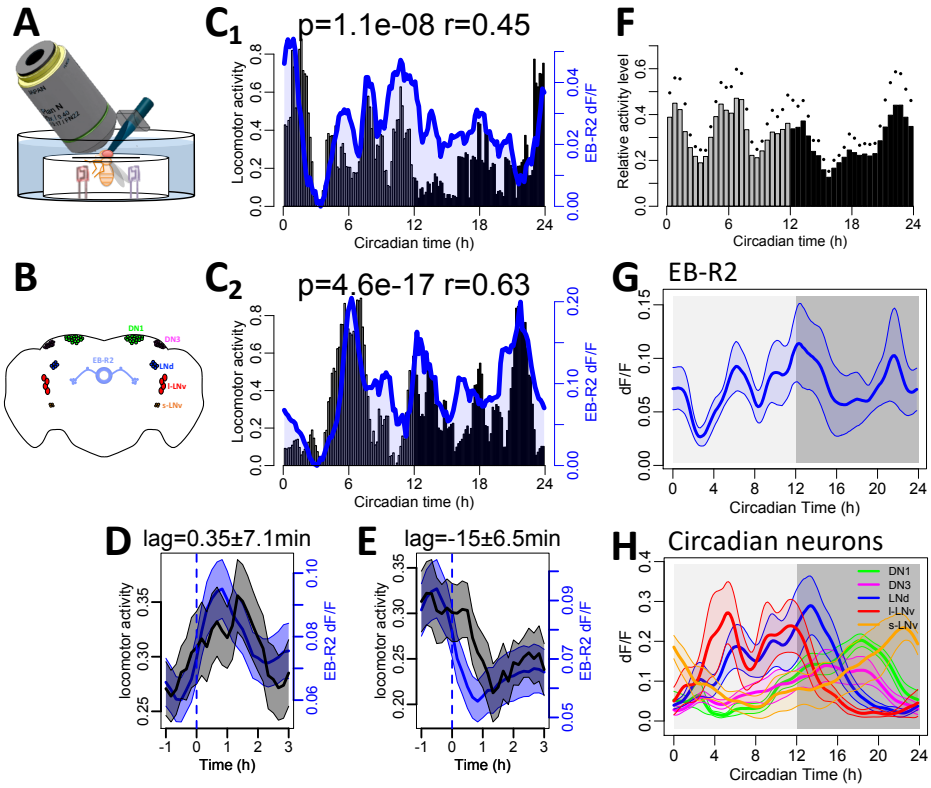


**Figure 2. EB ring neuron activity is correlated with locomotor activity.**
(**A**) Illustration of long-term *in vivo* imaging with infrared measurement of locomotor activity (see Methods).
(**B**) Map of the major circadian neuron groups and EB ring neurons.
(**C**) Representative recordings of two flies: bars, normalized locomotor activity counts per 10 m; blue traces, $Ca^{2+}$ activity of EB-R2 neurons in the same fly.
(**D-E**) Average locomotor activity (black) and $Ca^{2+}$ activity (blue) aligned by (D) increasing phase and (E) decreasing phase of $Ca^{2+}$ activity. The averaged phase lags were calculated by cross-correlation: (D) 0.35 ±7 min; (E) -15±0.5 min.
(**F-H**) Average locomotor activity (F) and average $Ca^{2+}$ transients of (G) EB-R2 neurons and (H) circadian pacemaker neurons in the same flies (n = 6 flies). Dots and shading indicate SEM.

# Figure 3

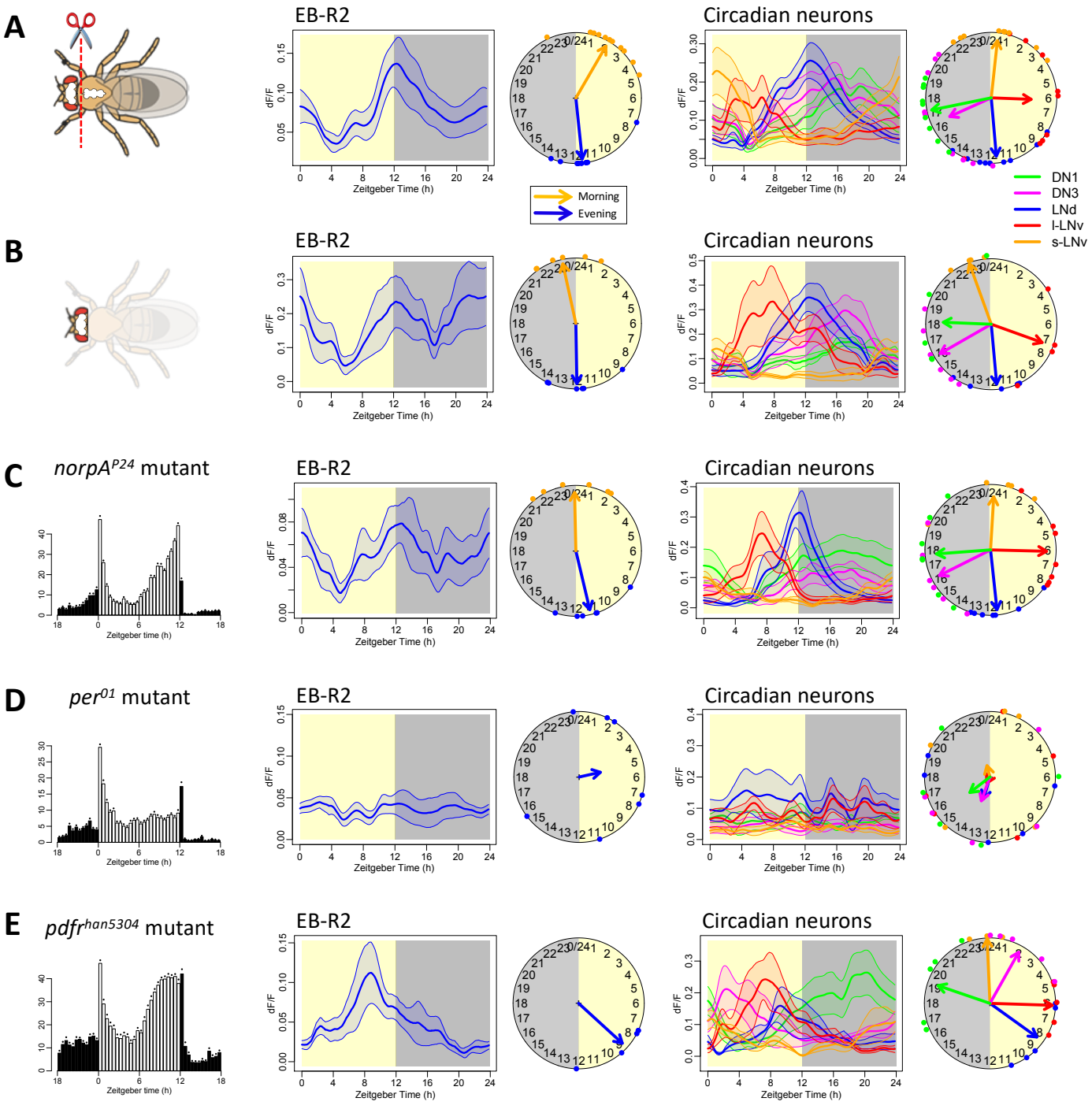


**Figure 3. EB ring neuron rhythms are driven by clocks, not in response to behavior or sensation.**
(**A**) Daily $Ca^{2+}$ activity patterns of (middle) EB-R2 neurons and (right) circadian neurons under LD immediately after cutting the connectives between brain and ventral nerve cord (n = 10 flies). (**B**) Daily $Ca^{2+}$ activity patterns of EB-R2 and circadian neurons under LD immediately after removing the bodies (n = 6 flies). (**C**) In blind *norpA*$^{p24}$ mutant flies, (left) average locomotor activity (n = 22 flies) and daily $Ca^{2+}$ activity patterns (middle) of EB-R2 neurons and (right) circadian neurons under LD (n = 6 flies). (**D**) In *per*$^{01}$ mutants, average locomotor activity (n = 16 flies) and arrhythmic $Ca^{2+}$ activity patterns of EB-R2 and of circadian neurons under LD (n = 7 flies). (**E**) In *pdfr*$^{han5304}$ mutants, average locomotor activity (n = 8 flies) and $Ca^{2+}$ activity patterns of EB-R2 and of circadian neurons under LD (n = 7 flies).

# Figure 4

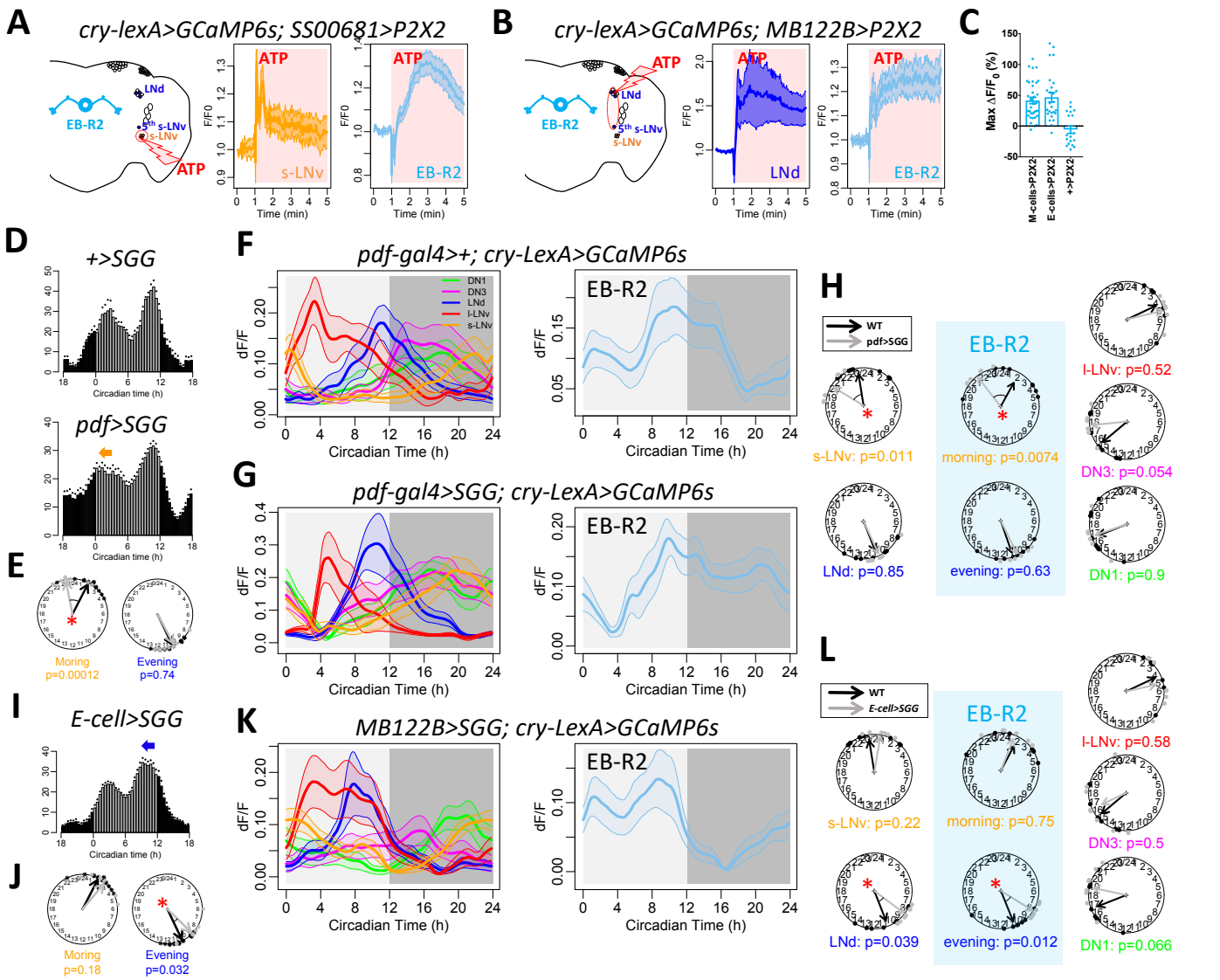


**Figure 4. Daily activity phases of EB-RNs are dictated by M and E cells.**
(**A**) Illustration and averaged response traces of M cells (s-LNv) and EB-R2 neurons to ATP application in flies with P2X2 expressed in M cells (n = 6 flies). (**B**) Illustration and averaged response traces of E cells (three LNd and the 5$^{th}$ s-LNv neurons) and EB-R2 neurons to ATP application in flies with P2X2 expressed in E cells (n = 5 flies). (**C**) Maximum $Ca^{2+}$ changes of EB-R2 after ATP application in experimental flies from panels A and B and from controls (n = 3 flies, also see Figure S2D-F). (**D**) Average locomotor activity in DD1 of (top) wild type (controls, n = 16 flies) and (bottom) flies expressing SGG in PDF neurons (PDF>SGG, n = 16). (**E**) Phase comparisons of morning and evening activity between WT and PDF>SGG. Note that only the morning activity phase was advanced (* $P < 0.05$, Watson-Williams test). (**F-G**) Daily $Ca^{2+}$ activity patterns during DD1 of (left) circadian neurons and (right) EB-R2 neurons in control flies (F, n = 10) and in M cell>SGG flies (G, n = 6). (**H**) Phase comparisons of $Ca^{2+}$ activity peaks between control and PDF>SGG flies, in each circadian neuron group and in the EB-R2 neurons. For the latter, the morning (orange) and evening (blue) activity peaks are displayed separately. Note that only M cells (s-LNv) and the morning peak of EB-R2 were significantly advanced in PDF>SGG. (**I**) Average locomotor activity of flies expressing SGG in E cells (using split-GAL4 line GMR_MB122B; E-cell>SGG, n = 16 flies) during DD1. **(J)** Phase comparisons of morning and evening locomotor activity between control and E-cell>SGG. Only evening activity phase was significantly different (advanced, * $P < 0.05$, Watson-Williams test). (**K**) Daily $Ca^{2+}$ activity patterns during DD1 of (left) circadian neurons and (right) EB-R2 neurons in E-cell>SGG flies (n = 8). (**L**) Phases comparisons of morning and evening activity between WT and E-cell>SGG. Note that only the morning activity phase was advanced. Phase comparisons of $Ca^{2+}$ activity peaks between control and E cell>SGG flies, in each circadian neuron group and in the EB-R2 neurons. For the latter, the morning (orange) and evening (blue) activity peaks are displayed separately. Note that only E cells (LNd) and the evening peak of EB-R2 were significantly different (advanced, * $P < 0.05$, Watson-Williams test).

# Figure 5

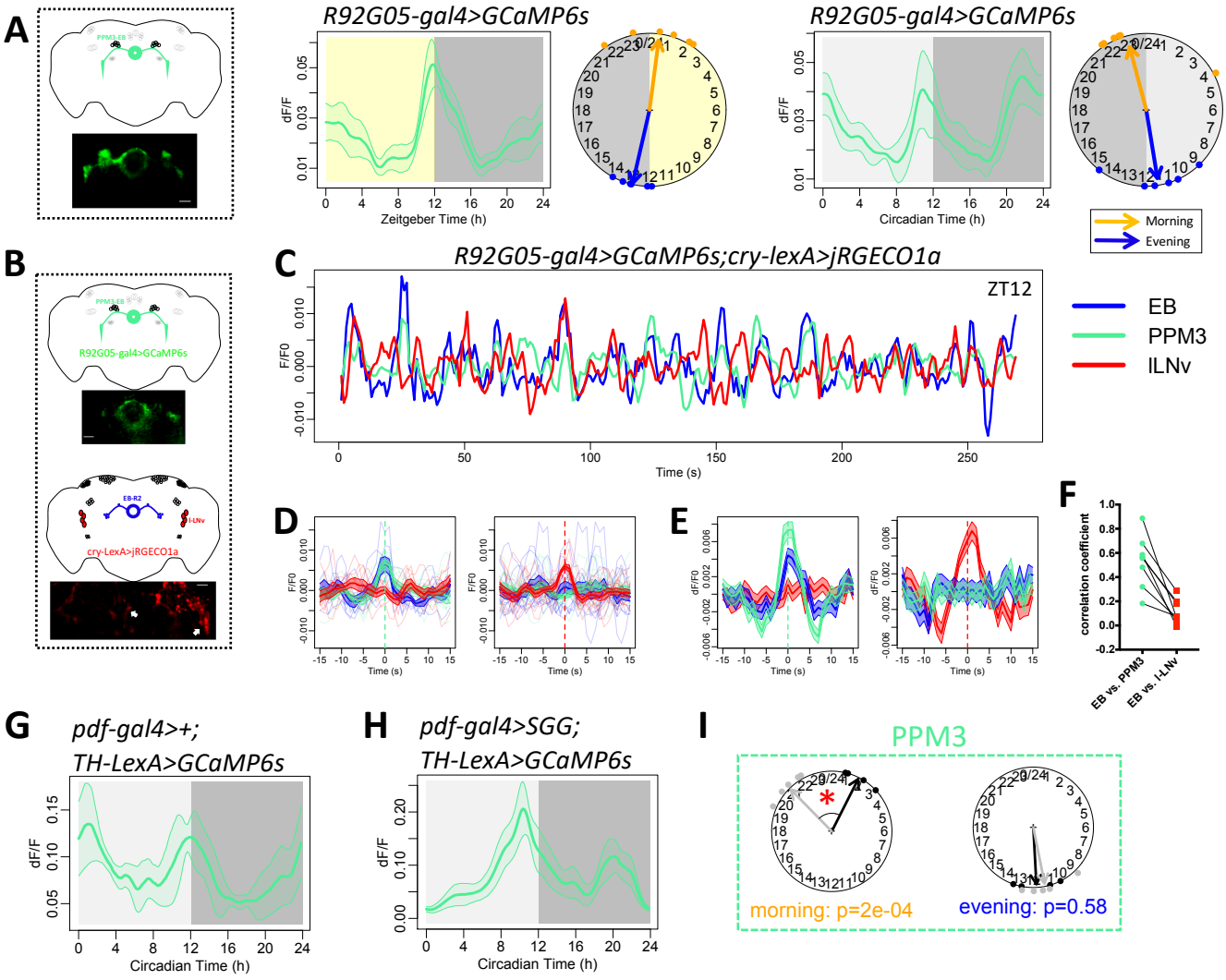


**Figure 5. Daily bimodal pattern of PPM3-EB.**

(**A**) Daily bimodal $Ca^{2+}$ activity patterns of PPM3-EB under LD and DD (n = 6 and 6 flies).

(**B**) Illustration of dual-color $Ca^{2+}$ imaging: GCaMP6s in PPM3-EB and jRGECO1a in EB-R2 and circadian neurons.

(**C**) Example traces of $Ca^{2+}$ activity in EB-R2, PPM3-EB, and l-LNv neurons (sampling rate, 1Hz).

(**D**) Average $Ca^{2+}$ activity traces from (C) aligned by (left) PPM3-EB peak and (right) l-LNv peak.

(**E**) As in (D), average $Ca^{2+}$ activity traces from all flies (n = 8 flies).

(**F**) Correlation of $Ca^{2+}$ activity (Pearson's r) between EB and PPM3 is considerably stronger than that between EB and l-LNv (p=0.0009, paired t-test after Fisher's Z-transform).

(**G-H**) Daily $Ca^{2+}$ activity patterns of PPM3 neurons during DD1 (G) in control flies (n = 4 flies) and (H) in PDF>SGG flies (n = 5 flies).

**(I)** Phase comparisons of PPM3 neuron activity peaks for both morning (orange) and evening (blue) phases between control and PDF>SGG flies. The morning PPM3 peak was significantly advanced in PDF>SGG, while the evening PPM3 peak was unaffected (Watson-Williams test).

# Figure 6

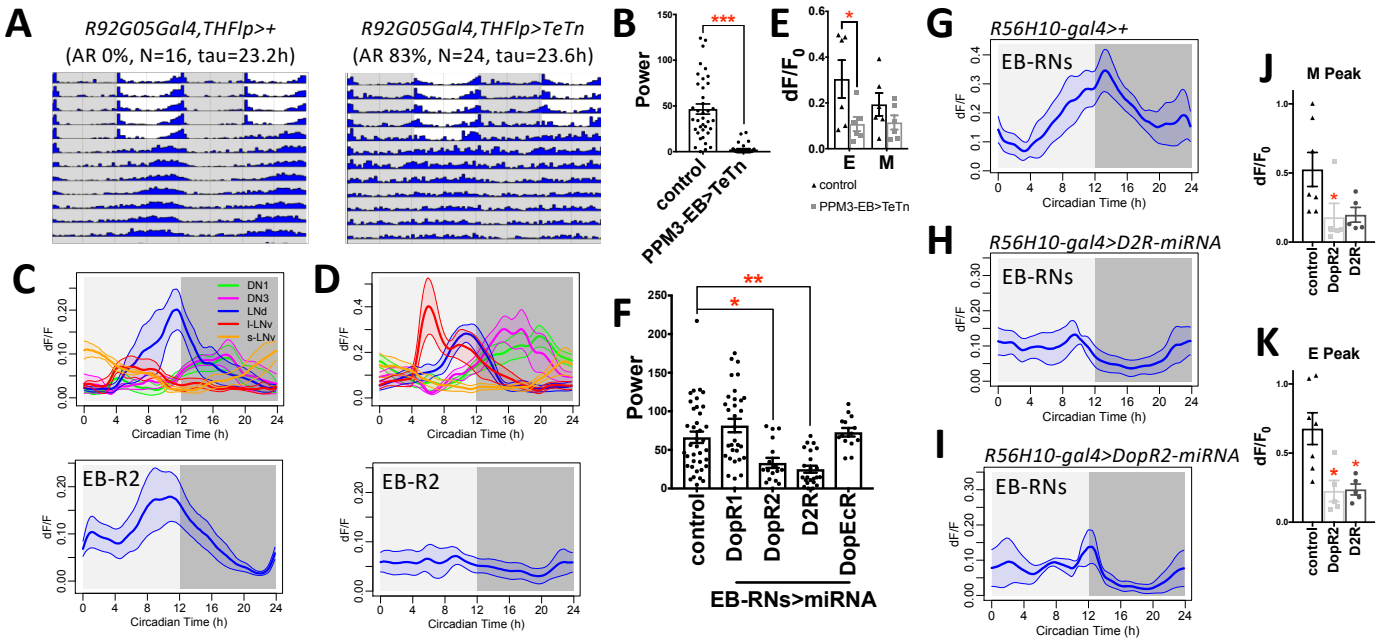


**Figure 6. PPM3-EB and EB-RNs constitute downstream elements of a circadian output motor circuit.**

(**A**) Group-averaged actograms of control flies (left) and one expressing tetanus toxin (TeTn) in PPM3-EB neurons to block neurotransmission (right).

(**B**) Average rhythm strength (power) of genotypes in (A) for 9 days under DD; asterisk denotes significant differences compared to control ($P < 0.0001$, Mann-Whitney test).

(**C-D**) Daily $Ca^{2+}$ activity patterns of circadian neurons (top) and EB-R2 neurons (bottom) during DD1 in (C) control flies (n = 6) and (D) ones with TeTn expressed in PPM3-EB neurons (n = 6).

(**E**) The amplitude of daily morning and evening $Ca^{2+}$ peak in EB-R2 neurons in control and PPM3>TeTn flies (*$P < 0.05$, Mann-Whitney test). The amplitude difference in the evening peak was significantly different.

(**F**) Average rhythm strength (power) of genotypes for 9 days under DD in which DA receptors are knocked down in EB-RNs using *R56H10-gal4*; asterisk denotes significant differences compared to control ($P < 0.05$, Kruskal-Wallis test followed by post hoc Dunn's tests).

(**G-I**) Daily $Ca^{2+}$ activity patterns of EB-R neurons under DD1 in (G) WT (n = 8 flies), (H) flies with (H) *D2R*-knockdown and (I) *DopR2*-knockdown in EB-R neurons (n = 5 and 5 flies).

(**J-K**) The amplitude of daily (J) morning and (K) evening $Ca^{2+}$ peak in EB-R neurons was reduced in DA-receptor-knockdown flies (*$P < 0.05$, Mann-Whitney test).

# Figure 7

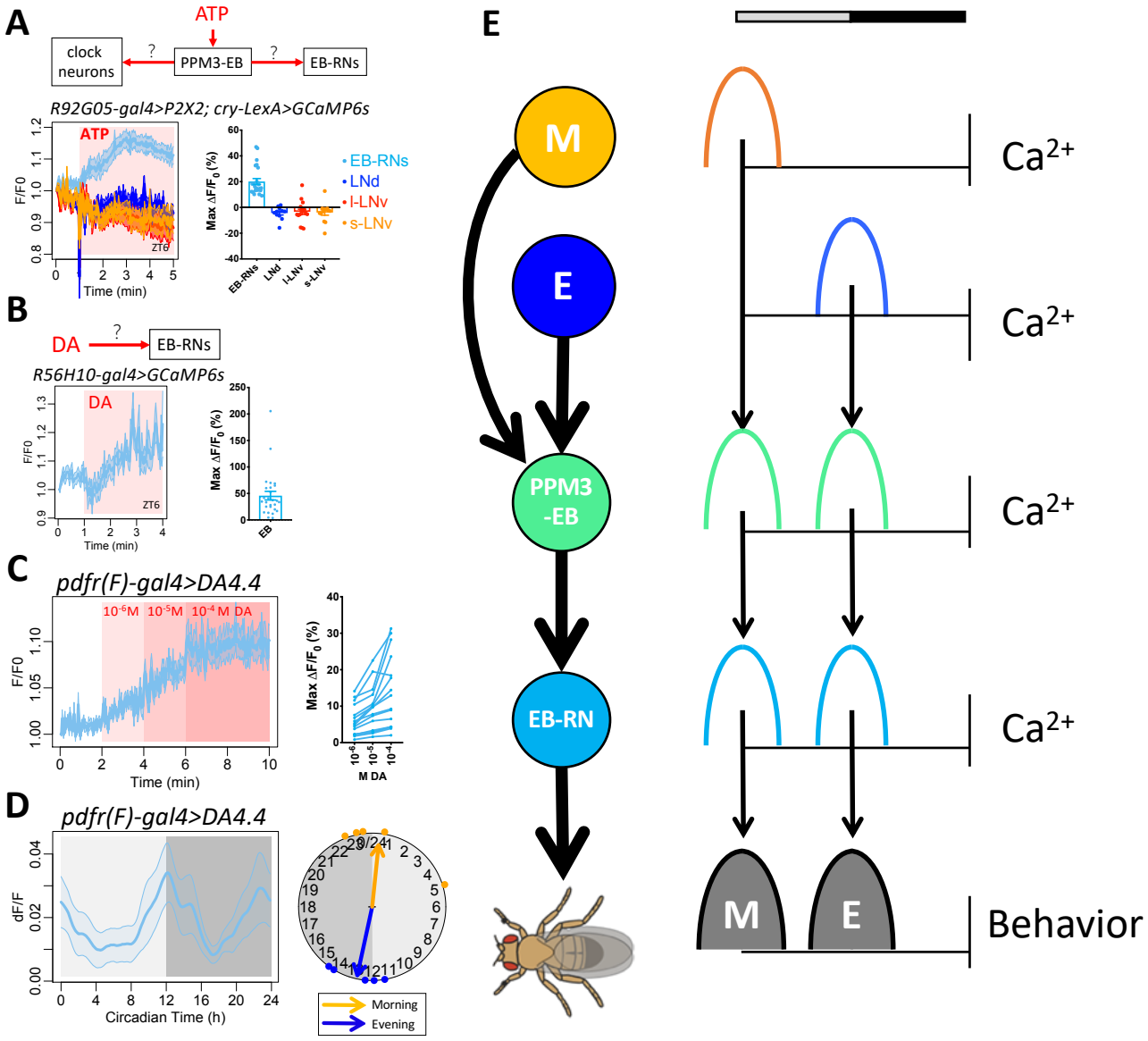


**Figure 7. EB-RNs receive daily bimodal dopamine inputs from PPM3-EB neurons.**

(**A**) Left - average traces of EB-R2 neurons, and circadian pacemaker neurons labelled by *cry-LexA,* responding to activation of P2X2-expressing PPM3-EB DA neurons by ATP (n = 5 flies). Shaded area indicates duration of drug application. Error bars denote SEM. Right - maximum $Ca^{2+}$ signal changes in individual cells within 4 min after ATP bath application.

(**B**) Left - average traces of EB-RNs responding to the bath-application of dopamine ($10^{-4}$ M) at ZT6 (n = 4 flies). Right - maximum $Ca^{2+}$ signal changes in individual cells within 3 min after DA bath application.

(**C**) Left – average traces of change from dopamine sensor $GRAB_{DA4.4}$ in EB-R3 neurons responding to steps of DA bath application ($10^{-6}$ M to $10^{-5}$ M to $10^{-4}$ M) at ZT6-8 (n = 4 flies). Right - maximum $Ca^{2+}$ signal changes in individual cells within 2 min after different concentration of DA.

(**D**) The daily spontaneous bimodal pattern of signal from dopamine sensor $GRAB_{DA4.4}$ in EB-R3 during DD1 (n = 5 flies).

(**E**) Model of the circadian output pathway for locomotor activity rhythms: circadian pacemaker M cells and E cells independently activate EB-RN pre-motor circuits around dawn and dusk through the relay of PPM3-EB dopaminergic neurons.

# Figure S1

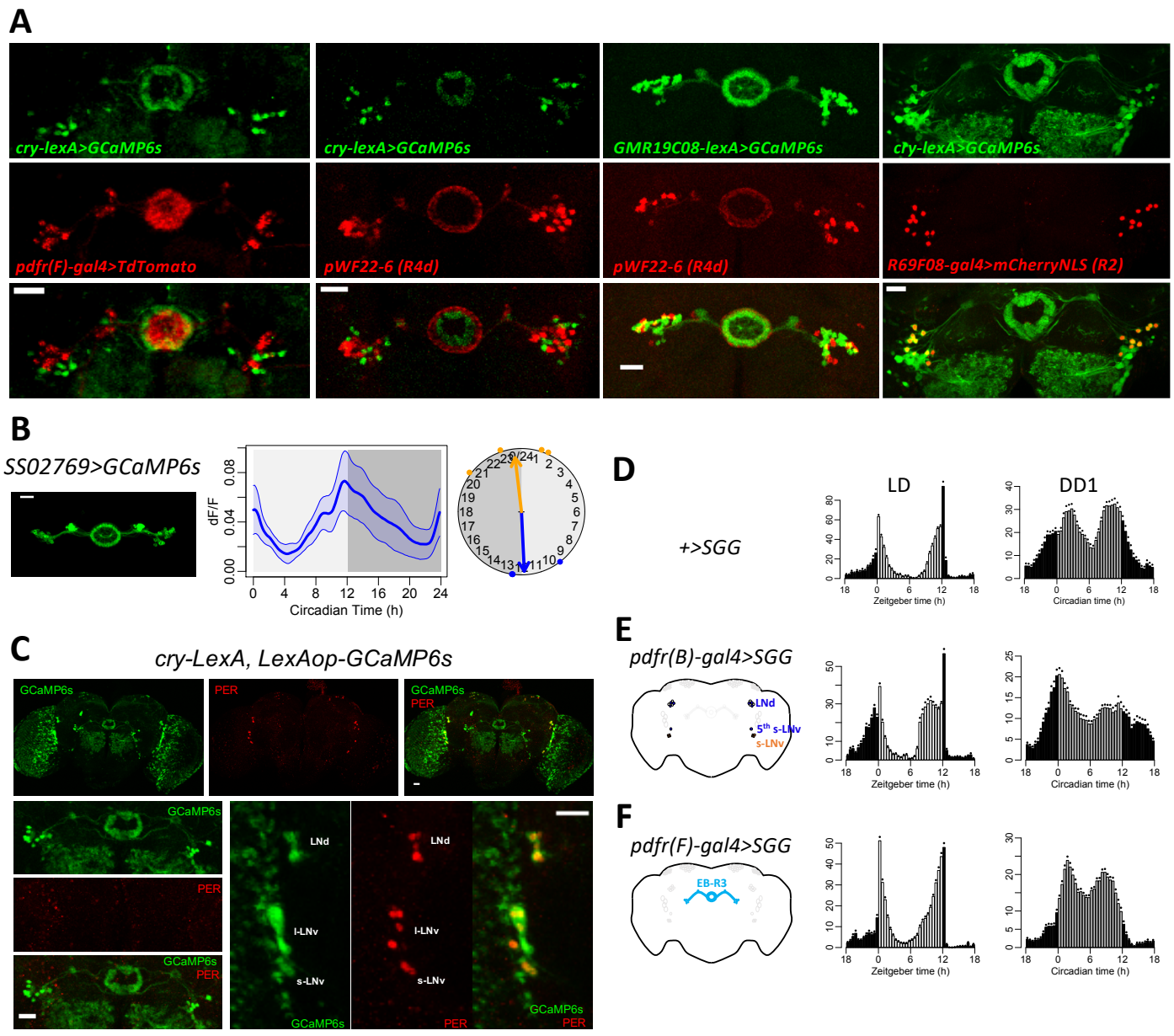


**Figure S1. The different subgroups of ellipsoid body (EB) ring neurons do not display circadian pacemaker cell properties.** Related to Figure 1.

(**A**) Confocal images of different subgroups of EB ring with different concentric arborization radii featured by different genetic drivers: the *cry-LexA* pattern did not overlap with that the *pdfr(F)-GAL4 pattern*; the *cry-LexA* pattern did not overlap with the *pWF22-6* pattern (R4d subgroup, see 30); the *GMR19C08(pdfr)-lexA* pattern did not overlap with the pattern of *pWF22-6*; the *cry-LexA* pattern did overlap with the that of *GMR69F08-GAL4* (R2 subgroup, see 69); Scale bars, 20 µm. (**B**) Daily $Ca^{2+}$ activity patterns of the EB-RN subgroup R4, labelled by split-GAL4 drivers which caused the strongest effect on increasing locomotor activity (18). (**C**) Immunostaining of PER protein in the *cry-LexA, LexAop-GCaMP6s* fly at ZT0. Scale bars, 20 µm. PER can be detected in circadian pacemaker neurons, but not in EB-RNs. (**D-F**) Average locomotor activity of (D) wild type (WT, n = 16 flies), (E) flies with Shaggy (SGG) expressed in s-LNv and three out of six LNd with *pdfr(B)-GAL4* (n = 16 flies), and (F) flies with SGG expressed in EB-R3 neurons with *pdfr(F)-GAL4* (n = 32 flies) under LD cycles and in the first day under DD (DD1). Accelerating molecular clocks in M and E cells (E) advanced both morning and evening behavioral phases, yet SGG over-expression in EB-RN neurons (F) was inconsequential.

# Figure S2

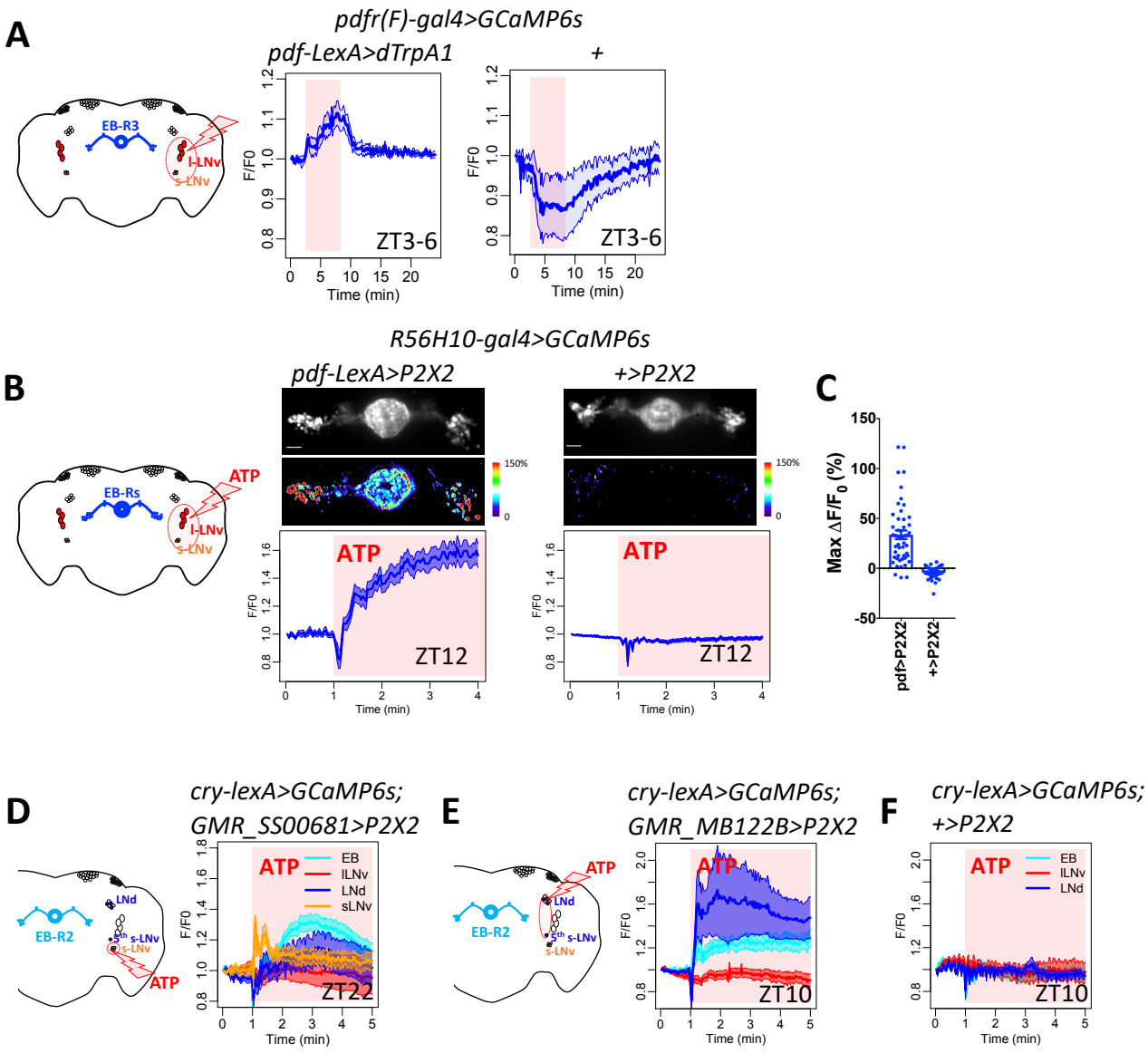


**Figure S2. EB-RNs respond to circadian neuron activation.** Related to Figure 4.

(**A**) Left, map of EB-RNs and circadian pacemaker neurons. Right, average traces of EB-R3 neurons responding to increase of temperature in flies with dTrpA1 expressed in PDF neurons (red, n = 7 flies) and in control flies without dTrpA1 expression (blue, n = 4 flies). Red aspect indicates duration of temperature increase.

(**B**) Responses of EB-RNs labelled by *R56H10-GAL4* to ATP application in flies with P2X2 expressed in PDF neurons (left, n = 5 flies) and in control flies without P2X2 expression (right, n = 3 flies). Red aspect indicates duration of ATP application. Above, example image baseline $Ca^{2+}$ signal and maximum $Ca^{2+}$ signal changes. Below, average traces of EB ring neurons.

(**C**) Maximum $Ca^{2+}$ signal changes after ATP application in individual EB-RNs in (B).

(**D**) Responses of EB-R2 neurons, and circadian pacemaker neurons labelled by *cry-LexA,* to ATP application in flies with P2X2 expressed in s-LNv (left, n = 6 flies).

(**E-F**) Responses of EB-R2 neurons and circadian pacemaker neurons labelled by *cry-LexA* to ATP application (E) in flies with P2X2 expressed in E cells: three LNd and the 5$^{th}$ s-LNv neurons (left, n = 5 flies) and (F) in control flies without P2X2 expression (right, n = 3 flies).

# Figure S3

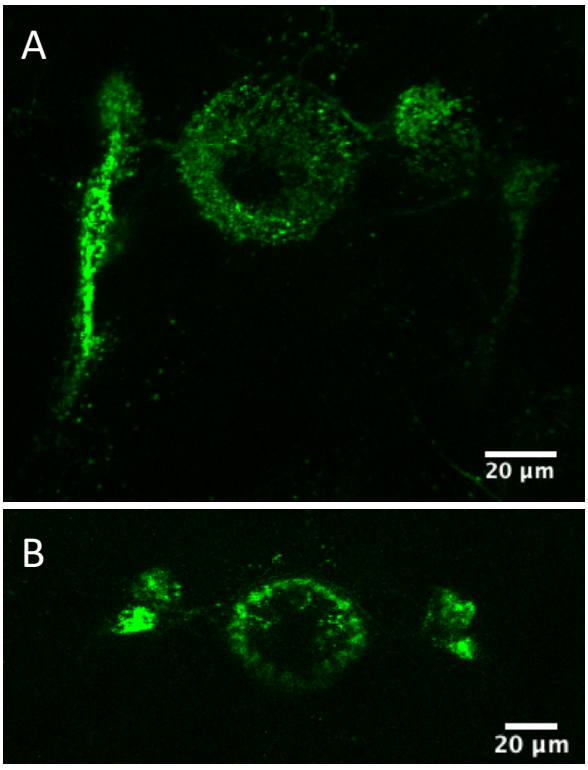


**Figure S3. GRASP analysis reveals synaptic connections between EB-RNs and PPM3-EB.** Related to Figure 5.
**(A)** *TH-LexA,LexAop-GFP11; R92G05-GAL4/UAS-GFP1-10* brain visualized for GFP in the entire processes of PPM3-EB neurons. **(B)** *R56H10-LexA,LexAop-GFP11; R92G05-GAL4/UAS-GFP1-10* brain visualized for GFP in the synapses between EB-RNs and PPM3-EB neurons.

# Figure S4

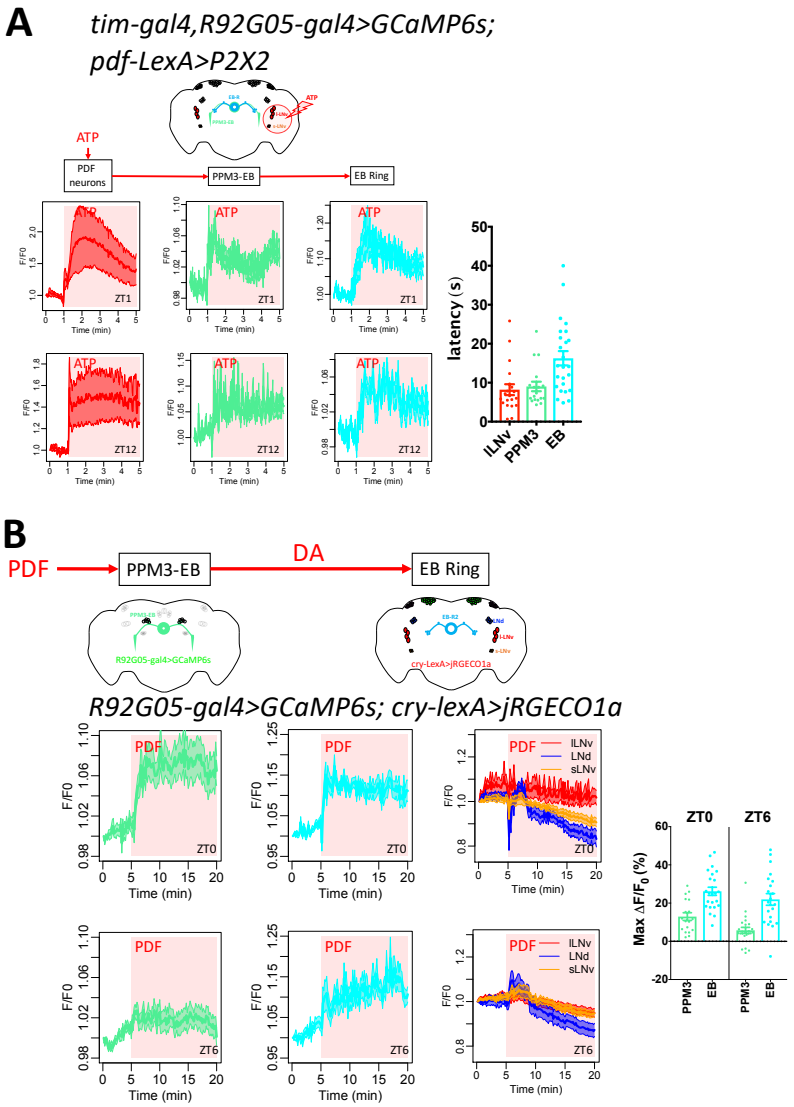


**Figure S4. Tests of connections from PDF neurons to PPM3-EB and to EB-RNs.** Related to Figure 5.
(**A**) Above, map of PPM3-EB DA neurons, EB-RNs, and circadian pacemaker neurons. Below-left, average traces of PDF neurons, PPM3-EB neurons, and EB-R1 neurons responding to activation of P2X2-expressing PDF neurons by ATP at two zeitgeber time points: ZT1 (n = 5 flies) and ZT12 (n = 4 flies). Below-right, response latency (onset time constant) of EB-RNs is longer than that of PPM3-EB neurons (p=0.0029, Mann-Whitney test).
(**B**) As in Figure 5B-F, dual-color $Ca^{2+}$ imaging: GCaMP6s in PPM3-EB and jRGECO1a in EB-R2 and circadian pacemaker neurons. Below-left, average traces of PPM3-EB neurons, EB-R2 neurons, and circadian pacemaker neurons responding to the bath-application of neuropeptide PDF ($10^{-5}$ M) at two zeitgeber time points: ZT0 (n = 3 flies) and ZT6 (n = 3 flies). Below-right, maximum $Ca^{2+}$ signal changes in individual cells after PDF bath application.

# Figure S5

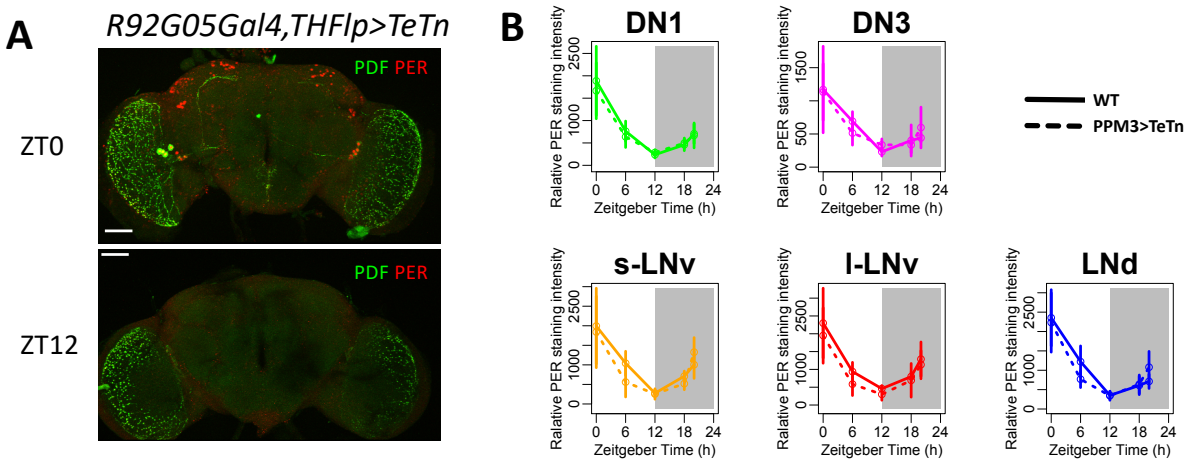


**Figure S5. PER protein rhythms of control flies and flies expressing tetanus toxin (TeTn) in PPM3-EB neurons in Figure 6A.** Related to Figure 6.
(**A**) Representative images of immunostaining against PDF and PER at two different time points: ZT0 and ZT12 of flies expressing TeTn in PPM3-EB. (**B**) Quantification of PER protein staining intensity at five different time points in five groups of circadian neurons from control flies and flies expressing TeTn in PPM3-EB (n > 3 flies for each time points).

# Table S1

**Manipulation of dopamine signal and EB-RNs impair circadian locomotor activity rhythms.**
Related to Figure 1 & 6.
AR, arrhythmic. Period and power are calculated by χ2 periodogram. Activity represents averaged activity count per 30 min.

| Genotype | N | AR | Period (h) | SEM | Power | SEM | Activity | SEM |
|---|---|---|---|---|---|---|---|---|
| ***R56H10-gal4>+*** | 15 | 7% | 23.50 | 0.10 | 88.36 | 10.97 | 20.53 | 2.27 |
| ***R56H10-gal4>UAS-TeTn*** | 14 | 64% | 24.00 | 0.97 | 10.69 | 3.12 | 6.07 | 1.25 |
| | | | | | | | | |
| ***TH-Flp/+; R92G05-gal4/+*** | 16 | 0% | 23.23 | 0.12 | 71.07 | 7.84 | 15.69 | 1.58 |
| ***TH-Flp/UAS-(FRT.stop)-TeTn;*** | 21 | 24% | 23.17 | 0.12 | 22.15 | 5.01 | 15.43 | 1.57 |
| ***TH-Flp/UAS-(FRT.stop)-TeTn; R92G05-gal4/+*** | 24 | 83% | 23.64 | 0.05 | 3.03 | 1.58 | 13.85 | 4.46 |
| | | | | | | | | |
| ***R56H10-gal4>+*** | 31 | 7% | 23.31 | 0.05 | 67.62 | 8.35 | 16.80 | 1.36 |
| ***R56H10-gal4>DopR1-miRNA*** | 32 | 3% | 23.63 | 0.05 | 84.18 | 8.57 | 22.21 | 1.22 |
| ***R56H10-gal4>DopR2-miRNA*** | 15 | 20% | 23.56 | 0.10 | 33.15 | 7.17 | 22.38 | 1.75 |
| ***R56H10-gal4>D2R-miRNA*** | 25 | 12% | 23.50 | 0.10 | 26.53 | 4.24 | 9.41 | 1.12 |
| ***R56H10-gal4>DopEcR-miRNA*** | 15 | 7% | 23.57 | 0.07 | 72.89 | 5.54 | 19.60 | 1.97 |

# Table S2

**List of driver/ reporter lines used in this study.** Related to Figure 1, 4, 5, S1, & S2.
The nomenclature of ellipsoid body ring neuron (EB-RN) subgroups used in this study – different from that in Omoto et al. (2017) - are here indicated.

| Driver / Reporter Lines | EB-RN subgroup | EB-RN subgroup nomenclature by Omoto et al. (2017) | other cell types |
|---|---|---|---|
| *tim(UAS)-GAL4* | R1 | R1 | All circadian pacemaker neurons and others |
| *pdfr(F)-GAL4* | R3 | R3 | N/A |
| *cry-LexA* | R2 | R5 | CRY-positive circadian pacemaker neurons and others |
| *GMR69F08-GAL4* | R2 | R5 | N/A* |
| *GMR_SS002769* | R2/R4m | R2 | N/A |
| *GMR19C08-LexA* | R4m | R2 | N/A |
| *GMR56H10-GAL4* | R1-4 | R1-5 | N/A |
| *pWF22-6-lacZ* | R4d | R4 | N/A |
| | | | |
| *pdfr(B)-GAL4* | N/A | N/A | all s-LNv, 3 CRY-positive LNd, and 2 DN1 |
| *GMR_SS00681* | N/A | N/A | 4 PDF-positive s-LNv |
| *GMR_MB122B* | N/A | N/A | the 5th s-LNv and 3 CRY-positive LNd |
| *pdf-LexA* | N/A | N/A | PDF-positive s-LNv and l-LNv |
| *GMR92G05-GAL4* | N/A | N/A | PPM3-EB and others |
| *GMR92G05-GAL4, TH-Flp* | N/A | N/A | PPM3-EB |

*N/A indicates invisible in the brain

# Chapter 5

# Circadian neurons orchestrate diverse neural activity rhythms in multiple parallel output circuits


**Abstract**

Circadian clocks align various physiological processes and behaviors to specific times of day that are most adaptive. To study how these timings are determined, I used brain-wide *in vivo* calcium imaging and measured neural activity patterns over 24-hour periods. I searched for neurons in *Drosophila* brain that displayed circadian rhythms in their neural activity. Such rhythms were widespread throughout the brain and driven by circadian clock activity within the well-described ~150 circadian pacemaker neuron network. I found that different sub-groups of pacemakers imposed neural activity rhythms onto different downstream non-clock neurons. Outputs from M and E pacemakers converged to generate a bimodal activity pattern in PPM3 dopaminergic (DA) neurons. E pacemakers also appeared to dictate the daily activity pattern in PPL1 and PAL DA neurons. l-LNv dictated the daily activity peak in PPM1 DA neurons and in specific neuroendocrine cells in the Pars Intercerebralis (PI). DN1 and DN3 appeared to co-regulate the daily activity pattern of antennal lobe local neurons. These output circuits downstream of circadian neurons were involved in regulating the circadian rhythms in sleep, feeding, and mating behaviors and in olfactory physiology. Through these circuits, synchronous circadian clocks can orchestrate multi-phasic diurnal outputs.

## Introduction

Animals have circadian rhythms in a variety of physiological processes and behaviors, such as locomotor activity, sleep/wake, feeding, and mating behaviors (Takahashi *et al.* 2008). These behaviors peak at different times of day, adapting species-specific requirements to daily changes of light, temperature, food, and mate availability. Under laboratory conditions, the locomotor activity of the fruit fly *Drosophila* peaks twice a day, in the morning and in the evening. During the morning peak, the fly shows a daily peak of feeding behavior; while during the evening peak, the fly shows the daily tough of mating behavior. Following each of these two activity peaks, the fly rests: it falls asleep around mid-day and again in the night. These behavioral rhythms are driven by synchronous clock gene oscillations (molecular clocks) in ~150 circadian pacemaker neurons (Nitabach & Taghert 2008). How a small population of circadian neurons, sharing a mono-phase molecular clock, regulates all the different phases of behavioral rhythms required for fitness of a species remains poorly understood.

Previously we reported (Liang *et al.* 2016) that molecular clocks generate circadian neural activity rhythms with diverse phases among different circadian neuron groups. Each group peaks at a specific time of day. Three laterally localized circadian neuron groups: s-LNv (M cells), l-LNv, and LNd (E cells) display spontaneous activity peaks in the morning, at mid-day, and in the evening, respectively. Two dorsally localized circadian neuron groups: DN3 and DN1 became sequentially active during the nighttime. These five pacemaker groups differentiate their activation times by neuropeptide-mediated modulations within the circadian neuron circuit (Liang *et al.* 2017). The peak time of each circadian neuron group may therefore represent a temporal mark by which different downstream output circuits may be temporally ordered. However, output circuits for different behavioral rhythms remain to be characterized.

Furthermore, how output circuits are regulated by phase-diverse circadian pacemaker neurons is a fundamental problem in the field of biological rhythms that remains to be studied.

To begin characterizing the complete map of circadian output circuits, I conducted an *in vivo* brain-wide screen for neurons showing circadian rhythms in their neural activity. I was particularly interested to relate daily patterns of spontaneous activity with previous ascribed roles in modulating diurnal rhythms of behavior. I found that a majority of dopaminergic (DA) neurons, and many of the major neuroendocrine peptidergic cells, exhibit diverse spontaneous daily neural activity patterns. Their patterns correspond to rhythms in sleep, locomotor activity, feeding, and mating behaviors. Furthermore, I found that the patterns were imposed by differentially-timed outputs from different circadian neurons groups. By whole-brain pan-neuronal imaging, I also found that circadian neural activity rhythms are widespread throughout the brain, including in neuroendocrine centers (the Pars Intercerebralis, PI) and in sensory systems (the local neurons in the antennal lobes) that receive inputs from olfactory sensory neurons. Together my findings indicate that synchronized timing information from molecular clocks spreads broadly through different downstream pathways to generate physiological and behavioral rhythms with diverse patterns.

## Results

### Daily neural activity rhythms of dopaminergic neurons

Several aspects of fly physiology and behavior, such as locomotor activity, sleep, feeding, and mating behaviors, are temporally organized by circadian clocks (Allada & Chung 2010). These aspects of behavior are also regulated by a neuromodulatory system in the fly's brain: the dopaminergic (DA) neurons (Kim *et al.* 2017). Thus, I asked whether the neural

activity of DA neurons is regulated by circadian clocks. Using *TH (tyrosine hydroxylase)-GAL4* and through dorsal cranial holes, I imaged five clusters of DA neurons in fly's dorsal protocerebrum: PAM, PAL, PPL1, PPM1/2, and PPM3 (Figure 1A; Friggi-Grelin *et al.* 2003; Mao & Davis 2009; Xie *et al.* 2018). Except for PAM, each cluster displayed a unique circadian rhythmic $Ca^{2+}$ activity pattern (Figure 1B). Three clusters showed single prominent $Ca^{2+}$ activity peaks at different times of day: PAL peaked around dawn, followed by PPM1/2, which peaked around noon, and later, PPL1 peaked around dusk. In contrast, PPM3 showed a bimodal activity pattern with two peaks at dawn and dusk (reported in detail in Chapter 4). These diverse daily activity patterns of DA neuron clusters were further confirmed by using two independent genetic drivers: *TH-C-GAL4* and *TH-D-GAL4* (Figure S1AB), which separately label largely non-overlapping DA neuron clusters and together recapitulate most of the *TH-GAL4* expression pattern (Liu *et al.* 2012). I also measured DA $Ca^{2+}$ activities at high frequency (1 Hz) for short periods *in vivo* in brains exposed acutely at different times of day. I found that DA neurons at the time of daily $Ca^{2+}$ level peak also displayed a more dynamic fast $Ca^{2+}$ fluctuations than those at the trough time (Figure S1D-K). Collectively, neurons of the *Drosophila* dopaminergic system exhibit diverse and cluster-specific daily neural activity patterns.

I also found that the daily neural activity patterns of DA neurons were completely arrhythmic in the circadian-defective $per^0$ mutant flies (Figure 1C & S1C). To study how molecular clocks in pacemaker neurons regulate DA neuron activity, I selectively activated PDF neurons by expressing ATP-gated P2X2 receptors (Lima and Miesenböck 2005) and applying ATP when imaging from DA neurons (Figure 1DE). All four DA neuron clusters that had circadian $Ca^{2+}$ activity rhythms (PAL, PPL1, PPM1/2, and PPM3) were excited by PDF neuron activation. In contrast, the PAM cluster, which didn't show circadian rhythmic activity, was

reproducibly inhibited by PDF neuron activation. Thus, molecular clocks could regulate DA neuron daily activity patterns through pacemaker neuron outputs.

**Daily patterns of DA neurons in regulating sleep and mating behavior**

I then compared the diversity of DA neuron daily activity patterns with the functional diversity of DA neuron clusters described in previous studies. DA plays a key role in wake/sleep regulation as a wake-promoting factor (Andretic *et al.* 2005, Kume *et al.* 2005, Shang *et al.* 2011, Ueno *et al.* 2012). To promote wake, a pair of PPL1 DA neurons (which constitute a subset of the PPL1 group) projecting to the dorsal fan-shape body (dFSB) suppresses the dFSB sleep-promoting neurons (Donlea *et al.* 2011, Liu *et al.* 2012, Pimentel *et al.* 2016). Using highly specific split-GAL4 drivers (Xie *et al.* 2018), I found that the specific PPL1-dFSB subset of PPL1 DA neurons showed a prominent evening $Ca^{2+}$ activity peak (Figure 2AC), when the flies were most active under DD. Unlike the averaged $Ca^{2+}$ peak from entire PPL1 cluster (Figure 1B), $Ca^{2+}$ activity of PPL1-dFSB subset alone dropped immediately in the beginning of subjective night, consistent with the onset of nighttime sleep. Thus, the $Ca^{2+}$ activity pattern of wake-promoting PPL1-dFSB precisely matched the daily sleep/wake pattern around dusk. In addition to sleep/wake cycles, specific DA neurons also regulate courtship and mating behavior. The internal drive of male mating behavior is encoded by the activity level of a pair of *fruitless*-positive DA neurons from the PAL cluster (*Fru*+ PAL, Figure 2B) (Zhang *et al.* 2015). I found that these *Fru*+ PAL neurons showed a morning $Ca^{2+}$ peak (Figure 2D), matching the daily behavioral mating activity pattern (Sakai & Ishida 2001, Fujii *et al.* 2007). Together, these observations suggest that for two distinct subsets of DA groups, their diverse daily $Ca^{2+}$ activity

patterns are congruent with their correlated behaviors. These spontaneous activity patterns may therefore contribute to the mechanistic basis that differentially times diverse behavioral rhythms.

**Daily neural activity rhythms of peptidergic neurons**

Neuroendocrine cells, that release different neuropeptides and peptide hormones, represent a second major neuromodulatory system. Many neuroendocrine cell bodies localize in the Pars Intercerebralis (PI), which as a functional homolog of the mammalian hypothalamus. PI neurons have been implicated in regulating sleep (Crocker *et al.* 2010; Park *et al.* 2014), locomotion (Cavanaugh *et al.* 2014), and metabolism (Barber *et al.* 2016). I identified these neuroendocrine cells by a peptidergic neuron marker DIMMED, which is bHLH transcription factor associated with neuroendocrine cell differentiation (Park *et al.* 2011). With a *dimm*-promoter reporter *c929-GAL4* (Park *et al.* 2008), I simultaneously imaged from all neuroendocrine cells in the PI and also from a circadian neuron group, l-LNv. I found that in average, PI neurons showed a daily $Ca^{2+}$ activity peak around mid-day, with approximately the same phase as the l-LNv (Figure 3C). The neuroendocrine cells in the PI are heterogeneous; different neurons release different neuropeptides and might regulate different physiological and behavioral functions (Park *et al.* 2008). I genetically dissected PI neurons based on types of neuropeptides they released, including insulin-like-peptides (dILPs), DH44, dromyosuppressin (DMS), and SIFamide (SIFa). Most PI groups, when analyzed with these more specific driver Gal4s, had activity peaks prominently at mid-day (Figure 3B, E-G), consistent with the averaged signal from the entire PI group (Figure 3C). I noted one exception to this: the insulin-producing cells (IPCs, labeled by *dILP2-GAL4*) peaked in the morning, earlier than the group average (Figure 3D). This pattern is consistent with previous observations that IPC display a higher firing

rate when recorded in vitro in the morning than at other times of day (Barber *et al.* 2016). The morning peak of IPC activity suggested that the release of insulin-like peptides peaks in the morning, coincident with the peak phase of feeding rhythm (Xu *et al.* 2008). Outside of the PI, a pair of neuroendocrine neurons releasing leucokinin (LK) has been showed to be involved in regulating locomotor activity rhythms (Cavey *et al.* 2016) and feeding behavior (Yurgel *et al.* 2018; Zanwadala *et al.* 2018). I found the LK neurons showed a daily activity peak in the evening, clearly different from the other neuroendocrine cells I studied. This pattern is consistent with the prediction (Cavey *et al.* 2016) that LK neurons were suppressed by PDF neurons that are active in the morning. Together, my results show that many neuroendocrine cells have circadian rhythms in their neural activity and like DA neurons groups, they exhibit diverse phase patterns, consistent with the hypothesis that the release of many different neuroendocrine factors is under circadian regulation.

**Circadian neurons dictate phases of output circuits**

Different output circuits showed diverse daily neural activity patterns. I developed several lines of evidence to suggest these patterns were temporally organized by molecular clocks through outputs of circadian neurons. I asked whether different groups of circadian neurons regulate different downstream output circuits. For instance, do circadian neurons that peak in the morning generate corresponding morning output peaks? Likewise, do circadian neurons that peak at other phases of the 24-hr day produce corresponding co-phasic outputs? I tested this hypothesis using the power of *Drosophila* genetics to selectively shift the activity phase of single circadian neuron groups. I tested the consequences by comparing the daily activity patterns of multiple output circuits. Overexpressing Shaggy(SSG) in morning

pacemakers using *pdf-GAL4* (*pdf>SGG*) to accelerate the M molecular clocks selectively advanced the M-cell (s-LNv) $Ca^{2+}$ peak and the morning peak of locomotor activity (Stoleru *et al.* 2005; Figure 4AB; also see Chapter 4 Figure 4DE). Among downstream circuits, I found that only the morning peaks of PPM3 DA neurons were advanced, while their evening peaks remained unaffected (Figure 4C-F; as reported in Chapter 4 Figure 5G-I). The DA neuron cluster PAL normally displays a morning peak and it was unaffected by the phase shift of M cells. These results suggest that some downstream rhythmic neurons that display a spontaneous morning phase (PPM3) are triggered by the morning peak of M cell neural outputs. However, others (PAL) are not so simply explained. To test the contribution of E-cell outputs, I overexpressed SSG both in M and E pacemakers using *dvpdf-GAL4* (*dvpdf>SGG*) to accelerate both M and E molecular clocks and thus to advance both the morning and evening peaks of locomotor activity (Stoleru *et al.* 2005; Figure 4GH). Corresponding to the behavioral phenotype, I found that both morning and evening peaks of PPM3 were significantly advanced. Interestingly, the daily activity peaks of PAL neurons and PPL1 neurons were also advanced (Figure 4IJ). Comparison between *pdf>SGG* and *dvpdf>SGG* flies suggested that E pacemakers might dictate activity phases of multiple downstream neuron groups; shifting E-cell activity phases shifted the downstream PAL, PPL1, and the evening phase of PPM3.

We further asked whether the third circadian neuron group may dictate daily activity patterns of other downstream output neurons. Ectopic PDFR expression using *pdf-GAL4* (*pdf>PDFR*) selectively delayed $Ca^{2+}$ phases in l-LNv (Liang *et al.* 2017; Figure 4K-N). In downstream circuits we found that PPM1 DA neurons, which peaked around the same time as l-LNv in WT, were selectively delayed together with l-LNv in *PDF>PDFR* flies (Figure 7OP). This result suggests that the spontaneous PPM1 activity phase is normally triggered by l-LNv.

This effect was confirmed in newly-eclosed flies, in which l-LNv transiently expresses PDFR for the first 24-48 hr of adult life (M Klose and P Shaw, personal communication) and displays a 4-5 hr delayed $Ca^{2+}$ phase. Strikingly, the $Ca^{2+}$ peak phases of both PPM1 and DIMM-positive PI neurons were delayed together with l-LNv at this specific developmental stage (Figure S2). Collectively, I found that many of the group-specific phases of circadian neurons dictated corresponding phases of downstream output circuits. In this way, synchronized molecular clocks use their sequential circadian neuronal outputs to assign different physiological processes and behaviors to different times of day.

**Circadian neural activity rhythms throughout the brain**

I found circadian rhythms in neural activity in all circadian pacemaker neurons, in the majority of DA neurons, and in many neuroendocrine cells. I then asked whether the circadian regulation of neural activity is a widespread phenomenon throughout the *Drosophila* brain. To test that hypothesis, I used a pan-neuronal driver *nSyb-GAL*4 and imaged the majority of the protocerebral volume for 24 hours in living flies. To estimate the rhythmicity of $Ca^{2+}$ signals from whole-brain 4D volumetric images, I utilized JTK_CYCLE analysis for each voxel and generated whole-brain maps of rhythmicity p values and activity peak phases (Figure 5A) (Hughes *et al.* 2010). In control flies under DD, I found that 27.9 ± 6.6% of the brain volume imaged showed significant circadian rhythms ($p<1e-5$, FDR=0.0099). The definition of significance rested in the comparison to rhythmicity of the comparable volume in the circadian defective $per^{01}$ flies (Figure 5B-D). Different brain regions showed different phases of peak activity. The majority of regions peaked around the middle of the day, or the middle of the night (Figure 5D). This activity phase pattern reflected intrinsic circadian patterning because different

recordings, begun at different circadian times, showed similar spatial phase patterns (Figure 5A). Furthermore, a small proportion of brain volume showed daily bimodal activity patterns (5.3±1.1%, Figure S3). Therefore, spontaneous circadian rhythms in neural activity are widespread throughout the brain and demonstrate diverse peak phases.

From the whole brain circadian phase pattern, I noted that the area encompassing the PI displayed a circadian activity peak around midday, which is consistent with daily activity patterns that I measured in the majority of neuroendocrine cells in PI (Figure 3). Another notable region was the antennal lobe (AL) with a daily $Ca^{2+}$ activity peak around midnight: that pattern is strikingly consistent with previous observations that circadian rhythms in olfactory responses peak around midnight (Krishnan *et al.* 1999). I further confirmed this midnight pattern by measuring 24-hr $Ca^{2+}$ activity rhythms in AL local neuron groups that are labelled by either *tim-GAL4* or *cry-LexA* (Figure 6 and S4). Daily rhythms of these AL neurons were dependent on circadian clocks (Figure 5B, 6B, and S4C). I then asked whether $Ca^{2+}$ rhythms in AL neurons are dictated by the circadian neuron groups that peak that are co-phasic at night, such as DN1 and DN3. However, in $pdf^{01}$ mutants, when the phases of DN3 were shifted to the morning (Liang *et al.* 2017), AL neurons remained rhythmic with a phase still at midnight (Figure 6B and S4C). Likewise, in sNPF or sNPFR knockdown, when DN1 were arrhythmic (Liang *et al.* 2017), AL neurons were still rhythmic and AL neurons remained rhythmic and their phase was unaffected (Figure 6B and S4C). However, with sNPF or sNPFR knockdown, the amplitude of daily $Ca^{2+}$ variations in AL neurons were strongly reduced (ANOVA followed by Dunnett's test, $P < 0.01$). These results suggested that AL neurons might be regulated synergistically, by both DN1 and DN3. A linear regression model, using the daily activity pattern of five major circadian neuron groups to predict the daily pattern of AL neurons, showed that both DN1 and DN3 (and only

those groups) have significant effects on predicting the activity of AL neurons (Figure 6BC, $R^2$ = 0.8261). Taken together, circadian rhythms in neural activity have diverse phases among brain regions. Different brain regions were regulated by the different combinations of outputs from circadian neuron groups. These findings reflect fundamental mechanisms to explain how the occurrence of different physiological processes and behaviors are aligned to different times of day.

**Discussion**

By searching across the whole brain for neurons that display circadian neural activity rhythms, I found several output circuits downstream of the circadian pacemaker network. These different circuits show diverse daily activity patterns – different neural centers exhibit activity peak at different time of day. PPM3 dopaminergic (DA) neurons display daily bimodal rhythms and they were essential for the locomotor activity rhythms (also see Chapter 4). *Fru*+ PAL DA neurons display a morning activity peak, which is a time consistent with their driving a morning-biased mating rhythm. PPL1-dFSB DA neurons displayed an evening activity peak, which is consistent with their involvement in controlling the sleep/wake profile around dusk. In Pars Intercerebralis (PI), insulin producing cells peaked in the morning consistent with their involvement in feeding rhythms. Other PI neuroendocrine cells displayed daily activity rhythms that peaked around mid-day, and likely underlie rhythms of hormone secretion for various neuroendocrine systems. Olfactory sensory neurons innervating the antennal lobes displayed a midnight activity peak. Daily neural activity rhythms of these output circuits were driven by circadian neural activity rhythms of pacemaker neurons. Groups of circadian neurons peaking at different times of day sent outputs to different downstream circuits to generate diverse phases, by

which various physiological processes and behaviors were aligned to times of day that are most adaptive (Figure 7).

The daily bimodal pattern of PPM3 group was consistent with the daily activity pattern and function of its subset which projects to EB - the PPM3-EB subgroup. The PPM3-EB neurons regulate the pre-motor ellipsoid body (EB) ring neurons and thus generate daily bimodal pattern in locomotor activity (See Chapter 4). Besides PPM3, other three groups of DA neurons: PAL, PPL1, and PPM1 were also under circadian control. Previous studies have described synaptic connections between DA neurons and circadian neurons (Shang *et al.* 2011): they suggested that DA regulates circadian neuron activity. My findings and also a recent study (Potdar and Sheeba 2018) both showed that circadian neurons regulate DA neuron activity. DA neurons responded to circadian neuron outputs (Figure 1D) and showed circadian neural activity rhythms (Figure 1B). DA neural activity rhythms required functional clock gene oscillations (Figure 1C). The different phases of DA neural activity rhythms were dictated by phases of different circadian neuron groups (Figure 4).

Circadian rhythms in the DA neurons might drive circadian rhythms in behaviors in addition to locomotor activity. My data implicates spontaneous activity in DA neurons that were previously associated with rhythmic arousal and with rhythmic male reproductive activity. *Drosophila* exhibit a midday siesta (daytime sleep) in between the morning and evening activity periods. DA promotes wakefulness and arousal (Andretic *et al.* 2005), in part through a pair of PPL1-dFSB neurons that inhibit the sleep-promoting dFSB neurons (Liu *et al.* 2012; Pimentel *et al.* 2016). I found that PPL1-dFSB neurons were spontaneously active around dusk (Figure 2C), which might be driven by the output of E cells (Figure 4G-J). The activity pattern suggested that PPL1-dFSB might selective regulate afternoon wakefulness. I speculate that the morning

wakefulness might be controlled by a separate circuit, such as through neuropeptide DH31 released from DN1 neurons (Kunst *et al.* 2014). Regarding reproductive behavior, circadian mating rhythms peak in the morning and could be driven by males (Sakai & Ishida 2000; Fujii *et al.* 2007). Zhang *et al.* (2016) showed that another pair of DA neurons, the *fruitless*-positive (*Fru*+) PAL, encode internal mating drive in male flies by regulating P1 neurons. I found that *Fru*+ PAL neurons were spontaneously active in the morning (Figure 2D), a phase consistent with the expectation that spontaneous *Fru*+ PAL activity promotes mating drive in the morning. It was striking that the morning activity peak of PAL neurons, unlike that of the PPM3 and EB ring neurons, was not dictated by M-cell activity (Figure 4F). Instead, the activity peak of PAL appeared to be dictated by E-cell activity (Figure 4J), consistent with previous observation that impairing clocks in E cells (LNd) and in DN1 caused more severe mating rhythm deficits (Hamasaka *et al.* 2010). Interestingly, E cells were in antiphase to PAL. It suggested that E cells inhibit PAL neurons, while they activate PPL1 and PPM3 neurons. Thus, E cells generate the daily tough of mating behavior during the evening peak via PAL neurons. The third DA neuron group PPM1 peaked at mid-day, and its phase was clearly dictated by l-LNv activity (Figure 4K-P). However, the function of PPM1 has not been described yet.

In addition to neuromodulatory DA systems, I also found a substantial region of the fly brain showed circadian rhythms in spontaneous neural activity by whole-brain pan-neuronal imaging (Figure 5A). These rhythmic brain regions were not homogeneously active but showed diverse phasic patterns and mainly peaked around mid-day or midnight (Figure 5C). Brain regions peaking around mid-night included the antennal lobes (AL). Olfactory sensory neurons (OSNs) of the antennae project axons to the AL and there make connections with 2$^{nd}$ order interneurons. OSNs display a daily circadian rhythm of sensitivity to odorants that peaks around

mid-night (Krishnan *et al.* 1999). These circadian olfaction rhythms are considered autonomous to the OSNs, dependent on circadian pacemaking within the sensory neurons (Tanoue *et al.* 2004). Interestingly, my observations revealed that antennal lobe local neurons (AL-LN), from flies without antennae, still demonstrated circadian neural activity rhythms (Figure 6 & S4). Moreover, the phase of the spontaneous AL-LN activity rhythms appeared to match that of the OSNs. Impairing PDF neuron outputs reduced the amplitude of AL-LN rhythms (Figure 6 & S4). However, even the ablation of PDF neurons didn't diminish Al-LN rhythms (Figure S4), suggesting that AL-LN might be driven by groups of non-PDF circadian neurons. Together with the linear regression model (Figure 6C), I suggest that AL-LN daily activity may reflect synergistic activation by the DN1 and DN3. Alternatively, AL-LN might have their own autonomous molecular clocks, which are yet to be identified.

Brain regions peaking around noon include the principle neuroendocrine centers: the Pars Lateralis (PL) and Pars Intercerebralis (PI). In the PI, I found several groups of neuroendocrine cells exhibiting spontaneous circadian neural activity rhythms, including the dILP2, SIFa, DMS, and DH44 neurons (Figure 3). dILP2 neurons (aka. insulin-producing cells, IPC), which are involved in regulating feeding rhythms and promoting wake (Barber *et al.* 2016; Crooker *et al.* 2010), peaked in the morning. The other PI neurons peaked later around midday, including the sleep-promoting SIFa and SIFR neurons (Park *et al.* 2014) and DH44 neurons. DH44 neurons together with a pair of leucokinin (LK) neurons in lateral horns (LH) regulate locomotor activity rhythms (Cavanaugh *et al.* 2014; Cavey *et al.* 2016). I found that DH44 neuron activity peaked around midday, whereas that of LK neurons peaked in early evening (Figure 3), consistent with the activity patterns of LK neurons when measured in acutely dissected brains (Cavey *et al.* 2016; Bai *et al.* 2018). However, the activity patterns of DH44 and LK neurons were different

from the daily patterns of locomotor activity. Further studies are required to determine how the activity patterns of DH44 and LK neurons specifically contribute to the daily bimodal pattern of locomotor rhythms.

In summary, I found circadian neural activity rhythms in diverse downstream neuronal circuits throughout the fly brain (Figure 7). M cells and E cells generated morning and evening activity peaks respectively in the pre-motor circuit of PPM3, and subsequently in EB ring neurons. E cells might also generate the daily activity peak in PPL1 neurons and the daily activity tough in PAL neurons in the evening. The circadian neuron group l-LNv controlled the midday phase of dILP-negative PI neurons and PPM1 DA neurons. Besides these one-to-one determinations, my data indicates that certain circadian neuron groups may work in concert to regulate specific activity rhythms, as in the case of output circuits like antennal lobe local neurons.

**Methods**

I did not use statistical methods to predetermine sample sizes. I randomly selected flies from vials for imaging and behavioral tests. I was aware of fly genotypes during the course of obtaining and analyzing the data.

**Fly stocks.** Flies were reared on standard cornmeal/agar food at room temperature. Before imaging experiments, flies were entrained under 12 h light: 12 h dark (LD) cycles at 25°C for at least 3 days or under 10 h light: 14 h dark (short day, SD) cycles at 25°C for at least 5 days. All experiments used male flies older than three days after eclosion except for Figure S8F-K, in which flies within one day after eclosion were used.

The following fly lines have been described previously: *tim(UAS)-GAL4* (Blau & Young 1999), *TH-GAL4* (Friggi-Grelin *et al.* 2003), *TH-C-GAL4* and *TH-D-GAL4* (Liu *et al.* 2012), *nSyb-GAL4* (Pauli *et al.* 2008), *dILP2-GAL4* (Rulifson *et al.* 2002), *DH44-GAL4* (Cavanaugh *et al.* 2014), *DMS-GAL4* (Park *et al.* 2008), *SIFa-GAL4* (Terhzaz *et al.* 2007), *c929-GAL4* (Hewes *et al.* 2003), *dvpdf-GAL4* (Bahn *et al.* 2009); split-GAL4 lines: *R76F01-DBD* and *R76F02-AD* (Xie *et al.* 2018); *TH-LexA* (Berry *et al.* 2015), *cry-LexA* (Liang *et al.* 2017), *pdf-LexA* (Shang *et al.* 2008); *Fru-Flp* (Yu *et al.* 2010); *UAS-SGG* (Stoleru *et al.* 2005), *UAS-pdfr* (Mertens *et al.* 2005), *UAS-P2X2* and *LexAop-P2X2* (Yao *et al.* 2002), *UAS-GCaMP6s* and *LexAop-GCaMP6s* (Chen *et al.* 2013); $per^{01}$ (Konopka & Benzer1 971) and $pdfr^{han5403}$ (Hyun *et al.* 2005).

The *cry-LexA* line was a gift from Dr. F Rouyer (CNRS Gyf, Paris). The *UAS-(FRT.stop)-tdTomato* line was a gift from Dr. S. Lawrence Zipursky (UCLA).

**In vivo fly preparations.** The surgical procedure for fly in vivo calcium imaging was as described in Liang *et al.* (2016, 2017). I mounted flies by inserting the neck into a narrow cut in a piece of aluminum foil. Thus, the foil separated the head from the body and permitted me to present saline to the exposed brain, while leaving the body in an oxygen-normal environment. During brain-exposing surgery and in vivo imaging, the head was immersed in saline, while the body remained in an air-filled enclosure. To access circadian pacemaker neurons on one side of the head, one antenna, a portion of the dorso-anterior head capsule, and a small part of one compound eye were removed. For pan-neuronal imaging, both antennae and a portion of the dorso-anterior head capsule were removed, while the compound eyes remained intact. To access dopaminergic (DA) neurons, a portion of the dorsal head capsule and the ocelli were removed, while the compound eyes and antennae remained intact. The orientation of fly was then tilted for a more optimal view of DA neurons in the posterior brain.

**In vivo calcium imaging.** Imaging was conducted with custom Objective Coupled Planar Illumination (OCPI) microscopes (Holekamp *et al.* 2008), as described in Liang *et al.* (2016, 2017). Briefly, OCPI used a cylindrical lens to generate a ~5 μm thick light sheet, which was set to the focal plane of the objective. For 24-hr imaging, the objective coupled light sheet was scanned across the fly brain through a small cranial window every 10 min to capture stacks of images. Each stack contained 20 to 40 separate images with a step size of 10 microns. For each image, exposure time was not more than 0.1 s. During 24-hr imaging, fresh haemolymph-like saline (HL3; 5 mM KCl, 1.5 mM CaCl2, 70 mM NaCl, 20 mM MgCl2, 10 mM NaHCO3, 5 mM trehalose, 115 mM sucrose, and 5 mM HEPES; pH 7.1) was perfused continuously (0.1-0.2 mL/min). Light-dark cycle stimulation during in vivo calcium imaging was delivered using a

white Rebel LED (Luxeon) controlled by an Arduino UNO board (Smart Projects, Italy) as described in Liang *et al.* (2017). For short term high frequency imaging, stacks of images were captured every 10 s (Figure 4D). For each image, exposure time was not more than 0.04 s. For pharmacological tests, after 5-min baseline recordings, 10 mM ATP solution (pH was adjusted to 7) was manually added into a 9 ml static HL3 bath over a ~2 s period. PDF was purchased from Neo-MPS (San Diego, CA, USA) at a purity of 86%.

**Imaging data analysis.** I analyzed calcium imaging data as described previously (Liang *et al.* 2016, 2017). Images were acquired by custom software (Imagine - Holekamp *et al.* 2008) and processed in Julia 0.6, including non-rigid registration, alignment and maximal projection along z-axis. Then ImageJ-based Fiji (Schindelin *et al.* 2012) was used for rigid registration and to manually select regions of interest (ROIs) over individual cells or groups of cells. Average intensities of ROIs were measured through the time course and divided by the average of the whole image to subtract background noise.

For spontaneous calcium transients, each time trace was calculated as $dF/F=(F-F_{min})/F_{mean}$. For 24-hr time traces, traces of certain cell type ROIs were firstly aligned based on Zeitgeber Time and then averaged across different flies. The phase relationship between traces was estimated by cross-correlation analysis. The 24-hr-clock circular plot of phases reflected both mean peak time and phase relationship of the same cell-group traces from different flies. For neurons with daily bimodal patterns (PPM3 DA neurons), each trace was split into two parts: ZT18-ZT6 (morning) and ZT6-ZT18 (evening) to estimate the morning and evening peak phases respectively.

For pharmacological calcium responses, each time trance was normalized by the initial intensity ($F/F_0$). The maximum change was calculated by the maximum difference of normalized

intensities between baseline and following drug application. The latency (onset time constant) was calculated by the duration from drug application to the time when the trace reached 63.2% of maximum change. Trace analysis and statistics were performed using R 3.3.3 and Prism 7 (GraphPad, San Diego CA).

**Estimated rhythmicity for pan-neuronal imaging.** To estimate the rhythmicity of calcium signals from whole brain pan-neuronal 4D volumetric images, I used the Jonckheere-Terpstra-Kendall (JTK) algorithm (Hughes *et al.* 2010). After non-rigid registration, each frame of the 4D volumetric images was firstly filtered by a high pass filter (Gaussian filter, 500X500 pixel, 162.5 μm X 162.5 μm) to remove fixed-pattern noise generated by the camera. Each frame was then filtered by a low pass filter (Gaussian filter, 5X5 pixel, 1.6 μm X 1.6 μm). A threshold was set by a selected background region outside of the head. Time traces of voxels that reached the threshold were then averaged by one-hour bin. For each voxel, time trace with 24 time-points was analyzed by the JTK algorithm. Briefly, this nonparametric test estimates the amplitude and phase of rhythmic data based on the order of the data for a selected period. A 24-hr period was used to estimate circadian rhythmicity. A 12-hr period was used to estimate ultradian rhythmicity of the daily bimodal patterns. For each brain, I generated 3D maps of rhythmicity p-values and activity peak phases. p-values for the entire brain were adjusted by a Bonferroni correction for multiple testing. Imaging data processing and JTK_CYCLE analysis was performed using Julia 0.6.

Figure 1

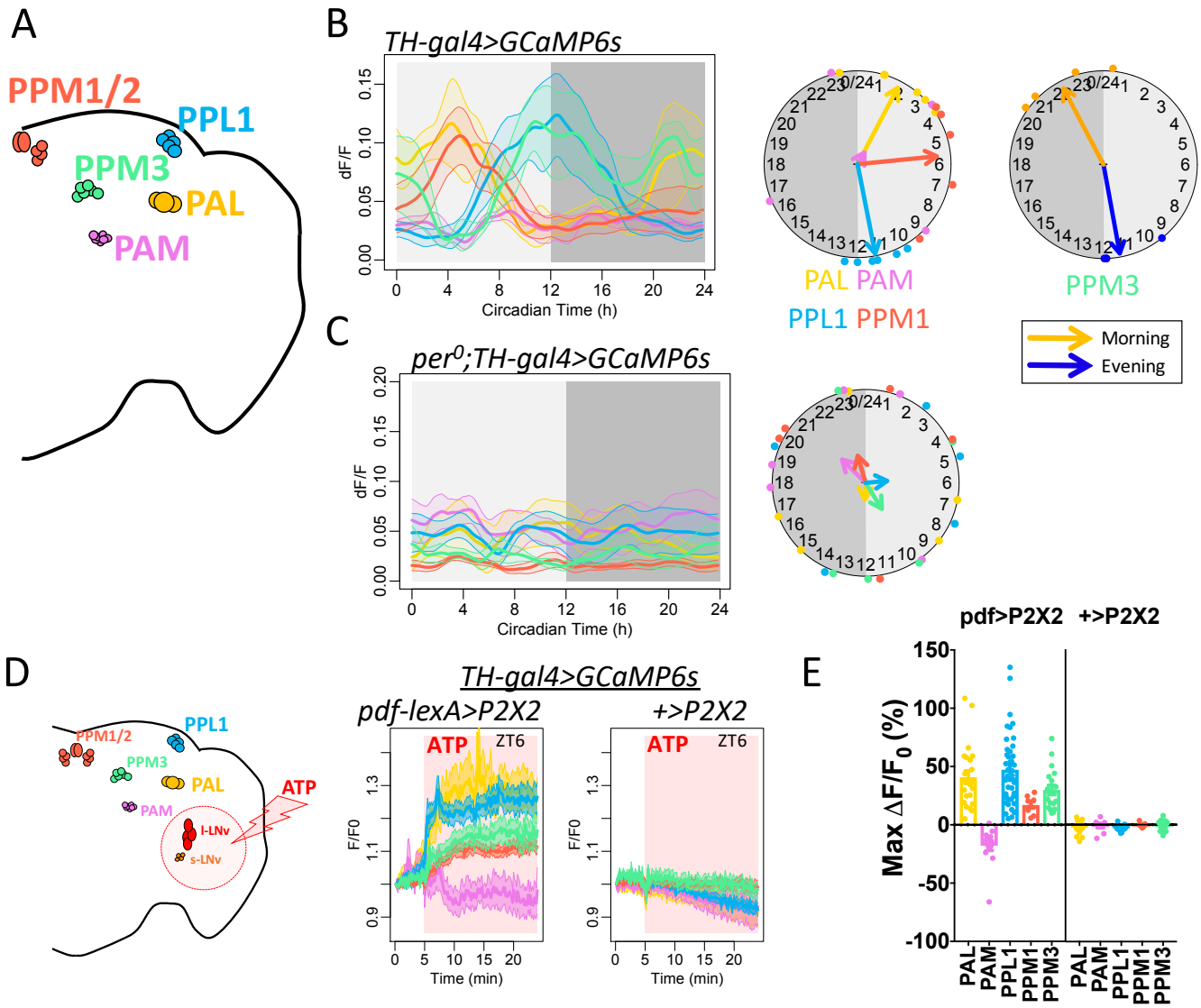


**Figure 1. Diverse daily neural activity patterns of DA neuron clusters.**
(**A**) Map of the five DA neuron clusters accessible via in vivo imaging.
(**B**) Left, daily $Ca^{2+}$ activity patterns of DA neuron clusters under DD (n = 6 flies). Middle, $Ca^{2+}$ phase distribution of DA neuron clusters showing single peaks (PAL, PPL1, and PPM1) or arrhythmic activity (PAM). Right, $Ca^{2+}$ phase distribution of PPM3 for both morning peaks (orange) and evening peaks (blue).
(**C**) Arrhythmic $Ca^{2+}$ activity patterns of DA neuron clusters under DD in *per*$^{01}$ mutants (n = 5 flies).
(**D**) Average traces of DA neuron clusters responding to ATP application in flies with P2X2 expressing in PDF neurons (left, n = 7 flies) and in control flies without P2X2 expression (right, n = 4 flies). Red aspect indicates duration of ATP application.
(**E**) Maximum $Ca^{2+}$ signal changes after ATP application in individual cells in (E).

Figure 2

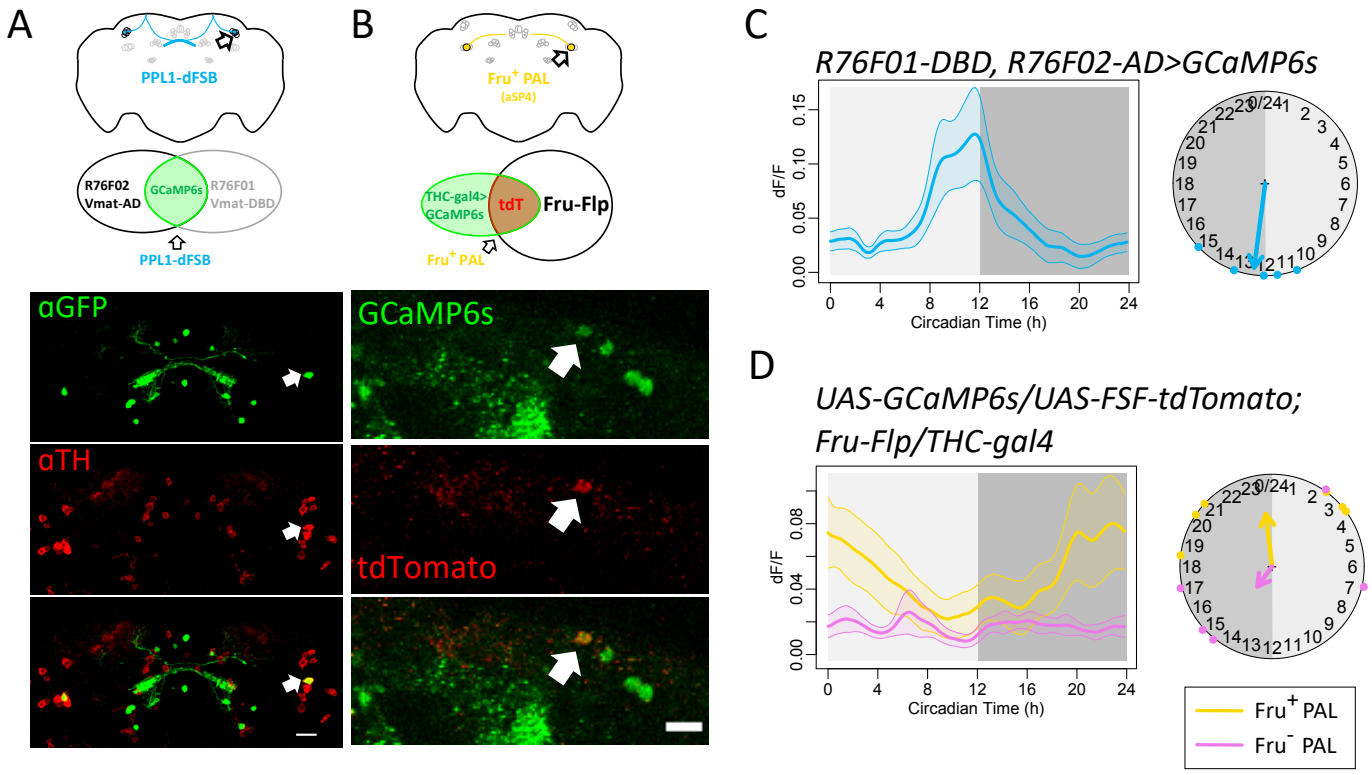


**Figure 2. Daily patterns of DA neurons in regulating sleep and mating behavior.**

(**A**) Diagram and confocal images of a pair of PPL1 projecting to dorsal fan-shape body (dFB) neurons co-localized with immunostaining signal of tyrosine hydroxylase (TH). Scale bar, 20 µm.

(**B**) Diagram and confocal images of a pair of fruitless positive PAL was labeled by tdTomato with intersection of TH-C-Gal4 and Fru-Flp.

(**C**)Daily $Ca^{2+}$ activity patterns of PPL1-dFB shown in (D) under DD (n = 5 flies).

(**D**) Daily $Ca^{2+}$ activity patterns of Fruitless-positive and -negative PAL shown in (E) under DD (n = 6 flies).

Figure 3

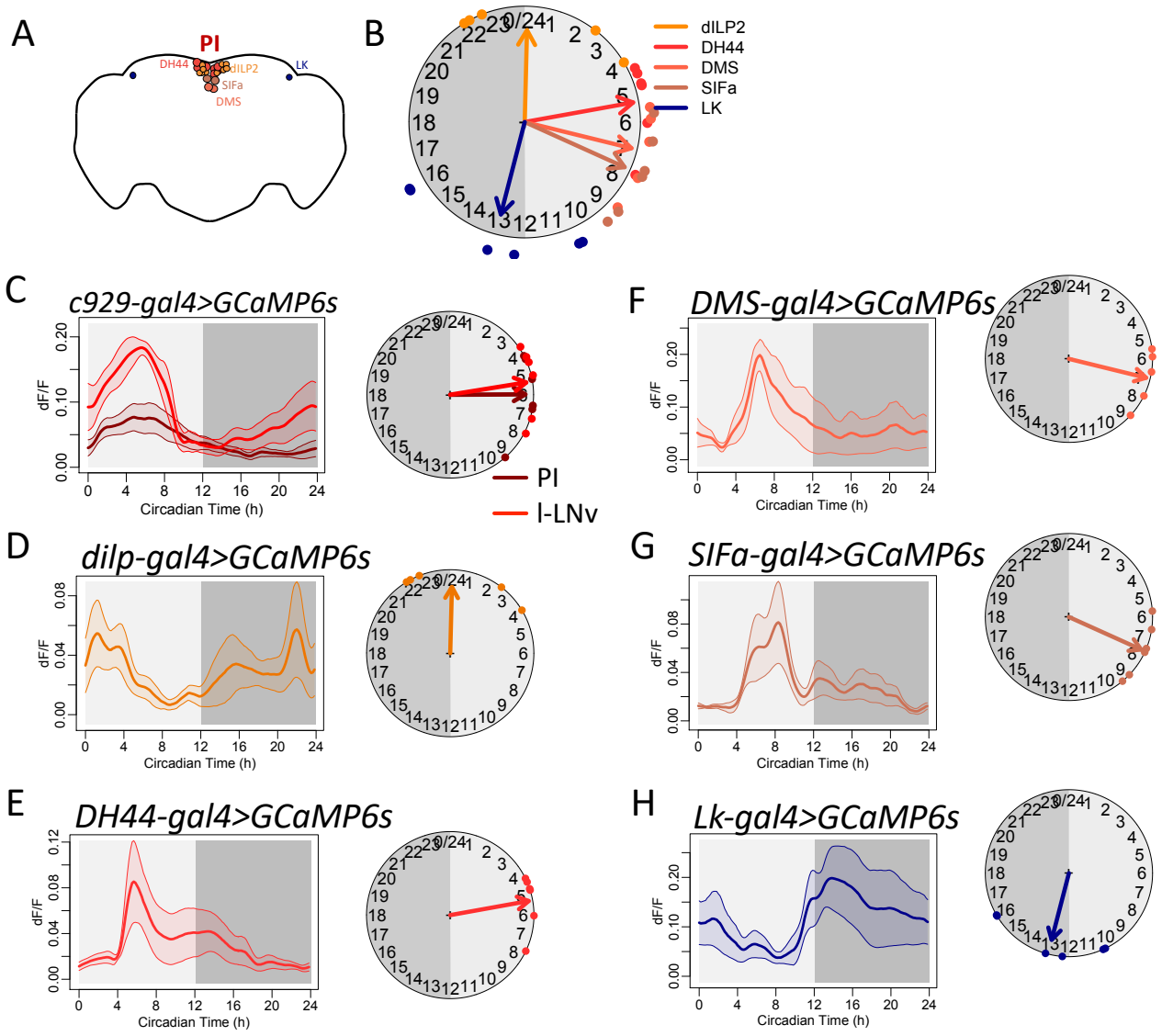


**Figure 3. Daily neural activity patterns of neuroendocrine cells.**

(**A**) Diagram of peptidergic neurons in the brain.

(**B**) Summary of phase distribution of different peptidergic neurons in (D-H).

(**C**) Averaged $Ca^{2+}$ activity rhythms of pars intercerebralis (PI) neuropeptidergic neurons and circadian neurons l-LNv labelled by *dimm(c929)-gal4* (n = 6 flies).

(**D-G**) Daily neural activity patterns of four different of PI subgroups: insulin producing cells (labelled by *dilp2-gal4*), diuretic hormone 44 (DH44) neurons, dromyosuppressin (DMS) neurons, and SIFamide (SIFa) neurons (n = 5, 6, 5, and 6 flies).

(**H**) Daily neural activity patterns of leucokinin (LK) neurons (n = 6 flies).

Figure 4

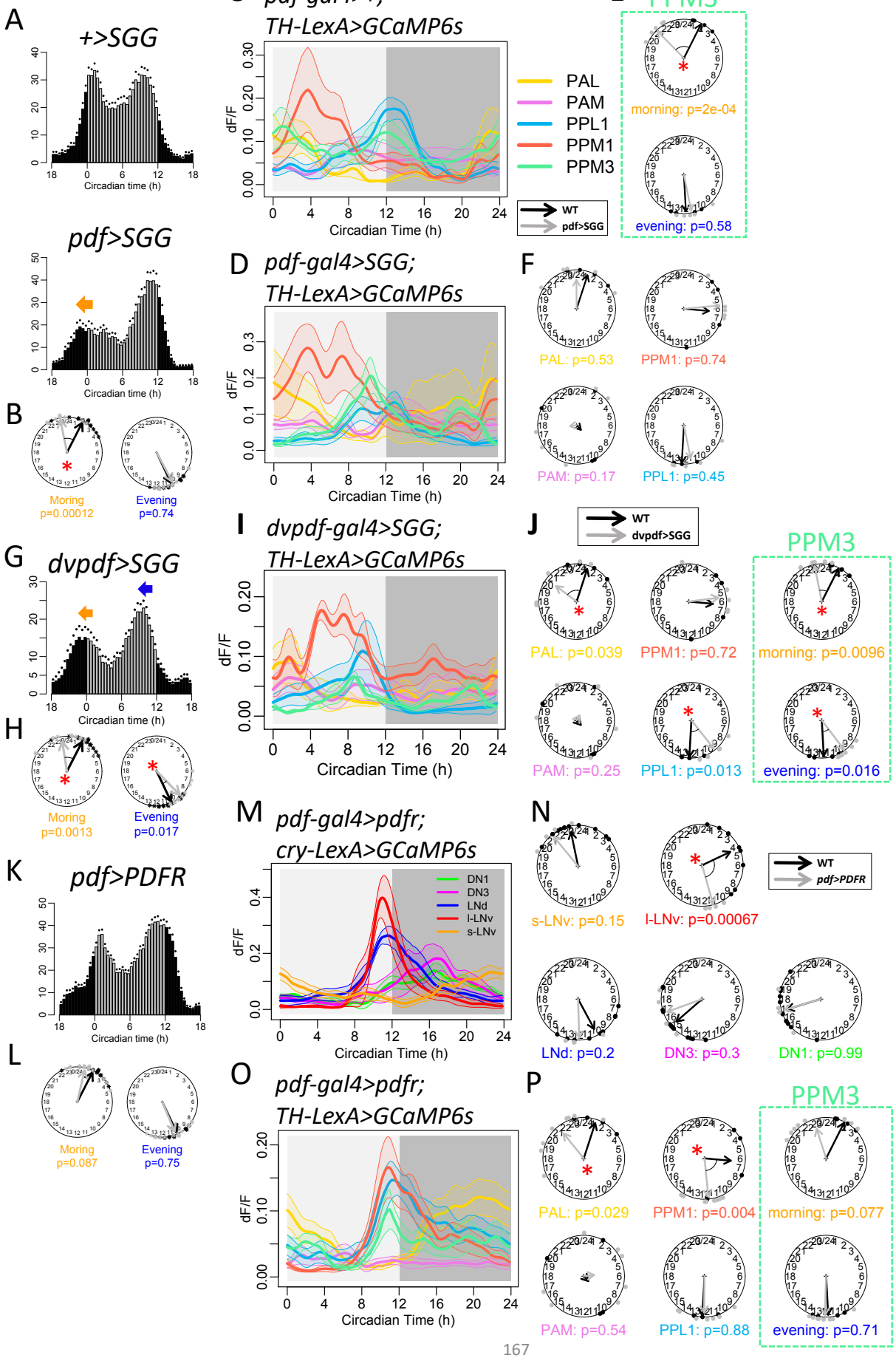
A
+>SGG
pdf>SGG
Circadian time (h)
B
Moring p=0.00012
Evening p=0.74
C pdf-gal4>+; TH-LexA>GCaMP6s
D pdf-gal4>SGG; TH-LexA>GCaMP6s
dF/F
Circadian Time (h)
PAL
PAM
PPL1
PPM1
PPM3
WT
pdf>SGG
E PPM3
morning: p=2e-04
evening: p=0.58
F
PAL: p=0.53
PPM1: p=0.74
PAM: p=0.17
PPL1: p=0.45
G dvpdf>SGG
H
Moring p=0.0013
Evening p=0.017
I dvpdf-gal4>SGG; TH-LexA>GCaMP6s
J
WT
dvpdf>SGG
PPM3
PAL: p=0.039
PPM1: p=0.72
morning: p=0.0096
PAM: p=0.25
PPL1: p=0.013
evening: p=0.016
K pdf>PDFR
L
Moring p=0.087
Evening p=0.75
M pdf-gal4>pdfr; cry-LexA>GCaMP6s
DN1
DN3
LNd
l-LNv
s-LNv
N
WT
pdf>PDFR
s-LNv: p=0.15
l-LNv: p=0.00067
LNd: p=0.2
DN3: p=0.3
DN1: p=0.99
O pdf-gal4>pdfr; TH-LexA>GCaMP6s
P
PPM3
PAL: p=0.029
PPM1: p=0.004
morning: p=0.077
PAM: p=0.54
PPL1: p=0.88
evening: p=0.71

Figure 5

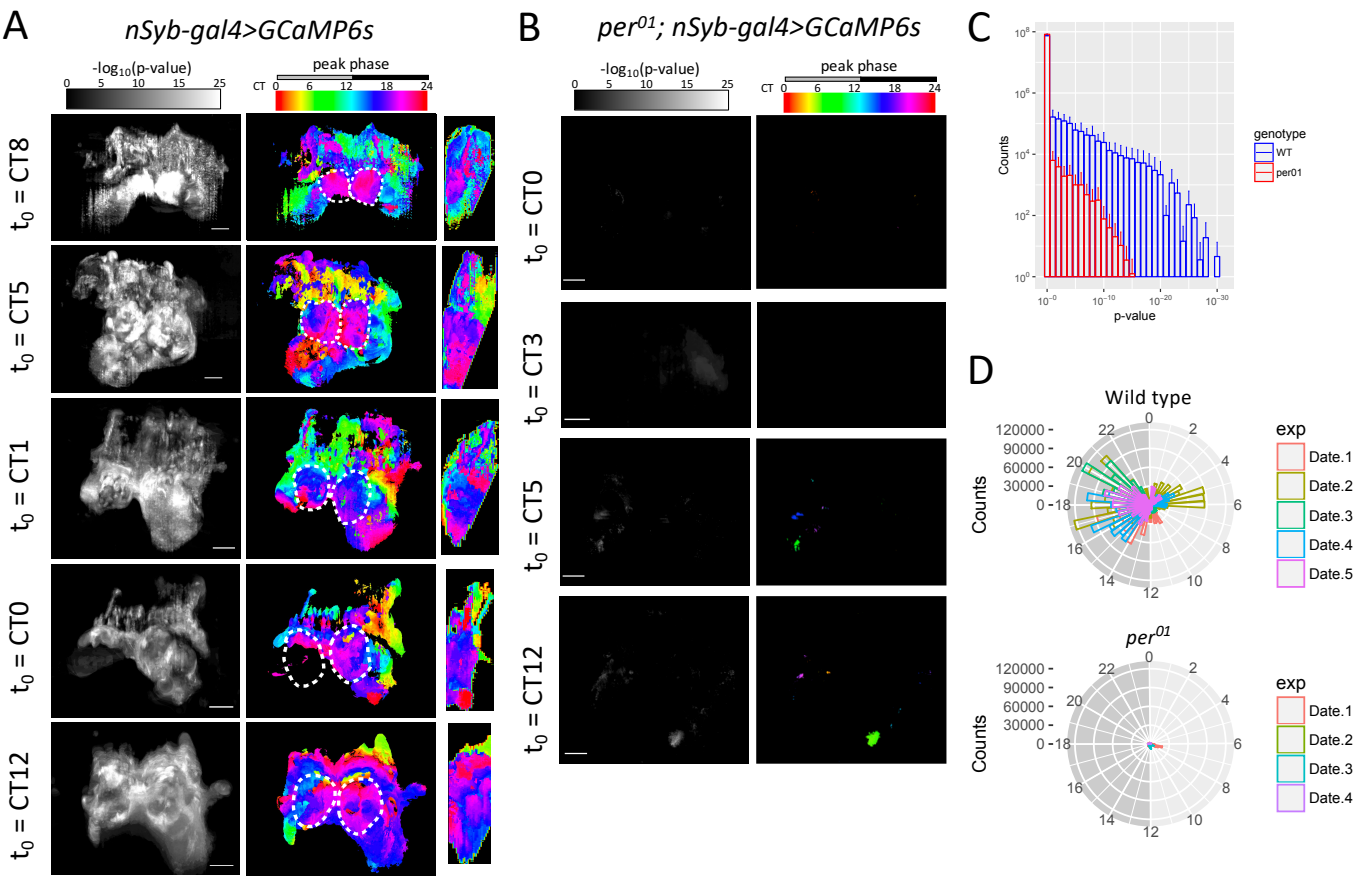


**Figure 5. Circadian rhythms in neural activity are widespread across the brain.** (**A**) Circadian rhythmicity of neural activity estimated by 24-hr in vivo pan-neuronal $Ca^{2+}$ imaging in wild type flies under DD. Left, maximum projection of rhythmicity map. (-log(p-value) for 24-hr period, JTK_CYCLE). Right, $Ca^{2+}$ activity peak phase map corresponding to voxels with maximum rhythmicity (shown in left). $t_0$ indicates circadian time when recording began. Scale bars, 100 µm. (**B**) Same analysis as (A) failed to identify strong circadian rhythmicity of neural activity in *per*$^{01}$ mutants. (**C**) p-value distribution of individual voxels in wild type flies (blue) and *per*$^{01}$ mutants (red). (**D**) Activity peak phase distribution of rhythmic voxels (p<1e-5) in wild type flies (above) and *per*$^{01}$ mutants (below).

---

**Figure 4. Daily activity phases of DA neurons are dictated by different groups of circadian neurons.**
(**A**) Average locomotor activity in DD1 of (top) wild type (WT, n = 16 flies) and (bottom) flies expressing *SGG* in PDF neurons using *pdf-GAL4* (*pdf>SGG*, n = 16 flies). (**B**) Phases comparisons of morning and evening activity between WT and *pdf>SGG*. Note that only the morning activity phase was advanced (* P < 0.05, Watson-Williams test). (**C-D**) Daily $Ca^{2+}$ activity patterns of DA neurons (C) in WT flies under DD (n = 4 flies) and (D) neurons in *pdf>SGG* flies under DD (n = 5 flies). (**E**) Phase comparison of morning peaks (orange) and evening peaks (blue) of PPM3 neurons between WT and *pdf>SGG* flies (Data was replotted from Chapter 4 Figure 5I). Morning peak of PPM3 were significantly advanced in *pdf>SGG*. (**F**) Phase comparison of other DA neurons between WT and *pdf>SGG* flies. (**G**) Average locomotor activity in DD1 of flies expressing *SGG* in PDF neurons and E cells using *dvpdf-GAL4* (*dvpdf>SGG*, n = 16 flies). (**H**) Phase comparisons of morning and evening activity between WT and *dvpdf>SGG*. (**I**) Daily $Ca^{2+}$ activity patterns of DA neurons in *dvpdf>SGG* flies under DD (n = 6 flies). (**J**) Phase comparison of DA neurons between WT and *dvpdf>SGG* flies. The daily peak phases of PAL and PPL1 and both morning and evening phases of PPM3 were advanced in *dvpdf>SGG* flies (* P < 0.05, Watson-Williams test). (**K**) Average locomotor activity in DD1 of flies expressing *PDFR* in PDF neurons using *pdf-GAL4* (*pdf>PDFR*, n = 16 flies). (**L**) Phase comparisons of morning and evening activity between WT and *pdf>PDFR*. (**M-N**) Daily $Ca^{2+}$ activity patterns of circadian neurons in *pdf>PDFR* and the phase comparisons of *pdf>PDFR* with WT. The phase of l-LNv was delayed. (**O-P**) Daily $Ca^{2+}$ activity patterns of DA neurons in *pdf>PDFR* and the phase comparisons of *PDF>PDFR* with WT. The phase of PPM1 was delayed.

# Figure 6

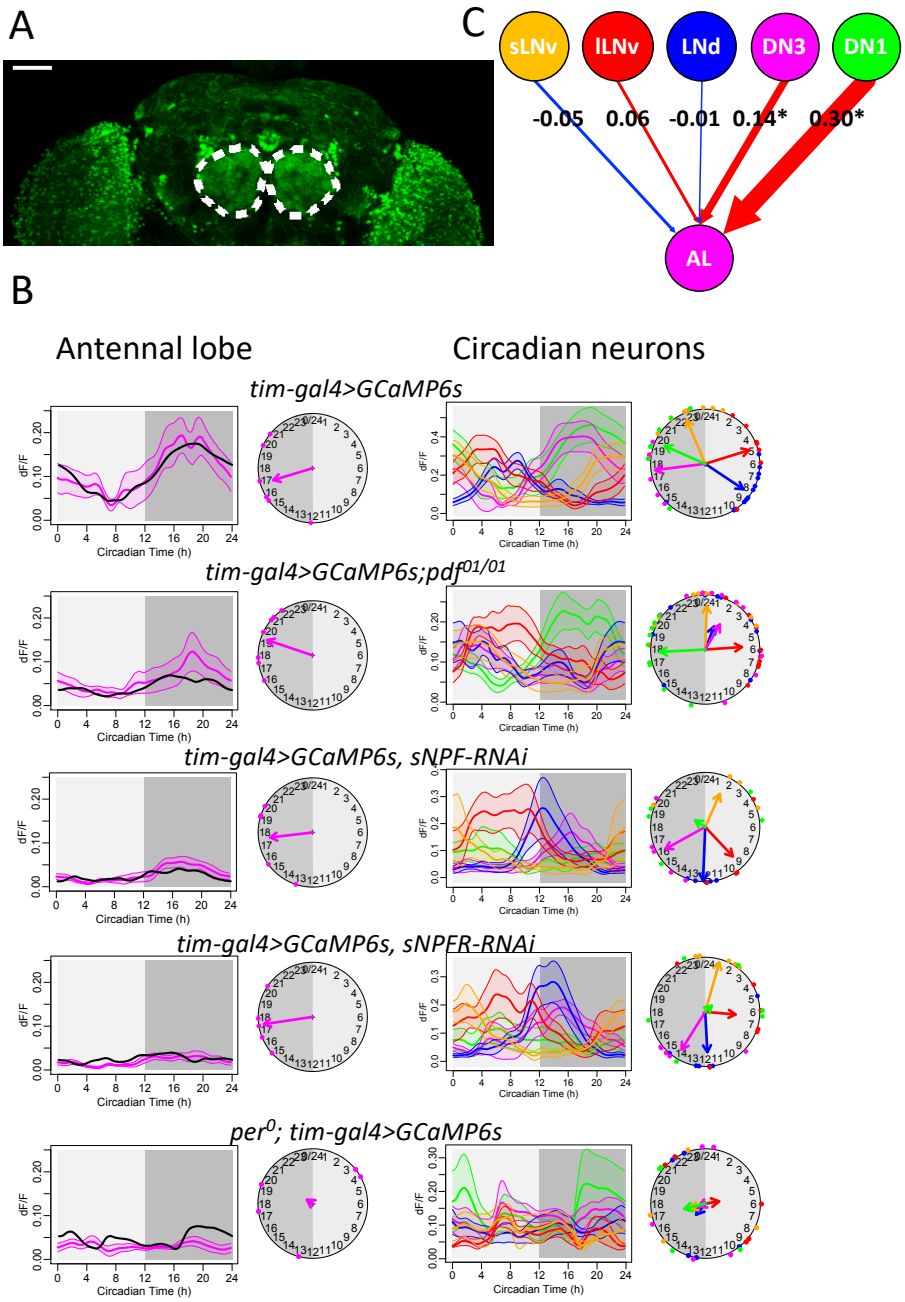


**Figure 6. Daily neural activity patterns of antennal lobe local neurons.**

(**A**) *tim-gal4* labelled a subgroup of antennal lobe local neurons (AL-LN). Scale bars, 100 µm.

(**B**) Daily neural activity patterns of AL-LN and circadian neurons labelled by *tim-gal4* in WT flies and deficiencies of PDF or sNPF neuropeptide signaling (Data from Liang et al 2017). The black traces are AL-LN activity predicted by circadian neuron activity in the genotypes based on the model in (C).

(**C**) Diagram of the linear model to generate the black traces in the left panel of (B). The width of and the number on the lines from different groups of circadian neurons to AL indicate the effect size of circadian neuron activity pattern contributing to AL activity pattern. (Linear model, *P < 1e-10)

Figure 7

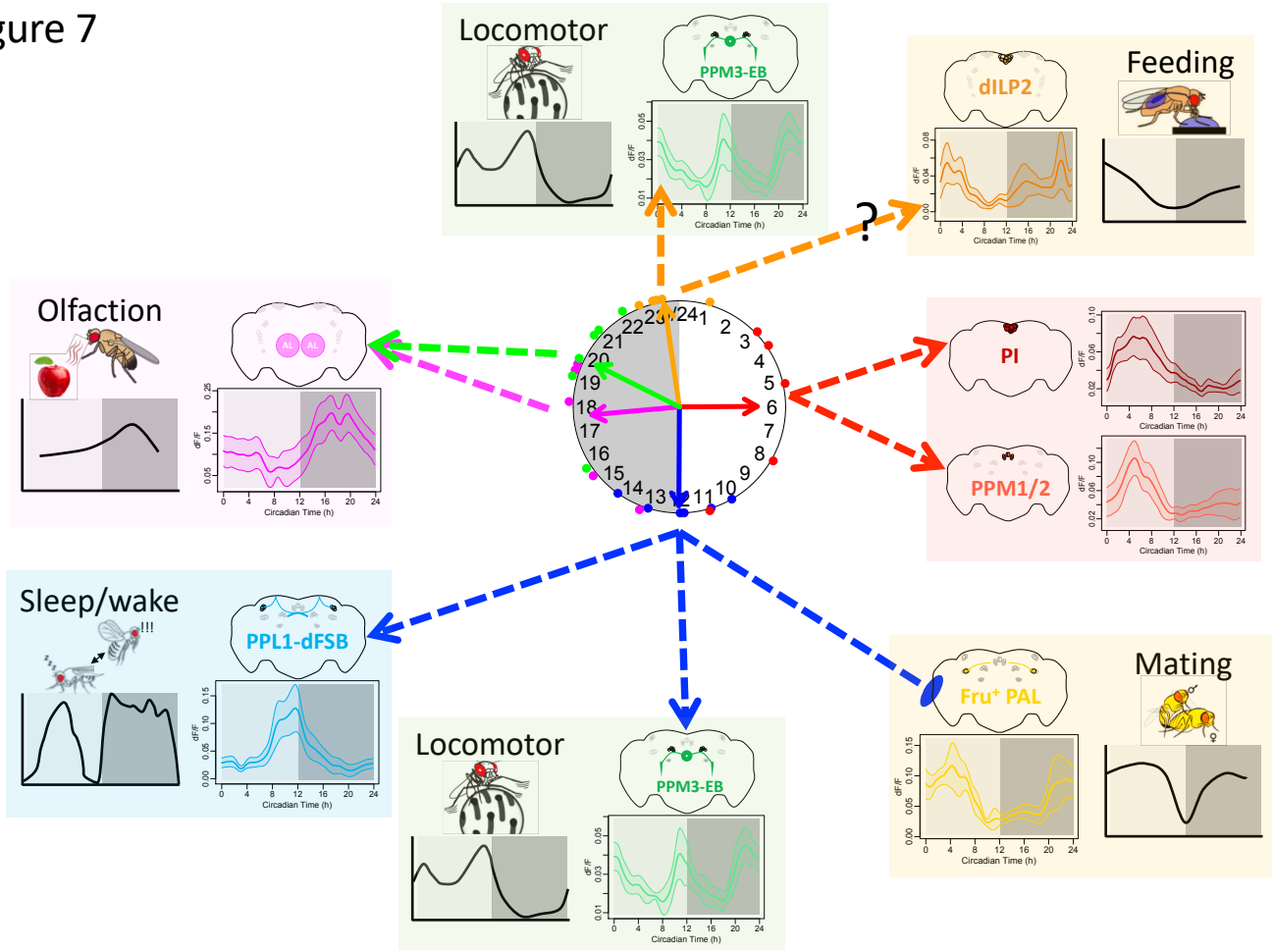


**Figure 7. Model of circadian output pathways.**
Groups of circadian neurons peaking at different times of day (center clockface) sent outputs to different downstream circuits (surrounding panels) to generate diverse phases. Circadian pacemaker M cells (orange arrows) and E cells (blue arrows) independently activate PPM3 neurons around dawn and dusk, which drive the locomotor activity rhythms (See Chapter 4). E cells (blue arrows) activate PPL1-dFSB neurons to suppress sleep around dusk (the daily sleep pattern was redrawn from Liu *et al.* 2012). E cells inhibit Fru+ PAL neurons to suppress the mating drive around dusk (the daily mating pattern was redrawn from Sakai and Ishida 2001). l-LNv (red arrows) controls the midday phase of dILP-negative PI neurons and PPM1 DA neurons. DN1 and DN3 (green and magenta arrows) work in concert to regulate activity rhythms in antennal lobe local neurons, which are involved in regulating the midnight peak of olfactory sensitivity (the daily pattern of olfactory responses was redrawn from Krishnan *et al.* 1999). The dILP2-positive PI neurons might regulate daily feeding rhythms and might be dictated by M cells (the daily feeding pattern was redrawn from Xu *et al.* 2008). The morning activity peaks of dILP2 neurons may also contribute to suppress sleep around dawn.

Fig. S1

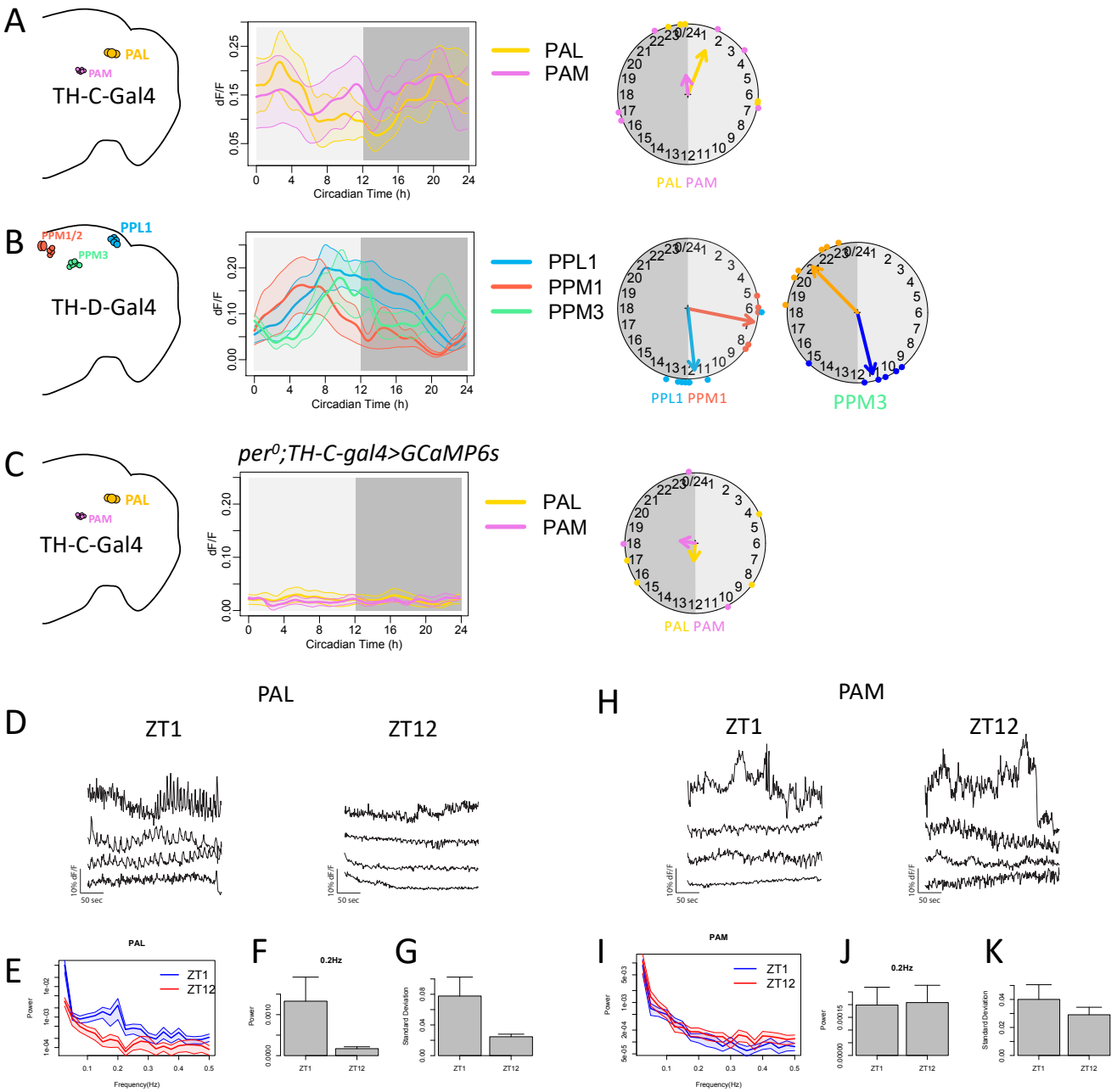


**Figure S1. Diverse daily $Ca^{2+}$ activity patterns of DA neuron clusters.** (**A**) Left, map of the two DA neuron clusters: PAL and PAM, accessible via in vivo imaging labelled by *TH-C-Gal4*. Right, daily $Ca^{2+}$ activity patterns of these two DA neuron clusters under DD (n = 6 flies). (**B**) Left, map of the three DA neuron clusters: PPL1, PPM1/2, and PPM3, labelled by *TH-D-Gal4*. Right, daily $Ca^{2+}$ activity patterns of these three DA neuron clusters under DD (n = 6 flies). (**C**) Arrhythmic $Ca^{2+}$ activity patterns of two DA neuron clusters labelled by *TH-C-Gal4* under DD in $per^{01}$ mutants (n = 5 flies). (**D-K**) Fast $Ca^{2+}$ activity of two DA clusters: PAL (D-G) and PAM (H-K), measured by 1Hz imaging at two zeitgeber time points: ZT1 (n = 7 flies) and ZT12 (n = 5 flies). (**E & I**) Power spectrums (fast Fourier transform) of PAL and PAM activity at two ZTs. (**F**) For PAL, power at 0.2Hz is stronger in the morning than in the evening. (**J**) For PAM, power at 0.2Hz is not different between morning and evening. (**G**) For PAL, overall standard deviation is higher in the morning than in the evening. (**K**) For PAM, overall standard deviation is not different between morning and evening.

Fig. S2

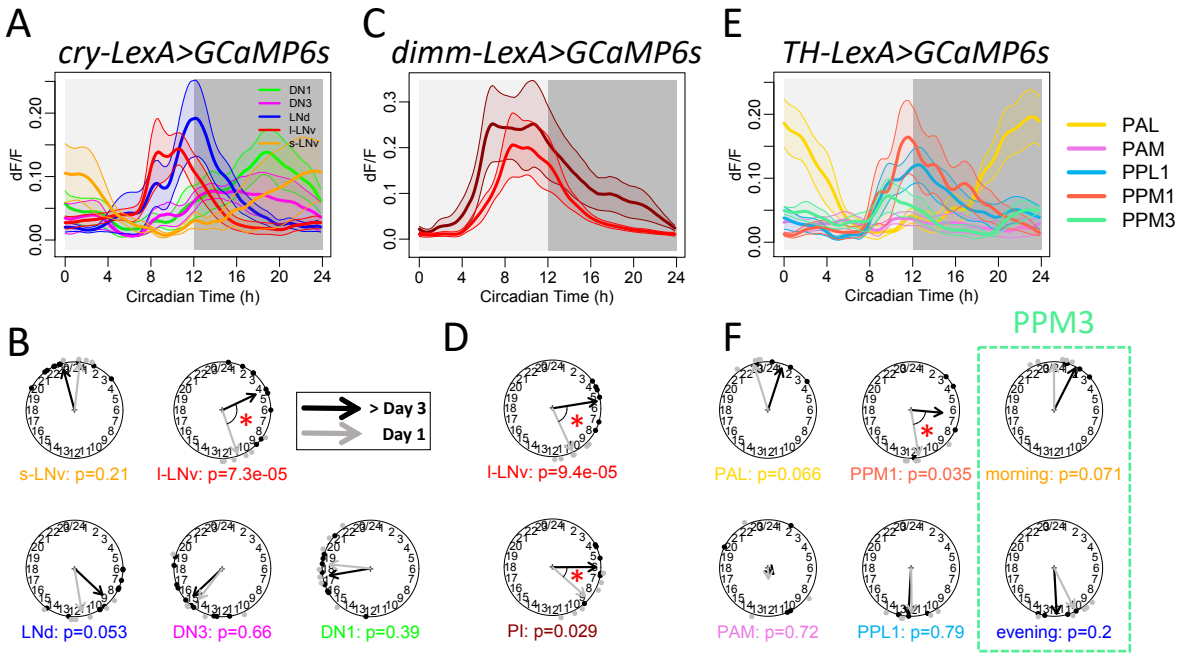


**Figure S2. Daily activity patterns of circadian neurons and output circuits in the first day after eclosion.**
(**A**) Daily $Ca^{2+}$ activity patterns of circadian neurons in flies within one day after eclosion (n = 7 flies).
(**B**) Phase comparison between aged and newly eclosed flies. Note that l-LNv phases in newly eclosed flies were latter than that in aged flies. (*p < 0.05, Watson-Williams test).
(**C**) Daily $Ca^{2+}$ activity patterns of l-LNv and PI cells in newly eclosed flies (n = 6 flies).
(**D**) l-LNv and PI cell phases in newly eclosed flies were latter than that in aged flies.
(**E**) Daily $Ca^{2+}$ activity patterns of dopaminergic neurons in newly eclosed flies (n = 5 flies).
(**F**) PPM1 phases in newly eclosed flies were latter than that in aged flies.

Fig. S3

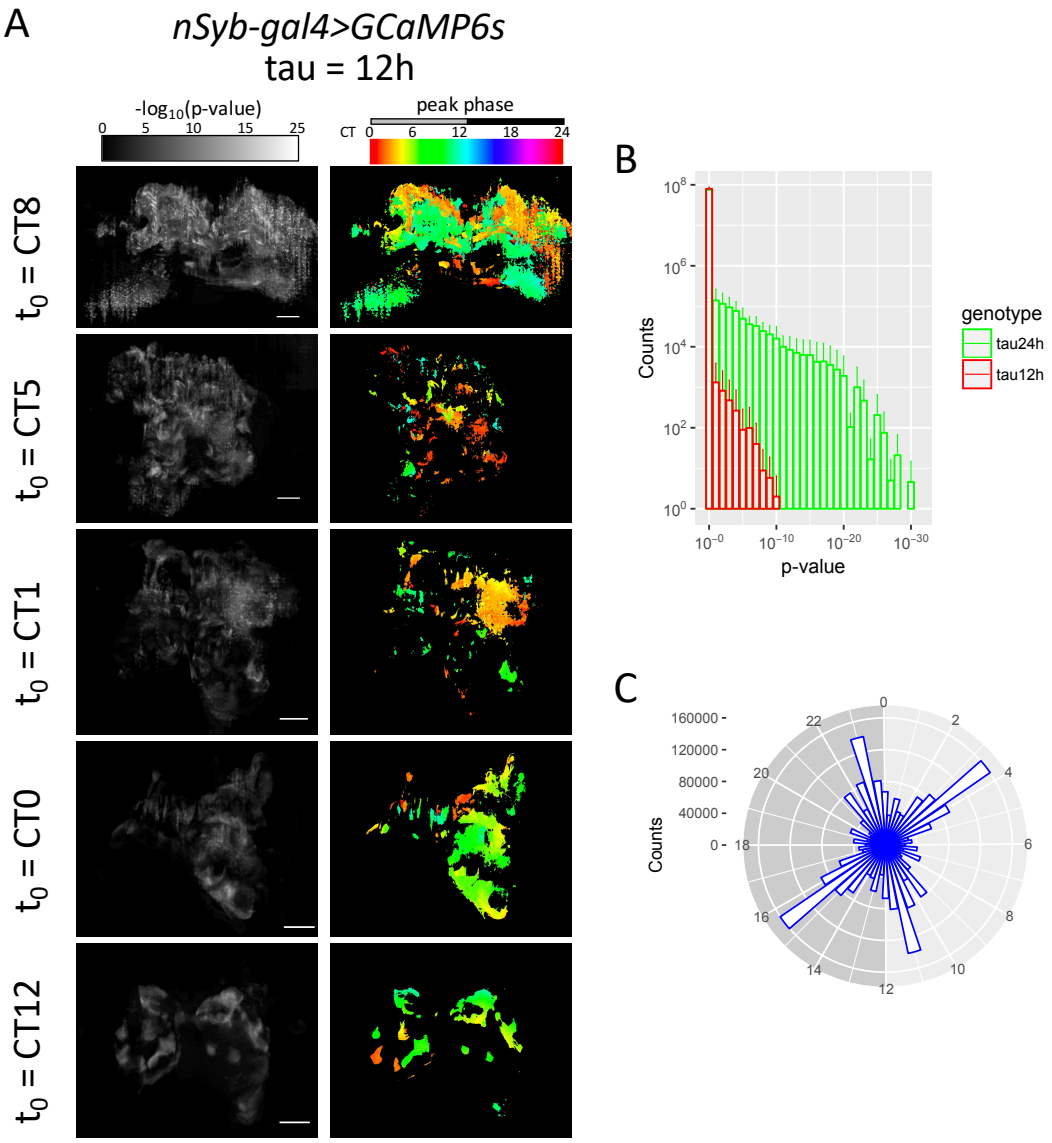


**Figure S3. Daily bimodal neural activity patterns are widespread across the brain**

(**A**) Ultradian rhythmicity (12-hr period) estimation for daily bimodal neural activity patterns in the same five wild type flies in Figure 6A and S5A. Left, maximum projection of rhythmicity map. (-log(p-value) for 12-hr period, JTK_CYCLE). Right, $Ca^{2+}$ activity peak phase map.

(**B**) Distribution of p-values for 24-hr period (green) and for 12-hr period (red) of individual voxels in wild type flies.

(**C**) Distribution of activity phases of rhythmic voxels with 12-hr period (p<1e-5) in wild type flies.

Fig. S4

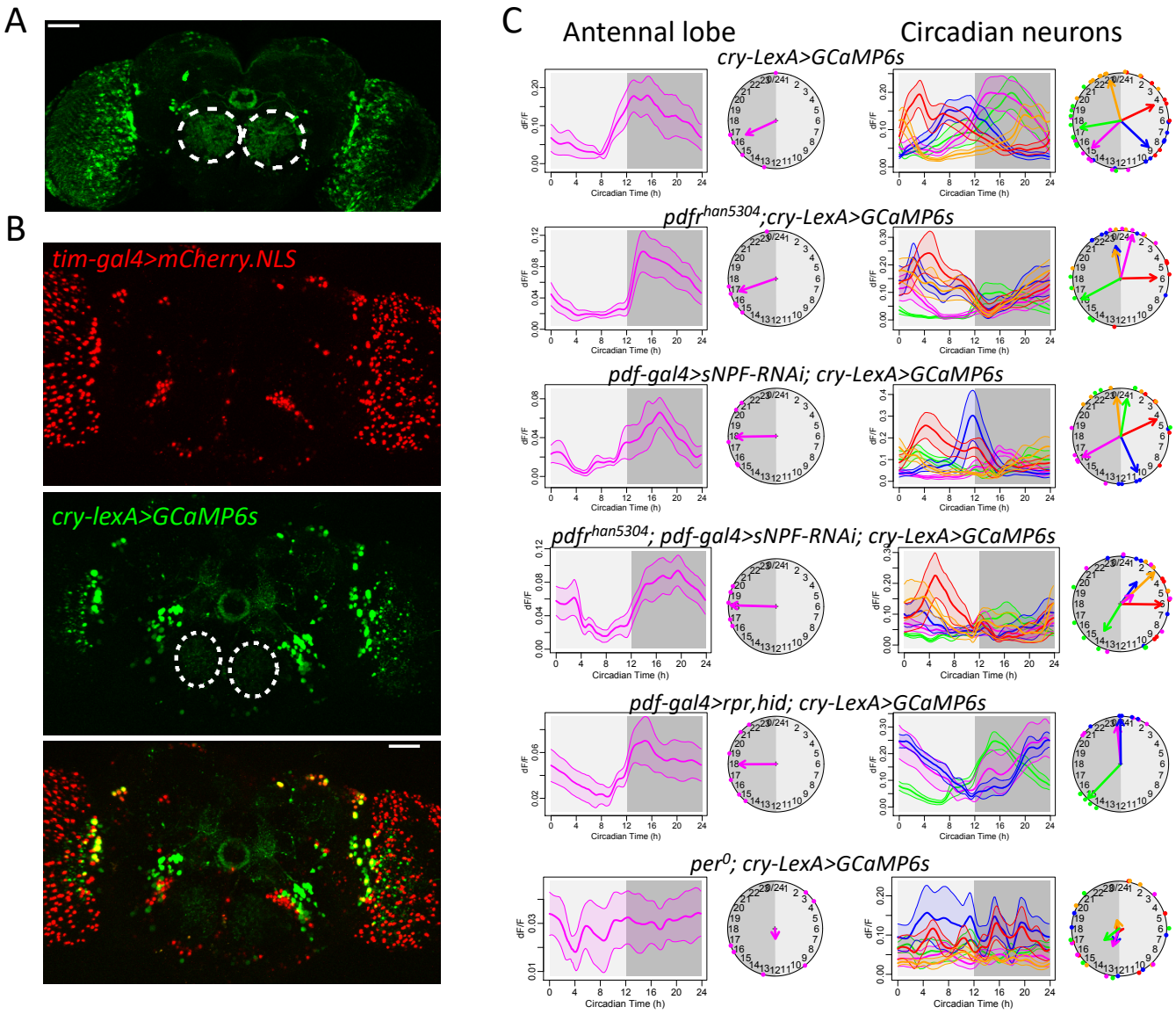


**Figure S4. Daily neural activity patterns of antennal lobe local neurons** (Data from Liang et al 2017).
(**A**) *cry-lexA* labelled a subgroup of antennal lobe local neurons (AL-LN). Scale bars, 100 µm.
(**B**) *cry-lexA* labelled a different subgroup of AL-LN. mCherry.NLS driven by *tim-gal4* was not overlapped with GCaMP6s driven by *cry-lexA*.
(**C**) Daily neural activity patterns of AL-LN and circadian neurons labelled by *cry-lexA* in WT flies and deficiencies of PDF and/or sNPF and $per^{01}$ null mutants.

# Chapter 6

## Circadian pacemaker neurons display daily rhythms in basal calcium level and in fast calcium fluctuations


### Abstract

Circadian pacemaker neurons in *Drosophila* brain display daily rhythms in the levels of intracellular calcium. These calcium rhythms are driven by molecular clocks and are required for normal circadian behavior. To study their biological basis, I employed genetic manipulations in conjunction with *in vivo* light-sheet microscopy to measure calcium dynamics in individual pacemaker neurons over complete 24-hour periods. I found co-phasic rhythms in basal calcium levels and in high-frequency calcium fluctuations. Further I found that the rhythms of basal calcium levels required the activity of the *IP3R*, a channel that mediates calcium fluxes from internal endoplasmic reticulum (ER) calcium stores. Independently, the rhythms of fast calcium fluctuations required the T-type voltage-gated calcium channel, a conductance that mediates extracellular calcium influx. These results suggest that molecular clocks regulate *IP3R* and T-type channels to generate coupled rhythms on the basal calcium level and the fast calcium fluctuations, respectively. I propose that both internal and external calcium fluxes are essential for circadian pacemakers to provide rhythmic outputs and thereby regulate the activities of downstream brain centers.

## Introduction

Circadian rhythms in multiple aspects of cellular physiology help organisms across taxa, from unicellular cyanobacteria to multicellular animals, adapt to environmental day-night changes (Dunlap 1999; Herzog 2007). In mammals, neurons in the hypothalamic suprachiasmatic nucleus (SCN) shows circadian rhythms in gene expression, intracellular calcium, neural activity, and other cellular properties (Welsh *et al.* 2010). Circadian rhythms in SCN neuronal outputs coordinate circadian rhythms in other cells throughout the body and generate behavioral rhythms (Mohawk *et al.* 2012). The rhythms of SCN neuronal outputs can be generated intrinsically by the negative transcription/translation feedback loop of core clock genes, as a molecular clock, which then generates 24-hour oscillations in a series of genes (Welsh *et al.* 1995; Dunlap 1999; Panda *et al.* 2002; Colwell 2011). These gene oscillations then regulate different aspects of membrane physiology such as the expression levels of channels for potassium ($K^+$), sodium ($Na^+$), and calcium ($Ca^{2+}$) (Pennartz *et al.* 2002; Itri *et al.* 2005; Pitts *et al.* 2006; Meredith *et al.* 2006; Flourakis *et al.* 2015). It remains unclear however, how these different aspects of membrane physiology interact and coordinate to generate circadian rhythms in pacemaker neural activity.

Calcium signaling regulates many cellular processes, such as neural excitability, neurotransmitter release, and gene expression (Berridge 1998). Intracellular calcium can be regulated from extracellular calcium influx, as well as from intracellular calcium storage in the endoplasmic reticulum (ER) and mitochondria (Syntichaki & Tavernarakis 2003). Studies on SCN neurons *in vitro* (Colwell 2000; Ikeda *et al.* 2003) and recently *in vivo* (Jones *et al.* 2018) showed circadian calcium rhythms in SCN neurons. Some studies suggested that calcium rhythms were driven by neuronal firing and voltage-gated calcium channels (Colwell 2000;

Enoki *et al.* 2017), while others suggested that were driven by intracellular stores via the ER channels ryanodine receptor *RyR* (Ikeda *et al.* 2003). These conflicting hypotheses may be due to the technical differences in the various studies, including the details of *in vitro* preparations, but also due to a lack of single-cell resolution in the calcium measurements.

In *Drosophila*, circadian pacemaker neurons also show clock-driven circadian calcium rhythms (Liang *et al.* 2016). The calcium rhythms in five major pacemaker groups: s-LNv, l-LNv, LNd, DN1, and DN3, exhibit distinct and sequential daily peak phases. The phase diversity requires environmental light and non-cell-autonomous modulation mediated by neuropeptides (Liang *et al.* 2017). Precisely how neuropeptide signaling regulates calcium activity in pacemaker neurons is unknown. In *Drosophila*, many calcium channels are encoded by single genes (Chorna & Hasan 2012), which provides a great opportunity to use genetics to study their potential roles in generating pacemaker calcium rhythms.

In this study, I used *in vivo* calcium imaging at singe-cell resolution with a high-speed light-sheet microscope. As described below, I simultaneously measured both basal calcium levels and fast calcium fluctuations over entire 24-hr periods. I found circadian rhythmicity in both basal calcium levels and the power of high-frequency calcium fluctuations. I consider the fast calcium fluctuations to represent events closely coupled to neuronal firing, as have previous related studies (Pologruto *et al.* 2004, Yaksi and Friedrich 2006). In all pacemaker neurons I studied, these two layers of calcium rhythms shared the same daily temporal pattern (i.e., they were co-phasic). In this chapter, I present results of experiments in which I knocked down different calcium channels selectively in all or a subset of pacemakers. I aimed to determine which channel(s) gate calcium stores that underlie changes in basal levels and which gate stores for changes in fast fluctuations. Also, as measured by PERIOD staining levels and by behavioral

consequences, I asked which channels feedback to influence the molecular clock and which are required for normal circadian output from the pacemaker network.

## Results

### The calcium rhythms in basal levels and fast fluctuations show similar daily patterns

Previously I reported that five major groups of circadian pacemaker neurons each exhibit daily calcium rhythms with distinct phases (Chapter 2; Liang *et al.* 2016). These results stand in contrast to descriptions of synchronous daily electrical neural activity rhythms in three groups of circadian pacemaker neurons, s-LNv, l-LNv, and DN1, by electrophysiological recordings (Cao and Nitabach 2008; Sheeba *et al.* 2008; Flourakis *et al.* 2015). The electrical activity rhythms were recorded *ex vivo* from different brains isolated at four to six different time points of the day. In contrast, I measured calcium rhythms *in vivo* by scanning individual flies every 10 min for 24 hours. Because of the close peak phases of s-LNv, l-LNv, and DN1 (from late night to mid-morning; Liang *et al.* 2016), and because of the coarse sampling of electrophysiological studies, whether calcium and electrical activity show different patterns remains uncertain. To help clarify apparent differences between results from calcium imaging vs. from electrophysiological recordings, I performed short-term high-frequency (1 Hz) *in vivo* calcium imaging on fly brains that were exposed acutely before each imaging experiment at five different time of day. Thus, I first used an *in vivo* experimental design akin to my earlier studies, but I represented the daily rhythm from population measures, not from single flies. I focused on the LNd because this group has the most different phase of calcium rhythms compared to s-LNv, l-LNv, and DN1 and the daily electrophysiological activity pattern of LNd has never been reported before. I found that around the daily calcium peak time (ZT8 - ZT10), LNd showed stronger fast calcium

fluctuations than other time points (Figure S1). The time course of fast calcium fluctuations in the evening indicates that these calcium fluctuations might be caused by the calcium influx during single action potentials or bursts of them (Figure S1a, Yaksi and Friedrich 2006). This result suggests that LNd might exhibit a daily rhythm in electrical neural activity, and that it is co-phasic with this pacemaker group's slow calcium rhythm.

Because the slow and fast calcium LNd rhythms are synchronous as measured, it is formally possible that one rhythm is downstream of the other: for example, the slow calcium rhythm could be the consequence of a rhythm in the fast. Alternatively, these two processes could be completely distinct. To better compare the basal calcium level with fast calcium fluctuations, I performed a series of short-term (1 min) high-frequency (5 Hz) *in vivo* calcium imaging at 1-hr intervals using the light-sheet microscope (OCPI-II). In so doing, I tracked both basal calcium level and fast calcium fluctuations in the same individual neurons, from all five major circadian pacemaker groups: importantly, made these measures consecutively from single brains for entire 24-hr periods (Figure 1a and Figure S2). I found that within all five pacemaker groups, changes in basal calcium levels and in fast calcium fluctuations shared similar daily patterns: when basal calcium levels were high, neurons tended to have more fast calcium fluctuations. The genotype of the flies I studied in these experiments flies were null mutants for the internal photoreceptor CRYPTOCHROME (*cry*[01]), to ensure minimal disruption to the circadian clocks due to repeated optical scanning. On average, all circadian neuron groups displayed slow calcium rhythms comparable to those I previously reported (Liang *et al.* 2016), expect for the l-LNv, which showed a second daily calcium activation right after the time of light off. Because l-LNv innervates optic lobes and receives large-scale visual inputs (Ashmore and Sehgal 2003), I speculate that the repeated optical scanning might activate l-LNv in the evening

via visual systems. Nevertheless, all pacemaker groups displayed daily changes in the minimal calcium level, suggesting that their basal calcium levels cycle with a daily rhythm (Figure 1c). Power spectrum analysis clearly revealed that, for individual neurons within each pacemaker group, calcium activity at all frequency domains increased when the basal calcium level was high (Figure 1d). These results support the hypothesis that fast calcium fluctuations in each of the circadian pacemaker groups exhibit a daily rhythmic pattern that is synchronized with a similar rhythm in basal calcium levels.

**An RNAi screen to identify potential contributions of different calcium channels**

The observations just described support the conclusion that for individual pacemakers, the level of basal calcium covaries with changes in the incidence of fast calcium fluctuations. Yet, these observations do not reveal whether the slow and fast calcium activities are mechanistically linked or represent distinct functions. To identify the sources for the calcium rhythms, I used RNAi to knockdown different calcium channels. I performed an extensive but incomplete screening for calcium channels, including three subtypes of α1 subunits and one type of α2δ subunits of voltage-gated calcium channels; two types of store-operated calcium entry (SOCE): *dSTIM* and *dOrai*; two types of calcium channels on ER: ryanodine receptor (*RyR*) and inositol trisphosphate receptor (*IP3R*); and sarco/endoplasmic reticulum calcium-ATPase (*SERCA*). By knocking down these genes selectively in circadian pacemaker neurons using *tim-GAL4* or in a subset of eight PDF-positive pacemaker neurons using *pdf-GAL4*, I first tested whether any of these genes are required for normal circadian behavioral rhythms (Figure 2a) and found evidence for the involvement of three (Figure 2b and Table 1). Reduced expression of a channel on the cytoplasmic membrane, *α1T* which encodes the α1 subunit for T-type voltage-

gated calcium channel caused the strongest behavioral arrhythmicity when driven by either *pdf-GAL4* or by *tim-GAL4* (65% and 83%) with one of the RNAi lines (KK100082). Knockdown of expression of the calcium pump on the ER membrane, encoded by *SERCA* likewise caused strong arrhythmicity in two different RNAi lines. Yet knocking down *SERCA* with the stronger RNAi line in all circadian pacemakers by *tim-GAL4* also shortened the flies' lifespans: most flies died during behavioral experiments. Reduced expression of another calcium channel on ER membrane, *IP3R,* also affected the circadian rhythm in behavior, when knocked down broadly with *tim-GAL4*. These behavioral deficits suggested that *α1T*, *SERCA*, and *IP3R* might be involved in the regulation of calcium rhythms in circadian pacemaker neurons.

**Slow calcium rhythms require IP3R**

We then asked whether *α1T*, *SERCA*, and *IP3R* regulate circadian behavior by regulating calcium rhythms, by measuring GCaMP6-signal levels during *in vivo* 24-hr recordings calcium imaging at 10-min sampling rate in *Drosophila* with these genes knocked down in all, or in just the subset of PDF-positive, circadian neurons (Figure 2c-j). Although knocking down *α1T* caused the strongest behavioral deficits, the slow calcium rhythms of all pacemaker neuron groups in these flies were generally as normal as those in the control genotype (Figure 2c-f). The amplitude of DN1 and DN3 calcium rhythms were reduced in flies with *α1T* knocked down in all pacemaker neurons, while their activity phases were still normal (Figure S3). In contrast, when *SERCA* was knocked down in PDF neurons (Figure 2g), or in all circadian neurons (Figure 2h), using the stronger RNAi line (KK107371), the slow calcium activities of these neurons were largely arrhythmic. The amplitudes of calcium fluctuations were reduced, and the coherence was lost within groups (Rayleigh test, $P > 0.2$). Likewise, the calcium rhythms were still normal

when *IP3R* was knocked down in PDF neurons (Figure 2i) but became largely arrhythmic when *IP3R* was knocked down in all circadian neurons (Figure 2j). The latter results are consistent with the behavioral phenotypes of the two manipulations for *IP3R* RNAi. In the latter case, knocking down *IP3R* in all circadian neurons caused stronger deficits in the calcium rhythms of non-PDF-positive neurons (LNd, DN1, and DN3) than in those of PDF-positive neurons (s-LNv and l-LNv). The difference in the vulnerability to IP3R disruption between PDF-negative and PDF-positive neurons might interpret why the *PDF-GAL4*-driven knockdown of *IP3R* didn't affect either calcium rhythms or behavior. Together, these results implicate SERCA and IP3R channel activities as essential for slow calcium rhythms and suggest the ER may be a key calcium source for the daily fluctuations of the basal calcium levels in circadian pacemaker neurons.

Because the slow calcium rhythms are driven by molecular clock gene oscillations (Liang *et al.* 2016), we asked whether the molecular clock generates the slow calcium rhythms by regulating *SERCA* and *IP3R*. If *SERCA* and *IP3R* are downstream of the molecular clock, knocking down these genes would affect calcium rhythms and behavior but not affect the molecular clock itself. I examined PERIOD (PER) protein levels in all five circadian pacemaker groups at four LD time points and found that PER cycling appeared robust in *IP3R*-knockdown flies, but was clearly diminished in *SERCA*-knockdown flies (Figure 3). Therefore, *IP3R* may be required to mediate regulation from the molecular clock to generate daily rhythms in basal calcium levels.

**Fast calcium fluctuations require voltage-gated T-type calcium channels**

Knocking down the *α1T* voltage-gated calcium channels impaired circadian rhythms in behavior, but did not affect circadian rhythmicity in basal calcium levels within pacemaker neurons. Therefore, I next asked whether *α1T* may underlie the circadian rhythm of fast calcium fluctuations in pacemakers. To test this, I again performed imaging across a series of short-term (5 min) high-frequency (1 Hz) calcium measurements on the same flies for a 24-hour day with 1-hour intervals (similar to Figure 1, yet with a slightly lower sampling rate). By comparing between control *Drosophila* and those with *α1T* knocked down in all circadian pacemaker neurons by *tim-GAL4,* I found that knocking down *α1T* did not affect the daily rhythms in the basal calcium level in any pacemaker groups, except for the DN1, which showed a reduction in the day-night difference of basal calcium level (Figure 4a-i and Figure S4). These high-frequency measures of slow basal calcium levels largely conform with those obtained with the slow-frequency (every 10 m) recording sessions (cf. Figure 2f). However, the high-frequency recording revealed that fast calcium fluctuations were significantly reduced in all circadian pacemaker neurons of the *α1T*-knockdown flies, except for the l-LNv, (Figure 4a-h & 4j and Figure S5). That specific pacemaker group instead displayed higher levels of fast calcium fluctuations. These results indicated that, at least in the majority of circadian pacemaker neurons, *α1T* is required for strong daily rhythms in fast calcium fluctuations and that the rhythm of fast calcium fluctuations can be selectively impaired, in distinction to manipulations that selectively affect the slow calcium rhythm.

**Discussion**

In this study, I used *in vivo* 24-hour high-frequency calcium imaging and genetic screening to study the cellular biology of daily calcium rhythms in circadian pacemaker neurons

of *Drosophila*. I found that the calcium rhythm is in fact composite: it reflects daily fluctuations in both a slow component (basal levels) and a fast one (high-frequency fluctuations). I have interpreted fast calcium fluctuations as representations of calcium dynamics that occur as neurons fire single action potentials or bursts of them. For individual identified pacemakers, these two calcium rhythms share the same daily pattern, yet different calcium sources appear to contribute differentially to these two rhythms. A calcium flux from ER via the channel *IP3R* is required for the slow rhythms in the basal calcium levels. Whereas an extracellular calcium influx, through cytoplasmic membrane calcium channels that include the *α1T* subunit, is critical for the fast calcium fluctuations. Importantly, both channels are essential for normal circadian behavior. Thus, the molecular clocks may drive circadian rhythms in pacemaker neuron output by regulating different calcium sources to generate coordinate, but distinct rhythms in its calcium activities.

Circadian calcium rhythms (CCR) are widespread across taxa (Knight *et al.* 1991; Colwell 2000). Calcium rhythms are required for circadian pacemaker functions in both *Drosophila* and rodents (Lundkvist *et al.* 2005; Harrisingh *et al.* 2007). Studies on mammalian circadian pacemakers in the suprachiasmatic nucleus (SCN) are controversial regarding the temporal relationship between the CCR and rhythms in electrical activity, such as spontaneous firing rate (SFR) and resting membrane potential (RMP). Recordings from SCN slice cultures showed that the phases of CCR in individual pacemakers are diverse and could be different from the populational phase of SFR rhythms (Ikeda *et al.* 2003; Enoki *et al.* 2012). However, it is unclear on the individual cell level, whether the phases of SFR rhythms are in phase with the populational SFR phase and/or with the phases of CCR. Imaging using both voltage sensor and calcium sensor on SCN slices, Brancaccio *et al.* (2017) showed that RMP rhythms and CCR

were in phase, yet Enoki *et al.* (2017) showed that RMP rhythms and CCR were in phase in the ventral SCN, but in dorsal SCN, the CCR phase-led the RMP rhythms by about 2 hours. This phase difference results from the 2-hour phase-lag in CCR between the ventral and dorsal SCN. However, this study didn't detect similar 2-hour phase-lag in RMP rhythms. Cellular interpretations in that case can be problematic in that the voltage sensor signal measured from dorsal SCN could derive from the neural processes of ventral SCN neurons. It is also possible that the neural activity pattern of dorsal SCN neurons is imposed by inputs from ventral SCN, as we previous showed in the case of the DN1 pacemaker group in *Drosophila* (Liang *et al.* 2017). Another possibility for the inconsistency might be the culture conditions: when SCN neurons were recorded *in vivo* by photometry, the rhythms in fast calcium activity were in phase with slow calcium rhythms (Jones *et al.* 2018). However, without comparisons made at the single-cell level, these studies remain inconclusive. Our recordings tracking individual pacemaker neurons from different groups *in vivo* for 24 hours showed that, at the single-cell level, slow calcium rhythms (CCR) were in phase with rhythms in fast calcium fluctuations, which likely reflect rhythms in SFR (Figure 1).

The causal relationships between clock gene rhythms, calcium rhythms, and electrical activity rhythms in the SCN remain generally unresolved. Treating SCN slices with TTX (to block Na-dependent action potentials) diminished SFR rhythms (Ikeda *et al.* 2003), partially affected RMP rhythms and CCRs (Hong *et al.* 2012; Enoki *et al.* 2012; Enoki *et al.* 2017), and slowly affected clock gene rhythms over several days (Yamaguchi *et al.* 2003). Dispersed SCN cells *in vitro* showed a TTX-resistant CCR, suggesting that CCR is driven by clock gene rhythms (Noguchi *et al.* 2017). Thus, the variation in CCR sensitivity to TTX treatment might be caused by the degree to which clock gene rhythms *in vitro* become progressively dysfunctional. In

*Drosophila*, my findings suggested that clock gene rhythms drive CCR in both basal calcium levels and fast calcium fluctuations via circadian regulation on both ER channel *IP3R* and membrane voltage-gated calcium channel *α1T*, respectively. The latter might then contribute to SFR and RMP rhythms. Similarly, in SCN pacemakers, pharmacologically blocking another ER channel *RyR* affected both CCR and SFR rhythms (Ikeda *et al.* 2003), suggesting that rhythms in basal calcium level are regulated by calcium from ER and are required for fast electric activity rhythms. In addition, SCN pacemakers also showed a circadian rhythm in fast calcium activity mediated by L-type voltage-gated calcium channels (Pennartz *et al.* 2002). Pharmacologically blocking these membrane channels affected SFR rhythms and in some case affected CCR (Ikeda *et al.* 2003; Enoki *et al.* 2017). In our studies, manipulating membrane voltage-gated calcium channel in all or a subset of pacemakers selectively affected rhythms in fast calcium fluctuations, which likely reflected SFR rhythms and thus impaired circadian outputs, but didn't significantly affect the slow rhythms in basal calcium levels (Figure 4). Therefore, in parallel to mammalian SCN neurons, *Drosophila* circadian pacemakers generate calcium rhythms by regulating both ER and extracellular calcium sources. Yet the regulation acts on a different set of ER and cytoplasmic membrane channels from mammalian pacemakers.

The RNAi knockdown experiments indicate a role for the ER calcium channel SERCA in supporting slow calcium rhythms in *Drosophila* pacemakers and behavioral rhythms. Yet the very high degree of lethality and the strong effects of SERCA-knockdown on the PER molecular oscillation precluded a clear assessment of its precise role. I can conclude that *SERCA*, which maintains the ER-cytoplasmic calcium gradient, is essential for the normal physiology of the cells, and suggest that future studies employing a conditional strategy – to knock SERCA down in mature neurons only – may help clarify its direct versus indirect contributions to the CCRs in

*Drosophila*. In contrast to *SERCA*, my results support a hypothesis that *IP3R* is a specific output molecule of the molecular clock. Previous transcriptomic analysis also supports that possibility: in circadian neurons, *IP3R* displays rhythmic expression, while *SERCA* does not (Figure S6; Abruzzi *et al.* 2017). Finally, the RNAi knockdown of plasma membrane calcium channel *α1T* indicated a role for voltage-gated T-type calcium channels in the final rhythmic output of the pacemakers. Furthermore, and consistent with a role as the presumed output pathway, impairing the rhythm of fast calcium activity strongly affected circadian behavior but did not affect the molecular clock, or the slow calcium rhythms. Remarkably, expression of *α1T* displays a circadian rhythm, with distinct phases in different groups of pacemaker neurons (Figure S3; Abruzzi *et al.* 2017). Collectively, these results suggest that *α1T* channel activity is critical to the regulation from the molecular clock to the rhythm of fast calcium activity.

**Methods**

**Fly stocks.**

Flies were reared on standard yeast-supplemented cornmeal/agar food at room temperature. After eclosion, male flies were entrained under 12 h light: 12 h dark (LD) cycles at 25°C for at least 3 days. The *tim>GCaMPS6s; cry*$^{01/01}$ flies were entrained under LD for more than 6 days.

The following fly lines were previously described: *tim(UAS)-GAL4* (Blau & Young 1999), *pdf-GAL4* (Renn *et al.* 1999), *cry-LexA* (Liang *et al.* 2017), *UAS-GCaMP6s* and *LexAop-GCaMP6s* (Chen *et al.* 2013). *UAS-dSTIM* and *UAS-dOrai* (Agrawal *et al.* 2010) were gifts from Dr. G Hasan (NCBS, India). *UAS-ip3rRNAi* (Liu *et al.* 2016) was a gift from Dr. M Wu (Johns Hopkins U.). Stable line: *UAS-dcr2; tim(UAS)-GAL4; UAS-GCaMP6s* and *pdf-GAL4;UAS-dcr2;cry-LexA,LexAop-GCaMP6s* were created for RNAi screening of calcium channels. The *cry-LexA* line was a gift from Dr. F Rouyer (CNRS Gyf, Paris).

RNAi lines were obtained from Bloomington Stock Center, Vienna Drosophila Resource Center, and Tokyo Stock Center. Two lines for *cac* (CG43368): *UAS-KK101478-RNAi* (VDRC 104168) and *UAS-JF02572-RNAi* (BDSC 27244). Two lines for *α1T* (CG15899): *UAS-KK100082-RNAi* (VDRC 108827) and *UAS-JF02150-RNAi* (BDSC 26251). Three lines for *α1D* (CG4894): *UAS-GD1737-RNAi* (VDRC 51491), *UAS-JF01848-RNAi* (BDSC 25830), and *UAS- HMS00294-RNAi* (BDSC 33413). Two lines for *α2δ* (CG12295): *UAS-KK101267-RNAi* (VDRC 18569) and *UAS-JF01825-RNAi* (BDSC 25807). One line for *Orai* (CG11430) *UAS-HMC03562-RNAi* (BDSC 53333). Three lines for *dSTIM* (CG9126): *UAS- KK102366-RNAi* (VDRC 106256), *UAS- GLC01785-RNAi* (BDSC 51685), and *UAS- JF02567-RNAi* (BDSC 27263). Two lines for *SERCA* (CG3725): *UAS- KK107371-RNAi* (VDRC 107446) and *UAS- JF01948-RNAi* (BDSC

25928). Three lines for *RyR* (CG19844): *UAS- KK101716-RNAi* (VDRC 109631), *UAS-HM05130-RNAi* (BDSC 28919), and *UAS- JF03381-RNAi* (BDSC 29445).

***In vivo* fly preparations and calcium imaging.**

The fly surgery followed procedures I previously described (Liang *et al.* 2016; 2017). Flies were first anesthetized by $CO_2$ and immobilized by inserting the neck into a narrow cut in an aluminum foil base. A portion of the dorso-anterior cuticle on one side of the head, an antenna, and a small part of one compound eye were then removed. For slow calcium rhythm measurements, imaging was conducted with a custom horizontal-scanning Objective Coupled Planar Illumination (hsOCPI) microscope (Holekamp *et al.* 2008). The scanning was done by moving the stage horizontally every 10 min for 24 hours. Each scan contained 20-40 separate frames with a step size of 5 to 10 microns. For fast calcium rhythm measurements, imaging was conducted with a custom high-speed dual-channel Objective Coupled Planar Illumination (OCPI-II) microscope (Greer *et al.* in prep). Each scanning session involved moving the objective using a piezo motor at 1-5 Hz for 1-5 min. The same scans were then repeated on the same specimens every hour, for 24 hrs. During both slow and fast imaging modes, HL3 saline was continuously perfused (0.1-0.2 mL/min).

**Locomotor activity rhythm.**

Trikinetics *Drosophila* Activity Monitor (DAM) system was used to monitor the locomotor activity rhythms of individual flies. 4-6-day-old male flies were monitored for 6 days under light-dark (LD) cycles and then for 9 days under constant darkness (DD) condition. The circadian rhythmicity and periodicity were measured by $\chi^2$ periodogram with a 95% confidence

cutoff and SNR analysis (Levine *et al.* 2002). Arrhythmicity were defined by a power value ($\chi^2$ power at best period) less than 10, width lower than 1, a period less than 18 hours or more than 30 hours.

**Immunocytochemistry.**

The flies were entrained for 6 days under LD and dissected at ZT0, ZT6, ZT12, and ZT18. After dissected in ice-cold, calcium-free saline, fly brains were fixed for 15 min in 4% paraformaldehyde containing 7% picric acid (v/v) in PBS. Primary antibodies were rabbit anti-PER (1:5000; kindly provided by Dr. M. Rosbash, Brandeis Univ.; Stanewsky *et al.* 1997). Secondary antisera were Cy3-conjugated (1:1000; Jackson Immunoresearch, West Grove, PA). Images were taken on the Olympus FV1200 confocal microscope. PER protein immunostaining intensity was measured in ImageJ-based Fiji (Schindelin *et al.* 2012).

**Imaging data analysis.**

Calcium imaging data was acquired by a custom software, Imagine (Holekamp *et al.* 2008) and pre-processed using custom scripts in Julia 0.6 for including non-rigid registration, alignment and maximal projection along z-axis. The images were then visualized and analyzed in ImageJ-based Fiji by manually selecting regions of interest (ROIs) over individual cells or groups of cells and measuring the intensity of ROIs over time. Slow calcium activity was analyzed as described previously (Liang *et al.* 2016, 2017). Fast calcium activity in each scanning session was analyzed similarly. Between sequential scanning sessions, the ROIs for individual neurons were manually corrected for position drifts. For the calcium signal of each ROI in each session, the mean of calcium intensity and the range of calcium intensity change was measured, and the

power spectrum was generated by fast Fourier transform. Then the calcium signal was filtered by a high-pass filter (1/15 Hz) and the standard deviation of calcium changes was measured. Calcium activity trace analysis and statistics were performed using R 3.3.3 and Prism 7 (GraphPad, San Diego CA).

Figure 1

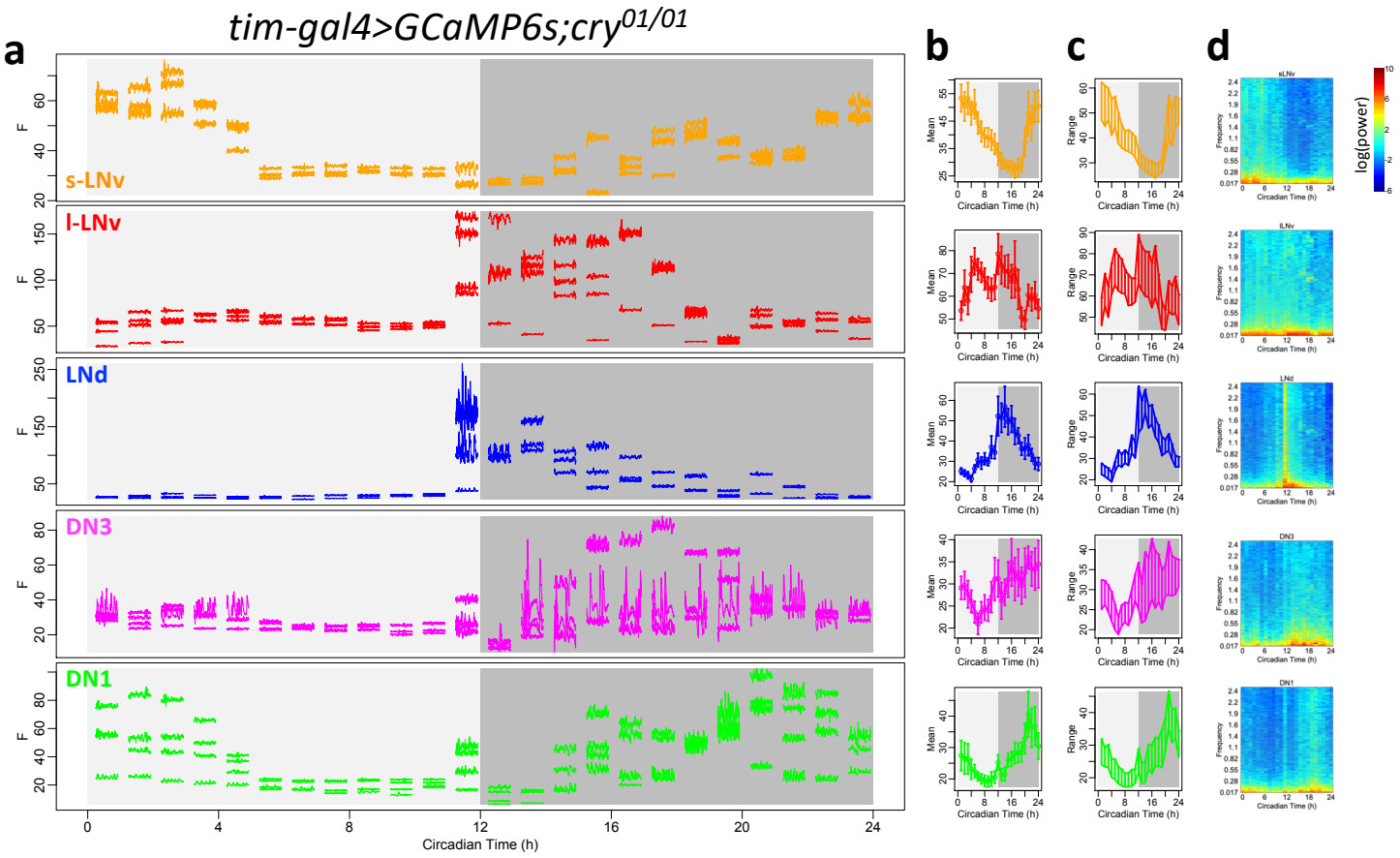


**Figure 1. Daily pattern of fast calcium activity in circadian pacemaker neurons.**
**(a)** Raw calcium activity traces from one representative fly (n = 6 flies). Each segmented trace is 1-min activity recorded at 5Hz. 24 segments are recorded over 24 hours with 1-hour intervals. Activity traces of five circadian pacemaker groups are plotted in separate panels and color-coded. For each group, only cells that can be tracked throughout all 24 recording sessions are showed. In this specific fly, 3 s-LNv, 4 l-LNv, 3 LNd, 4 DN3, and 4 DN1 can be reliably tracked across 24 recording sessions. Circadian pacemaker neurons exhibit daily modulation in basal calcium level and in the frequency of fast calcium spikes. **(b)** Daily pattern of mean calcium intensity over the 1-min recording session at each of the 24 timepoints, averaged across all 6 flies studied. Error bars denote SEM. **(c)** Daily patterns of the range of calcium transients over the 1-min recording session at each of the 24 timepoints, averaged across all 6 flies studied. **(d)** Daily pattern of the power spectrum over the 1-min recording session at each of 24 timepoints, averaged across all 6 flies studied.

Figure 2

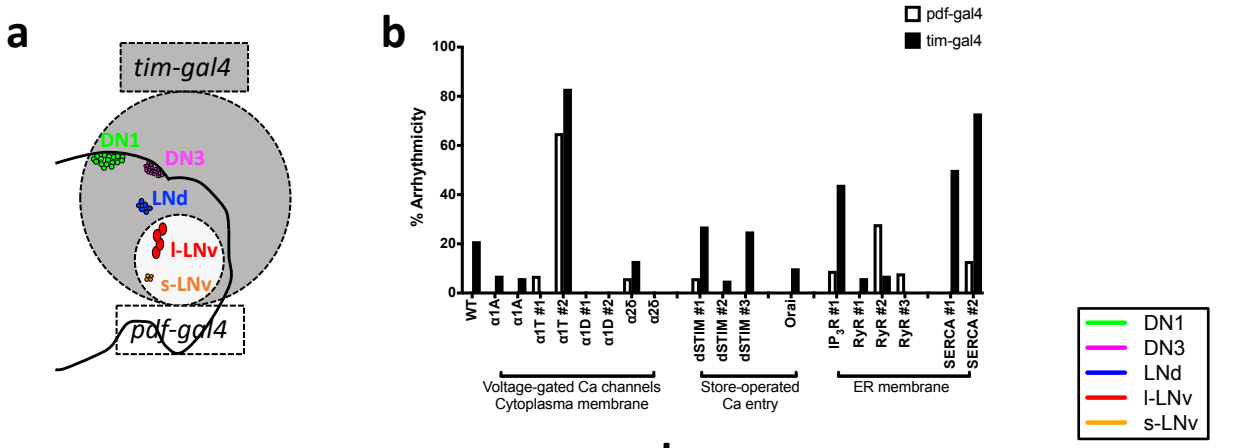
a
tim-gal4
DN1
DN3
LNd
l-LNv
s-LNv
pdf-gal4
b
pdf-gal4
tim-gal4
% Arrhythmicity
WT
α1A
α1A
α1T #1
α1T #2
α1D #1
α1D #2
α2δ
α2δ
dSTIM #1
dSTIM #2
dSTIM #3
Orai
IP3R #1
RyR #1
RyR #2
RyR #3
SERCA #1
SERCA #2
Voltage-gated Ca channels Cytoplasma membrane
Store-operated Ca entry
ER membrane
DN1
DN3
LNd
l-LNv
s-LNv

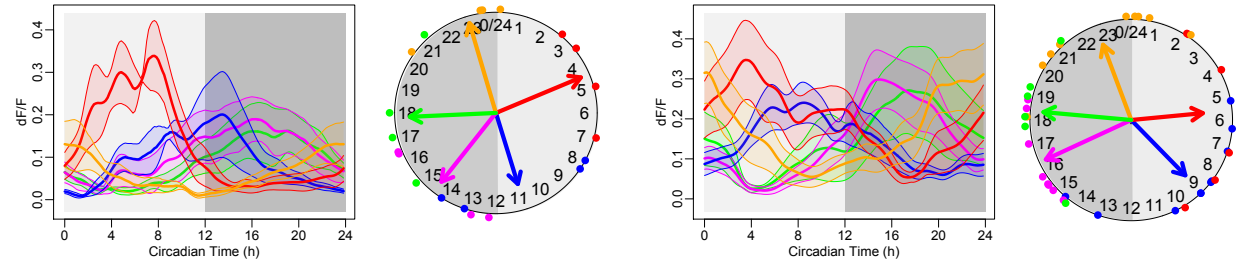
c
pdf-gal4>dcr2; cry-LexA>GCaMP6s
d
tim-gal4>GCaMP6s, dcr2
dF/F
Circadian Time (h)

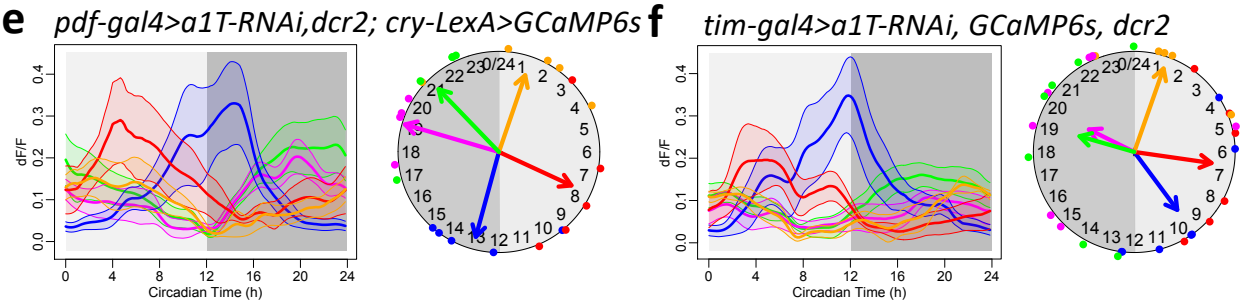
e
pdf-gal4>a1T-RNAi,dcr2; cry-LexA>GCaMP6s
f
tim-gal4>a1T-RNAi, GCaMP6s, dcr2
dF/F
Circadian Time (h)

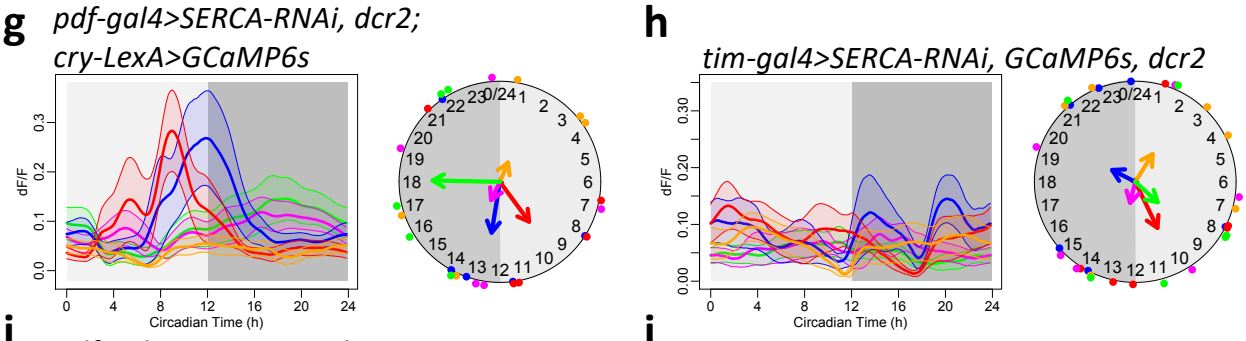
g
pdf-gal4>SERCA-RNAi, dcr2;
cry-LexA>GCaMP6s
h
tim-gal4>SERCA-RNAi, GCaMP6s, dcr2
dF/F
Circadian Time (h)

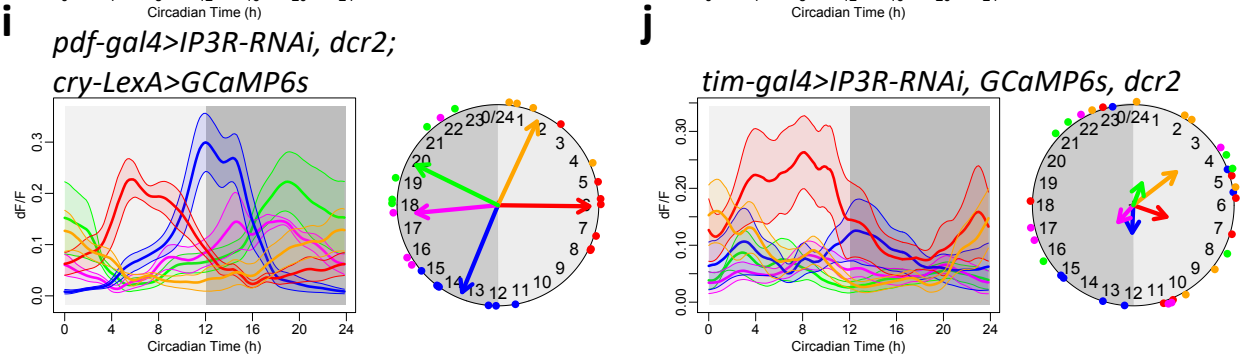
i
pdf-gal4>IP3R-RNAi, dcr2;
cry-LexA>GCaMP6s
j
tim-gal4>IP3R-RNAi, GCaMP6s, dcr2
dF/F
Circadian Time (h)

**Figure 2. RNAi-screening for calcium channels required for circadian calcium rhythms.**
**(a)** Illustration of *tim-GAL4* driving expression in all pacemaker groups and *pdf-GAL4* driving expression in a subset of pacemakers: the PDF-positive s-LNv and l-LNv groups. **(b)** Summary of behavioral screening for calcium-channel knockdowns that cause arrhythmicity in locomotor activity under DD (also see Table 1). **(c-d)** Daily calcium activity rhythms of five major circadian pacemaker groups in control flies for (c) *pdf-GAL4*-driven knockdown (n = 4 flies) and (d) *tim-GAL4*-driven knockdown (n = 12 flies) in first day under constant darkness (DD1). **(e-f)** Daily calcium activity rhythms are normal in (e) *pdf-GAL4*-driven *a1T* knockdown flies (n = 5 flies) and (f) *tim-GAL4*-driven *a1T* knockdown flies (n = 7 flies). **(g-h)** Daily calcium activity rhythms are partially impaired in (g) *pdf-GAL4*-driven *SERCA* knockdown flies (n = 5 flies) and completely impaired in (g) *tim-GAL4*-driven *SERCA* knockdown flies (n = 6 flies). **(i-j)** Daily calcium activity rhythms are normal in (i) *pdf-GAL4*-driven *ip3r* knockdown flies (n = 7 flies) and partially impaired in (j) *tim-GAL4*-driven *ip3r* knockdown flies (n = 7 flies).

Table 1. The rhythm strength and period of Locomotor activity under constant darkness of flies expressing calcium channel RNAi transgenes in PDF neurons or all clock neurons.

| GENE | CG# | Genotype* | N | %AR | Period | pwr | wid | SNR | ACT-day | ACT-night | ACT-cycle |
|---|---|---|---|---|---|---|---|---|---|---|---|
| Control | - | pdf>dcr2 | 16 | 0% | 25.0 | 96.7 | 6.8 | 1.8 | 23.7 | 27.9 | 25.8 |
| | | tim>dcr2 | 14 | 21% | 24.2 | 66.3 | 5.1 | 1.6 | 20.4 | 10.2 | 15.3 |
| α1A cac | 43368 | tim>JF02572 | 16 | 0% | 24.1 | 49.8 | 4.5 | 0.5 | 19.9 | 10.7 | 15.3 |
| | | pdf>JF02572 | 16 | 6% | 24.5 | 81.0 | 4.1 | 0.7 | 16.4 | 16.1 | 16.2 |
| | | pdf>kk104178 | 16 | 0% | 25.4 | 138.5 | 8.6 | 3.1 | 13.9 | 28.7 | 21.3 |
| | | tim>kk104178 | 14 | 7% | 24.4 | 41.1 | 4.9 | 1.0 | 14.8 | 21.0 | 17.9 |
| α1T | 15899 | pdf>JF02150 | 14 | 7% | 24.5 | 75.1 | 4.9 | 1.5 | 22.1 | 15.6 | 18.8 |
| | | tim>JF02150 | 16 | 0% | 23.6 | 59.0 | 4.4 | 1.1 | 14.3 | 2.4 | 8.4 |
| | | pdf>KK100082 | 23 | 65% | 24.4 | 21.4 | 3.0 | 0.7 | 14.4 | 11.9 | 13.2 |
| | | tim>KK100082 | 23 | 83% | 24.2 | 13.2 | 2.0 | 0.4 | 13.5 | 12.5 | 13.0 |
| α1D | 4894 | pdf>JF01848 | 14 | 0% | 24.3 | 66.7 | 4.4 | 0.9 | 18.7 | 13.4 | 16.1 |
| | | tim>JF01848 | 16 | 0% | 24.3 | 28.1 | 4.1 | 0.5 | 14.3 | 5.7 | 10.0 |
| | | pdf>GD1737 | 16 | 0% | 24.7 | 159.8 | 6.4 | 2.4 | 19.8 | 10.2 | 15.0 |
| | | tim>GD1737 | 23 | 0% | 24.4 | 170.8 | 6.3 | 2.3 | 18.4 | 14.8 | 16.6 |
| | | pdf>HMS00294 | 16 | 0% | 24.5 | 162.5 | 5.4 | 1.9 | 25.7 | 30.2 | 27.9 |
| | | tim>HMS00294 | 16 | 0% | 24.0 | 87.9 | 4.1 | 0.8 | 19.7 | 7.9 | 13.8 |
| α2δ | 12295 | pdf>JF01825 | 16 | 6% | 24.3 | 50.8 | 4.6 | 0.7 | 27.1 | 18.0 | 22.6 |
| | | tim>JF01825 | 16 | 13% | 23.9 | 62.7 | 5.9 | 1.0 | 25.0 | 13.7 | 19.4 |
| | | pdf>KK101267 | 16 | 0% | 24.7 | 183.1 | 6.2 | 2.6 | 17.0 | 21.3 | 19.1 |
| | | tim>KK101267 | 15 | 0% | 24.0 | 115.5 | 4.9 | 1.4 | 20.7 | 11.8 | 16.2 |
| Orai | 11430 | pdf>HMC03562 | 15 | 0% | 24.6 | 167.6 | 6.3 | 2.5 | 10.4 | 14.2 | 12.3 |
| | | tim>HMC03562 | 20 | 10% | 23.6 | 78.9 | 4.1 | 0.8 | 10.6 | 4.2 | 7.4 |
| | | pdf>uas-dOrai | 13 | 0% | 24.9 | 108.9 | 5.6 | 1.0 | 24.8 | 26.2 | 25.5 |
| | | tim>uas-dOrai | 15 | 0% | 24.3 | 115.4 | 5.7 | 1.2 | 16.1 | 8.8 | 12.4 |
| dSTIM | 9126 | pdf>GLC01785 | 16 | 6% | 24.2 | 91.8 | 7.4 | 2.0 | 21.4 | 18.6 | 20.0 |
| | | tim>GLC01785 | 15 | 27% | 23.7 | 31.9 | 3.6 | 0.7 | 13.3 | 6.0 | 9.7 |
| | | pdf>KK102366 | 23 | 0% | 25.4 | 118.3 | 6.2 | 1.2 | 11.4 | 12.6 | 12.0 |
| | | tim>KK102366 | 22 | 5% | 23.9 | 105.5 | 4.8 | 1.6 | 11.9 | 12.6 | 12.2 |
| | | pdf>JF02567 | 16 | 0% | 24.5 | 113.5 | 5.3 | 1.3 | 23.5 | 24.5 | 24.0 |
| | | tim>JF02567 | 12 | 25% | 23.8 | 24.7 | 3.3 | 0.6 | 7.3 | 3.4 | 5.3 |
| | | pdf>uas-dSTIM | 15 | 0% | 24.3 | 129.4 | 5.8 | 1.2 | 23.6 | 11.5 | 17.5 |
| | | tim>uas-dSTIM | 14 | 0% | 23.7 | 137.1 | 5.3 | 1.4 | 21.1 | 6.2 | 13.7 |
| SERCA | 3725 | pdf>JF01948 | 14 | 0% | 25.2 | 84.1 | 6.4 | 1.3 | 33.6 | 35.2 | 34.4 |
| | | tim>JF01948 | 12 | 50% | 25.3 | 12.7 | 2.8 | 1.4 | 13.1 | 10.1 | 11.6 |
| | | pdf>KK107371 | 16 | 13% | 24.5 | 40.9 | 4.4 | 0.7 | 28.3 | 29.1 | 28.7 |
| | | tim>KK107371** | 15 | 73% | 23.7 | 65.4 | 3.4 | 0.7 | 14.9 | 8.7 | 11.8 |
| RyR | 10844 | pdf>HM05130 | 15 | 0% | 24.7 | 94.0 | 6.2 | 1.7 | 19.0 | 19.1 | 19.0 |
| | | tim>HM05130 | 16 | 6% | 24.0 | 49.8 | 4.6 | 0.8 | 17.4 | 6.7 | 12.0 |
| | | pdf>JF03381 | 39 | 28% | 24.4 | 55.2 | 3.4 | 0.7 | 16.5 | 11.7 | 14.1 |
| | | tim>JF03381 | 28 | 7% | 23.9 | 128.1 | 5.3 | 1.4 | 19.1 | 10.1 | 14.6 |
| | | pdf>KK101716 | 13 | 8% | 24.7 | 165.1 | 6.6 | 2.5 | 15.1 | 17.1 | 16.1 |
| | | tim>KK101716 | 16 | 0% | 24.8 | 101.1 | 4.9 | 1.1 | 12.1 | 17.6 | 14.8 |
| IP3R | 1063 | pdf>ip3rRNAi#1 | 23 | 9% | 24.5 | 69.8 | 4.1 | 0.9 | 22.8 | 23.6 | 23.2 |
| | | tim>ip3rRNAi#1 | 16 | 44% | 24.3 | 18.0 | 2.6 | 0.6 | 12.1 | 4.9 | 8.5 |

*All genotypes include *UAS-dcr2* if it is not mentioned.

**In this genotype, most flies died during the behavioral experiment.

Figure 3

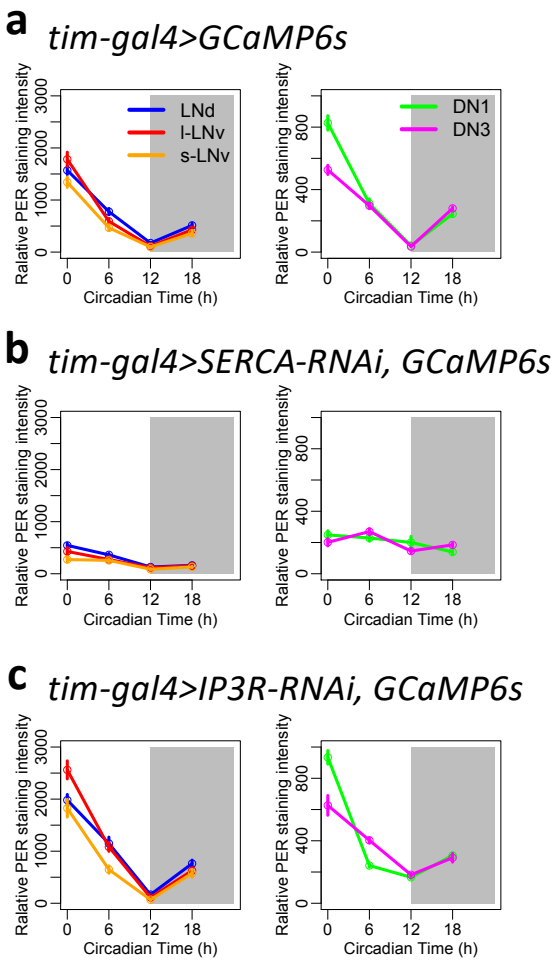


**Figure 3. PER protein rhythms of control flies and flies with *SERCA* or *ip3r* knocked down in all pacemaker neurons.**

**(a)** Averaged PER protein staining intensity at four different time points (ZT0, ZT6, ZT12, and ZT18) in five groups of circadian pacemaker neurons from control flies. **(b)** PER protein rhythms are diminished when knocking down *SERCA* in all pacemaker neurons by *tim-GAL4*. **(c)** PER protein rhythms are robustly cycling when knocking down *ip3r* in all pacemaker neurons by *tim-GAL4*. (n > 3 flies at each time point for each genotype).

Figure 4

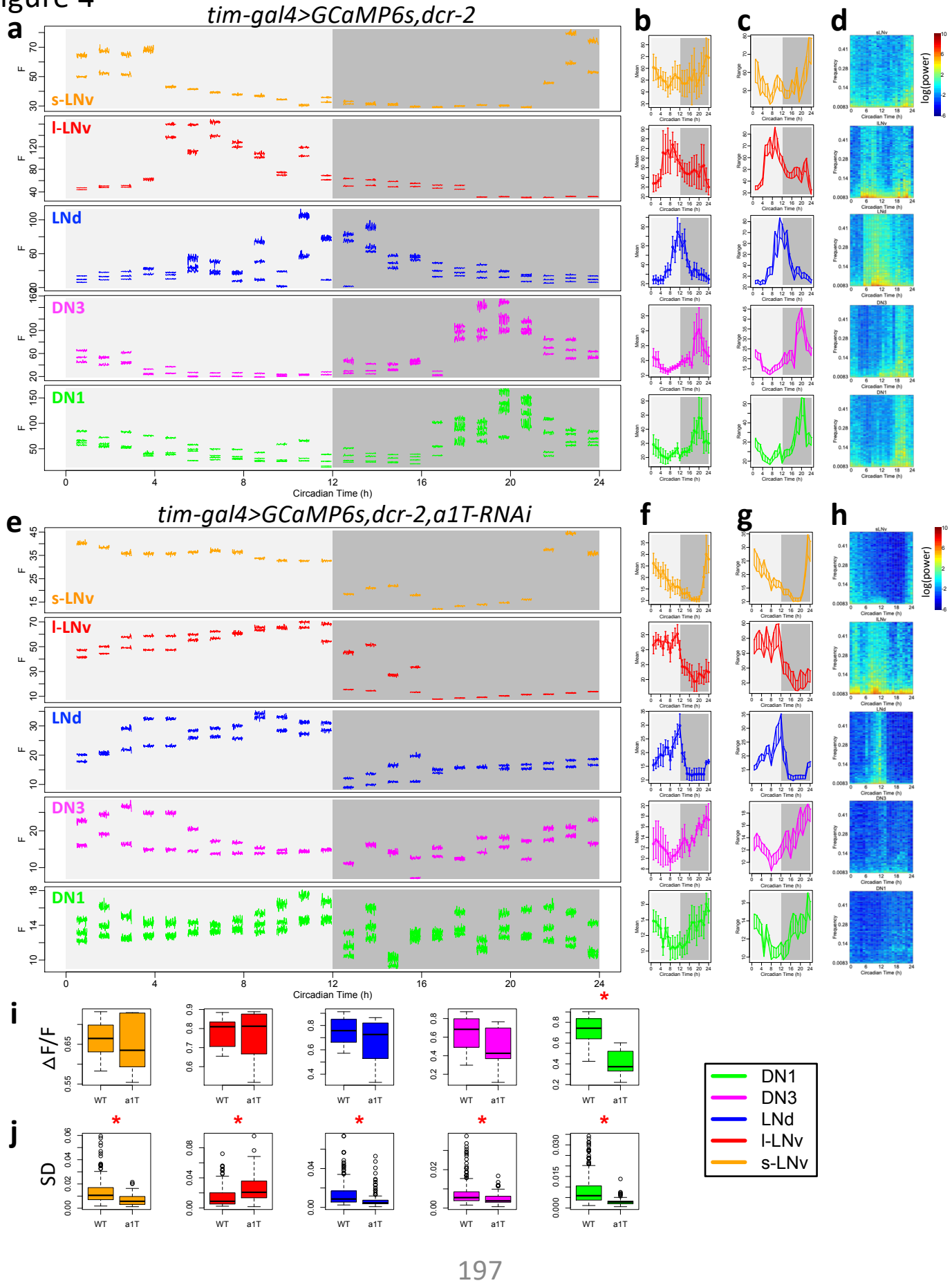
a
tim-gal4>GCaMP6s,dcr-2
s-LNv
l-LNv
LNd
DN3
DN1
F
Circadian Time (h)
b
c
d
log(power)
e
tim-gal4>GCaMP6s,dcr-2,a1T-RNAi
f
g
h
i
ΔF/F
WT
a1T
j
SD
DN1
DN3
LNd
l-LNv
s-LNv

**Figure 4. *α1T* knockdown reduces fast calcium fluctuations.**
**(a-d)** As Figure 1a-d, (a) raw calcium activity traces from one representative control fly. Each segmented trace is 5-min activity recorded at 1Hz. Averaged daily patterns of (b) mean calcium intensity, (c) the range of calcium transient, and (d) the power spectrum (n = 4 flies). **(e-h)** As in (a-d), raw calcium activity traces from one representative fly with *α1T* knockdown in all pacemaker neurons and averaged daily patterns of mean, range, and power spectrum in this genotype (n = 4 flies). **(i)** Box plot of daily range of calcium signal for individual neurons of five pacemaker groups between control flies and *α1T*-knockdown flies. The daily variation of DN1 calcium reduces in *α1T*-knockdown flies (t-test, *P < 0.05). **(j)** Box plot of standard deviations of calcium signal in each recording session for individual neurons of five pacemaker groups between control flies and *α1T*-knockdown flies. The standard deviations of fast calcium fluctuations in s-LNv, LNd, DN3, and DN1 are smaller, while that in l-LNv is larger in *α1T*-knockdown flies than that in control (t-test, *P < 0.05).

Figure S1

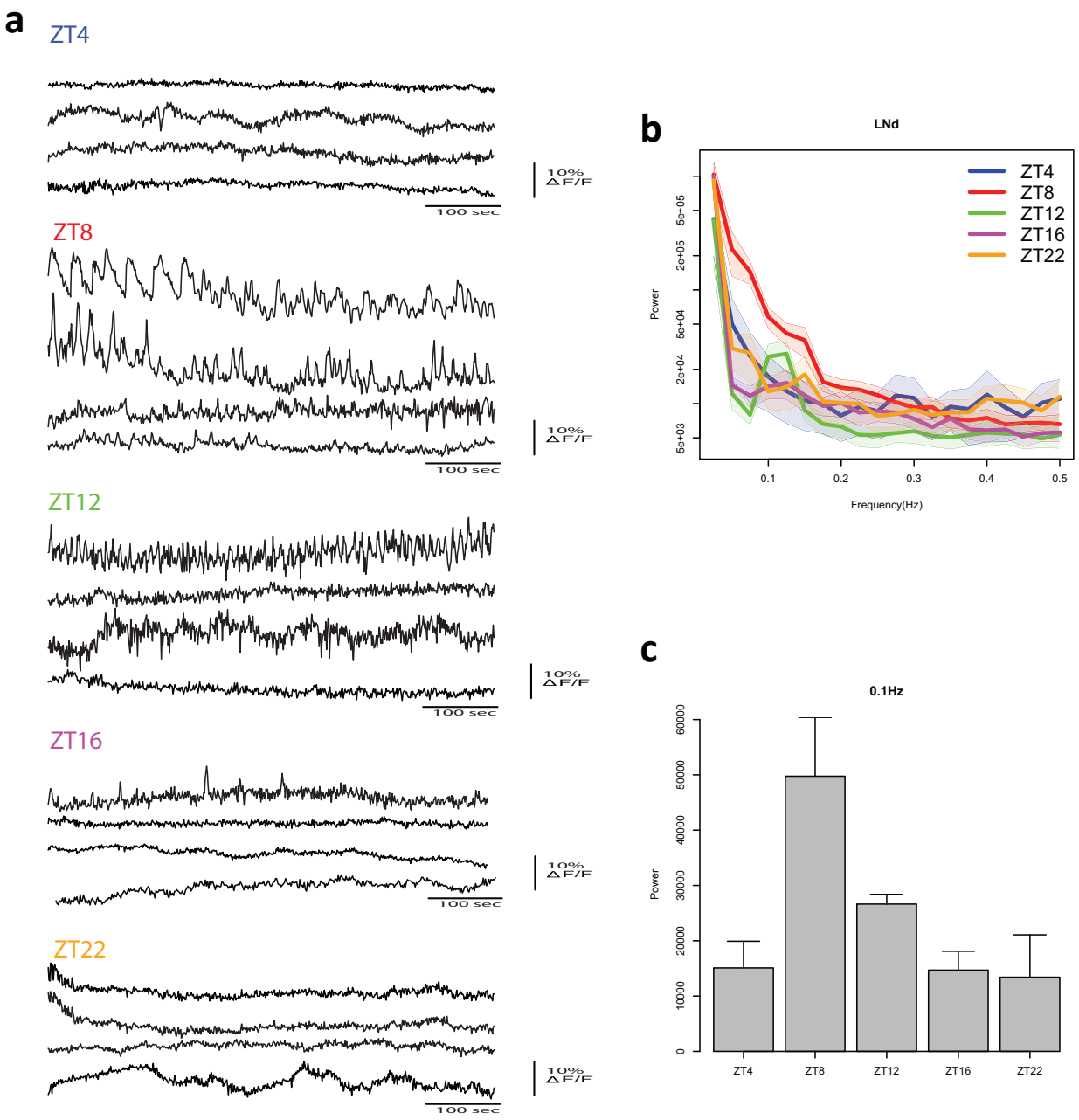


**Figure S1. Daily pattern of fast calcium activity in LNd.**
**(a)** Representative calcium activity traces of LNd recorded at 1Hz from five different times of day: ZT 4, ZT8, ZT 12, ZT16, and ZT22. For each timepoint, the fly's brains are acutely exposed for short-term imaging. **(b)** Averaged power spectrums for five different timepoints (n > 6 flies for each timepoint). **(c)** Averaged power at 0.1Hz for five different timepoints shows a similar daily pattern as LNd slow calcium rhythms.

Figure S2

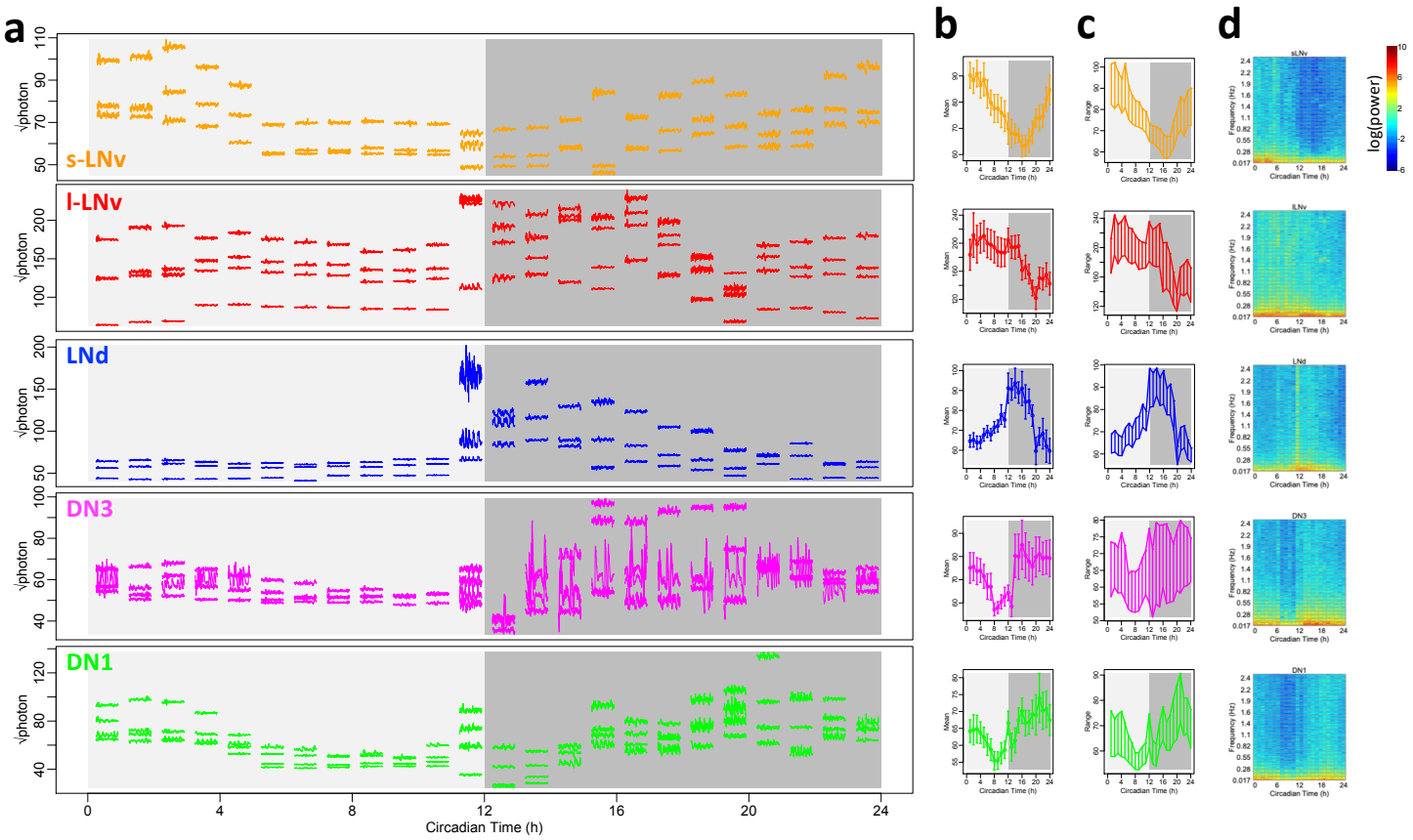


**Figure S2. Daily pattern of fast calcium activity in circadian pacemaker neurons.**
**(a)** Raw calcium activity traces from the representative fly shown in Figure 1a. The intensity of calcium signal was calculated as the square root of photon number collected from individual region of interest (ROI), in order to normalize the effect of shut noise. **(b)** The mean of the photon number square root over the 1-min recording session at each of the 24 timepoints, averaged across all 6 flies studied. Error bars denote SEM. **(c)** Daily patterns of the range of calcium transients based on the square root of photon number collected from individual ROI, over the 1-min recording session at each of the 24 timepoints, averaged across all 6 flies studied. **(d)** Daily pattern of the power spectrum based on the square root of photon number collected from individual ROI, over the 1-min recording session at each of 24 timepoints, averaged across all 6 flies studied.

Figure S3

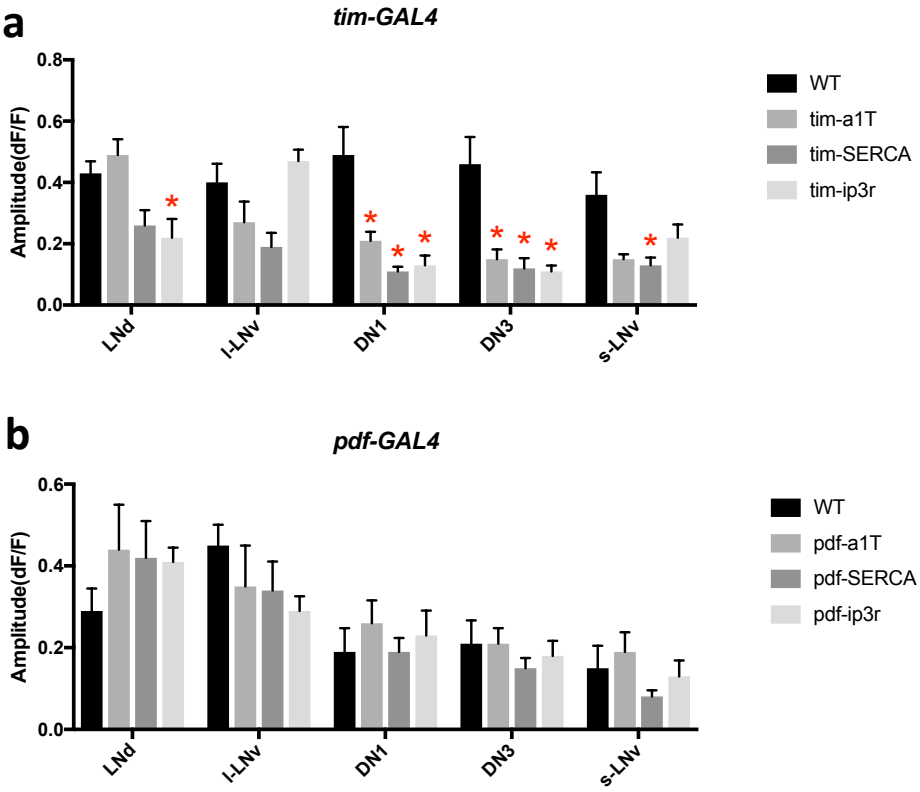


**Figure S3. Amplitude of daily calcium peaks in calcium-channel-knockdown flies.**
**(a)** The averaged amplitude of daily calcium peaks of five pacemaker groups in flies measured in Figure 2d, 2f, 2h, and 2j, with calcium channels knockdown by *tim-GAL4* (two-way ANOVA followed by Dunnett's multiple comparisons test, *P < 0.05). **(b)** The averaged amplitude of daily calcium peaks of five pacemaker groups in flies measured in Figure 2c, 2e, 2g, and 2i, with calcium channels knockdown by *pdf-GAL4*.

Figure S4

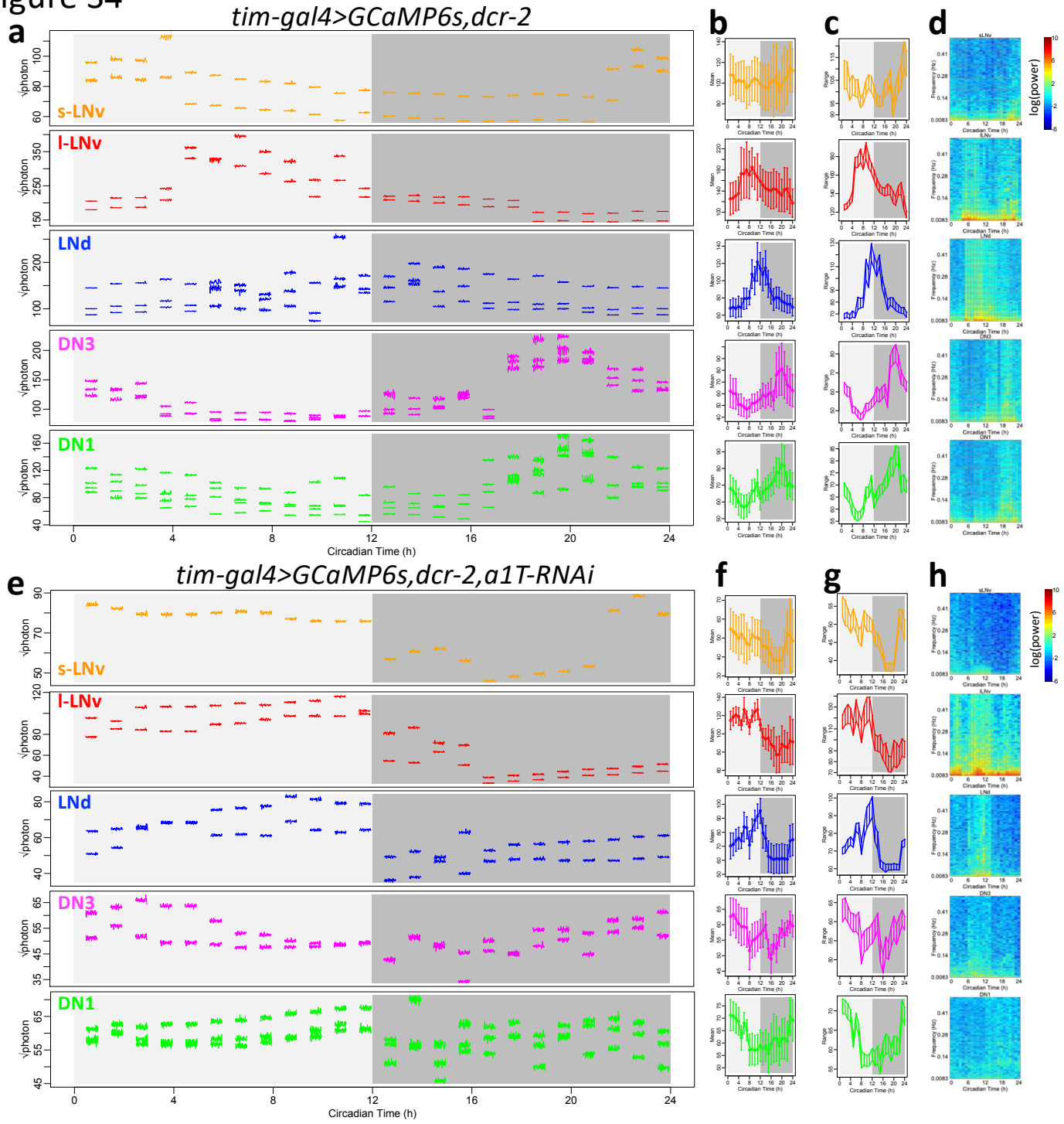
a
tim-gal4>GCaMP6s,dcr-2
s-LNv
l-LNv
LNd
DN3
DN1
√photon
Circadian Time (h)
b
c
d
log(power)
e
tim-gal4>GCaMP6s,dcr-2,a1T-RNAi
f
g
h

**Figure S4. *α1T* knockdown reduces fast calcium fluctuations.**
**(a-d)** As Figure S2a-d, (a) raw calcium activity traces from the representative fly shown in Figure 4a. The intensity of calcium signal was calculated as the square root of photon number collected from individual region of interest (ROI), in order to normalize the effect of shut noise. Averaged daily patterns of (b) mean calcium intensity, (c) the range of calcium transient, and (d) the power spectrum were calculated based on on the square root of photon number collected from individual ROIs (n = 4 flies). **(e-h)** As in (a-d), raw calcium activity traces from one representative fly shown in Figure 4e with *α1T* knockdown in all pacemaker neurons and averaged daily patterns of mean, range, and power spectrum in this genotype calculated based on on the square root of photon number collected from individual ROIs (n = 4 flies).

Figure S5

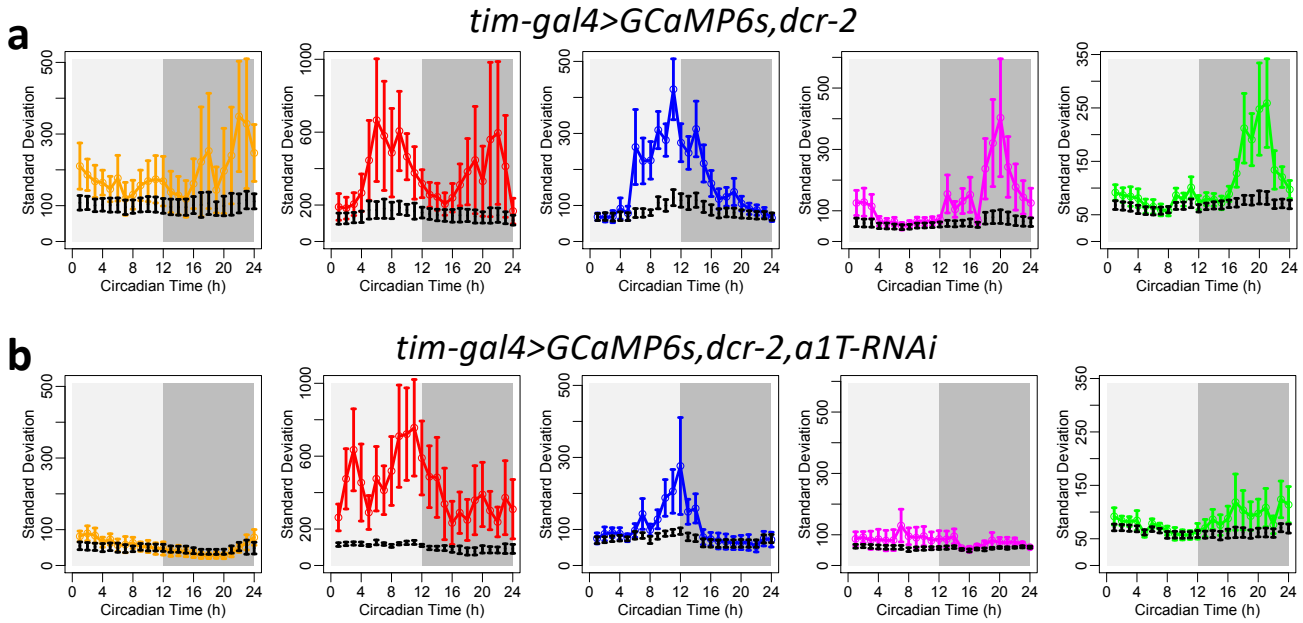


**Figure S5. Fast calcium fluctuations of *a1T* knockdown are below the range of shut noise.**
**(a)** Comparison of standard deviations between calcium activity and shut noise in wild type flies. Color lines, daily pattern of the standard deviations of calcium intensity (calculated as the collected photon number from individual ROIs) over the 1-min recording session at each of the 24 timepoints, averaged across all wide-type 4 flies studied in Figure 4a-d. Error bars denote SEM. For each timepoint, black error bars were the standard deviations of shut noise estimated by the square root of photon number collected from individual ROIs. At those time of day when mean calcium signal was high (shown in Figure 4b), the standard deviations of calcium signal were significantly higher than the standard deviations generated by shut noise, suggesting that the calcium fluctuation was generated by physiologically-relevant events.
**(b)** Comparison of standard deviations between calcium activity and shut noise in flies shown in Figure 4e-h with *a1T* knockdown. Except for LNd and l-LNv, the standard deviations of calcium signal were not significantly different from the standard deviations generated by shut noise at any time of day.

Figure S6

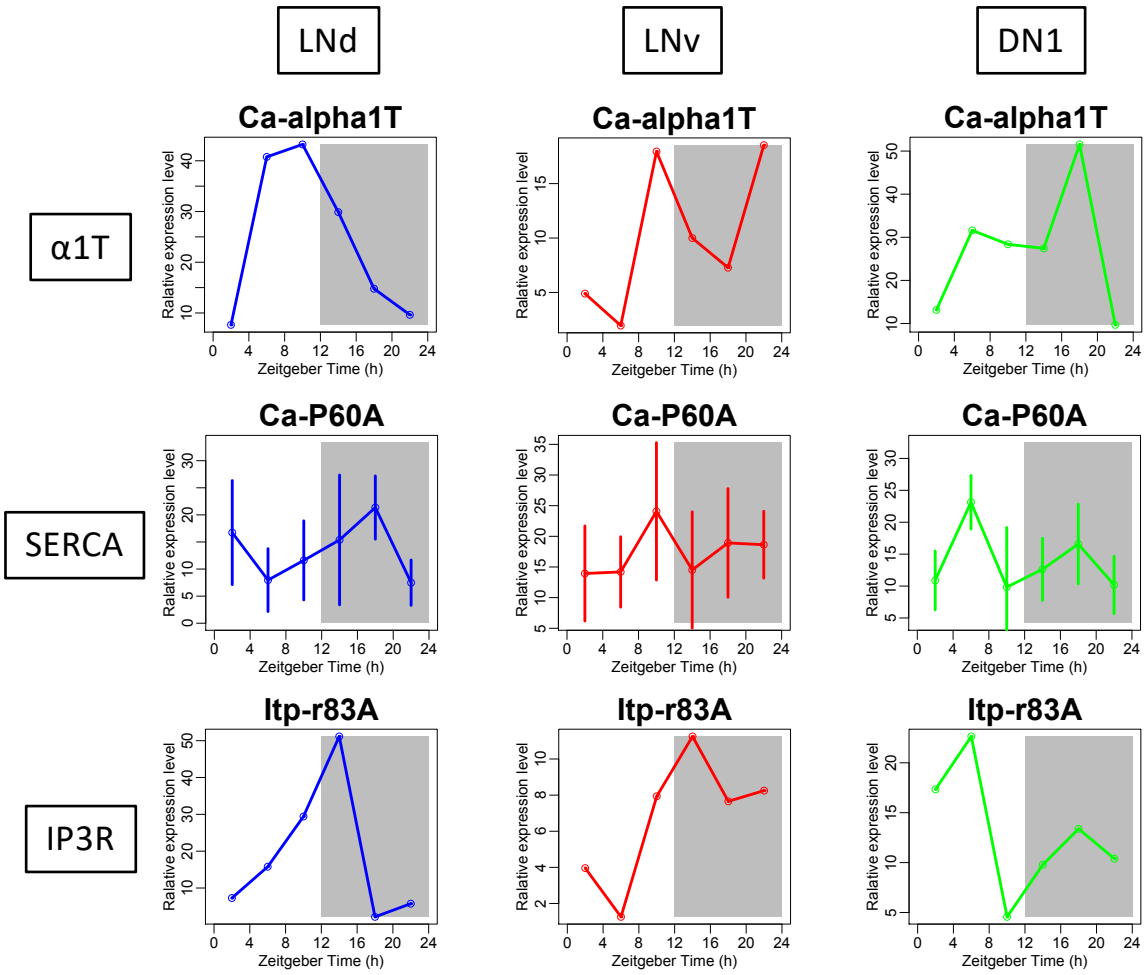


**Figure S6. Daily rhythms in expression level of different calcium channels.**
The daily expression pattern of *α1T*, *SERCA,* and *ip3r* in three different pacemaker groups LNd, PDF-positive LNv neurons, and DN1. Data is obtained from Abruzzi et al 2017, in which each pacemaker group was sorted and analyzed by RNA sequencing for two continuous days with 4-hour intervals.

# Chapter 7

# Conclusions and Future Directions

My thesis begins to bridge the gaps between genes and neural circuits, and the gaps between neural circuits and behaviors in the *Drosophila* circadian system. I ask two major questions: how molecular circadian clocks control the outputs of circadian pacemaker neurons, and how the outputs of circadian pacemaker neurons control rhythms in different downstream biological processes? I found that molecular circadian clocks generate daily neural activity rhythms in circadian pacemaker neurons (Chapter 2). The molecular circadian clocks regulate distinct calcium channels to generate circadian rhythms in both basal calcium level and fast calcium fluctuations (Chapter 6). Although the molecular circadian clocks are synchronized among different groups of circadian neurons, they generate phase-diverse activity rhythms in different neurons (Chapter 2). Groups of circadian neurons inhibit each other via long-duration neuromodulation, mediated by neuropeptides PDF and sNPF, such that their activity phases are properly staggered across the day and night; certain activity phases are also regulated by environmental light inputs (Chapter 3). Together, the circadian pacemaker neural circuit sends out sequential timing information across all phases of the day and night. The broadcast timing signals are then received by different downstream output circuits. Directly or indirectly, the timing signals generate circadian rhythms in spontaneous neural activity throughout the entire brain (Chapter 5). Among the downstream output circuits, I found a key neural pathway for the locomotor activity rhythm, by which M and E pacemakers independently regulate a common

pre-motor center, the ellipsoid body ring neurons (EB-RNs), through the agency of dopaminergic interneurons called PPM3-EB (Chapter 4). Additionally, my findings also suggest that several output circuits, including different groups of dopaminergic neurons and neuroendocrine cells might regulate different behavioral outputs including sleep, olfaction, mating, and feeding rhythms (Chapter 5). Together, my thesis establishes a framework for circadian clock genes to generate daily rhythms in diverse biological processes; circadian clock genes generate multi-phasic pacemaker neuronal outputs that propagate through multiple downstream output circuits. In creating this framework, my work helps formulate a new set of questions with which the field can better understand pacemaker circuit operations and downstream circadian timing.

**From genes to neural circuits**

In Chapter 3, I showed that neuropeptides PDF and sNPF can suppress and delay neural activity peaks in several groups of circadian pacemaker neurons. Three major questions remain unexplored. First, how can the regulation of PDF and sNPF last for such a long time, to delay the activity peak by up to 17 hours? One possibility is that the M and E cells release PDF and/or sNPF for a long time to continuously suppress the neural activity of other pacemaker neurons. PDF levels show circadian rhythms in M-cell terminals (Park *et al.* 2000) and so does the PDFR sensitivity (Klose *et al.* 2016). However, there is no direct observation showing the daily pattern of PDF release. Because PDFR is a G-protein coupled receptor (GPCR) that causes the elevation of cAMP in the cells, using a cAMP reporter *Epac1-camps* (Shafer *et al.* 2016), 24-hr *in vivo* imaging might reveal the daily pattern of PDFR signaling in different circadian pacemaker neurons. However, as a key second massager, cAMP is the convergent point for input from many different GPCRs. PDF/PDFR signaling cannot be disambiguated from other GPCRs that change

global cAMP levels. Alternatively, it will be helpful to directly visualize PDF release or PDFR activation. To visualize PDF release, one way is to fuse PDF peptide with the pH-sensitive green fluorescent protein pHluorin (Miesenböck *et al.* 1998). When the reporters are released from acidic secretory vesicles into the neutral extracellular environment, the excitation spectrum of pHluorin changes. Expressing the PDF-pHluorin in PDF neurons might help to visualize the daily pattern of PDF release. Complementally, PDFR activation might be visualized by developing a genetically encoded GPCR activation-based sensors (Sun *et al.* 2018), which couples a conformationally sensitive circular-permutated GFP to the PDFR. Although it might not be compatible with PDFR (discussed below), TANGO assay might also be used to measure daily pattern of sNPF-R activity (Barnea *et al.* 2008). TANGO assay combines a GPCR fused with a transcription factor (tTA) and a β-arrestin fused with a TEV protease; when the GPCR is activated, it recruits the β-arrestin and the fused TEV protease releases tTA to activate the expression of a reporter gene. The mechanism of the long-term effect of PDF and sNPF could also be on the post-synaptic side. The signaling pathways downstream of GPCRs might switch the neural activity states. The signaling pathways of PDFR have been studied but not yet fully understood (Seluzicki *et al.* 2014, Duvall and Taghert 2012). Efforts on screening for downstream molecules that are regulated by PDFR signaling will provide the starting points for this question.

Second, how can PDF from the same PDF neuron groups delay activity phases in different neurons by different time, ~10 hours for LNd vs. ~17 hours for DN3? In LNd and DN3, signaling pathways downstream of PDFR could be different, as PDFR is coupled with different subtypes of adenylate cyclase in M and E pacemakers (Duvall and Taghert 2013). In addition, the circadian remodeling of M cells (s-LNv) projections suggests that M cells may change

synaptic contacts with LNd and with DN3 across the day (Fernández *et al.* 2008, Gorostiza *et al.* 2014). Recently developed anterograde transsynaptic circuit tracing techniques *trans*-Tango (Talay *et al.* 2017) and TRACT (Huang *et al.* 2017) can be adopted to visualize daily synaptic connectivity changes by using a short lifetime reporter.

Third, how is the mid-day phase of l-LNv activity determined? I established major inputs that dictate the activity phases of three of the four non-morning pacemaker groups, the LNd, the DN3, and the DN1. However, the l-LNv calcium activity phase was not affected in loss-of-function genetic manipulations for neuropeptides including PDF, sNPF, NPF, ITP, and NPLP1. They were altered by manipulations for DH31 and the DH31-R1, but only moderately, which suggests that other factor(s) regulate daily l-LNv calcium activity and remain to be identified. Unlike other pacemaker groups, l-LNv PER rhythms are lost under constant conditions, suggesting they behave more like hour glasses, than durable oscillators (Lin *et al.* 2004). l-LNv calcium phase could be determined by the intrinsic property of l-LNv cells, in which the mechanism for transforming molecular circadian clocks into neural activity rhythms is different from other pacemaker neurons. This possibility is supported by the observation in Chapter 6 that α1T-knockdown caused an opposite effect on l-LNv compared to other pacemaker groups. Alternatively, l-LNv calcium phase could be set by classical small molecule neurotransmitters released from other pacemaker neurons, as l-LNv activity is inhibited by GABA (Parisky *et al.* 2008, Chung *et al.* 2009), or by an as yet unidentified neuropeptide within the pacemaker system. l-LNv activity could also be determined by some factors from outside the central pacemaker network, such as inputs from visual systems or perhaps by regulation from glia.

In Chapter 6, using an extensive, but still incomplete RNAi screen for calcium channels, I found that IP3R channels appear to generate rhythms in basal calcium level and that T-type

calcium channels appear to generate rhythms in fast calcium fluctuations. However, the relationship between these two channels, and thus the relationship between these two calcium processes, are unknown. These two processes can be distinct as was shown in mammalian astrocytes (Srinivasan *et al.* 2015). I showed that α1T-knockdown impaired rhythms in fast calcium fluctuations without affecting rhythms in basal calcium level. However, I did not have the opportunity to also ask the opposite question: whether pacemaker neurons still show rhythms in the fast calcium activity following *ip3r*-knockdown. Other ion channels, including the sodium channel *Na (narrow abdomen)*(Lear *et al.* 2005, Flourakis *et al.* 2015), the calcium activated potassium channel *slo (slowpoke)* (Jaramillo *et al.* 2004), and the potassium channel *Ir* (Ruben *et al.* 2012) have also been implicated in the regulation of neural activity rhythms in some of *Drosophila* circadian pacemaker neurons. How these different ion channels interact with the calcium channels in the regulation of circadian pacemaker neural activity is also unclear.

**From neural circuits to behaviors**

In Chapter 4, I found that M and E pacemakers independently regulate a common pre-motor center, the ellipsoid body ring neurons (EB-RNs), through the agency of dopaminergic interneurons called PPM3-EB. Although a recent study suggested the anatomical and functional connection between M cells and PPM3 neurons (Potdar and Sheeba 2018), the connection from E cells to PPM3 neurons is still unknown. To study the connection from M and E cells to PPM3-EB, the anterograde transsynaptic circuit tracing techniques *trans*-Tango (Talay *et al.* 2017) and TRACT (Huang *et al.* 2017) can be used to identify neurons to which M and E cells project. From the recently available electron microscopy volume of the fly brain, and from improvements in the EM reconstruction and automatic connectome mapping techniques (Zheng *et al.* 2018), the

connectivity from M and E cells could also be tracked down. However, both M and E cells release multiple neuropeptides besides classical small molecule neurotransmitters. These neuropeptides are important intra-pacemaker network signals that diversify neural activity phases in different pacemaker groups as described in Chapter 2 & 3. These neuropeptides may also be used to signal the downstream non-clock neurons. Neuropeptides might diffuse certain distance and act at variable spatial ranges, even extrasynaptically far from the release site (Jan and Jan 1982). Therefore, synaptic contacts might not be required for the outputs of M and E cells to regulate downstream neurons. The TANGO assay fuses a neuropeptide-GPCR with the transcription factor (tTA) then can be used to characterize what downstream cells are activated by certain types of neuropeptides (Barnea *et al.* 2008). The TANGO assay may require modification for profiling of the spatial pattern of PDFR activation, because the activation of tTA requires the GPCR to recruit β-arrestin (discussed above) but PDFR recruits β-arrestin very poorly, compared to every other *Drosophila* GPCR so far tested (Johnson *et al.* 2003; Klose *et al.* 2016). Such modification could be to fuse the *trans*-Tango ligand glucagon with the PDF peptide, which could activate the glucagon receptor of *trans*-Tango postsynaptic reporter system (Talay *et al.* 2017).

In Chapter 5, I suggested that circadian neural activity rhythms in different groups of dopaminergic neurons and neuroendocrine cells might regulate different behavior outputs. For each of the candidate output circuits, functional evidence that the specific circuit regulates the specific behavioral rhythm is critical. For instance, the *fruitless*-positive PAL neurons have been showed to regulate the mating drive of male flies (Zhang *et al.* 2016). Based on the superficial similarity between the daily neural activity pattern of the PAL neurons and the daily mating behavioral rhythms, it raises that possibility that PAL neurons might mediate the circadian

regulation to mating behavior. However, direct evidence to show that neural activity rhythms in PAL neurons are necessary and sufficient for the circadian mating rhythms remains to be established. Similarly, several neuron groups, including the PPL1-dFSB dopaminergic neurons, dILP2, and SIFa neurons, have been implicated in sleep/wake regulation. The PPL1-dFSB and dILP2 neurons suppress sleep. Their neural activity peaks around dawn and dusk respectively, patterns that suggest they may be responsible for the suppression of sleep during the two daily active episodes. SIFa neurons promote sleep and are active around mid-day, which might be responsible for the daytime sleep and the mid-day activity siesta. However, many other neuron groups, including different subclasses of mushroom body Kenyon cells, the dFSB neurons, and a subset of EB-RNs, have been shown to regulate sleep. It will be interesting to characterize the daily neural activity patterns of these sleep-regulated neurons, and important to study the hierarchical relationship between all these sleep-relevant neurons. Furthermore, other neuromodulatory systems: octompaminergic (OA) neurons, serotonergic (5-HT) neurons, cholinergic (ACh) neurons, and other neuropeptidergic neurons like NPF, sNPF, Allatostatin, Tachykinin (and others), are possibly also regulated by circadian pacemaker signaling and be responsible for rhythms in other physiological functions and behaviors. Brain-wide imaging strategies will permit researchers to address these challenging issues.

In Chapter 5, I employed the whole-brain pan-neuronal imaging to estimate how widespread the circadian rhythms of neural activity are in the *Drosophila* brain. To learn more from whole-brain pan-neuronal imaging, the future directions of this analysis are to achieve single-cell resolution and to register individual recorded brains to a template brain, the fly brain atlas using Computational Morphometry Toolkit (CMTK) algorithms. After registering each experiment to the template, the daily activity-phase patterns then could be compared across

different genotypes. Comparison among genotypes in which the oscillators in each of circadian pacemaker groups are selectively accelerated (by expressing SGG with group-specific split-GAL4 lines) should reveal how different pacemaker groups dictate activity rhythms in different brain regions. Combined with anterograde trans-synaptic tracing from each of pacemaker groups, these experiments may reveal how the circadian pacemaker circuit generates brain-wide circadian rhythms in spontaneous neural activity, with region-specific (likely circuit-specific) phases.

Circadian neural activity rhythms of non-clock neurons could be simply imposed by circadian neural activity rhythms of pacemaker neurons via direct excitation or inhibition. Other mechanisms might be involved as well. Pacemaker outputs may switch activity states of certain downstream neurons or neuronal networks via neuropeptide-mediated modulation. Similar to the long-term effect of PDF and sNPF on pacemaker neural activity, through downstream signaling pathways, neuropeptides could cause changes in gene expression, neuronal excitability, synaptic strength, and connectivity pattern. Furthermore, outputs of circadian pacemaker neurons can also regulate the circadian clocks in peripheral tissues (Mohawk *et al.* 2012). In *Drosophila* several peripheral tissues have been shown to have circadian rhythms in gene expression. These peripheral circadian rhythms can be regulated directly or indirectly by the brain pacemaker outputs, such as in the prothoracic gland (Morioka *et al.* 2012, Iga *et al.* 2014, Selcho *et al.* 2017), in the oenocytes (Krupp *et al.* 2013), and in the fat body (Xu *et al.* 2011, Barber *et al.* 2016, Erion *et al.* 2016). It would be of interest to measure daily rhythms of cellular properties including calcium activity in peripheral tissues and study how such rhythms regulate circadian rhythms in physiological functions and behaviors.

# References:


Abruzzi, K.C., Zadina, A., Luo, W., Wiyanto, E., Rahman, R., Guo, F., Shafer, O., and Rosbash, M. (2017). RNA-seq analysis of Drosophila clock and non-clock neurons reveals neuron-specific cycling and novel candidate neuropeptides. PLOS Genet. 13, e1006613.

Agrawal, N., Venkiteswaran, G., Sadaf, S., Padmanabhan, N., Banerjee, S., & Hasan, G. (2010). Inositol 1, 4, 5-trisphosphate receptor and dSTIM function in Drosophila insulin-producing neurons regulates systemic intracellular calcium homeostasis and flight. Journal of Neuroscience, 30(4), 1301-1313.

Akten, B., Jauch, E., Genova, G. K., Kim, E. Y., Edery, I., Raabe, T., & Jackson, F. R. (2003). A role for CK2 in the Drosophila circadian oscillator. Nature neuroscience, 6(3), 251.

Allada, R., & Chung, B. Y. (2010). Circadian organization of behavior and physiology in Drosophila. Annual review of physiology, 72, 605-624.

An, S., Harang, R., Meeker, K., Granados-Fuentes, D., Tsai, C. a, Mazuski, C., Kim, J., Doyle, F.J., Petzold, L.R., and Herzog, E.D. (2013). A neuropeptide speeds circadian entrainment by reducing intercellular synchrony. Proc. Natl. Acad. Sci. U. S. A. 110, E4355-61.

Andretic R, van Swinderen B, Greenspan RJ. (2005) Dopaminergic modulation of arousal in Drosophila. Curr Biol. 15:1165–1175.

Ashmore, L.J., and Sehgal, A. (2003). A Fly's Eye View of Circadian Entrainment. J. Biol. Rhythms 18, 206–216.

Aton, S.J., and Herzog, E.D. (2005). Come together, right...now: synchronization of rhythms in a mammalian circadian clock. Neuron 48, 531–534.

Aton, S.J., Huettner, J.E., Straume, M., and Herzog, E.D. (2006). GABA and Gi/o differentially control circadian rhythms and synchrony in clock neurons. Proc. Natl. Acad. Sci. U. S. A. 103, 19188–19193.

Bahn, J. H., Lee, G. G., & Park, J. H. (2009). Comparative analysis of Pdf-mediated circadian behaviors between Drosophila melanogaster and Drosophila virilis. Genetics.

Bai, L., Lee, Y., Hsu, C.T., Williams, J.A., Cavanaugh, D., Zheng, X., Stein, C., Haynes, P., Wang, H., Gutmann, D.H., *et al.*. (2018). A Conserved Circadian Function for the Neurofibromatosis 1 Gene. Cell Rep. 22, 3416–3426.

Barber, A. F., Erion, R., Holmes, T. C., & Sehgal, A. (2016). Circadian and feeding cues integrate to drive rhythms of physiology in Drosophila insulin-producing cells. Genes & Development, 30(23), 1–11.

Barnea, G., Strapps, W., Herrada, G., Berman, Y., Ong, J., Kloss, B., ... & Lee, K. J. (2008). The genetic design of signaling cascades to record receptor activation. Proceedings of the National Academy of Sciences, 105(1), 64-69.

Berridge, M.J. (1998). Neuronal calcium signaling. Neuron 21, 13–26.

Berry, J. A., Cervantes-Sandoval, I., Chakraborty, M., & Davis, R. L. (2015). Sleep facilitates memory by blocking dopamine neuron-mediated forgetting. Cell, 161(7), 1656-1667.

Birman S. (2005) Arousal mechanisms: speedy flies don't sleep at night. Curr Biol. 15:R511–513.

Blau, J., and Young, M.W. (1999). Cycling vrille expression is required for a functional Drosophila clock. Cell 99, 661–671.

Brancaccio, Marco, Elizabeth S. Maywood, Johanna E. Chesham, Andrew SI Loudon, and Michael H. Hastings. "A Gq-Ca2+ axis controls circuit-level encoding of circadian time in the suprachiasmatic nucleus." Neuron 78, no. 4 (2013): 714-728.

Cao, G., & Nitabach, M. N. (2008). Circadian control of membrane excitability in Drosophila melanogaster lateral ventral clock neurons. Journal of Neuroscience, 28(25), 6493-6501.

Cao, G., Platisa, J., Pieribone, V. a, Raccuglia, D., Kunst, M., and Nitabach, M.N. (2013). Genetically targeted optical electrophysiology in intact neural circuits. Cell 154, 904–913.

Caussinus, E., Colombelli, J., & Affolter, M. (2008). Tip-cell migration controls stalk-cell intercalation during Drosophila tracheal tube elongation. Current biology, 18(22), 1727-1734.

Cavanaugh, D.J.J., Geratowski, J.D.D., Wooltorton, J.R.A.R.A., Spaethling, J.M.M., Hector, C.E.E., Zheng, X., Johnson, E.C.C., Eberwine, J.H.H., and Sehgal, A. (2014). Identification of a Circadian Output Circuit for Rest:Activity Rhythms in Drosophila. Cell 157: 689–701.

Cavey, M., Collins, B., Bertet, C., & Blau, J. (2016). Circadian rhythms in neuronal activity propagate through output circuits. Nature Neuroscience, 19, 1–11.

Ceriani, M.F., Darlington, T.K., Staknis, D., Más, P., Petti, A.A., Weitz, C.J., and Kay, S.A. (1999). Light-dependent sequestration of TIMELESS by CRYPTOCHROME. Science 285, 553–556.

Chang HY, Grygoruk A, Brooks ES, Ackerson LC, Maidment NT, Bainton RJ, Krantz DE. (2006) Overexpression of the Drosophila vesicular monoamine transporter increases

motor activity and courtship but decreases the behavioral response to cocaine. Mol. Psychiatry. 11:99–113.

Chatterjee, A., Lamaze, A., De, J., Mena, W., Chélot, E., Martin, B., ... & Rouyer, F. (2018). Reconfiguration of a Multi-oscillator Network by Light in the Drosophila Circadian Clock. Current Biology.

Chen, J., Reiher, W., Hermann-Luibl, C., Sellami, A., Cognigni, P., Kondo, S., Helfrich-Förster, C., Veenstra, J.A., and Wegener, C. (2016). Allatostatin A Signalling in Drosophila Regulates Feeding and Sleep and Is Modulated by PDF. PLOS Genet. 12, e1006346.

Chen, T.-W., Wardill, T.J., Sun, Y., Pulver, S.R., Renninger, S.L., Baohan, A., Schreiter, E.R., Kerr, R. a, Orger, M.B., Jayaraman, V., *et al.* (2013). Ultrasensitive fluorescent proteins for imaging neuronal activity. Nature 499, 295–300.

Choi, C., Cao, G., Tanenhaus, A.K., McCarthy, E. v., Jung, M., Schleyer, W., Shang, Y., Rosbash, M., Yin, J.C.P., and Nitabach, M.N. (2012). Autoreceptor Control of Peptide/Neurotransmitter Corelease from PDF Neurons Determines Allocation of Circadian Activity in Drosophila. Cell Rep. 2, 332–344.

Chorna, T., and Hasan, G. (2012). The genetics of calcium signaling in Drosophila melanogaster. Biochim. Biophys. Acta - Gen. Subj. 1820, 1269–1282.

Collins, B., Kane, E. a, Reeves, D.C., Akabas, M.H., and Blau, J. (2012). Balance of activity between LN(v)s and glutamatergic dorsal clock neurons promotes robust circadian rhythms in Drosophila. Neuron 74, 706–718.

Collins, B., Kaplan, H.S., Cavey, M., Lelito, K.R., Bahle, A.H., Zhu, Z., Macara, A.M., Roman, G., Shafer, O.T., and Blau, J. (2014). Differentially Timed Extracellular Signals Synchronize Pacemaker Neuron Clocks. PLoS Biol. 12, e1001959.

Colwell, C.S. (2000). Circadian modulation of calcium levels in cells in the suprachiasmatic nucleus. Eur. J. Neurosci. 12, 571–576.

Colwell, C.S. (2011). Linking neural activity and molecular oscillations in the SCN. Nat. Rev. Neurosci. 12, 553–569.

Coomans, C.P., Ramkisoensing, A., and Meijer, J.H. (2015). The suprachiasmatic nuclei as a seasonal clock. Front. Neuroendocrinol. 37, 29–42.

Crocker, A., Shahidullah, M., Levitan, I. B., & Sehgal, A. (2010). Identification of a neural circuit that underlies the effects of octopamine on sleep: wake behavior. Neuron, 65(5), 670-681.

Cusumano, P., Klarsfeld, A., Chélot, E., Picot, M., Richier, B., and Rouyer, F. (2009). PDF-modulated visual inputs and cryptochrome define diurnal behavior in Drosophila. Nat. Neurosci. 12, 1431–1437.

Dana, H., Mohar, B., Sun, Y., Narayan, S., Gordus, A., Hasseman, J. P., ... & Patel, R. (2016). Sensitive red protein calcium indicators for imaging neural activity. Elife, 5: e12727.

De La Iglesia HO, Meyer J, and Schwartz WJ (2003) Lateralization of circadian pacemaker output: activation of left- and right-sided luteinizing hormone-releasing hormone neurons involves a neural rather than a humoral pathway. J Neurosci 23:7412-7414.

Depetris-Chauvin, A., Berni, J., Aranovich, E.J., Muraro, N.I., Beckwith, E.J., and Ceriani, M.F. (2011). Adult-specific electrical silencing of pacemaker neurons uncouples molecular clock from circadian outputs. Curr. Biol. 21, 1783–1793.

Diaz, M. M., Schlichting, M., Abruzzi, K., & Rosbash, M. (2018). Allatostatin C/AstC-R2 is a Novel Pathway to Modulate Circadian Activity Pattern in Drosophila. bioRxiv, 361048.

Dissel, S., Hansen, C.N., Özkaya, Ö., Hemsley, M., Kyriacou, C.P., and Rosato, E. (2014). The Logic of Circadian Organization in Drosophila. Curr. Biol. 2257–2266.

Dolezelova, E., Dolezel, D., and Hall, J.C. (2007). Rhythm defects caused by newly engineered null mutations in Drosophila's cryptochrome gene. Genetics 177, 329–345.

Donlea, J. M., Thimgan, M. S., Suzuki, Y., Gottschalk, L., & Shaw, P. J. (2011). Inducing sleep by remote control facilitates memory consolidation in Drosophila. Science, 332(6037), 1571-1576.

Donlea, J.M., Pimentel, D., Talbot, C.B., Kempf, A., Omoto, J.J., Hartenstein, V., and Miesenböck, G. (2018). Recurrent Circuitry for Balancing Sleep Need and Sleep. Neuron. 97: 378-389

Dunlap, J. (1999). Molecular bases for circadian clocks. Cell, 96, 271–290.

Duvall, L.B., and Taghert, P.H. (2012). The circadian neuropeptide PDF signals preferentially through a specific adenylate cyclase isoform AC3 in M pacemakers of Drosophila. PLoS Biol. 10, e1001337.

Duvall, L.B., and Taghert, P.H. (2013). E and M circadian pacemaker neurons use different PDF receptor signalosome components in drosophila. J. Biol. Rhythms 28, 239–248.

Emery, P., So, W. V, Kaneko, M., Hall, J.C., and Rosbash, M. (1998). CRY, a Drosophila clock and light-regulated cryptochrome, is a major contributor to circadian rhythm resetting and photosensitivity. Cell 95, 669–679.

Emery, P., Stanewsky, R., Helfrich-Förster, C., Emery-Le, M., Hall, J.C., and Rosbash, M. (2000). Drosophila CRY is a deep brain circadian photoreceptor. Neuron 26, 493–504.

Enoki, R., Kuroda, S., Ono, D., Hasan, M.T., Ueda, T., Honma, S., Honma, K., and Sens, H. (2012). Topological specificity and hierarchical network of the circadian calcium rhythm in the suprachiasmatic nucleus. Proc. Natl. Acad. Sci. U. S. A. 109, 21498–21503.

Enoki, R., Oda, Y., Mieda, M., Ono, D., Honma, S., and Honma, K.-I. (2017). Synchronous circadian voltage rhythms with asynchronous calcium rhythms in the suprachiasmatic nucleus. Proc. Natl. Acad. Sci. 114, E2476–E2485.

Erion, R., King, A. N., Wu, G., Hogenesch, J. B., & Sehgal, A. (2016). Neural clocks and Neuropeptide F/Y regulate circadian gene expression in a peripheral metabolic tissue. Elife, 5, e13552.

Evans, J. A., Leise, T. L., Castanon-Cervantes, O., & Davidson, A. J. (2013). Dynamic interactions mediated by nonredundant signaling mechanisms couple circadian clock neurons. Neuron, 80(4), 973-983.

Feinberg, E.H., *et al.* GFP Reconstitution Across Synaptic Partners (GRASP) defines cell contacts and synapses in living nervous systems. Neuron, 2008. 57(3): p. 353-63.

Feng, G., Reale, V., Chatwin, H., Kennedy, K., Venard, R., Ericsson, C., Yu, K., Evans, P.D., and Hall, L.M. (2003). Functional characterization of a neuropeptide F-like receptor from Drosophila melanogaster. Eur. J. Neurosci. 18, 227–238.

Fiala, A., & Spall, T. (2003). In vivo calcium imaging of brain activity in Drosophila by transgenic cameleon expression. Science Signaling, 2003(174), pl6-pl6.

Fifel, K., Meijer, J. H., & Deboer, T. (2018). Circadian and Homeostatic Modulation of Multi-Unit Activity in Midbrain Dopaminergic Structures. Scientific reports 8: 7765.

Flourakis, M., Kula-Eversole, E., Hutchison, A.L.L., Han, T.H.H., Aranda, K., Moose, D.L.L., White, K.P.P., Dinner, A.R.R., Lear, B.C.C., Ren, D., *et al.* (2015). A Conserved Bicycle Model for Circadian Clock Control of Membrane Excitability. Cell 162, 836–848.

Fogle, K.J., Parson, K.G., Dahm, N. a, and Holmes, T.C. (2011). CRYPTOCHROME is a blue-light sensor that regulates neuronal firing rate. Science 331, 1409–1413.

Freeman Jr, G. M., Krock, R. M., Aton, S. J., Thaben, P., & Herzog, E. D. (2013). GABA networks destabilize genetic oscillations in the circadian pacemaker. Neuron, 78(5), 799-806.

Friggi-Grelin, F., Coulom, H., Meller, M., Gomez, D., Hirsh, J., & Birman, S. (2003). Targeted gene expression in Drosophila dopaminergic cells using regulatory sequences from tyrosine hydroxylase. Journal of Neurobiology, 54(4), 618–627.

Froy, O., Gotter, A. L., Casselman, A. L., & Reppert, S. M. (2003). Illuminating the circadian clock in monarch butterfly migration. Science, 300: 1303-1305.

Fujii, S., Krishnan, P., Hardin, P., & Amrein, H. (2007). Nocturnal Male Sex Drive in Drosophila. Current Biology, 17(3), 244–251.

Fujiwara, Y., Hermann-Luibl, C., Katsura, M., Sekiguchi, M., Ida, T., Helfrich-Förster, C., & Yoshii, T. (2018). The CCHamide1 neuropeptide expressed in the anterior dorsal neuron 1 conveys a circadian signal to the ventral lateral neurons in Drosophila melanogaster. Frontiers in physiology, 9, 1276.

Grima, B., Chélot, E., Xia, R., and Rouyer, F. (2004). Morning and evening peaks of activity rely on different clock neurons of the Drosophila brain. Nature 431, 869–873.

Guo, F., Cerullo, I., Chen, X., and Rosbash, M. (2014). PDF neuron firing phase-shifts key circadian activity neurons in Drosophila. Elife e02780.

Guo, F., Holla, M., Díaz, M. M., & Rosbash, M. (2018). A Circadian Output Circuit Controls Sleep-Wake Arousal in Drosophila. Neuron.

Guo, F., Yu, J., Jung, H. J., Abruzzi, K. C., Luo, W., Griffith, L. C., & Rosbash, M. (2016). Circadian neuron feedback controls the Drosophila sleep–activity profile. Nature, 536(7616), 292.

Hall, J.C. (2003). Genetics and molecular biology of rhythms in Drosophila and other insects. Adv. Genet. 48, 1–280.

Hamasaka, Y., Rieger, D., Parmentier, M.-L., Grau, Y., Helfrich-Förster, C., and Nässel, D.R. (2007). Glutamate and its metabotropic receptor in Drosophila clock neuron circuits. J. Comp. Neurol. 505, 32–45.

Hamasaka, Y., Suzuki, T., Hanai, S., & Ishida, N. (2010). Evening circadian oscillator as the primary determinant of rhythmic motivation for Drosophila courtship behavior. Genes to Cells, 15(12), 1240–1248.

Hardin, P. E., Hall, J. C., & Rosbash, M. (1990). Feedback of the Drosophila period gene product on circadian cycling of its messenger RNA levels. Nature, 343(6258), 536.

Harrisingh, M.C., Wu, Y., Lnenicka, G. a, and Nitabach, M.N. (2007). Intracellular Ca2+ regulates free-running circadian clock oscillation in vivo. J. Neurosci. 27, 12489–12499.

Hartigan, J. A. and Hartigan, P. M. (1985). The Dip Test of Unimodality, Journal of the American Statistical Association, 86, 738–746.

Hastings, M.H., Brancaccio, M., and Maywood, E.S. (2014). Circadian pacemaking in cells and circuits of the suprachiasmatic nucleus. J. Neuroendocrinol. 26, 2–10.

Heinze, S., and Reppert, S.M. (2011). Sun Compass Integration of Skylight Cues in Migratory Monarch Butterflies. Neuron 69: 345–358.

Helfrich-Förster C. (2005) Neurobiology of the fruit fly's circadian clock. Genes Brain Behav. 24: 65-76.

Helfrich-Förster, C. (2002). The circadian system of Drosophila melanogaster and its light input pathways. Zoology (Jena). 105, 297–312.

Helfrich-Förster, C. (2003). The neuroarchitecture of the circadian clock in the brain of Drosophila melanogaster. Microsc. Res. Tech. 62, 94–102.

Hermann-Luibl, C. (2014). The Role of the Neuropeptides NPF , sNPF , ITP and PDF in the Circadian Clock of Drosophila melanogaster. Universität Würzburg.

Hermann, C., Yoshii, T., Dusik, V., and Helfrich-Förster, C. (2012). Neuropeptide F immunoreactive clock neurons modify evening locomotor activity and free-running period in Drosophila melanogaster. J. Comp. Neurol. 520, 970–987.

Herzog, E.D. (2007). Neurons and networks in daily rhythms. Nat. Rev. Neurosci. 8, 790–802.

Hewes, R. S., Park, D., Gauthier, S. A., Schaefer, A. M., & Taghert, P. H. (2003). The bHLH protein Dimmed controls neuroendocrine cell differentiation in Drosophila. Development, 130(9).

Hirsh J, Riemensperger T, Coulom H, Iché M, Coupar J, Birman S. (2010) Roles of dopamine in circadian rhythmicity and extreme light sensitivity of circadian entrainment. Curr Biol. 20: 209-14. PMID: 20096587

Hogenesch, J.B., and Herzog, E.D. (2011). Intracellular and intercellular processes determine robustness of the circadian clock. FEBS Lett. 585, 1427–1434.

Holekamp, T.F., Turaga, D., and Holy, T.E. (2008). Fast three-dimensional fluorescence imaging of activity in neural populations by objective-coupled planar illumination microscopy. Neuron 57, 661–672.

Hong, J.H., Jeong, B., Min, C.H., and Lee, K.J. (2012). Circadian waves of cytosolic calcium concentration and long-range network connections in rat suprachiasmatic nucleus. Eur. J. Neurosci. 35, 1417–1425.

Huang, T., Niesman, P., Arasu, D., Lee, D., De La Cruz, A., Callejas, A., Hong, E.J., and Lois, C. (2017). Tracing neuronal circuits in transgenic animals by transneuronal control of transcription (TRACT). Elife 6, e32027.

Hughes, A.T.L., Croft, C.L., Samuels, R.E., Myung, J., Takumi, T., and Piggins, H.D. (2015). Constant light enhances synchrony among circadian clock cells and promotes behavioral rhythms in VPAC2-signaling deficient mice. Sci. Rep. 5, 14044.

Hughes, M. E., Hogenesch, J. B., & Kornacker, K. (2010). JTK_CYCLE: An Efficient Nonparametric Algorithm for Detecting Rhythmic Components in Genome-Scale Data Sets. Journal of Biological Rhythms, 25(5), 372–380.

Hyun, S., Lee, Y., Hong, S.-T., Bang, S., Paik, D., Kang, J., Shin, J., Lee, J., Jeon, K., Hwang, S., *et al.* (2005). Drosophila GPCR Han is a receptor for the circadian clock neuropeptide PDF. Neuron 48, 267–278.

Iga, M., Nakaoka, T., Suzuki, Y., and Kataoka, H. (2014). Pigment dispersing factor regulates ecdysone biosynthesis via Bombyx neuropeptide G protein coupled receptor-B2 in the prothoracic glands of Bombyx mori. PLoS One 9.

Ikeda, M., Sugiyama, T., Wallace, C.S., Gompf, H.S., Yoshioka, T., Miyawaki, A., and Allen, C.N. (2003). Circadian dynamics of cytosolic and nuclear Ca2+ in single suprachiasmatic nucleus neurons. Neuron 38, 253–263.

Im, S.H., and Taghert, P.H. (2010). PDF Receptor Expression Reveals Direct Interactions between Circadian Oscillators in Drosophila. J. Comp. Neurol. 518, 1925–1945.

Im, S.H., Li, W., and Taghert, P.H. (2011). Pdfr and cry signaling converge in a subset of clock neurons to modulate the amplitude and phase of circadian behavior in Drosophila. PLoS One 6.

Inagaki, N., Honma, S., Ono, D., Tanahashi, Y., & Honma, K. I. (2007). Separate oscillating cell groups in mouse suprachiasmatic nucleus couple photoperiodically to the onset and end of daily activity. Proceedings of the National Academy of Sciences, 104(18), 7664-7669.

Itri, J.N., Michel, S., Vansteensel, M.J., Meijer, J.H., and Colwell, C.S. (2005). Fast delayed rectifier potassium current is required for circadian neural activity. Nat. Neurosci. 8, 650–656.

Jan, L. Y., & Jan, Y. N. (1982). Peptidergic transmission in sympathetic ganglia of the frog. The Journal of physiology, 327(1), 219-246.

Jaramillo, A. M., Zheng, X., Zhou, Y., Amado, D. A., Sheldon, A., Sehgal, A., & Levitan, I. B. (2004). Pattern of distribution and cycling of SLOB, Slowpoke channel binding protein, in Drosophila. BMC neuroscience, 5(1), 3.

Johard, H. a D., Yoishii, T., Dircksen, H., Cusumano, P., Rouyer, F., Helfrich-Förster, C., and Nässel, D.R. (2009). Peptidergic clock neurons in Drosophila: Ion transport peptide and short neuropeptide F in subsets of dorsal and ventral lateral neurons. J. Comp. Neurol. 516, 59–73.

Johnson, E. C., Bohn, L. M., Barak, L. S., Birse, R. T., Nässel, D. R., Caron, M. G., & Taghert, P. H. (2003). Identification of Drosophila neuropeptide receptors by G protein-coupled receptors-β-arrestin2 interactions. Journal of Biological Chemistry, 278(52), 52172-52178.

Johnson, E.C., Shafer, O.T., Trigg, J.S., Park, J., Schooley, D.A., Dow, J.A., and Taghert, P.H. (2005). A novel diuretic hormone receptor in Drosophila: evidence for conservation of CGRP signaling. J. Exp. Biol. 208.

Joiner, W.J., Crocker, A., White, B.H., and Sehgal, A. (2006). Sleep in Drosophila is regulated by adult mushroom bodies. Nature 441, 757–760.

Jones, J. R., Simon, T., Lones, L., & Herzog, E. D. (2018). SCN VIP neurons are essential for normal light-mediated resetting of the circadian system. Journal of Neuroscience, 38(37), 7986-7995.

Kalsbeek A, Palm IF, La Fleur SE, Scheer FA, Perreau-Lenz S, Ruiter M, Kreier F, Cailotto C, Buijs RM. (2006) SCN outputs and the hypothalamic balance of life. J Biol Rhythms. 21: 458-469.

Kaneko, M., and Hall, J.C. (2000). Neuroanatomy of cells expressing clock genes in Drosophila: transgenic manipulation of the period and timeless genes to mark the perikarya of circadian pacemaker neurons and their projections. J. Comp. Neurol. 422: 66–94.

Kim, S. M., Su, C.-Y., & Wang, J. W. (2017). Neuromodulation of Innate Behaviors in Drosophila. Annual Review of Neuroscience, 40(1)

King, A.N., Barber, A.F., Smith, A.E., Dreyer, A.P., Sitaraman, D., Nitabach, M.N., Cavanaugh, D.J., and Sehgal, A. (2017). A Peptidergic Circuit Links the Circadian Clock to Locomotor Activity. Curr. Biol.

Klarsfeld, A., Malpel, S., Michard-Vanhée, C., Picot, M., Chélot, E., and Rouyer, F. (2004). Novel Features of Cryptochrome-Mediated Photoreception in the Brain Circadian Clock of Drosophila. J. Neurosci. 24.

Klose, M., Duvall, L.B.B., Li, W., Liang, X., Ren, C., Steinbach, J.H.H., and Taghert, P.H. (2016). Functional PDF Signaling in the Drosophila Circadian Neural Circuit Is Gated by Ral A-Dependent Modulation. Neuron 90: 1–14.

Kloss, B., Price, J. L., Saez, L., Blau, J., Rothenfluh, A., Wesley, C. S., & Young, M. W. (1998). The Drosophila clock gene double-time encodes a protein closely related to human casein kinase Iε. Cell, 94(1), 97-107.

Knight, M.R., Campbell, A.K., Smith, S.M., and Trewavas, A.J. (1991). Transgenic plant aequorin reports the effects of touch and cold-shock and elicitors on cytoplasmic calcium. Nature 352, 524–526.

Koh, K., Zheng, X., & Sehgal, A. (2006). JETLAG resets the Drosophila circadian clock by promoting light-induced degradation of TIMELESS. Science, 312(5781), 1809-1812.

Kong, E.C., Woo, K., Li, H., Lebestky, T., Mayer, N., Sniffen, M.R., Heberlein, U., Bainton, R.J., Hirsh, J., and Wolf, F.W. (2010). A pair of dopamine neurons target the D1-like dopamine receptor dopr in the central complex to promote ethanol-stimulated locomotion in Drosophila. PLoS One 5: e9954.

Konopka, R.J., and Benzer, S. (1971). Clock mutants of Drosophila melanogaster. Proc. Natl. Acad. Sci. U. S. A. 68: 2112–2116.

Krishnan, B., Dryer, S. E., & Hardin, P. E. (1999). Circadian rhythms in olfactory responses of Drosophila melanogaster. Nature, 400(6742), 375–378.

Krupp, J. J., Billeter, J. C., Wong, A., Choi, C., Nitabach, M. N., & Levine, J. D. (2013). Pigment-dispersing factor modulates pheromone production in clock cells that influence mating in Drosophila. Neuron, 79(1), 54-68.

Kudo, T., Loh, D. H., Truong, D., Wu, Y., & Colwell, C. S. (2011). Circadian dysfunction in a mouse model of Parkinson's disease. Experimental neurology, 232: 66-75.

Kume, K., Kume, S., Park, S. K., Hirsh, J., & Jackson, F. R. (2005). Dopamine is a regulator of arousal in the fruit fly. Journal of Neuroscience, 25(32), 7377-7384.

Kunst, M., Hughes, M. E., Raccuglia, D., Felix, M., Li, M., Barnett, G., & Duah, J. (2014). Calcitonin Gene-Related Peptide Neurons Mediate Sleep-Specific Circadian Output in Drosophila. Current Biology, 24(22), 2652–2664.

Lamaze, A., Krätschmer, P., Chen, K. F., Lowe, S., & Jepson, J. E. (2018). A Wake-Promoting Circadian Output Circuit in Drosophila. Current Biology.

Lamba, P., Bilodeau-Wentworth, D., Emery, P., and Zhang, Y. (2014). Morning and evening oscillators cooperate to reset circadian behavior in response to light input. Cell Rep. 7, 601–608.

Landgraf D, Joiner WJ McCarthy MJ, Kiessling S, Barandas R, Young JW, Cermakian N, Welsh DK. (2016) The mood stabilizer valproic acid opposes the effects of dopamine on circadian rhythms. Neuropharmacology. 107: 262-270.

Lear, B.C., Lin, J.-M., Keath, J.R., McGill, J.J., Raman, I.M., and Allada, R. (2005). The ion channel narrow abdomen is critical for neural output of the Drosophila circadian pacemaker. Neuron 48, 965–976.

Lear, B.C., Zhang, L., and Allada, R. (2009). The neuropeptide PDF acts directly on evening pacemaker neurons to regulate multiple features of circadian behavior. PLoS Biol. 7, e1000154.

Lebestky T, Chang JS, Dankert H, Zelnik L, Kim YC, Han KA, Wolf FW, Perona P, Anderson DJ. (2009) Two different forms of arousal in Drosophila are oppositely regulated by the dopamine D1 receptor ortholog DopR via distinct neural circuits. Neuron. 64: 522-536.

Lee, K.S., You, K.H., Choo, J.K., Han, Y.M., and Yu, K. (2004). Drosophila short neuropeptide F regulates food intake and body size. J. Biol. Chem. 279, 50781–50789.

Lehman MN, Silver R, Gladstone WR, Kahn RM, Gibson M, and Bittman EL (1987) Circadian rhythmicity restored by neural transplant. Immunocytochemical characterization of the graft and its integration with the host brain. J Neurosci 7: 1626-1638.

Levine, J., Funes, P., Dowse, H., and Hall, J. (2002). Signal analysis of behavioral and molecular cycles. BMC Neurosci. 25, 1–25.

Li MT, Cao LH, Xiao N, Tang M, Deng B, Yang T, Yoshii T, Luo DG. Hub-organized parallel circuits of central circadian pacemaker neurons for visual photoentrainment in Drosophila. Nat Commun. 2018 Oct 12;9(1):4247.

Li, Y., Guo, F., Shen, J., and Rosbash, M. (2014). PDF and cAMP enhance PER stability in Drosophila clock neurons. Proc. Natl. Acad. Sci. U. S. A. 111, E1284-90.

Liang, X., Holy, T. E., & Taghert, P. H. (2016). Synchronous Drosophila circadian pacemakers display nonsynchronous Ca2+ rhythms in vivo. Science, 351(6276), 976–981.

Liang, X., Holy, T. E., & Taghert, P. H. (2017). A series of suppressive signals within the Drosophila circadian neural circuit generates sequential daily outputs. Neuron, 94(6), 1173-1189.

Lim, C., & Allada, R. (2013). Emerging roles for post-transcriptional regulation in circadian clocks. Nature neuroscience, 16(11), 1544.

Lima, S. Q., & Miesenböck, G. (2005). Remote control of behavior through genetically targeted photostimulation of neurons. Cell, 121(1), 141-152.

Lin, J. M., Kilman, V. L., Keegan, K., Paddock, B., Emery-Le, M., Rosbash, M., & Allada, R. (2002). A role for casein kinase 2α in the Drosophila circadian clock. Nature, 420(6917), 816.

Lin, Y., Stormo, G.D., and Taghert, P.H. (2004). The neuropeptide pigment-dispersing factor coordinates pacemaker interactions in the Drosophila circadian system. J. Neurosci. 24, 7951–7957.

Liu, Q., Liu, S., Kodama, L., Driscoll, M. R., & Wu, M. N. (2012). Two dopaminergic neurons signal to the dorsal fan-shaped body to promote wakefulness in Drosophila. Current Biology, 22(22), 2114–2123.

Liu, Q., Tabuchi, M., Liu, S., Kodama, L., Horiuchi, W., Daniels, J., Chiu, L., Baldoni, D., and Wu, M.N. (2017). Branch-specific plasticity of a bifunctional dopamine circuit encodes protein hunger. Science (80-. ). 356, 534–539.

Liu, S., Liu, Q., Tabuchi, M., & Wu, M. N. (2016). Sleep drive is encoded by neural plastic changes in a dedicated circuit. Cell, 165(6), 1347-1360.

Lucassen, E.A., van Diepen, H.C., Houben, T., Michel, S., Colwell, C.S., and Meijer, J.H. (2012). Role of vasoactive intestinal peptide in seasonal encoding by the suprachiasmatic nucleus clock. Eur. J. Neurosci. 35, 1466–1474.

Luibl, C. (2014). The Role of the Neuropeptides NPF, sNPF, ITP and PDF in the Circadian Clock of Drosophila melanogaster (Doctoral dissertation, Universität Würzburg).

Lundkvist, G.B., Kwak, Y., Davis, E.K., Tei, H., and Block, G.D. (2005). A calcium flux is required for circadian rhythm generation in mammalian pacemaker neurons. J. Neurosci. 25, 7682–7686.

Luo, A. H., & Aston-Jones, G. (2009). Circuit projection from suprachiasmatic nucleus to ventral tegmental area: a novel circadian output pathway. European Journal of Neuroscience, 29: 748-760.

Mabuchi, I., Shimada, N., Sato, S., Ienaga, K., Inami, S., and Sakai, T. (2016). Mushroom body signaling is required for locomotor activity rhythms in Drosophila. Neurosci. Res. 111, 1–9.

Mao, Z., & Davis, R. L. (2009). Eight different types of dopaminergic neurons innervate the Drosophila mushroom body neuropil: anatomical and physiological heterogeneity. Frontiers in neural circuits, 3, 5.

Martín-Peña, A., Acebes, A., Rodríguez, J.R., Chevalier, V., Casas-Tinto, S., Triphan, T., Strauss, R., and Ferrús, A. (2014). Cell types and coincident synapses in the ellipsoid body of Drosophila. Eur. J. Neurosci. 39: 1586–1601.

Martinek, S., Inonog, S., Manoukian, A. S., & Young, M. W. (2001). A role for the segment polarity gene shaggy/GSK-3 in the Drosophila circadian clock. Cell, 105(6), 769-779.

Meijer, J.H., and Schwartz, W.J. (2003). In search of the pathways for light-induced pacemaker resetting in the suprachiasmatic nucleus. J. Biol. Rhythms 18, 235–249.

Meijer, J.H., Michel, S., Vanderleest, H.T., and Rohling, J.H.T. (2010). Daily and seasonal adaptation of the circadian clock requires plasticity of the SCN neuronal network. Eur. J. Neurosci. 32, 2143–2151.

Menegazzi, P., Vanin, S., Yoshii, T., Rieger, D., Hermann, C., Dusik, V., Kyriacou, C.P., Helfrich-Förster, C., and Costa, R. (2013). Drosophila clock neurons under natural conditions. J. Biol. Rhythms 28, 3–14.

Meredith, A.L., Wiler, S.W., Miller, B.H., Takahashi, J.S., Fodor, A. a, Ruby, N.F., and Aldrich, R.W. (2006). BK calcium-activated potassium channels regulate circadian behavioral rhythms and pacemaker output. Nat. Neurosci. 9, 1041–1049.

Mertens, I., Vandingenen, A., Johnson, E.C., Shafer, O.T., Li, W., Trigg, J.S., De Loof, A., Schoofs, L., and Taghert, P.H. (2005). PDF receptor signaling in Drosophila contributes to both circadian and geotactic behaviors. Neuron 48, 213–219.

Miesenböck, G., De Angelis, D. A., & Rothman, J. E. (1998). Visualizing secretion and synaptic transmission with pH-sensitive green fluorescent proteins. Nature, 394(6689), 192.

Miyawaki, A., Griesbeck, O., Heim, R., & Tsien, R. Y. (1999). Dynamic and quantitative Ca2+ measurements using improved cameleons. Proceedings of the National Academy of Sciences, 96(5), 2135-2140.

Mohawk, J. a, Green, C.B., and Takahashi, J.S. (2012). Central and peripheral circadian clocks in mammals. Annu. Rev. Neurosci. 35, 445–462.

Moore RY, Klein DC. (1974) Visual pathways and the central neural control of a circadian rhythm in pineal serotonin N-acetyltransferase activity. Brain Res. 71:17-33.

Morioka, E., Matsumoto, A., and Ikeda, M. (2012). Neuronal influence on peripheral circadian oscillators in pupal Drosophila prothoracic glands. Nat. Commun. 3, 909.

Nässel, D.R. (2018). Substrates for Neuronal Cotransmission With Neuropeptides and Small Molecule Neurotransmitters in Drosophila. Front. Cell. Neurosci. 12, 1–26.

Neuser, K., Triphan, T., Mronz, M., Poeck, B., & Strauss, R. (2008). Analysis of a spatial orientation memory in Drosophila. Nature 453: 1244.

Ni, J.D.; Baik, L.S.; Holmes, T.C., Montell, C. (2017). A rhodopsin in the brain functions in circadian photoentrainment in Drosophila. Nature 545, 340–344.

Nitabach, M. N., & Taghert, P. H. (2008). Organization of the Drosophila circadian control circuit. Current Biology, 18(2), R84-93.

Noguchi, T., Leise, T.L., Kingsbury, N., Diemer, T., Wang, L.L., Henson, M.A., and Welsh, D.K. (2017). Calcium Circadian Rhythmicity in the Suprachiasmatic Nucleus: Cell Autonomy and Network Modulation. Eneuro ENEURO.0160-17.2017.

Ofstad, T. A., Zuker, C. S., and Reiser, M. B. (2011). Visual place learning in Drosophila melanogaster. Nature, 474, 204.

Omoto, J.J., Keleş, M.F., Nguyen, B.C.M., Bolanos, C., Lovick, J.K., Frye, M.A., and Hartenstein, V. (2017). Visual Input to the Drosophila Central Complex by Developmentally and Functionally Distinct Neuronal Populations. Curr. Biol. 27, 1098–1110.

Ostroy, S. E., & Pak, W. L. (1974). Protein and electroretinogram changes in the alleles of the norp Ap12 Drosophila phototransduction mutant. Biochimica et Biophysica Acta (BBA)-Bioenergetics, 368(2), 259-268.

Panda, S., Antoch, M. P., Miller, B. H., Su, A. I., Schook, A. B., Straume, M., ... & Hogenesch, J. B. (2002). Coordinated transcription of key pathways in the mouse by the circadian clock. Cell, 109(3), 307-320.Pennartz, C.M. a, de Jeu, M.T.G., Bos, N.P.A., Schaap, J., and Geurtsen, A.M.S. (2002). Diurnal modulation of pacemaker potentials and calcium current in the mammalian circadian clock. Nature 416, 286–290.

Parisky, K.M., Agosto, J., Pulver, S.R., Shang, Y., Kuklin, E., Hodge, J.J.L., Kang, K., Kang, K., Liu, X., Garrity, P. a, *et al.* (2008). PDF cells are a GABA-responsive wake-promoting component of the Drosophila sleep circuit. Neuron 60, 672–682.

Park, D., Hadžić, T., Yin, P., Rusch, J., Abruzzi, K., Rosbash, M., ... & Taghert, P. H. (2011). Molecular Organization of Drosophila Neuroendocrine Cells by Dimmed. Current Biology, 18(21), 1515-1524.

Park, D., Veenstra, J. A., Park, J. H., & Taghert, P. H. (2008). Mapping peptidergic cells in Drosophila: where DIMM fits in. PloS one, 3(3), e1896.

Park, J. H., Helfrich-Förster, C., Lee, G., Liu, L., Rosbash, M., & Hall, J. C. (2000). Differential regulation of circadian pacemaker output by separate clock genes in Drosophila. Proceedings of the National Academy of Sciences, 97(7), 3608-3613.

Park, S., Sonn, J. Y., Oh, Y., Lim, C., & Choe, J. (2014). SIFamide and SIFamide Receptor Defines a Novel Neuropeptide Signaling to Promote Sleep in Drosophila. Molecules and Cells, 37(4), 295–301.

Partch, C. L., Green, C. B., & Takahashi, J. S. (2014). Molecular architecture of the mammalian circadian clock. Trends in cell biology, 24(2), 90-99.

Pauli, A., Althoff, F., Oliveira, R. A., Heidmann, S., Schuldiner, O., Lehner, C. F., ... & Nasmyth, K. (2008). Cell-type-specific TEV protease cleavage reveals cohesin functions in Drosophila neurons. Developmental cell, 14(2), 239-251.

Peng, Y., Stoleru, D., Levine, J.D., Hall, J.C., and Rosbash, M. (2003). Drosophila free-running rhythms require intercellular communication. PLoS Biol. 1, E13.

Pennartz, C.M. a, de Jeu, M.T.G., Bos, N.P.A., Schaap, J., and Geurtsen, A.M.S. (2002). Diurnal modulation of pacemaker potentials and calcium current in the mammalian circadian clock. Nature 416, 286–290.

Pfeiffer, K., and Homberg, U. (2014). Organization and Functional Roles of the Central Complex in the Insect Brain. Annu. Rev. Entomol. 59: 2014.

Pimentel, D., Donlea, J. M., Talbot, C. B., Song, S. M., Thurston, A. J. F., & Miesenböck, G. (2016). Operation of a homeostatic sleep switch. Nature, 536(7616), 333–337.

Pírez, N., Christmann, B.L., and Griffith, L.C. (2013). Daily rhythms in locomotor circuits in Drosophila involve PDF. J. Neurophysiol. 110, 700–708.

Pitman, J.L., McGill, J.J., Keegan, K.P., and Allada, R. (2006). A dynamic role for the mushroom bodies in promoting sleep in Drosophila. Nature 441, 753–756.

Pittendrigh, C. S., & Daan, S. (1976). A functional analysis of circadian pacemakers in nocturnal rodents. Journal of comparative physiology, 106(3), 223-252.

Pittendrigh, C., Bruce, V., and Kaus, P. (1958). on the Significance of Transients in Daily Rhythms. Proc. Natl. Acad. Sci. U. S. A. 44, 965–973.

Pitts, G.R., Ohta, H., and McMahon, D.G. (2006). Daily rhythmicity of large-conductance Ca2+ -activated K+ currents in suprachiasmatic nucleus neurons. Brain Res. 1071, 54–62.

Pologruto, T. A., Yasuda, R., & Svoboda, K. (2004). Monitoring neural activity and [Ca2+] with genetically encoded Ca2+ indicators. Journal of Neuroscience, 24(43), 9572-9579.

Potdar, S., & Sheeba, V. (2018). Wakefulness Is Promoted during Day Time by PDFR Signalling to Dopaminergic Neurons in Drosophila melanogaster. eNeuro, 5(4).

Price, J. L., Blau, J., Rothenfluh, A., Abodeely, M., Kloss, B., & Young, M. W. (1998). double-time is a novel Drosophila clock gene that regulates PERIOD protein accumulation. Cell, 94(1), 83-95.

Ralph, M.R., Foster, R.G., Davis, F.C., and Menaker, M. (1990). Transplanted suprachiasmatic nucleus determines circadian period. Science 247, 975–978.

Renn, S.C., Park, J.H., Rosbash, M., Hall, J.C., and Taghert, P.H. (1999). A pdf neuropeptide gene mutation and ablation of PDF neurons each cause severe abnormalities of behavioral circadian rhythms in Drosophila. Cell 99, 791–802.

Renn, S.C.P., Armstrong, J.D., Yang, M., Wang, Z., An, X., Kaiser, K., and Taghert, P.H. (1999a). Genetic analysis of the Drosophila ellipsoid body neuropil: Organization and development of the central complex. J. Neurobiol. 41, 189–207.

Roberts, L., Leise, T. L., Noguchi, T., Galschiodt, A. M., Houl, J. H., Welsh, D. K., & Holmes, T. C. (2015). Light evokes rapid circadian network oscillator desynchrony followed by gradual phase retuning of synchrony. Current Biology, 25(7), 858-867.

Robie, A.A., Hirokawa, J., Edwards, A.W., Umayam, L.A., Lee, A., Phillips, M.L., Card, G.M., Korff, W., Rubin, G.M., Simpson, J.H., *et al.*. (2017). Mapping the Neural Substrates of Behavior. Cell 170: 393–406.e28.

Root, C.M., Ko, K.I., Jafari, A., and Wang, J.W. (2011). Presynaptic facilitation by neuropeptide signaling mediates odor-driven food search. Cell 145, 133–144.

Ruben, M., Drapeau, M. D., Mizrak, D., & Blau, J. (2012). A mechanism for circadian control of pacemaker neuron excitability. Journal of biological rhythms, 27(5), 353-364.

Rulifson, E. J., Kim, S. K., & Nusse, R. (2002). Ablation of insulin-producing neurons in flies: growth and diabetic phenotypes. Science, 296(5570), 1118-1120.

Sakai, T., & Ishida, N. (2001). Circadian rhythms of female mating activity governed by clock genes in Drosophila. Proceedings of the National Academy of Sciences, 98(16), 9221–9225.

Saunders, D.S., Gillanders, S.W., and Lewis, R.D. (1994). Light-pulse phase response curves for the locomotor activity rhythm in Period mutants of Drosophila melanogaster. J. Insect Physiol. 40, 957–968.

Schindelin, J., Arganda-Carreras, I., Frise, E., Kaynig, V., Longair, M., Pietzsch, T., Preibisch, S., Rueden, C., Saalfeld, S., Schmid, B., *et al.* (2012). Fiji: an open-source platform for biological-image analysis. Nat. Methods 9, 676–682.

Schwartz, W. J., & Gainer, H. (1977). Suprachiasmatic nucleus: use of 14C-labeled deoxyglucose uptake as a functional marker. Science, 197(4308), 1089-1091.

Seelig, J.D., and Jayaraman, V. (2013). Feature detection and orientation tuning in the Drosophila central complex. Nature 503: 262–266.

Selcho, M., Millán, C., Palacios-Muñoz, A., Ruf, F., Ubillo, L., Chen, J., Bergmann, G., Ito, C., Silva, V., Wegener, C., *et al.* (2017). Central and peripheral clocks are coupled by a neuropeptide pathway in Drosophila. Nat. Commun. 8: 15563.

Seluzicki, A., Flourakis, M., Kula-Eversole, E., Zhang, L., Kilman, V., and Allada, R. (2014). Dual PDF signaling pathways reset clocks via TIMELESS and acutely excite target neurons to control circadian behavior. PLoS Biol. 12, e1001810.

Shafer, O.T., Helfrich-Förster, C., Renn, S.C.P., and Taghert, P.H. (2006). Reevaluation of Drosophila melanogaster's neuronal circadian pacemakers reveals new neuronal classes. J. Comp. Neurol. 498, 180–193.

Shafer, O.T., Kim, D.J., Dunbar-Yaffe, R., Nikolaev, V.O., Lohse, M.J., and Taghert, P.H. (2008). Widespread receptivity to neuropeptide PDF throughout the neuronal circadian clock network of Drosophila revealed by real-time cyclic AMP imaging. Neuron 58, 223–237.

Shafer, O.T., Rosbash, M., and Truman, J.W. (2002). Sequential nuclear accumulation of the clock proteins period and timeless in the pacemaker neurons of Drosophila melanogaster. J. Neurosci. 22, 5946–5954.

Shafer, O.T., Wu, C., Helfrich-fo, C., Grieshaber, E.V.A., Rieger, D., and Taghert, P. (2007). Development and Morphology of the Clock-Gene-Expressing Lateral Neurons of Drosophila melanogaster. 70, 47–70.

Shang, Y., Donelson, N.C., Vecsey, C.G., Guo, F., Rosbash, M., and Griffith, L.C. (2013). Short neuropeptide F is a sleep-promoting inhibitory modulator. Neuron 80, 171–183.

Shang, Y., Griffith, L.C., and Rosbash, M. (2008). Light-arousal and circadian photoreception circuits intersect at the large PDF cells of the Drosophila brain. Proc. Natl. Acad. Sci. U. S. A. 105, 19587–19594.

Shang, Y., Haynes, P., Pírez, N., Harrington, K.I., Guo, F., Pollack, J., Hong, P., Griffith, L.C., and Rosbash, M. (2011). Imaging analysis of clock neurons reveals light buffers the wake-promoting effect of dopamine. Nat. Neurosci. 14: 889–895.

Sheeba, V., Sharma, V.K., Gu, H., Chou, Y.-T., O'Dowd, D.K., and Holmes, T.C. (2008). Pigment dispersing factor-dependent and -independent circadian locomotor behavioral rhythms. J. Neurosci. 28, 217–227.

Shiozaki, H.M., and Kazama, H. (2017). Parallel encoding of recent visual experience and self-motion during navigation in Drosophila. Nat. Neurosci. 20: 1395–1403.

Silverman, B. W. (1981). Using kernel density estimates to investigate multimodality, Journal of the Royal Statistical Society. Series B, 43, 97–99.

Sleipness, E. P., Sorg, B. A., & Jansen, H. T. (2007). Diurnal differences in dopamine transporter and tyrosine hydroxylase levels in rat brain: dependence on the suprachiasmatic nucleus. Brain research, 1129: 34-42.

Smith, A. D., Olson, R. J., & Justice Jr, J. B. (1992). Quantitative microdialysis of dopamine in the striatum: effect of circadian variation. Journal of neuroscience methods, 44: 33-41.

Srinivasan, R., Huang, B. S., Venugopal, S., Johnston, A. D., Chai, H., Zeng, H., ... & Khakh, B. S. (2015). Ca 2+ signaling in astrocytes from Ip3r2−/− mice in brain slices and during startle responses in vivo. Nature neuroscience, 18(5), 708.

Stanewsky, R., Frisch, B., Brandes, C., Hamblen-Coyle, M. J., Rosbash, M., & Hall, J. C. (1997). Temporal and Spatial Expression Patterns of Transgenes Containing Increasing Amounts of the Drosophila Clock Geneperiod and a lacZ Reporter: Mapping Elements of the PER Protein Involved in Circadian Cycling. Journal of Neuroscience, 17(2), 676-696.

Stanewsky, R., Jamison, C.F., Plautz, J.D., Kay, S. a, and Hall, J.C. (1997). Multiple circadian-regulated elements contribute to cycling period gene expression in Drosophila. EMBO J. 16, 5006–5018.

Stanewsky, R., Kaneko, M., Emery, P., Beretta, B., Wager-Smith, K., Kay, S. a, Rosbash, M., and Hall, J.C. (1998). The cryb mutation identifies cryptochrome as a circadian photoreceptor in Drosophila. Cell 95, 681–692.

Stephan, F.K., and Zucker, I. (1972). Circadian rhythms in drinking behavior and locomotor activity of rats are eliminated by hypothalamic lesions. Proc. Natl. Acad. Sci. U. S. A. 69, 1583–1586.

Stewart, B. A., Atwood, H. L., Renger, J. J., Wang, J., & Wu, C. F. (1994). Improved stability of Drosophila larval neuromuscular preparations in haemolymph-like physiological solutions. Journal of Comparative Physiology A, 175(2), 179-191.

Stoleru, D., Nawathean, P., Fernández, M.D.L.P., Menet, J.S., Ceriani, M.F., and Rosbash, M. (2007). The Drosophila circadian network is a seasonal timer. Cell 129, 207–219.

Stoleru, D., Peng, Y., Agosto, J., and Rosbash, M. (2004). Coupled oscillators control morning and evening locomotor behaviour of Drosophila. Nature 431.

Stoleru, D., Peng, Y., Nawathean, P., & Rosbash, M. (2005). A resetting signal between Drosophila pacemakers synchronizes morning and evening activity. Nature, 438(7065), 238–242.

Strauss, R., and Heisenberg, M. (1993). A higher control center of locomotor behavior in the Drosophila brain. J. Neurosci. 13: 1852–1861.

Sun, F., Zeng, J., Jing, M., Zhou, J., Feng, J., Owen, S.F., Luo, Y., Li, F., Wang, H., Yamaguchi, T., *et al.* (2018). A Genetically Encoded Fluorescent Sensor Enables Rapid and Specific Detection of Dopamine in Flies, Fish, and Mice. Cell 174, 481–496.e19.

Sun, Y., Nern, A., Franconville, R., Dana, H., Schreiter, E.R., Looger, L.L., Svoboda, K., Kim, D.S., Hermundstad, A.M., and Jayaraman, V. (2017). Neural signatures of dynamic stimulus selection in Drosophila. Nat. Neurosci. 20: 1104-1113

Sweeney, S. T., Broadie, K., Keane, J., Niemann, H., & O'Kane, C. J. (1995). Targeted expression of tetanus toxin light chain in Drosophila specifically eliminates synaptic transmission and causes behavioral defects. Neuron, 14(2), 341-351.

Syntichaki, P., & Tavernarakis, N. (2003). The biochemistry of neuronal necrosis: rogue biology?. Nature Reviews Neuroscience, 4(8), 672.

Takahashi, J. S., Hong, H. K., Ko, C. H., & McDearmon, E. L. (2008). The genetics of mammalian circadian order and disorder: implications for physiology and disease. Nature Reviews Genetics, 9(10), 764.

Talay, M., Richman, E.B., Snell, N.J., Hartmann, G.G., Fisher, J.D., Sorkaç, A., Santoyo, J.F., Chou-Freed, C., Nair, N., Johnson, M., *et al.* (2017). Transsynaptic Mapping of Second-Order Taste Neurons in Flies by trans-Tango. Neuron.

Tang, C.-H.A., Hinteregger, E., Shang, Y., and Rosbash, M. (2010). Light-mediated TIM degradation within Drosophila pacemaker neurons (s-LNvs) is neither necessary nor sufficient for delay zone phase shifts. Neuron 66, 378–385.

Tanoue, S., Krishnan, P., Krishnan, B., Dryer, S. E., & Hardin, P. E. (2004). Circadian Clocks in Antennal Neurons Are Necessary and Sufficient for Olfaction Rhythms in Drosophila. Current Biology, 14(8), 638–649.

Taylor, T. N., Caudle, W. M., Shepherd, K. R., Noorian, A., Jackson, C. R., Iuvone, P. M., ... & Miller, G. W. (2009). Nonmotor symptoms of Parkinson's disease revealed in an animal model with reduced monoamine storage capacity. Journal of Neuroscience, 29(25), 8103-8113.

Terhzaz, S., Rosay, P., Goodwin, S. F., & Veenstra, J. A. (2007). The neuropeptide SIFamide modulates sexual behavior in Drosophila. Biochemical and biophysical research communications, 352(2), 305-310.

Thevenaz, P., Ruttimann, U. E., & Unser, M. (1998). A pyramid approach to subpixel registration based on intensity. IEEE transactions on image processing, 7(1), 27-41.

Turaga, D., & Holy, T. E. (2012). Organization of vomeronasal sensory coding revealed by fast volumetric calcium imaging. Journal of Neuroscience, 32(5), 1612-1621.

Ueno, T., Tomita, J., Tanimoto, H., Endo, K., Ito, K., Kume, S., & Kume, K. (2012). Identification of a dopamine pathway that regulates sleep and arousal in Drosophila. Nature neuroscience, 15(11), 1516.

van Swinderen B, Andretic R. (2003). Arousal in Drosophila. Behavioural Processes. 64:133–144.

VanderLeest, H. T., Houben, T., Michel, S., Deboer, T., Albus, H., Vansteensel, M. J., ... & Meijer, J. H. (2007). Seasonal encoding by the circadian pacemaker of the SCN. Current Biology, 17(5), 468-473.

Vecsey, C.G., Pírez, N., and Griffith, L.C. (2014). The Drosophila neuropeptides PDF and sNPF have opposing electrophysiological and molecular effects on central neurons. J. Neurophysiol. 111, 1033–1045.

Videnovic, A., and Golombek, D. (2017). Circadian dysregulation in Parkinson's disease. Neurobiol. Sleep Circadian Rhythm. 2: 53–58.

Vinayak, P., Coupar, J., Hughes, S.E., Fozdar, P., Kilby, J., Garren, E., Yoshii, T., and Hirsh, J. (2013). Exquisite light sensitivity of Drosophila melanogaster cryptochrome. PLoS Genet. 9, e1003615.

Vosko, A.M., Schroeder, A., Loh, D.H., and Colwell, C.S. (2007). Vasoactive intestinal peptide and the mammalian circadian system. Gen. Comp. Endocrinol. 152, 165–175.

Wei, H., Yasar, H., Funk, N.W., Giese, M., Baz, E.-S., and Stengl, M. (2014). Signaling of Pigment-Dispersing Factor (PDF) in the Madeira Cockroach Rhyparobia maderae. PLoS One 9, e108757.

Welsh, D. K., Takahashi, J. S., & Kay, S. A. (2010). Suprachiasmatic nucleus: cell autonomy and network properties. Annual review of physiology, 72, 551-577.

Welsh, D.K., Logothetis, D.E., Meister, M., and Reppert, S.M. (1995). Individual neurons dissociated from rat suprachiasmatic nucleus express independently phased circadian firing rhythms. Neuron 14, 697–706.

Welsh, D.K., Logothetis, D.E., Meister, M., and Reppert, S.M. (1995). Individual neurons dissociated from rat suprachiasmatic nucleus express independently phased circadian firing rhythms. Neuron 14, 697–706.

Welsh, D.K., Takahashi, J.S., and Kay, S. a (2010). Suprachiasmatic nucleus: cell autonomy and network properties. Annu. Rev. Physiol. 72, 551–577.

Winfree, A.T. (1970). Integrated view of resetting a circadian clock. J. Theor. Biol. 28, 327–374.

Wu MN, Koh K, Yue Z, Joiner WJ, Sehgal A. (2008). A genetic screen for sleep and circadian mutants reveals mechanisms underlying regulation of sleep in Drosophila. Sleep. 31: 465–472.

Wülbeck, C., Grieshaber, E., and Helfrich-Förster, C. (2008). Pigment-dispersing factor (PDF) has different effects on Drosophila's circadian clocks in the accessory medulla and in the dorsal brain. J. Biol. Rhythms 23, 409–424.

Xie, T., Ho, M.C.W., Liu, Q., Horiuchi, W., Lin, C.-C.C., Task, D., Luan, H., White, B.H., Potter, C.J., and Wu, M.N. (2018). A Genetic Toolkit for Dissecting Dopamine Circuit Function in Drosophila. Cell Rep. 23, 652–665.

Xu, K., Zheng, X., & Sehgal, A. (2008). Regulation of Feeding and Metabolism by Neuronal and Peripheral Clocks in Drosophila. Cell Metabolism, 8(4), 289–300.

Yaksi, E., & Friedrich, R. W. (2006). Reconstruction of firing rate changes across neuronal populations by temporally deconvolved Ca 2+ imaging. Nature methods, 3(5), 377.

Yamaguchi, S., Isejima, H., Matsuo, T., Okura, R., Yagita, K., Kobayashi, M., and Okamura, H. (2003). Synchronization of Cellular Clocks in the Suprachiasmatic Nucleus. Science (80-. ). 302, 1408–1412.

Yao Z, Shafer OT. (2014). The Drosophila circadian clock is a variably coupled network of multiple peptidergic units. Science. 343:1516-1520.

Yao, Z., Macara, A.M., Lelito, K.R., Minosyan, T.Y., and Shafer, O.T. (2012). Analysis of functional neuronal connectivity in the Drosophila brain. J. Neurophysiol. 108, 684–696.

Yoshii, T., Funada, Y., Ibuki-Ishibashi, T., Matsumoto, A., Tanimura, T., and Tomioka, K. (2004). Drosophila cryb mutation reveals two circadian clocks that drive locomotor rhythm and have different responsiveness to light. J. Insect Physiol. 50: 479–488.

Yoshii, T., Hermann-Luibl, C., Kistenpfennig, C., Schmid, B., Tomioka, K., and Helfrich-Forster, C. (2015). Cryptochrome-Dependent and -Independent Circadian Entrainment Circuits in Drosophila. J. Neurosci. 35, 6131–6141.

Yoshii, T., Todo, T., Wülbeck, C., Stanewsky, R., & Helfrich-Förster, C. (2008). Cryptochrome is present in the compound eyes and a subset of Drosophila's clock neurons. Journal of Comparative Neurology, 508(6), 952-966.

Yoshii, T., Vanin, S., Costa, R., & Helfrich-Förster, C. (2009). Synergic entrainment of Drosophila’s circadian clock by light and temperature. Journal of Biological Rhythms, 24(6), 452-464.

Yoshii, T., Wülbeck, C., Sehadova, H., Veleri, S., Bichler, D., Stanewsky, R., & Helfrich-Förster, C. (2009). The neuropeptide pigment-dispersing factor adjusts period and phase of Drosophila's clock. Journal of Neuroscience, 29(8), 2597-2610.

Yurgel, M. E., Kakad, P., Zandawala, M., Nassel, D. R., Godenschwege, T. A., & Keene, A. (2018). A single pair of leucokinin neurons are modulated by feeding state and regulate sleep-metabolism interactions. BioRxiv, 313213.

Zandawala M, Yurgel ME , Liao S , Texada MJ , Rewitz KF, Keene AC , and Nässel DR (2018) Orchestration of Drosophila post-feeding physiology and behavior by the neuropeptide leucokinin. bioRxiv, 355107.

Zhang, L., Chung, B.Y., Lear, B.C., Kilman, V.L., Liu, Y., Mahesh, G., Meissner, R.-A., Hardin, P.E., and Allada, R. (2010a). DN1(p) circadian neurons coordinate acute light and PDF inputs to produce robust daily behavior in Drosophila. Curr. Biol. 20, 591–599.

Zhang, L., Lear, B.C., Seluzicki, A., and Allada, R. (2009). The CRYPTOCHROME photoreceptor gates PDF neuropeptide signaling to set circadian network hierarchy in Drosophila. Curr. Biol. 19, 2050–2055.

Zhang, S. X., Rogulja, D., & Crickmore, M. A. (2016). Dopaminergic Circuitry Underlying Mating Drive. Neuron, 91(1), 168–181.

Zhang, Y., Liu, Y., Bilodeau-Wentworth, D., Hardin, P. E., & Emery, P. (2010). Light and temperature control the contribution of specific DN1 neurons to Drosophila circadian behavior. Current Biology, 20(7), 600-605.

Zheng, Z., Lauritzen, J. S., Perlman, E., Robinson, C. G., Nichols, M., Milkie, D., ... & Calle-Schuler, S. A. (2018). A complete electron microscopy volume of the brain of adult Drosophila melanogaster. Cell, 174(3), 730-743.